Titre: Title:	Integrated Fluidized Bed-Membrane Process for Advanced Iron and Manganese Control in Drinking Water
Auteur: Author:	Seyedeh Laleh Dashtban Kenari
Date:	2017
Type:	Mémoire ou thèse / Dissertation or Thesis
Référence: Citation:	Dashtban Kenari, S. L. (2017). Integrated Fluidized Bed-Membrane Process for Advanced Iron and Manganese Control in Drinking Water [Ph.D. thesis, École Polytechnique de Montréal]. PolyPublie. https://publications.polymtl.ca/2517/

Document en libre accès dans PolyPublie
Open Access document in PolyPublie

URL de PolyPublie: PolyPublie URL:	https://publications.polymtl.ca/2517/
Directeurs de recherche: Advisors:	Benoit Barbeau
Programme: Program:	Génie civil

UNIVERSITÉ DE MONTRÉAL

INTEGRATED FLUIDIZED BED-MEMBRANE PROCESS FOR ADVANCED
IRON AND MANGANESE CONTROL IN DRINKING WATER

SEYEDEH LALEH DASHTBAN KENARI

DÉPARTEMENT DES GÉNIES CIVIL, GÉOLOGIQUE ET DES MINES

POLYTECHNIQUE MONTRÉAL

THÈSE PRÉSENTÉE EN VUE DE L'OBTENTION

DU DIPLÔME DE PHILOSOPHIAE DOCTOR

(GÉNIE CIVIL)

AVRIL 2017

UNIVERSITÉ DE MONTRÉAL

POLYTECHNIQUE MONTRÉAL

Cette thèse intitulée :

INTEGRATED FLUIDIZED BED-MEMBRANE PROCESS FOR ADVANCED IRON AND
MANGANESE CONTROL IN DRINKING WATER

présentée par : DASHTBAN KENARI Seyedeh Laleh

en vue de l'obtention du diplôme de : Philosophiae Doctor

a été dûment acceptée par le jury d'examen constitué de :

M. COMEAU Yves, Ph. D., président

M. BARBEAU Benoit, Ph. D., membre et directeur de recherche

M. PERRIER Michel, Ph. D., membre

M. TOBIASON John E., Ph. D., membre

DEDICATION

To my beloved parents & ever-kind and supportive husband

ACKNOWLEDGEMENTS

This is the opportune moment to acknowledge all who in one way or another contributed to the completion of this thesis. First and foremost, I wish to express my deep and sincere gratitude to my supervisor Prof. Benoit Barbeau for his solid support, caring and patience, as well as providing me with an excellent atmosphere for conducting my research. His vast knowledge and logical way of thinking helped me throughout this process.

I acknowledge the members of my committee, Prof. John Tobiason, Prof. Michel Perrier and Prof. Yves Comeau, for taking interest in my work, examining my thesis and providing insightful comments.

I also gratefully acknowledge the financial support of RES'EAU-WATERNET, a NSERC (Natural Sciences and Engineering Research Council of Canada) collaborative strategic network, which made this research work possible.

Special thanks go to my friend, Émile Sylvestre, for translating the abstract of this thesis into French. I am very grateful to all my colleagues in our research group and my fellow labmates and officemates for their cooperative manner and friendly support.

My deepest appreciation goes to the technicians and research associates in the Department of Civil, Geological and Mining Engineering, particularly Mireille Blais, Yves Fontaine, Julie Philibert, Jacinthe Mailly, Marcellin Fotsing and Valentin Pfeiffer for their excellent assistance. In addition, I thank the secretaries of the Department of Civil, Geological and Mining Engineering for helping us and providing us with an ideal atmosphere in which to advance our projects.

I genuinely express my profound gratefulness to my beloved husband, Jaber Shabanian, as I owe my success to his love, patience, heartfelt sympathy, and support.

And last but not least, from the bottom of my heart, I would like to express my endless gratitude to my mother, father, lovely brothers and sister, and in-laws for the absolute support they have provided me throughout my entire life, and without whose love, spiritual encouragement and altruism I would not have finished this thesis. Words are powerless to express what I feel in my heart for them.

RÉSUMÉ

Le fer et le manganèse se retrouvent généralement dans les sources d'eau naturelles, particulièrement en eaux souterraines, qui contiennent fréquemment des niveaux élevés de ces minéraux sous forme dissoute. Les concentrations de fer et de manganèse peuvent causer des problèmes esthétiques à l'eau potable et entrainer des coûts supplémentaires pour le nettoyage ou le renouvellement des conduites obstruées. Les usines de traitement de l'eau ont donc intérêt à éliminer ces minéraux de l'eau potable. De plus, plusieurs préoccupations en santé publique sont liées à la consommation du manganèse à l'eau potable. Par conséquent, Santé Canada (2016) a récemment proposé des lignes directrices pour protéger les enfants de ses effets neurotoxiques. La stratégie traditionnelle d'élimination du fer et du manganèse, par oxydation et la filtration en profondeur, a certaines limites, comme le faible taux d'oxydation du manganèse dissous (Mn(II)) et la formation d'oxyde de manganèse colloïdal, ce dernier étant difficile à retenir par la filtration en profondeur. L'application de membranes d'ultrafiltration (UF)/microfiltration (MF) a récemment été proposée en alternative pour leur capacité à éliminer efficacement les matières particulaires/colloïdales, les organismes pathogènes et les virus (seulement l'UF) par un procédé compact. Ce choix, permet à l'utilisateur de répondre à des normes règlementaires de plus en plus strictes à l'eau traitée. Cependant, le colmatage des membranes limite l'application de ce procédé. Par conséquent, le développement d'un procédé de prétraitement, pouvant diminuer le colmatage de la membrane, est nécessaire. L'élimination du Mn(II) par adsorption sur des milieux recouverts d'oxyde de manganèse suivie d'une oxydation catalytique du manganèse adsorbé, est un procédé efficace et économique. Toutefois, comme la capacité des sites d'adsorption disponibles est principalement régi par le pH, la concentration en chlore et le niveau de recouvrement d'oxyde de manganèse, elle a un impact important sur la performance du procédé. De plus, le taux de charge hydraulique (TCH), la concentration de Mn(II), la température et la dureté peuvent influencer la performance du procédé. Cependant, peu d'informations sont présentement disponibles sur l'impact de ces paramètres. De plus, les milieux recouverts d'oxyde de manganèse ont uniquement été étudiés en lits fixes, ce qui amène certaines limitations, comme un mauvais contact fluide-solide, une accumulation rapide de pertes de charge et un rétro-lavage fréquent conduisant à des TCH faibles. Ainsi, le développement d'un procédé pouvant éliminé efficacement des niveaux élevés de fer et de manganèse et opéré à des TCH élevés est souhaitable.

L'objectif principal de ce projet de recherche est de développer un procédé hybride à lit fluidisé de pyrolucite (LFP)-membrane pour améliorer le contrôle du fer et du manganèse dans l'eau potable (la limite cible de 0,02 mg Mn/L et 0,02 mg Fe/L dans l'eau traitée). Les objectifs spécifiques du projet sont: (1) déterminer les caractéristiques (distribution de la taille des particules (DTP), potentiel ζ et dimension fractale) des colloïdes/particules de l'hydroxyde ferrique et du dioxyde de manganèse qui sont générés en conditions d'oxydation typiques prévalent dans l'eau sous différentes conditions physico-chimiques (pH, force ionique et dureté), (2) évaluer la performance du procédé par membrane UF pré-oxydée par rapport à l'élimination du fer et du manganèse et le niveau de colmatage sous différentes conditions chimiques de l'eau, (3) déterminer les mécanismes de colmatage et la réversibilité du colmatage pour les membranes UF tubulaires en céramique et à fibres creuses en polymères, (4) étudier l'application d'un contacteur LFP pour réduire la concentration de Mn(II) dans les eaux souterraines sous les 0,02 mg/L en opérant à des conditions de TCH élevées et sous autres conditions, (5) opérer une usine pilote pour comparer les performances d'un contacteur fixe par rapport à un contacteur à lit fluidisé pour le contrôle du fer et du manganèse dans une nappe phréatique naturelle en condition d'opération à long terme afin de d'évaluer la faisabilité de ce processus pour les petites collectivités et les communautés rurales, et (6) comparer la performance d'un procédé hybride membranaire LFP-MF/UF par rapport à un procédé classique avec MF/UF membrane incluant une pré-oxydation (en ce qui concerne l'élimination du fer et du manganèse ainsi que l'atténuation du colmatage) sous différentes conditions chimiques.

En première partie de ce projet, la performance des membranes UF en céramique et en polymère avec une pré-oxydation en ligne pour le contrôle du fer/manganèse a été évaluée. En raison de l'impact possible des caractéristiques du fer et du manganèse oxydés sur la performance membranaire, cette recherche vise d'abord à déterminer le diamètre (DTP), le potentiel ζ et la dimension fractale de ces agrégats, en fonction du pH, de la force ionique et de la dureté en utilisant la diffraction laser (DL), la diffusion dynamique de la lumière (DDL) et le fractionnement par filtration membranaire en série. Pour le dioxyde de manganèse, le potentiel ζ a proportionnellement diminué par rapport au pH mais la force ionique et, surtout, la dureté l'ont augmenté, entrainant la formation de plus gros agrégats. En revanche, le potentiel ζ et le DTP des agrégats d'hydroxyde ferrique n'ont pas été significativement altérés par la chimie de l'eau. À l'étape suivante, le colmatage des membranes UF en céramique et en polymère a été évalué en utilisant les

modèles de loi de blocage et de résistance en série. Les résultats montrent que les paramètres chimiques de l'eau testée n'ont pas eu d'impact significatif sur l'efficacité d'élimination du fer/manganèse (> 99,5% pour toutes les conditions), mais ils ont permis d'expliquer le niveau du colmatage causé par les agrégats de dioxyde de manganèse. Contrairement au manganèse, le gâteau formé par les agrégats d'hydroxyde ferrique a exercé une résistance très faible et comparable sur les deux membranes pour toutes les conditions testées en accord avec les caractéristiques d'agrégats similaires. En général, bien que qu'un comportement de colmatage similaire eût été observé pour les membranes de céramique et de polymère, la réversibilité du colmatage a différé.

Pour la deuxième partie de ce projet, un contacteur LFP a été utilisé comme processus autonome pour traiter les eaux souterraines contenant des niveaux élevés de Mn(II). Une étude à échelle pilote a été menée en conditions dynamiques en utilisant de l'eau souterraine synthétique pour déterminer l'impact des conditions d'opération (TCH et température) et de la composition de l'eau souterraine (concentration Mn(II), dureté calcique et pH) sur l'élimination de Mn(II). Les résultats montrent un enlèvement quasi-total du manganèse (≈ 100%) en moins de 1 min dans toutes les conditions testées. L'adsorption de Mn(II) sur la pyrolucite s'est avérée être le seul mécanisme responsable de l'élimination du manganèse. Un taux d'adsorption plus élevé a été obtenu avec des TCH élevés. L'augmentation du résiduel de chlore libre à l'effluent de 1,0 à 2,0-2,6 mg Cl_2/L a augmenté le temps d'opération nécessaire avant une nouvelle régénération de 6 jours à plus de 12 jours. La turbidité à l'eau traitée est restée inférieure à 0,2 NTU pendant toute la période d'essai.

Pour la partie suivante, des lits fixes et fluidisés de pyrolucite à échelle pilote ont été testés en parallèle pour comparer les performances à long terme de ces procédés pour éliminer le fer et/ou le manganèse d'une eau souterraine naturelle dans laquelle du Fe(II)/Mn(II) a parfois été ajouté. La configuration de la plaque de distribution située au fond du LFP a fortement influencé le relargage du manganèse particulaire de la pyrolucite et la turbidité à l'eau traitée. Après avoir installé une plaque de distribution optimale, un enlèvement efficace du manganèse (< 0,02 mg/L en sortie) a été obtenu par le contacteur LFP à un TCH très élevé (45 m/h). Le même résultat a également été obtenu pour le lit fixe à TCH de 20 m/h. En présence d'une concentration élevée de fer, le contacteur LFP n'a pas réussi à contrôler correctement la concentration de fer et de manganèse en dessous de la limite cible de 0,02 mg/L alors que le contacteur à lit fixe a permis à lui seul un enlèvement presque complet mais à défaut de lavages fréquents du lit filtrant (3 d). Une étude plus approfondie de l'application d'un processus rentable en aval du LFP serait nécessaire.

Enfin, un procédé hybride LFP-MF/UF intégré a été proposé pour améliorer le contrôle du fer et du manganèse. Une étude à échelle laboratoire a été faite pour évaluer la performance de ce procédé et la comparer avec le procédé classique de pré-oxydation-MF/UF sous différentes conditions. Les modèles de loi de blocage et de résistance en série ont été utilisés pour mieux comprendre les mécanismes de colmatage de la membrane et sa réversibilité. Le flux membranaire et les concentrations en calcium et en acides humiques dans les eaux d'alimentation ont eu un impact notable sur le comportement de filtration des membranes en céramique et en polymère. La présence d'acides humiques a influencé la compressibilité du gâteau formé par le fer oxydé et le manganèse. L'ion calcium favorise l'agrégation du dioxyde de manganèse et des acides humiques, ce qui a entrainé un colmatage considérable. L'application d'un LFP comme procédé de prétraitement a atténué le colmatage des membranes en éliminant plus de 75% du fer et 95% du manganèse dans l'eau. Dans l'ensemble, ce travail apporte des informations supplémentaires sur le colmatage du fer oxydé et du manganèse pour le traitement de l'eau et propose un nouveau procédé permettant un meilleur contrôle du fer et du manganèse.

ABSTRACT

Iron and manganese are commonly found in natural water supplies, particularly groundwater, which frequently contains high levels of these minerals in dissolved form. The occurrence of iron and manganese in drinking water mainly gives rise to aesthetic issues as well as additional cost for cleaning or renewing clogged pipes; thus, it is of interest for water treatment utilities to remove these minerals from drinking water. In addition, health concern is also associated with manganese intake from water ingestion. Consequently, Health Canada (2016) has recently proposed a health-based guidance to protect children from neurotoxic effects. The traditional removal strategy for iron and manganese, i.e., oxidation and depth filtration, is subject to some limitations, such as slow oxidation rate of dissolved manganese (Mn(II)) and formation of colloidal manganese oxide that is difficult to retain by depth filtration. Alternatively, application of ultrafiltration (UF)/microfiltration (MF) membrane has been proposed more recently because they can properly remove particulate/colloidal materials, pathogens and viruses (only UF) in a compact process. Thus, the treated water can meet the increasingly stringent regulations. However, membrane fouling has limited the application of this process. Therefore, developing a pretreatment process, which can alleviate membrane fouling is of great interest. The Mn(II) removal through sorption onto manganese oxide coated media followed by catalytic oxidation of adsorbed manganese, is an effective and economical method. Nonetheless, maintenance of available sorption sites, which is mainly governed by pH, chlorine concentration and manganese oxide coating level, strongly affects the process performance. In addition, hydraulic loading rate (HLR), Mn(II) concentration, temperature and hardness may further influence the process performance. However, there is currently little information available on the impact of these parameters. Moreover, manganese oxide coated media has been solely studied in fixed beds which have some limitations, such as poor fluid-solid contact, rapid head loss buildup and frequent backwash, leading to low HLRs. Thus, developing a process which can efficiently remove elevated levels of iron and manganese and be operated under high HLRs is of great interest.

The main objective of this research project is to develop an integrated pyrolucite fluidized bed (PFB)-membrane hybrid process for improved iron and manganese control in drinking water (target limit of 0.02 mg Mn/L and 0.02 mg Fe/L in treated water). On a more detailed level, the following specific objectives are defined: (1) determine the characteristics (i.e., particle size distribution

(PSD), ζ-potential and fractal dimension) of ferric hydroxide and manganese dioxide colloids/particles, which are generated during typical oxidation conditions prevailing in water of various physicochemical characteristics (i.e., pH, ionic strength and hardness), (2) evaluate the performance of pre-oxidation-UF membrane process with respect to iron and manganese removal, and the extent of fouling under various water chemistry conditions, (3) determine the fouling mechanisms and reversibility of the fouling in tubular ceramic and hollow fiber polymeric UF membranes, (4) investigate the potential application of a PFB contactor to remove elevated concentrations of Mn(II) from groundwater down to below 0.02 mg/L while operating under high HLRs and different conditions, (5) conduct a field pilot plant comparing the performances of a fixed vs. fluidized bed contactors for iron and manganese control on a natural groundwater during a long-term operation in order to demonstrate the feasibility of this process for small rural communities, (6) compare the performance of a PFB-MF/UF membrane hybrid process with the conventional pre-oxidation-MF/UF membrane process (with respect to iron and manganese removal as well as fouling mitigation) under variable water chemistry conditions.

In the first part of this project, the performance of a ceramic and a polymeric UF membrane with in-line pre-oxidation for iron/manganese control was evaluated. Due to the possible impact of oxidized iron/manganese characteristics on membrane performance, this research, first, focused on determining the PSD, ζ-potential and fractal dimension of these aggregates, as a function of pH, ionic strength and hardness using laser diffraction (LD), dynamic light scattering (DLS) and fractionation through serial membrane filtration techniques. For manganese dioxide, the ζ-potential was found to decrease as the pH decreased and the ionic strength and, especially, hardness increased, resulting in the formation of larger aggregates. In contrast, the ζ-potential and PSD of ferric hydroxide aggregates was not significantly altered by water chemistry. In the next step, fouling of a ceramic and a polymeric UF membranes was evaluated using the blocking law and resistance-in-series models. Results suggest that the water chemistry tested did not produce significant impacts on the iron/manganese removal efficiencies (> 99.5% under all conditions) while it did contribute to explain the extent of fouling caused by manganese dioxide aggregates. Unlike manganese, the cake formed by ferric hydroxide aggregates exerted very low and comparable resistance on both membranes under all conditions tested, in agreement with the similar aggregate characteristics. In general, although a similar fouling behavior was found for the ceramic and polymeric membranes, the reversibility of the fouling differed from one another.

In the second part of this project, a PFB contactor was introduced as a stand-alone process to treat groundwater containing high levels of Mn(II). A lab pilot-scale study was conducted under dynamic conditions using synthetic groundwater to elucidate the impact of operational conditions (HLR and temperature) and groundwater composition (Mn(II) concentration, calcium hardness and pH) on Mn(II) removal. Results indicated almost complete manganese removal ($\approx$ 100%) in less than 1 min under all conditions tested. Adsorption of Mn(II) onto pyrolucite was proven to be the only mechanism responsible for manganese removal. Higher adsorption rate was achieved under elevated HLRs. Increasing the effluent free chlorine residual from 1.0 to 2.0-2.6 mg Cl_2/L extended the operation time before further regeneration from 6 days to more than 12 days. Turbidity of the treated water remained below 0.2 NTU during the entire test period.

In the next part, pilot-scale pyrolucite fixed and fluidized bed contactors were tested in parallel to compare the long-term performance of these processes for iron and/or manganese removal from a natural groundwater which was occasionally supplemented with Fe(II)/Mn(II). The configuration of the distributor plate located at the bottom of the PFB strongly influenced the release of particulate manganese from pyrolucite and the turbidity of the treated water. After installing an optimal distributor plate, effective manganese removal (< 0.02 mg/L) was achieved through the PFB contactor at very high HLR (45 m/h). The same result was also found for the fixed bed at HLR of 20 m/h. Under elevated iron concentration, the PFB contactor failed to properly control the iron and manganese concentration below the target limit of 0.02 mg/L while the fixed bed contactor alone provided almost complete removal but required frequent backwash of the filter bed (3 d). Further study should address the application of a cost-effective process downstream of the PFB.

Finally, an integrated PFB-MF/UF hybrid process was proposed for improved iron and manganese control. A lab-scale study was undertaken to assess the performance of this process and compare it with the conventional pre-oxidation-MF/UF process under different conditions. Blocking law and resistance-in-series models were used to elucidate the membrane fouling mechanisms and its reversibility. Membrane flux and calcium and humic acids concentrations in the feed waters had both a notable impact on the filtration behavior of the ceramic and polymeric membranes. The presence of humic acids influenced the compressibility of the cake formed by oxidized iron and manganese. Calcium ion promoted aggregation of manganese dioxide and humic acids, thus, considerably impacted fouling. Application of a PFB as a pretreatment process mitigated membrane fouling by removing more than 75% and 95% of iron and manganese from water,

respectively. Overall, this work provides further insight on the fouling of oxidized iron and manganese in water treatment and proposes a new process, which can fulfil appropriate iron and manganese control.

TABLE OF CONTENTS

LIST OF TABLES

LIST OF FIGURES

LIST OF ABBREVIATIONS

APHA	American Public Health Association
Ca^{2+}	Calcium Ion
ClO_2	Chlorine Dioxide
CR	Continuous Regeneration
DBPs	Disinfection by Products
DLS	Dynamic Light Scattering
DM	Demineralized
DOC	Dissolved Organic Carbon
EDL	Electrostatic Double Layer
FBR	Fluidized Bed Reactor
Fe	Iron
Fe(II)	Ferrous Iron
Fe(III)	Ferric Iron
$Fe(OH)_3$	Ferric Hydroxide
GAC	Granular Activated Carbon
HLR	Hydraulic Loading Rate
HOCl	Hypochlorous Acid
H_2O_2	Hydrogen Peroxide
IOCS	Iron Oxide Coated Sand
IR	Intermittent Regeneration
$KMnO_4$	Potassium Permanganate
LD	Laser Diffraction
LPMs	Low Pressure Membranes

MDDELCC   Ministère du Développement Durable de l'Environnement et de la Lutte contre les Changements Climatiques

MF   Microfiltration

Mn   Manganese

Mn(II)   Reduced Manganese

MnO_2 Manganese Dioxide

MnO_4^- Permanganate

MW   Molecular Weight

MWCO   Molecular Weight Cut Off

MWH   Montgomery Watson Harza

NF   Nanofitration

NGE   Natural Greensand Effect

NOM   Natural Organic Matter

NSERC   Natural Sciences and Engineering Research Council of Canada

O_3 Ozone

OCl^- Hypochlorite

PAA   Poly-Acrylic Acid

PES   Polyethersulfone

PFB   Pyrolucite Fluidized Bed

PFBR   Pyrolucite Fluidized Bed Reactor

PSD   Particle Size Distribution

PVC   Polyvinyl Chloride

PVDF   Polyvinylidene Fluoride

PVP   Polyvinylpyrrolidone

RO   Reverse Osmosis

SFW	Synthetic Feedwater
SGW	Synthetic Groundwater
SiC	Silicon Carbide
SMCL	Secondary Maximum Contaminant Level
THM	Trihalomethane
TiO$_2$	Titanium dioxide
TMP	Transmembrane Pressure
TOC	Total Organic Carbon
UF	Ultrafiltration
USEPA	United States Environmental Protection Agency
WHO	World Health Organization
ZrO$_2$	Zirconium dioxide

CHAPTER 1   INTRODUCTION

1.1 Background

Iron and manganese naturally co-occur in surface and ground water supplies as a result of weathering and leaching of metal-bearing minerals, rocks and soils rich in organic matter, thermal stratification in lakes and contamination by industrial effluents. Among different water sources, groundwater frequently contains significant levels of dissolved iron (Fe(II)) and manganese (Mn(II)) due to more reduced redox conditions. Nearly 44% of population in United States and 30% of population in Canada, mostly living in small rural communities, relies on groundwater as a source of drinking water. The presence of iron and manganese in drinking water is principally regarded as creating aesthetic and operational issues, including colored water formation, increased turbidity, metallic taste and odor, staining of laundry and plumbing fixture, and pipeline clogging, which may result in customer complaints (World Health Organization (WHO), 2008). In this regard, the United States Environmental Protection Agency (USEPA) (2004) and the Canadian Drinking Water Quality Guidelines (Health Canada, 2014) have established an aesthetic objective limit of 0.3 and 0.05 mg/L for total iron and manganese concentrations in drinking water, respectively. However, iron and manganese concentrations as low as 0.05 (World Health Organization, 2003) and 0.02 mg/L (Sly et al., 1990), respectively, may still give rise to adverse aesthetic impacts. As a result, Health Canada (2016) has lately proposed an aesthetic objective limit of 0.02 mg/L for total manganese in drinking water. Furthermore, manganese control in drinking water is receiving more attention owing to its potential neurotoxicity (Wasserman et al., 2006; Tuschl et al., 2013). Epidemiological studies reported that exposure to manganese in drinking water is associated with neurological impacts in children, such as intellectual impairment and poor neurobehavioral function (Bouchard et al., 2011; Oulhote et al., 2014), even at fairly low manganese concentrations in treated water. Consequently, Health Canada (2016) has recently proposed a health-based maximum acceptable concentration of 0.1 mg/L for manganese in drinking water. Thus, effective iron and manganese removal (target limit of 0.02 mg Mn/L and 0.02 mg Fe/L) is becoming an important objective of drinking water treatment.

One of the common treatment strategies for Fe(II) and Mn(II) control in drinking water, especially in North America, includes oxidation of dissolved species to particulate forms, ferric hydroxide

and manganese dioxide, followed by separation of oxidized particles from water. Unlike Fe(II), which is rapidly oxidized by a weak oxidant, direct oxidation of Mn(II) requires the application of a strong oxidant, such as potassium permanganate ($KMnO_4$) or ozone (O_3) (Knocke et al., 1990b), which always brings the risk of permanganate (MnO_4^-) escaping into treated water and therefore producing pink water (Gregory and Carlson, 2003). In addition, traditional processes for particulate/colloidal matter removal from water include coagulation, flocculation, sedimentation and granular media filtration, which have drawbacks of operating in successive steps requiring significant contact time and, consequently, large process footprint. Moreover, oxidized manganese may not be effectively removed by such treatment technologies (Carlson et al., 1997) because of its propensity to form colloidal manganese dioxide (Morgan and Stumm, 1964). Alternatively, compact membrane processes, such as microfiltration (MF) and ultrafiltration (UF), are increasingly retrofitted in water treatment plants for filtration of dilute suspensions based on size exclusion (Crittenden et al., 2012). However, management of membrane fouling is an important limitation of this technology, which requires a systematic study to identify the contribution of different parameters. Although organic matter dominantly controls membrane fouling in surface water systems, management of fouling caused by iron/manganese is of importance for many MF/UF/NF/RO groundwater systems. This is particularly important for manganese removal since colloidal manganese oxides are prone to severely foul membranes (Choo et al., 2005). Thus, developing a pretreatment process, which can properly alleviate the fouling of the membrane, would be a good option.

Several factors influence the fouling of a MF/UF membrane; namely, membrane type (e.g., tubular vs. hollow fiber), material (e.g., ceramic vs. polymeric) and pore size (e.g., MF vs. UF), operating conditions (e.g., flux), process configuration (e.g., dead end vs. cross flow), cleaning strategies and feed water characteristics (Crittenden et al., 2012; Lee and Kim, 2014). Application of ceramic membrane has been receiving growing attention owing to its inherent advantages over the conventional polymeric membrane, such as superior chemical, thermal and mechanical stability, which allow water practitioners to exert more aggressive physical and chemical cleaning, prolonging the membrane life expectancy. Despite the high potential application of ceramic membrane for iron/manganese control, the fundamental fouling behavior caused by ferric hydroxide and manganese dioxide aggregates has not yet been documented. Previous studies on some inorganic minerals, rather than oxidized iron and manganese, have revealed the influence of

pH, ionic strength and salt valency on the characteristics of inorganic aggregates (Faibish et al., 1998; Ramachandra Rao et al., 1999; Zhao et al., 2005; Duan et al., 2014), and, subsequently, on the performance of the membrane due to their impact on particle-particle and particle-membrane interactions (Lee et al., 2003; Santiwong et al., 2008). Furthermore, permeability of MF/UF membranes may be also altered by these parameters, although salt rejection is negligible (Huisman and Dutre, 1997; Faibish et al., 1998; Zhao et al., 2005; Manttari et al., 2006). Thus, understanding the characteristics and behavior of oxidized iron and manganese aggregates is of interest for application of UF/MF membranes.

Considering the propensity of $MnO_{x(s)}$ to adsorb dissolved metal ions (Morgan and Stumm, 1964), a process, termed Natural Greensand Effect (NGE), was historically developed for Mn(II) control. Based on NGE process, Mn(II) removal is achieved through sorption of Mn(II) onto $MnO_{x(s)}$ surface, e.g. $MnO_{x(s)}$ coated sand, followed by auto-catalytic oxidation of adsorbed Mn(II) in the presence of an oxidant. NGE process allows two modes of operation depending on the presence of free chlorine: intermittent regeneration (IR) and continuous regeneration (CR) (Knocke et al., 1990a). In IR operation mode, the $MnO_{x(s)}$ surface adsorbs Mn(II) until available sorption sites are occupied and breakthrough arisen. $KMnO_4$ or free chlorine solution is then used to restore the adsorption capacity of the filter media (i.e., regeneration of the filter media). In CR mode, a free chlorine solution is continuously spiked into the feed water just prior entering the column, thus the adsorption sites are continuously regenerated and become available. Nevertheless, maintenance of available adsorption sites, which is governed by the $MnO_{x(s)}$ coating level, chlorine concentration and pH, strongly affect the performance of NGE process (Knocke et al., 1990a). In addition, the process performance may be further influenced by the hydraulic loading rate (HLR), Mn(II) concentration, temperature and hardness.

Adsorption of Mn(II) onto $MnO_{x(s)}$-coated sand is normally performed in packed bed contactors operated at relatively low HLRs (6-12 m/h) to remove low feed water Mn(II) concentrations (< 0.5 mg/L) (Hargette and Knocke, 2001; Yang et al., 2008; Piispanen and Sallanko, 2010). Under higher HLRs, rapid head loss buildup gives rise to frequent backwash, high energy expenses and large amount of backwash water production, which are important limitations of a packed bed configuration. Knocke et al. (2010) have shown that application of post-filtration adsorptive contactors filled with large size (2.0-2.4 mm) pyrolucite (a natural manganese dioxide ore) media could overcome these constraints. HLRs as high as 32-50 m/h (16-20 gpm/ft²) were successfully

tested under low manganese concentrations (< 0.1 mg/L). The backwash frequency was approximately every other month.

Alternatively, a fluidized bed adsorptive contactor could offer a number of promising benefits in comparison with the fixed bed contactors because the adsorption sites can be effectively used in fluidized state due to the better fluid-solid contact, which offers a higher adsorption rate. In addition, it allows application of small size pyrolucite media (effective diameter of 0.4 mm) with high specific surface area at high HLRs that is favorable for adsorption kinetic while it simultaneously eliminates the head loss increase.

In order to come up with a novel process, which can properly overcome the problems encountered in the abovementioned methods, a pyrolucite fluidized bed (PFB) contactor was proposed as a pretreatment for membrane filtration. Due to the specific configuration of the fluidized bed, the number of available active sites for sorption is more than for the fixed-bed and it allows operating at relatively high HLRs. An increased HLR reduces the process footprint and therefore capital costs. This hybrid process could be a promising alternative for the treatment of groundwater containing high levels of iron and manganese, especially for groundwaters requiring primary disinfection which could be achieved with UF membranes.

1.2 Structure of dissertation

This thesis is subdivided in eight chapters. Following an in-depth review on common methods for iron and manganese control in drinking water (Chapter 1), the research objectives and methodology are presented (Chapter 2). Chapters 3 through 7 present results of this research in the form of 4 published articles and 1 submitted manuscript. The first article intends to determine the characteristics of oxidized iron and manganese aggregates in water treatment under different water chemistry conditions (Chapter 3, published in *Journal of Environmental Engineering*). The second article aims at understanding UF fouling of ceramic and polymeric membranes caused by oxidized iron and manganese under different water quality (Chapter 4, published in *Journal of Membrane Science*). The next chapter proposes a PFB as a robust and compact process for manganese removal from groundwater (Chapter 5, published in *Water Research*). Chapter 6 compares the long-term performance of pilot-scale pyrolucite fixed and fluidized bed contactors for iron and manganese control in natural groundwater (submitted to the *Journal of Environmental Chemical Engineering*).

Chapter 7 proposes an integrated PFB-MF/UF hybrid process for improved iron and manganese control in drinking water (published in *Water Research*). Finally, a general discussion is provided in Chapter 8 followed by conclusions and recommendations.

CHAPTER 2   LITERATURE REVIEW

This chapter presents a summary of previous research studies conducted in areas relevant to the removal of soluble iron and manganese from water. It includes sections on the geochemistry of iron and manganese in natural water systems, water quality concerns and regulations, traditional methods for iron and manganese control in drinking water, and the use of membrane filtration for the removal of these species.

2.1 Iron and manganese in natural water systems

Iron and manganese are both abundant and naturally-occurring elements in the earth's crust that frequently co-occur in natural water sources. Manganese is commonly found at concentrations below 0.3 mg/L, while iron generally presents at concentrations five to twenty times higher than manganese (Buamah et al., 2008). They usually occur in groundwater and anoxic hypolimnion layer of reservoirs at high concentrations due to dissolution of these minerals from rocks and soils under low redox potential and pH values. Likewise, groundwater containing high levels of iron (7-15 mg Fe/L) and manganese (2 mg Mn/L) has been reported in the province of Quebec (Ellis et al., 2000). Another research by Barbeau et al. (2011) revealed that the concentration of manganese in drinking water supplied by groundwater in southern Quebec can reach up to 2.7 mg/L. In addition, the leakage of industrial wastewater might also be responsible for heavy metal contamination of water sources (United States Environmental Protection Agency (USEPA), 2004). Furthermore, agricultural applications of manganese-containing fungicides have also been identified as a possible source of groundwater manganese contamination (van Wendel de Joode et al., 2016).

Manganese can exist in numerous oxidation states between 0 and +7 (Trudinger, 1979). Among these oxidation states, Mn(II), Mn(III), Mn(IV) and Mn(VII) are commonly encountered in water treatment practices. In natural water sources with pH values between 5-8, manganese predominantly exists in dissolved form, Mn(II) or Mn^{+2}. Mn(III), MnOOH, and Mn(IV), MnO_2, are insoluble forms of manganese. Mn(VII), the highest oxidized form of manganese, is a strong oxidant, exists in the form of MnO_4^- anion. Morgan and Stumm (1964) revealed that insoluble manganese in water can also occur as mixed oxides, termed MnO_x (where $1 < x < 2$).

Iron compounds presents in natural waters in two oxidation states, Fe(II) and Fe(III). Dissolved state of iron, Fe(II), is generally unstable in surface waters and precipitated as insoluble Fe(III)

hydroxide, Fe(OH)$_3$ (World Health Organization (WHO), 2003). However, anaerobic groundwater sources may contain high levels of Fe(II).

The equilibrium between the various iron and manganese species are commonly determined by pH and redox potential as depicted in Figure 2.1 (Eh-pH stability diagram). Obviously, this figure illustrates that at any Eh, or redox potential, value, the pH level for the stability of soluble Mn(II) is considerably higher than Fe(II). Consequently, it can be concluded that manganese cannot be oxidized and removed from water as easily as iron. The diagram also shows that under reducing condition with pH above 8.0, solid MnCO$_3$ is the primary form of manganese. Generally, solubility of Fe(II) and Mn(II) is controlled by the concentration of carbonate (alkalinity) in water which may result in the precipitation of FeCO$_3$ and MnCO$_3$, respectively (Buamah et al., 2008). However, in the presence of O$_2$ and high pH levels, Mn(III) and Mn(IV) are favored. In addition, presence of iron and manganese oxidizing and reducing microorganisms can also govern the oxidation state of these minerals in natural water sources (Trudinger, 1979). Furthermore, formation of stable complexes between either Fe(II) or Mn(II) and various dissolved organic compounds can greatly increase the solubility of these metals, especially iron (Trudinger, 1979).
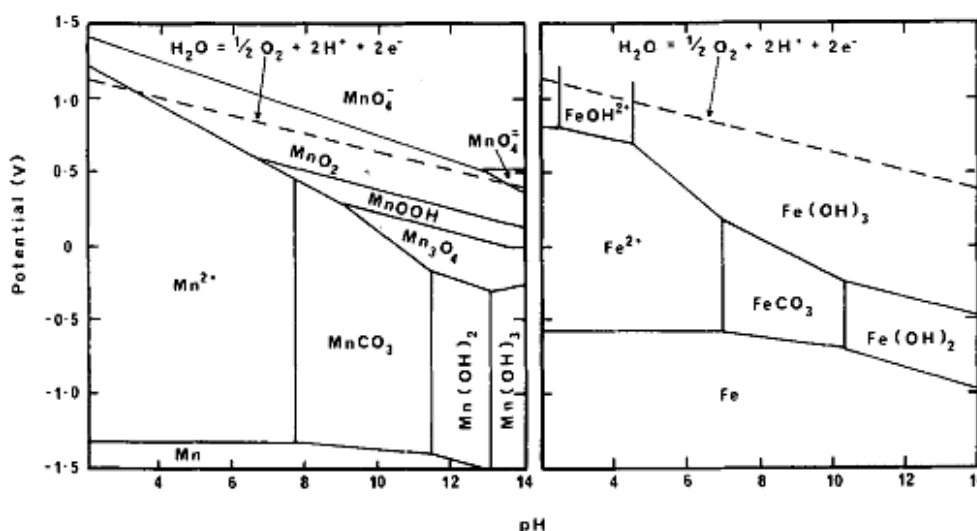
Figure 2.1. Eh-pH stability diagram for iron and manganese at 25°C and divalent species concentration (activity) of 10-5 M (Morgan and Stumm, 1965).

2.2 Water quality concerns and regulations

Iron and manganese are objectionable constituents of water mainly for aesthetic and/or operational issues. Soluble iron and manganese in water distribution systems may be oxidized by oxygen or free chlorine, which is applied as a secondary disinfectant, resulting in the deposition of blackish-brown manganese dioxide and/or reddish-brown iron hydroxide. This can cause discoloration of water, staining of laundry and plumbing fixtures, an unpleasant metallic taste to water, and, in severe case, the reduction in hydraulic capacity of pipes or an increase in required energy for pumping water through the pipes; hence, it represents additional costs to municipality. Furthermore, in the case of insufficient secondary disinfectant residual, the presence of these metals in distribution system may promote the growth of iron and manganese utilizing bacteria, resulting in clogging of the pipelines or creating additional aesthetic problems (Sly et al., 1990; World Health Organization (WHO), 2008). A recent study further revealed that bio-chemical oxidation and sorption of iron and manganese significantly influence the accumulation of these species in water distribution network (Prasad and Danso-Amoako, 2014). In this regard, the United States Environmental Protection Agency (USEPA), (2004) has established secondary maximum contaminant levels of 0.3 mg/L and 0.05 mg/L for total iron and manganese in drinking water, respectively. However, consumer complaints regarding aesthetic issues have been reported at concentrations of iron and manganese as low as 0.05 (World Health Organization (WHO), 2003) and 0.02 mg/L (Sly et al., 1990), respectively. Consequently, Health Canada (2016) has recently proposed an aesthetic objective limit of 0.02 mg/L for total manganese in drinking water. Therefore, it is recommended to keep the level of these minerals in drinking water as low as possible.

Over the last decade, numerous studies have reported adverse health impacts from manganese intake from drinking water. The reader is referred to the recent Health Canada (2016) literature review for a complete description of studies related to manganese neurotoxicity. For example, although manganese is an essential nutrient for human health, it has been indicated that exposure to elevated levels of manganese in drinking water may cause neurological disorders, especially, in children (Wasserman et al., 2006; Dion et al., 2016; Oulhote et al., 2014; Bouchard et al., 2011). Consequently, to prevent potential health effect, health-based guidelines of 0.5, 0.4, 0.3 and 0.1 mg/L manganese in drinking water have been recommended by California Department of Public

Health (CDPH) (2010), World Health Organization (WHO) (2008), United States Environmental Protection Agency (USEPA) (2004) and Health Canada (2016), respectively. The Health Canada guideline is currently under review and the final recommendation is expected in 2017. The Minnesota Department of Health followed the same approach as Health Canada and established a manganese level of 0.1 mg/L for infants less than 1 year old, and 0.3 mg/L for children > 1 year old and adults (MDH, 2012).

No health guideline value has been proposed for iron at concentrations normally found in drinking water (World Health Organization (WHO), 2008).

2.3 Traditional methods for iron and manganese control in drinking water

There are several available methods for iron and manganese removal from water depending on the speciation of these elements and water quality. The most common methods are as follows:

- Oxidation of Fe(II) and Mn(II) to particulate forms, ferric iron (Fe(III)) and manganic manganese (Mn(IV)), using a strong oxidant, followed by removal of the precipitates through depth granular media filtration;
- Sorption of Mn(II) onto manganese oxide coated media followed by autocatalytic oxidation of adsorbed manganese using oxygen or chlorine; however, in this process, Fe(II) may be readily oxidized in water and, thus, removed through granular media filtration.

These techniques are discussed in detail in the following sections.

2.3.1 Direct oxidation and particle removal

2.3.1.1 Oxidation of iron and manganese

In general, removal of manganese from water is more difficult than iron because of its slower oxidation rate (Knocke et al., 1991) and its tendency to form colloidal particles when it is rapidly oxidized in water (Morgan and Stumm, 1964).

Oxygen (from air), chlorine and $KMnO_4$ are the most common oxidants applied in water treatment practices. In addition to these, O_3, chlorine dioxide (ClO_2) and hydrogen peroxide (H_2O_2) are also used for iron/manganese oxidation (Sommerfeld, 1999).

Oxidation of Fe(II) and Mn(II) in water most often forms iron hydroxide (Fe(OH)$_3$) and manganese dioxide (MnO$_2$), respectively. Knocke et al. (1990a) revealed that oxidation from the bulk solution is the only mechanism responsible for Fe(II) removal in low-dissolved organic carbon (DOC) waters. However, oxidation of Mn(II) involves three steps: solution-phase oxidation, adsorption of Mn(II) onto MnO$_2$(s) particles and subsequent oxidation of adsorbed ions on the oxide surface, which are depicted on the following equations:

$$\text{Mn(II)} + \text{Ox} \rightarrow \text{MnO}_2(s) \qquad \text{(Oxidation)} \qquad (1.1)$$

$$\text{Mn(II)} + \text{MnO}_2(s) \rightarrow \text{Mn(II)}.\text{MnO}_2(s) \qquad \text{(Adsorption)} \qquad (1.2)$$

$$\text{Mn(II)}.\text{MnO}_2(s) + \text{Ox} \rightarrow 2\text{MnO}_2(s) \qquad \text{(Oxidation)} \qquad (1.3)$$

The following discussion reviews details of iron and manganese oxidation by different oxidants that are commonly used in water treatment plants:

Aeration. In many cases, aeration is the first pretreatment that has been used prior to filtration. It helps to oxidize iron in varying rates depending on the pH of water, temperature and the presence of organic matter (Sommerfeld, 1999; Azizi et al., 2013). Although aeration can theoretically be employed to oxidize Mn(II) to MnO$_{2(s)}$, the oxidation reaction is too slow under the pH of most natural waters, and thus a long detention time is required (Griffin, 1960; Wong, 1984). Likewise, Phatai et al. (2010) showed that the maximum Mn(II) removal efficiency using aeration alone was 40% even at pH 9.0. Under an elevated pH of 11.0 only 70% of Mn(II) could be oxidized by aeration (Kaya et al., 2005). Therefore, previous results indicate that aeration alone cannot satisfactorily oxidize Mn(II) even under high pH values (Azizi et al., 2013; Phatai et al., 2010). Another disadvantage related to this process is the high capital cost incurred due to the large-size retention tank that would be required.

Chlorination. Chlorine is a stronger oxidizing agent than oxygen which has been used for many years as a water treatment chemical because it is economical, readily available, easy to feed and can be used both for the oxidation of inorganic contaminants and as a disinfectant. There are two options for dosing chlorine, as a gas forced into water under pressure or as a solution of calcium hypochlorite or sodium hypochlorite pumped into water (Sommerfeld, 1999). The end-product is however the same: a mixture of hypochlorous acid (HOCl) and hypochlorite ion (OCl$^-$) which proportion is pH-dependent.

The stoichiometric amounts of chlorine required for oxidizing 1mg/L of Fe(II) and Mn(II) are 0.64 and 1.3 mg/L, respectively. However, in reality, the required chlorine has been found to be much higher than the stoichiometric amount owing to the additional chlorine demand caused by organic matter, ammonia and other reduced compounds in water such as hydrogen sulfide (Sommerfeld, 1999). Knocke et al. (1990a) found that Fe(II) and Mn(II) oxidation by chlorine was impacted by several factors including water pH, temperature, chlorine dosage and retention time. They revealed that the reaction rate between Fe(II) and chlorine was rapid even under low pH and temperature. Typically, at pH 5.0, complete oxidation of Fe(II) was observed within 10-15 seconds. Even though a considerable reduction in Fe(II) oxidation rate was noticed by decreasing temperature, effective Fe(II) oxidation was observed within 15 seconds (at pH 6.0) or 90 seconds (at pH 5.0) at 2°C (Knocke et al., 1990a).

The oxidation rate of Mn(II) by chlorine is highly dependent on pH. It has been indicated that even under a chlorine dosage 4 times greater than the stoichiometric value, a minimum of three hours contact time was necessary at pH 7.0 to oxidize 30% of Mn(II) in water (Knocke et al., 1990a). However, when the pH was increased to 9.0, Mn(II) was effectively controlled within 1 hour to below 0.05 mg/L. Also, it has been shown that the reduction of temperature from 25°C to 14°C declined the reaction rate significantly while increasing the reaction time by three or four times could not compensate this reduction (Knocke et al., 1990a). Consequently, direct oxidation of Mn(II) via chlorination is often unpractical because of the too slow oxidation rate even under high chlorine dosage (Griffin, 1960; Knocke et al., 1990a; Allard et al., 2013). In addition, the resultant oxidized Mn(II) may form negatively charged colloidal particles that can be difficult to remove by granular media filtration (Griffin, 1960; Wong, 1984). Nevertheless, chlorine is one of the most popular oxidant used for Mn removal applications in North America where it is combined with catalytic filters (e.g. greensand) to achieve removal trough adsorption-oxidation (cf. Eqs. 1.2 and 1.3). This treatment strategy will be further discussed in section 1.3.2

Chlorine dioxide treatment. ClO_2 is a powerful oxidant and disinfectant. It is being used for improving the removal of compounds that cause taste and odor, for the oxidation of iron and manganese and the inactivation of chlorine-resistant pathogens such as *Giardia*. Unlike chlorine, it does not produce organic disinfection by products (DBPs) (Gopal et al., 2007), although it generates chlorite and chlorate which are also regulated DBPs.

ClO_2 reacts quickly with the soluble forms of iron and manganese at pH ranges more than 7.0. The reaction rate increased when pH, temperature and initial Mn(II) concentration were increased (Vanbenschoten et al., 1992) and decreased in the presence of natural organic matter (NOM) (Gregory and Carlson, 2003). For Fe(II) and Mn(II) oxidation, the theoretical stoichiometric requirements of ClO_2 are 0.24 mg ClO_2/mg Fe(II) and 2.45 mg ClO_2/mg Mn(II). However, laboratory results showed that at least twice the theoretical value would be necessary for effective soluble manganese removal (Knocke et al., 1990a). This oxidant has been shown to be the most effective, more than $KMnO_4$ and O_3, for removing low initial Mn(II) concentrations (0.06 and 0.2 mg/L) in the presence of NOM (3.4 mg/L). It could consistently produce final Mn(II) < 0.01 mg/L within 1.5-3 minutes in various initial Mn(II) concentrations while the occurrence of undesirable MnO_4^- was not observed (Gregory and Carlson, 2003). Although ClO_2 is an effective oxidant for iron and manganese removal, its application has been limited due to the production of undesired by-products, i.e. chlorite and chlorate (Gopal et al., 2007). The USEPA (2004) regulated the combined residual of ClO_2, chlorite and chlorate in treated water at 1.0 mg/L. Therefore, the formation of chlorite often limits the maximum applicable ClO_2 dosage to 1.4 to 2.0 mg ClO_2/L, assuming that 50-70% of ClO_2 is converted into chlorite. Hence, with this high stoichiometric requirement, application of ClO_2 is only well suited for waters with very low oxidant demand.

In the province of Quebec (Canada), chlorine dioxide has been successfully used during the 1990s in settled waters to oxidize manganese in surface water applications. Even under very low water temperature (1°C), manganese oxidation was achieved by chlorine dioxide in the water column above the filter (contact time of approx. 20 min in winter). This practice was progressively abandoned due to the significant replacement costs of ClO_2 generators and concerns related to chlorite as a DBP.

Ozonation. O_3 is a powerful oxidant that is being employed extensively as a strong disinfectant owing to its numerous advantages over chlorine. Moreover, ozonation is efficient in removing taste and odor from water (Camel and Bermond, 1998).

The theoretical stoichiometric dose of O_3 for oxidation of Fe(II) and Mn(II) is 0.88 mg O_3/mg Mn(II) and 0.43 mg O_3/mg Fe(II). The second-order rate constant for the direct reaction of Mn(II) with O_3 is extremely fast as it was estimated as 1.5×10^3 M^{-1} s^{-1} (Jacobsen et al., 1998). However, in the presence of moderate concentrations of organic matter like humic substances, two to five

times as much O_3 dose was required (Knocke et al., 1990a; Reckhow et al., 1991). This was due to competition between Mn(II) and organic substances for the oxidant. Gregory and Carlson (2003) also revealed the importance of initial Mn(II) concentration, especially, in the presence of NOM. Accordingly, the oxidation kinetics for low Mn(II) concentrations (0.06 and 0.2 mg/L) were significantly slower than for high concentrations (1 mg/L), which resulted in soluble Mn(II) residual > 0.02 mg/L. The formation of MnO_4^- was observed in many cases in low Mn(II) source waters. The MnO_4^- formation was attributed to the higher required O_3 dose under elevated NOM content and the complexation of Mn(II) by NOM (Gregory and Carlson, 2003; Reckhow et al., 1991; Gregory and Carlson, 2001). However, a mechanistic study by Reisz et al. (2008) revealed that the MnO_4^- formation is most likely caused by the presence of Fe(II) in water rather than complexation of Mn(II) by NOM. MnO_4^- is an undesirable product in treated water since it is a Mn(II) species with a relatively long half-life and pink color, which may subsequently be slowly reduced to $MnO_2(s)$ in the distribution system and may contribute to water quality complaints due to turbidity and discoloration of water (Gregory and Carlson, 2001). At high Mn(II) concentrations, the formation of MnO_4^- is reduced as the theoretical oxidant dosage required is 2.2 mg O_3/mg Mn(II). In addition, under high initial Mn(II) concentrations, oxidized Mn(IV) progressively formed during the reaction may react with Mn(II) through the adsorption/oxidation pathway. Therefore, Mn(II) control via ozonation can be especially difficult to do in waters with low Mn(II) concentrations (e.g. < 100 µg/L) and/or in the presence of Fe(II).

Iron is rapidly oxidized by O_3 to an insoluble form in the absence of organic matter (Reckhow et al., 1991). The second-order kinetic rate constant has been estimated as 8.2 x 10^5 M^{-1} s^{-1} (Logager et al., 1992) which makes the reaction controlled by mass-transfer conditions. However, retardation in iron removal rate with increasing organic content has been shown (Reckhow et al., 1991). In fact, these substances inhibit oxidation of Fe(II) by O_3 by either complex formation with the Fe(II) or providing a competing oxidant demand. El Araby et al. (2009) showed that oxidation of Fe(II) was faster than Mn(II) while under low O_3 dose only iron removal was achieved. Although over ozonation did not affect iron removal, manganese removal efficiency was decreased because of MnO_4^- formation (Sung et al., 2015). In addition, the removal of Fe(II) and Mn(II) via ozonation is pH, temperature and alkalinity dependent, especially, for manganese (El Araby et al., 2009). As expected, increasing the temperature from 5 to 25°C slowed down the kinetic of iron and manganese oxidation by O_3 (El Araby et al., 2009). The removal performance was increased by

increasing the alkalinity, particularly for manganese, owing to the higher stability of dissolved O_3 in the presence of radical scavengers such as bicarbonate and carbonate.

In addition to the abovementioned defects, oxidation by O_3 is energy intensive and has the potential to produce bromate, a suspected carcinogen (Cavanagh et al., 1992). Moreover, O_3 is an expensive oxidant and requires more capital expenditures for its application than other oxidants. Susceptibility to the degradation of polymeric membranes due to its oxidative attack is another restriction encountered in ozonation (Montgomery Watson Harza (MWH), 2005) which limits its use prior to polymeric membrane filtration. In summary, ozonation is rarely selected for the oxidation of manganese in water, unless other treatment objectives (e.g. oxidation of geosmine) justify its application within the overall treatment strategy.

Potassium permanganate treatment. $KMnO_4$ is a strong oxidant that has been traditionally used for Fe(II) and Mn(II) oxidation. Theoretical stoichiometric dose of $KMnO_4$ for oxidizing 1 mg/L Fe(II) and Mn(II) is 0.94 and 1.92 mg/L, respectively. However, the presence of significant amount of dissolved organic matter will remarkably increase the oxidant demand to achieve effective Fe(II) and Mn(II) oxidation (Carlson and Knocke, 1999). In addition, the presence of organic matter retards the oxidation rate of these species (Carlson and Knocke, 1999; Vercellotti, 1988). These results emphasize the negative effect related to the formation of Fe(II) and Mn(II) complexes with organic substances found in water (Carlson and Knocke, 1999; Theis and Singer, 1974). For instance, the second order kinetic rate constant for oxidation of Mn(II) by MnO_4^- in water with < 0.5 mg/L and 3.3 mg/L dissolved organic matter is $10^{4.24}$ M^{-1} s^{-1} (Vanbenschoten et al., 1992) and $10^{1.90}$ M^{-1} s^{-1} (Carlson and Knocke, 1999), respectively. In addition, the rate of Fe(II) and Mn(II) oxidation by $KMnO_4$ is also influenced by pH, temperature and initial concentration of these species (Knocke et al., 1991; Vanbenschoten et al., 1992; Vercellotti, 1988) while the oxidation rate was increased by increasing these parameters. Van Benschoten et al. (1992) revealed that manganese oxidation at pH values between 6.0 and 8.0 occurred in less than 20 seconds at 25°C; however, this reaction was incomplete after 30 seconds at 7°C and pH 7.0. Gregory and Carlson (2003) found that the initial concentration of Mn(II) dramatically impacted the required contact time for oxidation. Accordingly, for an initial Mn(II) concentration of 0.06 mg/L, 20 min contact time was needed while the required contact time reduced to 3 min for an initial Mn(II) concentration of 1 mg/L (T = 9°C, pH = 7 and total organic carbon (TOC) = 3.4 mg/L).

Unlike chlorine, the reaction of $KMnO_4$ with organic compounds will not generate toxic trihalomethane (THM), but may even slightly reduce them by oxidizing certain THM precursors (Ficek and Boll, 1980). Other advantages of using this oxidant include the oxidation of compounds causing taste and odor (Ficek and Boll, 1980). The main disadvantages are related to the cost (which is higher than for bleach solution) and the formation of additional manganese as an oxidant by-product. Up to recently, the later was not perceived negatively but this consideration is slowly changing as manganese health-based regulations are being proposed (Health Canada, 2016) or put in place (MDH, 2012). Therefore, it becomes important to count on an efficient post-treatment of coagulation-granular media filtration or low-pressure membranes to remove the manganese oxides. In addition, if manganese level fluctuates, adjusting the $KMnO_4$ dose is critical and overdosing causes adverse effects (Azizi et al., 2013; Roccaro et al., 2007). Thus, the dosages must be monitored and optimized regularly. In summary, MnO_4^- is one of the most common oxidation strategy employed in the water industry for manganese control as it has been shown to be effective, even for the treatment of groundwaters with elevated manganese concentrations. As for any oxidant, its application conditions are highly site-specific and should account for the formation of the manganese oxides which must be adequately removed once formed.

Hydrogen peroxide treatment. H_2O_2 is a weak oxidant for Fe(II) and Mn(II) removal (Sommerfeld, 1999). Potgieter et al. (2005) revealed that oxidation by H_2O_2 yields unsatisfactory Fe(II) removal in water containing organic carbon and it shows no significant oxidative effect on Mn(II).

Theoretical reaction stoichiometry for oxidation of Fe(II) and Mn(II) with common oxidants are presented in Table 2.1.

As stated earlier, oxidation of Mn(II) involves solution-phase oxidation, adsorption and surface oxidation. Van Benschoten et al. (1992) developed a model to predict Mn(II) oxidation rate by ClO_2 and $KMnO_4$. They concluded that for these reactive oxidants, adsorption of Mn(II) to the $MnO_{2(s)}$ surface is the rate-limiting reaction since direct solution-phase oxidation is kinetically favored over surface oxidation except at low temperature and/or low pH when the solution-phase oxidation rate is expected to be slow (e.g., pH = 5.5, T = < 14°C). Considering this fact, Mn(II) removal by reactive oxidants is dependent upon oxidant addition at alkaline pH with a sufficient reaction time to allow oxidation of Mn(II) to $MnO_2(s)$. Subsequently, $MnO_{2(s)}$ must be removed by

a standard solid-liquid separation technique. In contrast, for weaker oxidants such as molecular oxygen and chlorine, the adsorption step was found to be faster than the solution-phase oxidation reaction (Casale et al., 2002). Thus Mn(II) removal successfully occurs in filters where oxide-coated media provides a large surface area for adsorption and evidently enhances the rate of surface oxidation of adsorbed manganese.

Table 2.1. Theoretical reaction stoichiometry for oxidation of Fe(II) and Mn(II) (Sommerfeld, 1999).

Oxidant	Oxidation reactions	Stoichiometric ratio (mg oxidant:mg Mn/Fe)
O_2 (aq)	$Mn^{2+} + 1/2O_2 + H_2O \Longrightarrow MnO_{2(s)} + 2H^+$	0.29:1
	$2Fe^{2+} + 1/2O_2 + 5H_2O \Longrightarrow 2Fe(OH)_{3(s)} + 4H^+$	0.14:1
HOCl	$Mn^{2+} + HOCl + H_2O \Longrightarrow MnO_{2(s)} + Cl^- + 3H^+$	1.30:1
	$2Fe^{2+} + HOCl + 5H_2O \Longrightarrow 2Fe(OH)_{3(s)} + Cl^- + 5H^+$	0.64:1
ClO_2	$Mn^{2+} + 2ClO_2 + 2H_2O \Longrightarrow MnO_{2(s)} + 2ClO_2^- + 4H^+$	2.45:1
	$5Fe^{2+} + ClO_2 + 13H_2O \Longrightarrow 5Fe(OH)_{3(s)} + Cl^- + 11H^+$	0.24:1
$KMnO_4$	$3Mn^{2+} + 2MnO_4^- + 2H_2O \Longrightarrow 5MnO_{2(s)} + 4H^+$	1.92:1
	$3Fe^{2+} + MnO_4^- + 7H_2O \Longrightarrow 3Fe(OH)_{3(s)} + MnO_{2(s)} + 5H^+$	0.94:1
O_3	$Mn^{2+} + O_3 + H_2O \Longrightarrow MnO_{2(s)} + O_2 + 2H^+$	0.88:1
	$2Fe^{2+} + O_3 + 5H_2O \Longrightarrow 2Fe(OH)_{3(s)} + O_2 + 4H^+$	0.43:1

2.3.1.2   Removal of oxidized particles by conventional treatment

Once Fe(II) and Mn(II) have been converted to particulate forms via oxidation, the particles must be removed by a solid-liquid separation technique. Commonly, utilities exploit the conventional treatment process consisting of coagulation, flocculation, clarification and filtration to remove particles (Potgieter et al., 2005; Zogo et al., 2011). Ferric sulfate, ferric chloride, aluminum sulfate (alum) and pre-hydrolyzed aluminum salts are the common coagulants used in water treatment plants. However, for utilities whose goal is to remove iron and manganese from water for drinking purposes, the application of ferric sulfate and ferric chloride at low pH (4.5- 5.5) for enhanced coagulation may lead to challenging conditions for manganese oxidation. Alum application is typically also optimal in a pH range of 5.8-6.3 which may slow down manganese oxidation kinetic (Knocke et al., 2010). Since oxidation of Mn(II) with strong oxidants may lead to the formation of colloidal solid (Morgan and Stumm, 1964; Tobiason et al., 2016), it may not be effictively removed through direct filtration without an optimized coagulation (Tobiason et al., 2016; Carlson et al.,

1997). The negative charge on the colloidal manganese oxides produce repulsion forces with the filter media which may prevent particle adhesion to the media.

In order to resolve the conflicting issue of NOM removal by coagulation (improved at lower pH) and the oxidation of manganese (improved at higher pH), many utilities will raise the pH of settled waters in the range of 6.5-7.0 and add chlorine before filtration in order to improve the filtration performance. Carlson et al. (1997) demonstrated that chlorine injection on top of the filter media, consisting of significant $MnO_{x(s)}$, improved manganese removal significantly. In this process the filter media would function to remove Mn(II) via surface adsorption followed by surface-catalyzed Mn(II) oxidation by chlorine (Knocke et al., 1990b). However, raising the pH too high before filtration (e.g. 8.0) may negatively impact manganese removal since elevated pH promotes solution phase oxidation of Mn(II) and generates colloidal manganese oxides which are hardly captured through filtration (Hargette and Knocke, 2001). Another treatment strategy has recently been proposed by Knocke et al. (2010). The treatment involves the construction of post-contactor (i.e. after the granular media filters) which are dedicated for the Mn(II) removal though sorption-oxidation on $MnO_{x(s)}$ filters (e.g. pyrolucite). The two main advantages of this techniques are (i) that the performance of the conventional coagulation/settling/filtration performance can be optimized for NOM/turbidity removal, (ii) chlorine addition in settled water can be abandoned which reduces THM/AHA formation and (iii) the operation of the post-contactor can be done at very high filtration rate (up to 49 m/h) since these filters do not remove particulate matter. Correspondingly, a recent study demonstrated a successful Mn(II) removal in full-scale plant at HLR of 25 m/h using second-stage contactors (Bazilio et al., 2016).

Mn(II) removal by sorption and subsequent autocatalytic oxidation is discussed in more details in the following section. Finally, membrane filtration as an alternative to traditional media filtration is being used more frequently in water treatment plants. More specific discussion regarding this process is presented in section 1.4.

2.3.2 Manganese removal by sorption and oxidation within filters

As discussed earlier, another method for manganese removal from aqueous solution is the adsorption of Mn(II) onto the $MnO_{x(s)}$ surface. Morgan and Stumm (1964) investigated the surface properties of hydrous $MnO_{2(s)}$, which has high specific surface area of 300 m^2/g of $MnO_{2(s)}$, and found that this oxide has a high affinity for Mn(II) adsorption, especially at alkaline pH values

above the zero point of charge. The point of zero charge of $MnO_{2(s)}$ lies between pH 1.5 and 4.6 (Healy et al., 1966). Mn(II) adsorption mechanism by $MnO_{x(s)}$ has been interpreted as ion exchange and/or surface complex formation where hydrogen ions are released while Mn(II) is adsorbed (Morgan and Stumm, 1964). Likewise, a study conducted by Hu et al. (2004) suggested that ion exchange might be the principal mechanism for Mn(II) adsorption onto $MnO_{x(s)}$.

The $MnO_{2(s)}$ can be employed as a coating on the surface of the filtration media (coated sand, anthracite and gravel) or as a natural ore (e.g., pyrolucite). Microscopic studies on manganese oxide coated media indicated that this coating has the capability to remove both particulate and dissolved inorganic species (Merkle et al., 1996). In addition, a strong adsorption capacity of $MnO_{x(s)}$ for other transition and heavy metal ions such as iron (He et al., 2010), copper (Lee et al., 2004) and arsenic (Chang et al., 2012) has been reported. In this process, $MnO_{x(s)}$ initially provides the sorption sites for Mn(II) and subsequently catalyzes the oxidation of adsorbed Mn(II) by free chlorine (autocatalytic oxidation) (Knocke et al., 1990b). This phenomenon has been termed the "NGE" process. Therefore, the media plays a dual function in NGE process, and thus, allowing two modes of operation to remove manganese: IR and CR. The regeneration is necessary to restore the adsorption capacity of the media (Knocke et al., 1990b).

IR process. The IR process is best suited for waters containing soluble Mn(II) concentrations of $\leq$ 0.2 mg/L (Knocke et al., 1990b) with low concentrations of iron. In this operation mode, the filter media adsorbs Mn(II) in the absence of a strong oxidant. After treating a specific quantity of water, since the adsorbed Mn(II) is hardly oxidized by the oxide coating (there is no evidence of auto-catalytic oxidation) at near neutral pH values (Knocke et al., 1990b), the adsorption capacity of the media is consumed (exhaustion of the filter media) and a regeneration is required. In order to regenerate the filter media, the appropriate concentration of $KMnO_4$ or chlorine must be applied whether in up-flow or down-flow mode (Knocke et al., 1990b).

Therefore, sorption of Mn(II) ions onto the oxide coated filter media appears to be the only mechanism responsible for Mn(II) removal (Knocke et al., 1990b), which can be illustrated in the following Eq. (1.4) that shows the ion exchange mechanism (Tiwari et al., 2007):

$$\equiv S-OH + Mn^{2+} \Longrightarrow \equiv S-O-Mn^+ + H^+ \tag{1.4}$$

where S is the manganese atom in the oxide surface.

Other restrictions facing to this type of operation are the recommended pH of water, which must be higher than 7.0, and the presence of a significant manganese oxide coating level on the filter media. Increasing the pH, especially, for utilities applying alum coagulation may cause problems due to elevated aluminum concentration in the treated water (Zogo et al., 2011). In addition, other drawbacks of this process are the production of a large volume of waste water during regeneration, which may contain high levels of oxidant, and the 15 to 30 minutes ripening period following filter re-start (to reduce the possible release of $MnO_{x(s)}$ into finished water) (Knocke et al., 1990b). However, IR might be an appropriate option for treating water supplies containing high levels of NOM (in order to prevent the possible formation of DBPs). It is also simpler to operate as no continuous chemical injection is required. This characteristic has made this treatment a common option for the treatment of iron/manganese in residential applications.

CR process. The CR process is well suited to treat waters with high levels of iron and manganese. The CR mode involves feeding an oxidant to raw water just prior to filtration. The Quebec Design Guidance Manual states that this configuration can treat up to 10, 5 and 2 mg/L of iron, manganese and hydrogen sulfide, respectively (Ministère du développement durable de l'environnement et lutte contre les changements climatiques (MDDELCC), 2016). However, for iron and manganese concentrations above 5 and 1 mg/L, respectively, providing a settler before filtration is recommended. Free chlorine is the ideal oxidant for CR process since it only promotes oxidation of adsorbed Mn(II) within the oxide coated media while stronger oxidants, such as $KMnO_4$, ClO_2 and O_3, promote solution phase oxidation of Mn(II) leading to generation of colloidal $MnO_{2(s)}$, which may not be removed through filtration. Moreover, free chlorine is a cheap and readily available oxidant. Thus, the filter media would function to remove Mn(II) via surface adsorption followed by surface-catalyzed Mn(II) oxidation by chlorine, as follows (Coffey et al., 1993):

$$Mn^{2+} + MnO(OH)_{2(s)} \Leftrightarrow MnO_2MnO_{(s)} + 2H^+ \qquad \text{(reversible adsorption)} \qquad (1.5)$$

$$MnO_2MnO_{(s)} + HOCl \Rightarrow 2MnO_2(s) + H^+ + Cl^- \qquad \text{(autocatalytic oxidation)} \qquad (1.6)$$

Thus, the maintenance of the available sorption site is an important issue. Accordingly, in order to achieve a continuous regeneration, free chlorine concentration should be adjusted such that a free chlorine residual of 0.5 - 1.0 mg/L is maintained in the effluent (Knocke et al., 1990b). In this process, the mechanism of iron removal mainly includes solution oxidation of Fe(II) by chlorine followed by removal of particulate $Fe(OH)_{3(s)}$ through the filter bed (traditional filtration).

2.3.2.1 Filter media for NGE process

Effective Mn(II) removal does not take place until a manganese oxide coating develops on the filter media (Griffin, 1960; Eley and Nicholson, 1993). It may take several weeks or even months to naturally develop this coating on the filter media (Azizi et al., 2013). The development period is mainly related to the oxidant concentration, pH and soluble Mn(II) level in the water supply (Knocke et al., 1990b). Another issue is associated with the stability and durability of this coating as it can be partially washed out during backwash (Azizi et al., 2013). The following sections presents the most common filtration media used in the NGE process.

Manganese greensand. Commercial manganese greensand is a well-known purple-black granular filter media having been used to remove iron, manganese and hydrogen sulfide from groundwater since the 1950s. The product was mined in New Jersey and sold by Inverness® which still supplies a similar product sold as the GreenSandPlus™. It is made from glauconite mineral (greensand) processed with $KMnO_4$ to produce a thin layer of $MnO_{2(s)}$ on the granules. According to the supplier, this media has typically an effective size of 0.3-0.35 mm, uniformity coefficient of less than 1.6, MnO_2 content of 25-45% and is commonly used at superficial flow rates of 7 to 12 m/h (3 to 5 gpm/ft^2) (Sommerfeld, 1999). The filter efficiency is severely reduced at pH values less than 6.8 (Barlokova and Ilavsky, 2009). In addition, organic substances, oils and hydrogen sulfide can adversely affect the process performance. Rapid media exhaustion was observed even at moderate levels of iron and manganese (0.4 mg/L of each metal) and pH 7.2 (Barlokova and Ilavsky, 2009).

Over the last decades, many other manganese-coated media were made commercially available (e.g. Katalox-Lite, MTM). These media are designed to have a lower density than greensand (e.g. MTM uses a plastic core while Katalox uses zeolite like Greensand but claims higher than 10% MnO_2 content).

Birm. Birm (Burgess Iron Removal Method) is another commercial manganese coated sand (aluminum silicate) having the capacity to oxidize iron. It is typically applied for household water treatment, but has been also used in municipal water treatment plants. According to the supplier, this media has typically an effective size of 0.48 mm, specific gravity of 2.0 and MnO_2 content of 25-45%. Birm is known as a catalytic media that can catalyze oxidation of iron by oxygen. In order to achieve an effective process, the water to be treated should have a pH of 6.8-9.0. It might be also

used for manganese removal, but in this case the pH of water should be preferably above 8.0. In this process, aeration is required for treating groundwater having low dissolved oxygen (Osmo Sistemi Company website). Lee et al. (2009) showed that although chlorination greatly increase the removal efficiency of laboratory prepared manganese coated sand, it does not have a significant effect on the removal capacity of Birm. Barlokova and Ilavsky (2009) revealed that a regeneration is necessary to restore media activity for manganese removal. In addition, the water to be treated must not contain oils (≈ 0 mg/L), sulfates (≈ 0 mg/L) and high level of organic substances (> 5 mg/L) and free chlorine (> 0.5 mg/L) (Barlokova and Ilavsky, 2009).

Pyrolucite. Pyrolucite or pyrolusite is the common name of black MnO_2 mineral consisting of 70 to 85% MnO_2 by weight, as is shown in Figure 2.2. The crushed and angular ore provides extensive surface sites available for iron and manganese removal. Thus, there is no need to develop a manganese oxide coating in order to remove manganese using this media. However, conditioning the virgin filter media with $KMnO_4$ or NaOCl solution is required to activate the sorption sites prior to filtration (Zuravnsky, 2006). Effective manganese removal can be achieved even at a high HLR of 24 to 29 m/h (10 to 12 gpm/ft^2). Typically, sufficient concentration of chlorine is supplied to keep the pyrolucite continuously regenerated (Osmo Sistemi Company website). Pyrolucite is a hard media with a high specific gravity of about 4.0. Thus, a high backwash rate is required to fluidize the bed at least 30%, which is a disadvantage of this media as it produces more wastewater during backwash than a lighter media such as Birm or greensand.

It has been shown that pyrolucite media has a larger capacity for Mn(II) removal than either manganese oxide coated gravel or torpedo sand (Knocke, et al. 2010; Zuravnsky, 2006). This can be attributed to both higher specific concentration of $MnO_{2(s)}$ on the media and larger specific surface area of pyrolucite, which provide high amount of available active sites on its surface. The pyrolucite is commercialized under various names (e.g., MangOX^{TM}, Pyrolox$^{®}$, Filox^{TM}, etc.).

Birnessite. Bruins et al. (2015b) revealed that the predominant component in $MnO_{x(s)}$ coatings extracted from conventional aeration-filtration groundwater treatment plants is Birnessite which provides a very effective manganese removal performance. Birnessite is a poorly crystalline structure of manganese oxides. The average valence number of manganese in Birnessite ranges from +3.5 to +3.9. This compound is extremely suitable for manganese removal because of its layered structure, which may readily undergo oxidation-reduction and cation-exchange reactions

(Post, 1999). This resulted in a very good adsorption and subsequent autocatalytic oxidation properties (Bruins et al., 2015b). However, noteworthy is the formation of this coating is initiated by bacterial activity (Bruins et al., 2015a) which may last several weeks to more than a year (Bruins et al., 2015b). Birnessite is currently not available commercially. It must be generated on-site biologically. It is the most common approach used in Europe in order to remove manganese from groundwaters as it does not require the use of a strong oxidant (which application is avoided in many jurisdictions). The Mangazur® process commercialized by Degremont® is an example of such application.

Figure 2.2. Pyrolucite ore.

Iron-based media. Rather than manganese oxide, iron oxide coated sand (IOCS) was shown to be a potential adsorbent for the removal of iron (Sharma et al., 1999) and manganese (Buamah et al., 2008). Likewise, Buamah et al. (2009) revealed that IOCS provided the highest adsorption capacity after manganese sand. In their study the adsorption capacity of six different filtration media, namely, manganese sand, IOCS, manganese green sand, laterite, iron ore and virgin sand, was investigated. This shows the potential application of naturally coated iron oxide in water treatment plants as a cheap media for iron and manganese removal. However, the application of iron-based filters is currently mostly recommended for arsenic removal.

Generally, the capacity of filter media for Mn(II) removal is a function of pH, NOM, presence of free chlorine and surface $MnO_{2(s)}$ coating level (Knocke et al., 1990b). In addition, HLR, temperature and initial Mn(II) concentration can further impact the process performance, as well. However, their effects have not been fully investigated. Coming sections detail the impact of these parameters on manganese uptake capacity of the filter media. In conclusion, it would be favorable to artificially create the manganese oxide coating on the surface of a filter media (sand, anthracite

or gravel). In addition, certain manufacturers supply commercial manganese oxide coated media (such as manganese greensand and Birm). Furthermore, application of natural manganese dioxide ore (e.g., pyrolucite) as a great source of MnO_2, is becoming more common recently.

2.3.2.2 Effect of surface manganese oxide coating level on manganese removal

Although manganese oxide coating changes physical appearance and color of a filter media, it does not alter the size, shape and density of the media and, hence, the hydraulic behavior of the filter during filtration or backwashing (Hargette and Knocke, 2001). The specific concentration of manganese oxide coating on the media (mg Mn/g media) has a significant impact on the Mn(II) uptake capacity (Islam et al., 2010). The Mn(II) adsorption breakthrough curves for four media having different manganese oxide coating levels were depicted in Figure 2.3 (Knocke et al., 1990b). From this figure, the media with the greatest manganese coating level (42 mg/g media) possessed a considerably greater Mn(II) uptake capacity. In addition, it has been shown that a lower Mn(II) uptake capacity under lower pH conditions can be compensated by a larger amount of coating on the media (Knocke et al., 1990b). Thus, water with a pH value of < 7.0 could be effectively treated applying media with high coating levels. The importance of coating level is more significant when the water to be treated contains greater amounts of soluble Mn(II).

According to the above mentioned discussion, the Mn(II) uptake capability of media generally increase with increasing manganese oxide coating level. However, some instances revealed that media containing higher manganese oxide coating level do not necessarily exhibit greater Mn(II) uptake capacity (Islam et al., 2010). One possibility is related to the oxidation state of the manganese oxide coating since it varies between $MnOOH_{(s)}$ (Mn(III)) and $MnO_{2(s)}$ (Mn(IV)) (Cerrato et al., 2010; Cerrato et al., 2011). Highly oxidized forms of $MnO_{x(s)}$ ($MnO_{1.8(s)} - MnO_{2(s)}$) coating have increased Mn(II) removal capacity (Knocke et al., 1990b). The other possibility is, as the $MnO_{x(s)}$ coating level increases, some of the coatings are deep enough and supports the hypothesis that only readily accessible adsorption sites contribute to the NGE process (Islam et al., 2010).
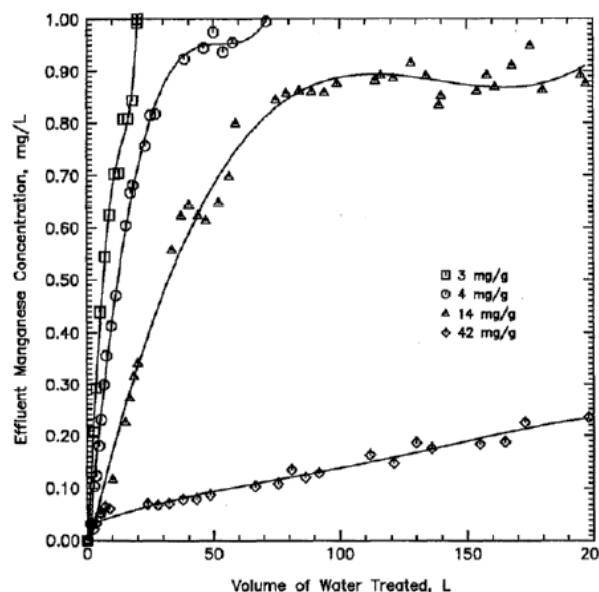
Figure 2.3. Effect of surface oxide coating level on Mn(II) uptake capacity of media. pH = 6-6.2, Mn(II)0 = 1.0 mg/L and in the absence of free chlorine (Knocke et al., 1990b).

2.3.2.3 Effect of pH on manganese removal

Morgan and Stumm (1964) first demonstrated that the adsorption of Mn(II) onto $MnO_{2(s)}$ is a highly pH-dependent process. As can be seen from Figure 2.4, the adsorption capacity of $MnO_{2(s)}$ is substantially reduced at pH below 7.
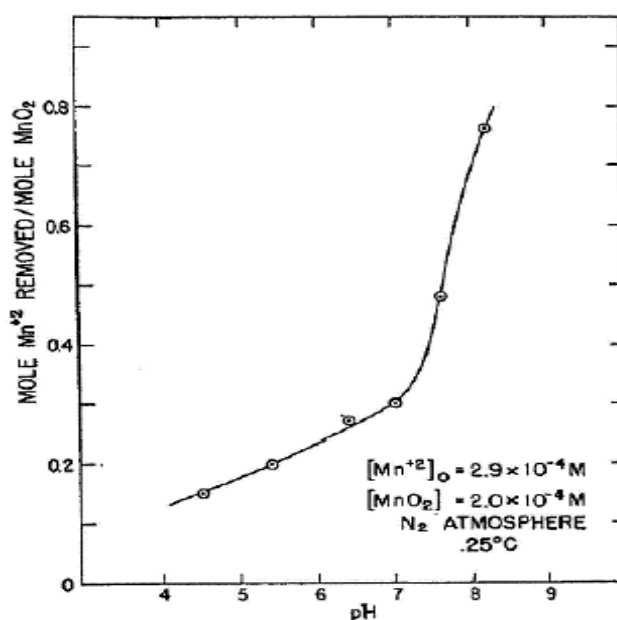
Figure 2.4. Influence of pH on the sorption of Mn(II) onto $MnO_2(s)$ (Morgan and Stumm, 1964).

Later, the same results were obtained by Knock et al. (1990b), as illustrated in Figure 2.5. This was attributed to the changes in the surface charge of the $MnO_{x(s)}$ due to pH changes. As the solution pH increases, the oxide surface charge become increasingly more negative (Knocke et al., 1990b; Hu et al., 2004). This lead to both an increase in Mn(II) adsorption rate as well as an increase in the adsorption capacity of manganese oxide due to the presence of more potential available sites for Mn(II) uptake (Knocke et al., 1990b). In addition, at low pH values H^+ ions may compete with metal ions for the $MnO_{x(s)}$ adsorption sites and render a decreased removal of Mn(II) (Lee et al., 2004). Desorption of Mn(II) from the $MnO_{x(s)}$ coating is more prevalent under lower pH conditions. Likewise, similar results have been found for the effect of pH in the CR process with the addition of free chlorine (Tiwari et al., 2007; Lee et al., 2009; Cerrato et al., 2011).
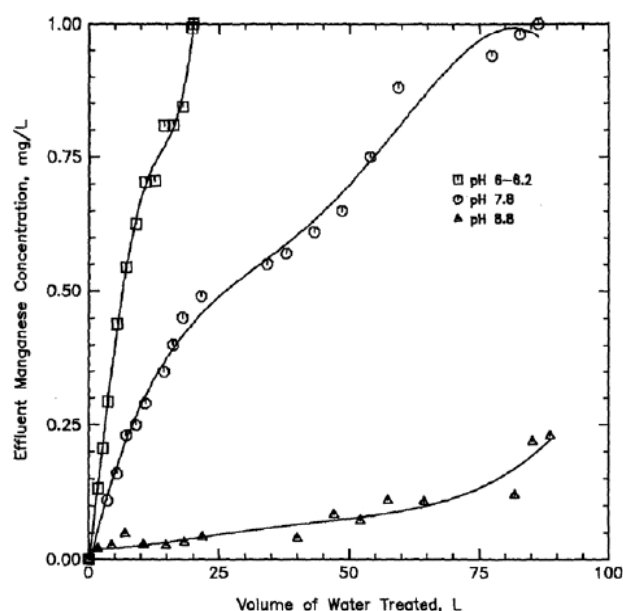
Figure 2.5. Effect of pH on Mn(II) uptake capacity of media: manganese oxide coating = 3 mg Mn/g media , Mn(II)0 = 1.0 mg/L and in the absence of free chlorine (Knocke et al., 1990b)**.**

Although higher pH value increases the adsorption capacity of $MnO_{x(s)}$, it might reduce the overall process performance in the presence of free chlorine. Hargette and Knocke (2001) revealed higher manganese removal at pH 6.0 (99.5%) than pH 7.3 (98.5%). This is attributed to the higher amount of solution phase particulate manganese formation under higher pH, which was hardly removed by filtration. Consequently, around 6% and 1.5% of Mn(II) was oxidized by chlorine prior to filtration at pH 7.3 and 6.0, respectively. In conclusion, it seems that further investigations must be conducted

in order to verify the effect of pH for a specific application, especially if very low manganese concentration (e.g. < 20 µg/L) is targeted in the effluent.

2.3.2.4 Effect of free chlorine on manganese removal

As discussed earlier, continuous feed of free chlorine can greatly enhance Mn(II) removal via $MnO_{x(s)}$ coated media. Figure 2.6 illustrates the results obtained by Knocke et al. (1990b) indicating the significance of free chlorine on Mn(II) uptake capacity of $MnO_{x(s)}$ coated filter media. From this figure, substantial column exhaustion in the presence of chlorine would not occur even under mildly acidic pH condition. Free chlorine also minimizes the potential for desorption of Mn(II) from the $MnO_{x(s)}$ surface under mildly acidic pH condition (Cerrato et al., 2011). Increasing the dosage of free chlorine under low pH values could significantly enhance Mn(II) removal performance (Tiwari et al., 2007). The role of free chlorine in increasing manganese uptake is related to the oxidation of previously adsorbed Mn(II) on $MnO_{x(s)}$ which also serves as a catalyst for this reaction (Lee et al., 2009). This allows keeping the number of $MnO_{x(s)}$ adsorption sites and the applicability of coated media, because the generated Mn_3O_4 on the $MnO_{2(s)}$ surface at the early stages of the process (Aguiar et al., 2013) does not have a high propensity for Mn(II) adsorption. Moreover, oxidation of adsorbed Mn(II) reduces its concentration on the media resulting in high Mn(II) gradient between the media and bulk solution, which increases mass transfer rate, and thus, Mn(II) removal rate (Knocke et al., 1990b).

It is worth noting that, although free chlorine oxidizes a significant portion of adsorbed Mn(II), a fraction of it may remain not oxidized (Knocke et al., 1990b). This is imaginable since the adsorption reaction (Eq. (1.5)) is very fast while the subsequent autocatalytic oxidation of adsorbed Mn(II) by chlorine (Eq. (1.6)) is slower (Morgan and Stumm, 1964). The oxidation rate can be slower and still produce acceptable process performance, which should be assessed for each treatment plant (Knocke et al., 1990b). Such condition should prevail when the filter media provides a high amount of adsorption sites and subsequently high sorption capacity, such as in the case of pyrolucite media (Zuravnsky, 2006).

Adequate free chlorine concentration is an important parameter to achieve an adequate process performance. Zuravnsky (2006) showed that increased free chlorine concentration resulted in higher process performance by rapid regeneration of occupied sorption sites. However, high free chlorine concentrations can result in the formation of DBP in water with high organic content,

which is often a concern in surface water applications. Therefore, water utilities should optimize their treatment train design.
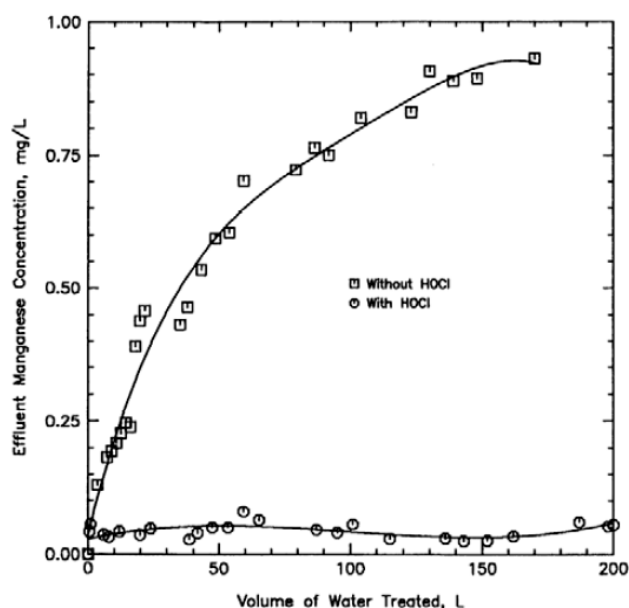
Figure 2.6. Effect of pre-filter chlorination on Mn (II) uptake capacity of media: manganese oxide coating level = 18 mg Mn/g media, Mn(II)0 = 1.0 mg/L and at pH = 6-6.2 (Knocke et al., 1990b)**.**

2.3.2.5   Effect of NOM on manganese removal

NOM can impact Fe(II) and Mn(II) removal in three ways: 1) it can exert additional oxidant demand, 2) it can form complexes with Fe(II) and Mn(II), and 3) it can impact adsorption of Mn(II) onto $MnO_{x(s)}$ coated filter media. Tobiason et al. (2008) revealed that the Mn(II) uptake capacity of $MnO_{x(s)}$ decreased with increasing NOM concentration in water. This might be attributed to the possible capability of $MnO_{x(s)}$ to adsorb NOM which, consequently, decreases the number of available sorption site for Mn(II) uptake (Tobiason et al., 2008). Another possible explanation is that a complexation reaction between Mn(II) and NOM took place and $MnO_{x(s)}$ surface was unable to adsorb the complex and thus the Mn(II) removal performance decreased (Tobiason et al., 2008).

As previously stated, the main concern regarding to NOM is its role on the formation of halogenated DBPs in CR with chlorine. One possibility to minimize the formation of these by-products is moving the chlorine injection point from pre-filtration to post-filtration. Thus, a treatment train containing second stage contactors whose sole purpose is Mn(II) sorption and catalytic oxidation

by free chlorine can be utilized, as described in a previous section (Knocke et al., 2010; Bazilio et al., 2016).

2.3.2.6 Effect of HLR, feed Mn concentration and temperature on manganese removal

HLR impacts the process performance in two ways. On one hand, increasing the HLR increases the mass transfer coefficient and hence the adsorption rate, which changes Mn(II) removal profile (Merkle et al., 1997). On the other hand, high HLR results in low contact time and increases the amount of Mn(II) loaded to the system. Zuravnsky (2006) showed that an increase in HLR (from 16 to 20 gpm/ft^2) had a negative impact on Mn(II) removal (15% reduction in process performance). This implies that increase in adsorption rate at higher HLR was not enough to compensate the reduced contact time and higher loading rate of Mn(II). In addition, elevated HLR results in more rapid head loss build up, and subsequently, more frequent backwashes are required.

Although Mn(II) uptake capacity increases with increasing feed concentration, Tobiason et al. (2008) showed that breakthrough occurs earlier under higher initial Mn(II) concentrations as this makes the IR process to be inapplicable even at Mn(II) level of 0.4 mg/L. They also revealed that even in CR mode using pyrolucite, increasing the concentration of Mn(II) from 0.035 to 0.107 mg/L resulted in 10% reduction in the process performance. This reduction was more significant for a $MnO_{x(s)}$ coated sand media than for pyrolucite.

Effect of temperature on the sorption of Mn(II) onto $MnO_{x(s)}$-coated filter media has not been well documented. Since adsorption onto $MnO_{2(s)}$ was expressed as an endothermic process (Ren et al., 2011), Mn(II) uptake capacity of $MnO_{x(s)}$-coated media is expected to increase under elevated temperatures. In addition to the effect of temperature on manganese sorption, it can also affect manganese removal in CR process with increasing solution oxidation of Mn(II) by free chlorine under elevated temperatures (e.g., 25°C vs. 10°C). Hence, the process performance might be reduced due to the formation of colloidal MnO_2, especially, under high feed Mn(II) concentrations, which can be hardly removed through sand filtration. As a conclusion, temperature provides both detrimental and beneficial impacts depending on the process conditions.

In summary, the significance of chlorine, pH, and oxide coating level on Mn(II) uptake capacity is related to their impacts on maintaining an appropriate number of $MnO_{x(s)}$ adsorption sites. Hence, the amount of available adsorption sites on the media plays a key role on Mn(II) removal efficiency within the filter. These adsorption sites can be used effectively through fluidized bed contactor

since adsorption is faster under fluidization state than for a fixed bed state owing to a better fluid-solid contact.

2.3.2.7 Effect of operation mode (fixed bed vs. fluidized bed state) on manganese removal

Fixed and fluidized beds are two common continuous adsorption contactor configurations. In the scientific literature, fixed bed contactor, in which the flow is directed downward, has been most commonly used for iron and manganese removal. In contrast, fluidized bed contactor, in which the fluid is forced through the filter media in upward direction at a velocity sufficiently high to fluidize the media, has been reported to effectively remove elevated concentrations of heavy metals (Nielsen et al., 1997) such as copper (Lee et al., 2004) and manganese (Takizawa et al., 2001) ions within a filter containing $MnO_{x(s)}$ coated sand and tubular polypropylene, respectively.

In fixed bed configuration, rapid head loss buildup limited the catalytic filtration of Mn(II) to relatively low HLRs (6-12 m/h) (Hargette and Knocke, 2001; Yang et al., 2008; Piispanen and Sallanko, 2010). Therefore, the size of contactor should be large enough to provide the required flow, and frequent backwash is required, which resulted in a large amount of wastewater production and high energy expenses. More recently, Knocke et al. (2010) applied high HLR (40-50 m/h or 16-20 gpm/ft^2) in a post-filtration sorptive contactor intended for surface water applications. However, in these experiments the initial manganese concentration was very low (< 0.1 mg/L) and the filter contained large-sized pyrolucite (2.0-2.4 mm diameter) (low specific surface area) that allowed working at high HLR in fixed bed state. However, even in this case where very low turbidity (< 0.1 NTU) were filtered, head loss accumulation (20 kPa) was observed due to the blockage of column void space, requiring backwash of the column every other two months (Subramaniam, 2010).

In fixed bed operation a portion of adsorption sites are lost due to the stationary state of the system in which particles support themselves to stay at this condition while this is a rather negligible issue when the bed is fluidized and nearly all adsorption sites are available (Lee et al., 2004). In addition, a uniform particle mixing and mass transfer rate are achieved which results in a uniform product and also higher efficiency due to better water-solid contact (Bošković-Vragolović et al., 2009). Furthermore, a lower susceptibility to plugging is another advantage of fluidized bed over fixed bed that allows operating continuously with a constant head loss independent of the fluid velocity. As a consequence, it permits working at higher HLRs (> 25 m/h) compared to fixed bed (< 12 m/h)

and provides higher adsorption rate that reduces the required contact time considerably (Nielsen et al., 1997). This results in a more compact process with a relatively smaller footprint.

Increase in mass transfer rate or, in fact, mass transfer coefficient at elevated Reynolds number or HLR results in high adsorption rate. Mass transfer coefficient is usually expressed by a combination of dimensionless groups. Dwivedi and Upadhyay (1977) developed Eq. (1.7) which can properly correlate the experimental data with an average deviation of 18% in the range of Reynolds number, Re ($U\,d_p/v$), from 0.01 up to 15,000 for both fixed and fluidized bed contactors.

$$\varepsilon J_d = \frac{0.765}{Re^{0.82}} + \frac{0.365}{Re^{0.386}} \tag{1.7}$$

Where ε is void fraction; and J_d is Chilton-Colburn mass transfer factor ((k_f/U) $Sc^{2/3}$).

Accordingly, mass transfer coefficient (k_f) can be expressed as follows (Eq. (1.8)):

$$k_f = \left(\frac{0.765}{Re^{0.82}} + \frac{0.365}{Re^{0.386}}\right) * \left(\frac{U}{\varepsilon\,Sc^{2/3}}\right) \tag{1.8}$$

Where U is superficial fluid velocity (m/s); and Sc is dimensionless Schmidt number (v/D).

Bošković-Vragolović et al. (2009) applied adsorption method as a suitable procedure for mass transfer studies. They concluded that Eq. (1.7) satisfactorily fits the experimental data obtained from diluted solution fluid-to-solid mass transfer in fluidized bed. This is consistent with Dwivedi and Upadhyay (1977) conclusion. In addition, it has been shown that, in dilute solution, mass transfer rate is only dependent upon the diffusion through the boundary layer.

Eq. (1.8) clearly depicted that mass transfer coefficients are directly proportional to fluid velocity, as expected. However, it is worth mentioning that in fluidized bed, increase in fluid velocity also results in increase in bed voidage or porosity which is inversely proportional to mass transfer coefficient. Bošković-Vragolović et al. (2009) computed the mass transfer coefficients at different fluid velocities in both fixed and fluidized bed states (Figure 2.7). Their results showed that the highest mass transfer coefficient can be achieved at minimum fluidization velocity, in which the adsorbent concentration is maximum, and then, by increasing the velocity up to a certain value, k_f remained contestant (Figure 2.7). After this plateau, mass transfer coefficients decreased with increasing velocity. The plateau demonstrates that there exists a certain bed expansion or HLR in which higher porosity can be compensated by higher velocity and results in a constant mass transfer

rate. The condition allows operating at higher velocity without reducing the mass transfer coefficient or adsorption rate.
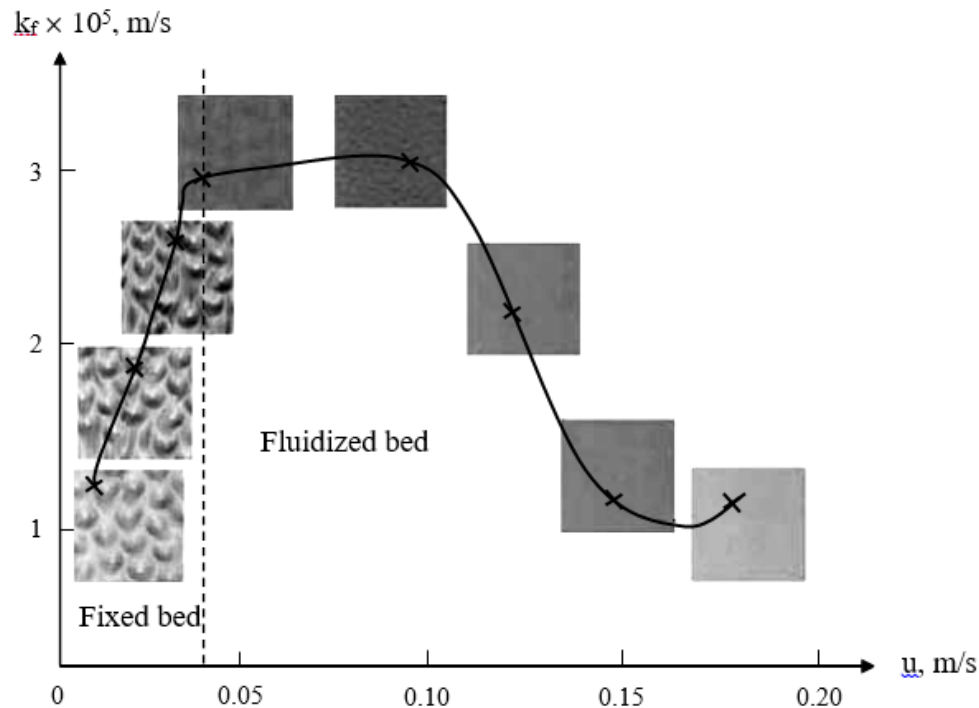
Figure 2.7. Effect of superficial fluid velocity on mass transfer coefficient in both fixed and fluidized bed contactors (Bošković-Vragolović et al., 2009).

As an alternative to granular media filtration, membrane technology has been proposed more recently to remove elevated levels of iron and manganese from groundwater. This treatment option is discussed in the next section.

2.4 Membrane filtration

Compact membrane processes, such as MF and UF, are increasingly used in water treatment facilities as an alternative process to conventional filtration for the removal of dilute suspensions containing fine particles and colloids based on size exclusion.

Application of UF membranes, with nominal pore size ranging from approximately 1 to 100 nm, are attractive for drinking water treatment because of:

- Strict solid-liquid separation that can remove particulate and colloidal materials (Choo et al., 2005) and macromolecular solutes (Choo et al., 2007). Thus, the treated water can meet increasing stringent regulations on drinking water production;
- Effective removal and control of the small pathogens such as protozoa and bacteria, and viruses (Montgomery Watson Harza (MWH), 2005);
- Limited use of chemicals;
- Small footprint and compact systems;
- Low sludge production;
- Easy and convenient operation which guaranties a more constant quality of treated water, regardless of the source water quality.

In addition, low pressure membranes (LPMs), MF/UF, are more economical than their high pressure counterparts (nanofitration, NF, and reverse osmosis, RO). However, since MF and UF membranes are microporous, dissolved inorganic constituents like metal ions cannot be removed without the use of pretreatment processes such as a strong oxidation.

In spite of the above mentioned advantages, application of MF/UF membranes in water treatment plants is still limited. The major obstacle facing this process is the decrease in membrane productivity or increase in energy consumption due to so-called membrane fouling (Gao et al., 2011). As opposed to surface water where organic fouling is dominant, management of inorganic fouling caused by iron/manganese is of importance for many UF/MF groundwater systems.

This section first provides background information on rejection and fouling mechanisms. Finally, it contains a review of literatures related to the removal of iron and manganese by LPMs.

2.4.1 Membrane rejection mechanisms

The pressure difference between the feed and permeate side (TMP gradient) is the driving force to transport water through LPMs. Particles and some dissolved compound are partially retained dependent upon their size, shape and charge. The rejection efficiency (R) for a given compound is expressed as follows:

$$R = \left(1 - \frac{C_P}{C_F}\right) \times 100 \tag{1.9}$$

Where C_P and C_F are concentrations of a component in permeate and feed water, respectively.

The log rejection is used for some compounds, such as microorganisms, for which their concentration in permeate would be several orders of magnitude lower than in the feed solution:

$$R_{LOG} = -\log(1-R) = \log\left(\frac{C_F}{C_P}\right) \qquad (1.10)$$

Although straining or sieving is the primary mechanism responsible for particle removal in UF/MF membrane filtration, removal is also impacted by adsorption and cake formation. These mechanisms are illustrated in Figure 2.8a-c (Montgomery Watson Harza (MWH), 2005). Straining is the dominant filtration mechanism in which the particles larger than membrane pore size are physically retained at the surface while water and smaller particles pass through the membrane, as schematically shown in Figure 2.8a. However, in reality, characteristics of the membrane and the particles and electrostatic interaction between particles and membrane impact this phenomenon (Montgomery Watson Harza (MWH), 2005). For instance, repulsive interactions between colloidal particles and membrane may prevent them entering the pores even with size smaller than the membrane pore size (Zydney and Pujar, 1998; Bernat et al., 2009).
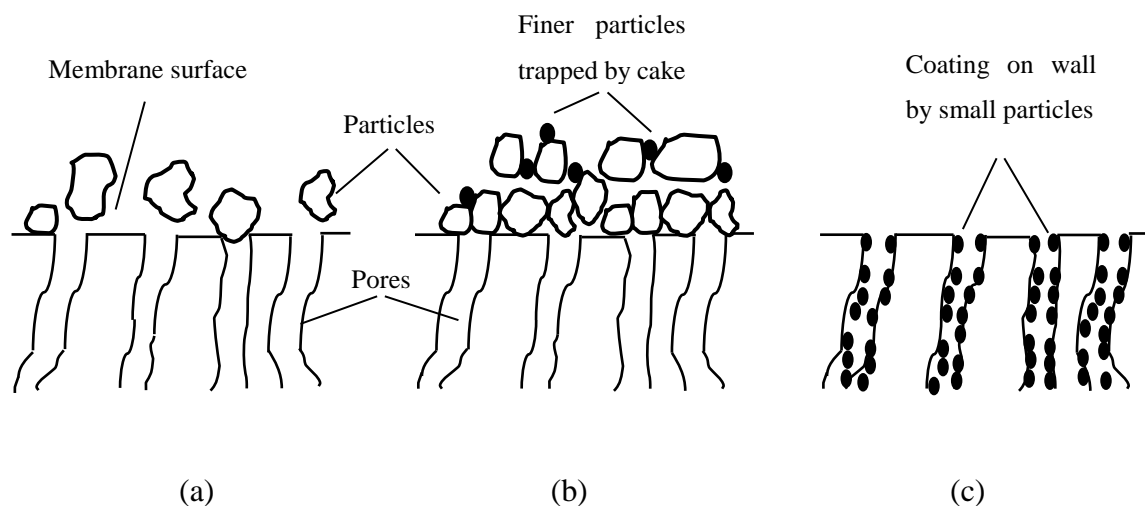
Figure 2.8. Membrane rejection mechanisms: (a) Straining (b) Cake filtration (c) Adsorption (Montgomery Watson Harza (MWH), 2005).

After a cake layer of large components is formed on the membrane surface, it will reduce the passage of particles that are small enough to pass through the membrane's pores (Figure 1.8b). Adsorption of organic contaminants (such as humic substances) or inorganic contaminants (such as manganese) is the other mechanism responsible for UF/MF membranes removal performance (Lee and Kim, 2014). These species may be adsorbed by the membrane surface especially during

the early stage of filtration cycle. However, since the adsorption capacity is quickly exhausted, it is not an effective mechanism in long term operation. As the filtration cycle progress, contaminants can be adsorbed inside the cake layer. As can be seen in Figure 1.8c, adsorbed materials may reduce the pore size of membrane and increase the rejection of small particles (Montgomery Watson Harza (MWH), 2005). In conclusion, the efficiency of cake filtration and adsorption mechanisms vary during the filtration cycle.

2.4.2 Parameters impact initial membrane permeability

Flux at a given temperature, J_T (m/s), which describes the filtration throughput, is defined as the filtrate flow, Q (m^3/s), per unit of membrane filtration area, A_0 (m^2). For porous membranes the flux is directly proportional to the TMP, ΔP_0 (kPa), and inversely proportional to the absolute viscosity of water, μ (kPa.s), as is described based on Darcy's law:

$$J_T = \frac{Q}{A_0} = \frac{\Delta P_0}{\mu * R_m} \tag{1.11}$$

where R_m is the hydraulic resistance (m^{-1}) of the clean membrane and is related to physical properties of membrane, as follows (American Water Works Association, 2005):

$$R_m = \frac{8 * \tau * \Delta z}{\pi * r^4 * P_{pore}} \tag{1.12}$$

where the pore density, P_{pore}, is the number of pores per unit of membrane area; r is the pore radius (m); τ is the tortuosity factor; and Δz is the pore length (m). However, for a typical membrane, R_m is commonly calculated from laboratory experiments employing Eq. (1.11).

Obviously, from Eq. (1.11), temperature has a significant impact on flux through viscosity, which decreases with increasing temperature. Thus, to eliminate the impact of temperature on flux, normalized flux at a reference temperature, 20°C, has been applied using an empirical relationship as follows (United States Environmental Protection Agency (USEPA), 2005):

$$J_{20} = \frac{J_T * \mu_T}{\mu_{20}} = J_T * [1.784 - 0.0575 * T + 0.0011 * T^2 - 10^{-5} * T^3] \tag{1.13}$$

where J_{20} is the flux at 20°C; and μ_T and μ_{20} are dynamic viscosity of water at temperature T and 20°C, respectively.

The change in membrane productivity is generally identified by variations in the pressure-normalized flux or specific flux, J_S, which is the flux at 20°C (J_{20}) divided by the TMP (Eq. (1.14)).

The specific flux is called membrane permeability when clean water is passed through the membrane (Montgomery Watson Harza (MWH), 2005).

$$J_S = \frac{J_{20}}{\Delta P} \tag{1.14}$$

It is worth noting that, in addition to temperature, the initial membrane permeability might be also impacted by pH, ionic strength and valency of the solute (Braghetta et al., 1997; Ito et al., 1992; Zhao et al., 2005; Nilsson et al., 2008). This is attributed to the electro-viscous effect that occurs due to the passage of an electrolyte solution through capillaries with charged surface, because the surface moves the ions away from their preferred place resulting in extra required energy and thus higher apparent viscosity (Huisman et al., 1997). Zhao et al. (2005) showed that the permeability of α-alumina (α-Al$_2$O$_3$) MF membrane is strongly affected by the zeta potential of the membrane surface, which is determined by the solution pH and ionic strength. They found that low pH values and high ionic strength led to low zeta potential or membrane surface charge and, consequently, the permeability increased due to the decrease in electro-viscous effects. The same results were reported for the permeability of zirconia (ZrO$_2$) UF membrane (Faibish et al., 1998). However, in polymeric membranes, which have slightly compressible characteristics in contrast to the rigid nature of ceramic membranes, both the electro-viscous effects and the membrane pore size variations account for the reported changes in membrane permeability (Zhao et al., 2011). In some cases, compaction of membrane matrix under low pH and/or high ionic strength and, thus, reduction of the membrane pore size has greater impact on permeability (Braghetta et al., 1997; Zhao et al., 2011; Mänttäri et al., 2006) than the electro-viscous effects. In addition, extension of chains in grafted polymeric membranes (e.g., polyvinylidene fluoride (PVDF) membrane grafted with poly-acrylic acid (PAA)) under high pH and/or low salt concentration led to blockage of the pores and reduction of membrane permeability (Kontturi et al., 1996). In summary, it is important that the initial membrane permeability be defined using the waters under investigation without particles rather than only ultrapure water.

2.4.3 Membrane fouling

One of the critical issues for applying LPMs technology in water treatment is the loss of membrane permeability, flux decline or increase in TMP, due to the adsorption or deposition of rejected species on the membrane surface or within the membrane pores. This phenomenon is termed

membrane fouling and characterized as reversible or irreversible. Reversible fouling can be removed by backwashing, termed physically reversible, or chemical cleaning, termed chemically reversible. Irreversible fouling reduces the membrane lifetime. Frequent chemical cleaning may also lead to a shorten membrane lifetime (Li et al., 2014). Fouling, whether reversible or irreversible, exerts additional cost for industries due to the higher energy and chemical consumption as well as membrane replacement. Several factors impact the extent of membrane fouling such as membrane characteristics (e.g., material, hydrophobicity, pore size and surface charge), operational conditions (e.g., TMP, flux and flow mode) and physicochemical properties of feed water (Guo et al., 2012).

Pressure-driven membranes has been traditionally fabricated from polymers, such as PVDF and polyethersulfone (PES). However, recently, application of ceramic membranes, such as Al_2O_3, ZrO_2, titania (TiO_2) and silicon carbide (SiC), has been receiving growing attention due to their inherent advantages over conventional polymeric membranes. Namely, ceramic membranes offer superior chemical, thermal and mechanical stability allowing much more aggressive physical and chemical cleaning approaches which can prolong membrane lifespan. In addition, the higher integrity and reliability of ceramic membranes would reduce the repetitive testing, repair and replacement of membrane modules leading to savings in operation cost (Pendergast and Hoek, 2011). Moreover, ceramic membranes may have a lower fouling potential because of their higher hydrophilicity compared to polymeric membranes (Hofs et al., 2011). In order to increase the hydrophilicity of the polymeric membranes, a blend of polyvinylpyrrolidone (PVP) and a polymer is commonly used (Van Der Bruggen et al., 2003). Electrostatic charge at the membrane surface is also important for fouling management. More severe fouling can be found when membrane surface and suspensions carry opposite charges because of electro-sorption of the foulant on the membranes (Zuo and Wang, 2013).

Membrane fouling is also impacted by the flow regime near the membrane surface. Two operating configurations, cross-flow filtration and dead-end or direct filtration, have been developed. In cross-flow filtration, a portion of feed water is recycled at a high velocity, typically 0.5 to 1 m/s. This high velocity tangential flow to the membrane surface creates a shear force and turbulence that diminishes the development of cake layer on the membrane surface. In dead-end filtration mode, all feed water passes through the membrane. Therefore, suspensions larger than the membrane pore size accumulate on its surface resulting in a greater permeability decline compared

to cross-flow filtration. In spite of this fact, the dead-end flow mode is most commonly applied in membrane filtration for water treatment due to both relatively low feed water turbidity, less than 100 NTU, and the high fraction of concentrate stream in cross-flow filtration. Moreover, piping and electrical costs of cross-flow pumping can triple the operation cost and would require a much larger footprint (Montgomery Watson Harza (MWH), 2005).

In drinking water treatment, NOM, microorganisms, inorganic colloids/particles, pH, ionic strength and salt valency are important feed water characteristics influencing membrane fouling (Guo et al., 2012). NOM is a major contributor to fouling of polymeric membranes during MF/UF of surface water (Escobar et al., 2005). Humic substances are the major fraction of NOM, which comprise over 50% of DOC, while having both aromatic and aliphatic components with MW range from 1-100 kDa (Guo et al., 2012). Lee et al. (2008) revealed that medium to low MW components of NOM (0.3-1 kDa) are the major contributor to membrane fouling during the early stage of MF/UF while fouling of very high MW colloidal NOM (> 50 kDa) is predominant during the later stage of filtration. Fouling caused by inorganic colloids/particles is discussed in the following sections.

2.4.3.1 Models for membrane fouling mechanisms

LPMs fouling mechanisms are generally based on the cake formation, pore blocking and internal pore constriction. In cake layer formation, fouling occurs due to the resistance imposed to flow by the particle cake that accumulates on the membrane surface. In pore blocking, the pore mouth is plugged by the particles and the rate of fouling is proportional to the rate of pore sealing whereas pore constriction occurs due to the adsorption of dissolved matter or attachment of small particles (smaller than the pore size) on the pore walls which will reduce the membrane's pore radius (Montgomery Watson Harza (MWH), 2005).

Hermia (1982) has proposed models to simulate all the above mentioned mechanisms. Schematic diagrams of the four fouling mechanisms proposed by Hermia are illustrated in Table 2.2. These models that are derived based on constant-pressure and dead-end filtration mode, can be written in a consistent format as follows (blocking laws) (Hermia, 1982):

$$\frac{d^2t}{dV^2} = k \left(\frac{dt}{dV}\right)^{\emptyset} \qquad (1.15)$$
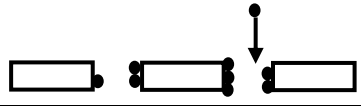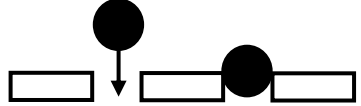
where t (s) is the filtration time; and V (m^3) is cumulative permeate volume; k and $\emptyset$ are two model parameters that their values depend on the fouling mechanism.

Although the majority of studies have delineated membrane fouling during constant TMP, membranes employed in water and wastewater treatment are commonly operated at constant flux mode and the data obtained from constant TMP experiments could not well predict the rate and extent of fouling in full-scale plant (Chellam and Xu, 2006). In this regard, the blocking laws model has been revised for constant flux membrane filtration (Eq. (1.16)) (Huang et al., 2008b):

$$\frac{dP'}{dV_s} = k_v P'^{n_1} \tag{1.16}$$

where P' is the TMP normalized to its initial value (ΔP_0), V_s is the volume of permeate per unit membrane area (m^3/m^2), and k_v and n_1 are model parameters representing blocking index and blocking constant, respectively. The blocking law exponent for incompressible cake formation, intermediate blocking, standard blocking and complete blocking is 0, 1, 1.5 and 2, respectively. However, fouling of many "real world" materials such as natural colloidal matter and microbial cells can be described by compressible cake formation. The blocking law model for compressible cake formation is delineated in the next section.

Table 2.2. Schematic diagrams of fouling mechanisms proposed by Hermia (1982).

Mechanisms	Concept	Description
Cake formation		$d_{particle} > d_{pore}$ Particles are retained due to sieving and form cake on the surface.
Intermediate blocking		$d_{particle} \approx d_{pore}$ Particles accumulate on each other and seal membrane pores.
Standard blocking		$d_{particle} < d_{pore}$ Particles deposit on the internal pore walls and decreasing the pore diameter.
Complete blocking		$d_{particle} \approx d_{pore}$ Particulates seal pores mouth and do not accumulate on each other.

2.4.3.2 Fouling of inorganic colloids/particles

Particulate matter in water has been classified in the following categories (Rudolfs and Balmat, 1952): 1) settable solids (> 100 µm), 2) supra-colloidal solids (1-100 µm), 3) colloidal solids (0.001-1 µm), and 4) dissolved solids (< 0.001 µm). Colloids/particles much larger than the membrane pore size lead to cake formation that is easily removed by physical backwash while those close to the size of membrane pores can cause pore blockage (Huang et al., 2008a). However in both cases, cake filtration mechanism can most commonly describe the pressure increase and membrane fouling at the later stage of filtration (Lim and Bai, 2003). Inorganic colloids in natural waters such as clay particles are commonly larger than the membrane pore size and hence collect on the membrane surface leading to the formation of a multilayered cake. According to the Darcy's law, the flow through the fouled membrane can be written as:

$$Q = \frac{\Delta P \, A_0}{\mu * (R_c + R_m)} \tag{1.15}$$

where R_c (m^{-1}) is the additional resistance due to the cake formation. Moreover, in the presence of other resistances, such as concentration polarization and internal pore fouling, they can be also included in this equation. For an incompressible cake composed of monodisperse spherical particles, the cake layer resistance can be computed applying Carman-Kozeny equation:

$$R_c = \frac{180 \, (1-\varepsilon)^2 \, \delta_c}{\varepsilon^3 \, d_p^2} \tag{1.16}$$

where d_p is the retained particle diameter (m); and ε and δ_c are the porosity and thickness of the filter cake, respectively.

In dead-end filtration mode, the thickness of the cake layer as a function of time can be derived as follows using the mass balance of particle toward the membrane surface:

$$\delta_c(t) = \frac{c_b \, V}{\rho_p \, A_0 \, (1-\varepsilon)} \tag{1.17}$$

where c_b is the bulk concentration (kg/m^3); and ρ_p is the density of deposited particles (kg/m^3) (Montgomery Watson Harza (MWH), 2005).

The cake layer resistance can be also expressed in terms of the average specific cake resistance, α_{ave} (m/kg), as follows:

$$R_c = \alpha_{ave} \, c_b \, V_s \tag{1.18}$$

Eq. (1.19) was derived from the combination of Eqs. (1.11), (1.15) and (1.18) that expresses the increase in TMP at constant flux during incompressible cake filtration, in which the specific cake resistance remains constant throughout the experiment.

$$\Delta P = \frac{Q \, \mu (\alpha \, c_b V_s + R_m)}{A_0} = \Delta P_0 + \frac{Q \, \mu \, \alpha \, c_b}{A_0} V_s \tag{1.19}$$

However, the filter cake of many natural materials, such as clays, microbial cells and flocculated colloidal maters, is compressible to some degree (Chellam and Xu, 2006; Singh and Song, 2006). Under this condition, after initial deposition of a cake layer and increase in TMP, a compact skin layer is formed next to the membrane surface, which gradually develops during the filtration period. Thus, the specific cake resistance gradually increases. During water and wastewater treatment, the specific cake resistance, α (m/kg), often increases according to a power law (Chellam and Xu, 2006; Chellam et al., 1998; Sørensen and Sorensen, 1997):

$$\alpha = \beta \Delta P^{n'} \tag{1.20}$$

where β (m/kg/kPa$^{n'}$) and n' are empirical constants. β is related principally to the size and shape of the particles, and the dimensionless parameter n' is the cake compressibility coefficient varying from zero for an incompressible cake to nearly 1 for a highly compressible cake. Substituting Eq. (1.20) in Eq. (1.19) gives rise to the following equation, which was derived by Chellam and Xu (2006):

$$\Delta P = \Delta P_0 + \frac{Q \, \mu \, c_b}{A_0} \beta \, \Delta P^{n'} V_s \tag{1.21}$$

Several studies have shown that, in addition to hydrodynamic operation conditions, productivity during colloidal MF/UF is also governed by physicochemical properties of the feed water such as pH, ionic strength, particle size distribution, shape, surface charge, fractal dimension and degree of aggregation (Singh and Song, 2006; Santiwong et al., 2008; Lee et al., 2003; Tiller et al. 1987). All of these parameters can alter the cake layer structure and its compressibility due to particle-particle and membrane-particle interactions.

Elzo et al. (1998) studied the effect of pH and ionic strength on the membrane performance during MF of 0.5 μm SiO$_2$ particles. They found that under high pH and/or low ionic strength, the specific cake resistance decreased, because the strong repulsion between the negatively charged particles

resulted in increase in cake layer porosity. This result is consistent with Faibish et al. (1998) findings who investigated the UF of smaller SiO_2 particles (47, 110 and 310 nm). In sharp contrast, Zhao et al. (2005) found that under high pH and low ionic strength, fouling dramatically increased during MF of TiO_2 suspensions. This was attributed to the tendency of TiO_2 particles to disperse under high charge density. However, near the zero-point of charge, suspensions tended to aggregate giving rise to the formation of a less compact cake with low resistance and high hydraulic permeability. The incoherence between the fouling behavior of SiO_2 and TiO_2 particles might be due to the non-flocculating character of SiO_2 colloids (Zhao et al., 2005). In conclusion, if the addition of salt and/or change in pH is not enough to destabilize the colloidal suspensions and aggregation of particles does not occur, it will reduce the thickness of electrostatic diffuse layer which result in a dense cake layer formation.

The influence of the aggregate fractal geometry has been reported as an important factor to explain dead-end (Santiwong et al., 2008; Lee et al., 2003; Xu et al., 2011) as well as cross flow (Zhang et al., 2010) filtration performances. Fractal dimension is a mathematical description of irregular geometric aggregates which gives insight into the compactness of the aggregates. The high fractal dimensions, values approaching 3, indicate compact nearly spherical aggregates, whereas more amorphous and less compact aggregates have low fractal dimensions, values approaching 1. Zhang et al. (2010) investigated the effect of particle size and fractal structure on critical flux (a flux below which a decline in flux or an increase in TMP does not occur over time) and fouling mechanisms. They found that critical flux increase with the particle size and fractal dimension. Lee et al. (2003) and Santiwong et al. (2008) revealed that the filter cake composed of aggregates with large size and low fractal dimension has high permeability, which impose low resistance to flow, due to the high inter-aggregate and intra-aggregate porosity, respectively. Previous studies on SiO_2 colloids (Singh and Song, 2006) and TiO_2 nanoparticles (Chowdhury et al., 2013) demonstrated that the fractal dimensions may be impacted by the solution chemistry. For instance, the fractal dimensions of these aggregates slightly increase with ionic strength due to the compression of the electrostatic double layer.

In conclusion, several parameters may play a substantial role on the fouling of MF/UF membrane. The significance of each parameter should be assessed during filtration of each specific component.

2.4.4 Iron and manganese removal by LPMs

LPMs cannot be used as standalone processes for removal of dissolved inorganic constituents such as Fe(II) and Mn(II) ions. Therefore, peroxidation is required in order to remove these elements via MF/UF membranes. Application of MF after oxidation by $KMnO_4$ (Côté et al., 1998) and ClO_2 (Schneider et al., 2001) was assessed to remove iron and/or manganese from water. Since sufficient retention time was allocated to oxidize Mn(II) and Fe(II) by these strong oxidants, satisfactory removal performance was achieved. Ellis et al. (2000) showed that the size distribution of oxidized iron and manganese ranged between 1.5 and 50 µm, and, consequently, concluded that cake formation is the dominant fouling mechanism responsible for the observed flux decline in MF membrane. However, oxidation of Mn(II) is limited by several parameters that were extensively described in the previous sections. Thus, this process might not be feasible for the treatment of drinking water containing high levels of iron and manganese. In addition, colloidal manganese oxide was reported to be the principal membrane foulant after NOM (Kaiya et al., 1996).

Choo et al. (2005) investigated the effect of prechlorination for Mn(II) and Fe(II) removal using UF membrane. The iron removal was very rapid and reached around 100% with only a small dosage of chlorine. However, only 80% of manganese was removed even with a chlorine dosage of around 200% of the stoichiometric requirement. Higher chlorine dosage did not increase manganese removal but even led to more serious membrane fouling. The severe fouling during this process was attributed to the slow oxidation rate of manganese by chlorine which may result in the formation of colloidal manganese that can pass through the membrane pores. These colloids may gradually grow in the pores and result in blockage of the pores during backwashing. Surprisingly, backwash had detrimental effect in their process; however, they did not measure the particle size distribution to support their hypothesis. Production of colloidal particles in this process (compared to much larger oxidized particles reported by Ellis et al. (2000)) may have been related to the low hardness of their raw water. Unfortunately, the hardness of the raw water, which can significantly impact the particle size, was not reported in their study.

In order to reduce the fouling caused by manganese oxides, it has been proposed to conduct a pretreatment process ahead of membrane filtration. Teng et al. (2001) studied the effect of stirred reactor containing manganese coated sand on the removal of Mn(II) and mitigation of MF membrane fouling. Although this hybrid process removed 95% of manganese at a pH of 9.3,

frequent regeneration was required due to the rapid exhaustion of manganese coated sand in the absence of a strong oxidant. In addition, membrane fouling was only slightly alleviated compared to the process without manganese coated sand. This might be due to the solution oxidation of Mn(II) at high pH of 9.3 which cannot be adsorbed by manganese coated sand resulting in the fouling of MF membrane. Takizawa et al. (2001) found that a fluidized bed contactor containing tubular polypropylene as a manganese-oxidizing catalyst along with chlorine can effectively remove manganese from water while preventing MF membrane fouling associated with manganese. However, even in the presence of catalyst, relatively high retention time (more than 30 minutes at 30°C) is required. Moreover, they showed that fixed-bed biological pretreatment can efficiently remove manganese and reduce membrane fouling (Takizawa et al., 2001). However, in biological processes, the removal efficacy is highly affected by the hydraulic retention time and raw water characteristics such as dissolved oxygen, pH, temperature, microbiological quality, NOM, and manganese and/or iron concentrations. Furthermore, it has been shown that simultaneous removal of Fe(II) and Mn(II) in a single bioreactor is not possible, unless it is achieved in a process with extremely high retention time. The problem is more significant when the water contains ammonia in addition to iron and manganese. Moreover, long start-up time (several weeks or months) is the other drawback of the biological process (Gouzinis et al., 1998), although this issue has been somewhat alleviated by seeding new filters using backwash waters from other existing biological filters.

Rather than oxidation of Fe(II) and Mn(II), another pretreatment was tested based on the capability of UF membranes to retain macromolecular solutes. In this regard, an extensive study was conducted to remove Mn(II) from groundwater by UF membranes through the addition of chelating PAA as a pretreatment (Choo et al., 2007; Han et al., 2005; 2007). Although this process was found to be effective for removing 80% of manganese, the removal efficiency severely depended upon the solution pH and the dosage of chelating polymers (PAA). The highest manganese removal efficiency (80%) only occurred at pH 9.0 with COOH/Mn molar ratio of 100, because the potential of Mn(II) to precipitate was higher under alkaline pH and more PAA-Mn complexes were created at high COOH/Mn ratio. The flux rapidly declined as the solution pH increased due to the deposition of manganese precipitates on the membrane surface and further flux decline was caused by addition of elevated amount of PAA (COOH/Mn = 100). The cost of using such a large dosage of PAA is another drawback of this procedure that prohibits its application in practice. Although

regeneration of the PAA via pH adjustment (pH 3.0) and UF membrane is accessible (Han et al., 2005), reuse of PAA gradually decreased the removal efficiency. Moreover, it has been revealed that calcium hardness had a great impact in manganese removal. Calcium ion, unlike magnesium that had no effect on manganese removal, reduced manganese removal performance by competing with manganese for the formation of metal-PAA chelates. Due to the inconveniences that were listed above, even if this procedure would be practically usable, it could not be applied even for water with moderate level of calcium.

Desalination membranes, such as NF and RO, can also be utilized to remove Fe(II) and Mn(II) from water (Richards et al., 2011; Al-Rashdi et al., 2013). However, the retention of manganese was found to be pH-dependent and the rejected species may be oxidized and precipitated on the membrane surface giving rise to membrane fouling (Richards et al., 2011). Most NF/RO membranes are commercialized as spiraled modules in which the fouling of the spacer by particulate matter, including oxidized iron and manganese, must be limited. Although application of NF and RO membranes for iron and manganese removal is uncommon, removal of these species by desalination membranes may occur in conjunction with other solutes that the membranes were designed to eliminate (e.g. hardness). Considering the higher costs of NF/RO application, it is not advised to use desalination membranes if Fe/Mn removal is the only treatment goal.

CHAPTER 3   RESEARCH OBJECTIVES, HYPOTHESES, AND METHODOLOGY

3.1 Critical review of previous research

Health concerns related to manganese intake from water ingestion on one hand, and the potential for aesthetic issues as well as maintenance cost for cleaning water mains on the other hand, make it desirable to minimize iron and manganese concentrations in drinking water. Based on the literature review, the traditional removal strategy, which involves oxidation of iron and manganese followed by removal of oxidized particles through depth filtration, is subject to the following limitations:

- Despite Fe(II) being readily oxidized by a weak oxidant such as oxygen, the direct oxidation of Mn(II) is difficult to achieve and therefore requires the use of a strong oxidant such as $KMnO_4$;

- Oxidation rate of Mn(II) strongly depends on feed water temperature, pH, initial concentration of manganese and NOM;

- Among the different strong oxidants, $KMnO_4$ and ClO_2 are generally argued to be the best options for the direct oxidation of Mn(II). However, fluctuations in Fe(II) and Mn(II) concentrations in raw water could limit the application of $KMnO_4$ due to the possible escape of $KMnO_4$ residual into treated water and pink water formation. ClO_2 dosage is limited due to the formation of chlorite and chlorate as disinfection by-products. The later must also be produced on-site;

- Efficient removal of particulate manganese through depth filtration may not be achieved due to the tendency of manganese to form negatively charged colloids via oxidation.

Biological oxidation is an attractive treatment option but its application in groundwaters with elevated Mn(II) and Fe(II) concentrations must be done in two sequential reactors, a process configuration which increases capital cost. Alternatively, application of LPMs has been proposed more recently since they can properly remove particulate and colloidal materials as well as small pathogens and viruses (only UF) through a more compact process while providing a stable process performance. Thus, the treated water can meet the increasingly stringent drinking water regulations. However, membrane fouling caused by oxidized iron and manganese, especially colloidal

manganese oxides, limits the application of this process. Therefore, developing a pretreatment strategy, which can reduce the fouling rate of LPMs while providing an appropriate removal performance is of great interest. In addition, based on the results found for other inorganic particles (e.g., SiO_2 and TiO_2), the potential influence of water characteristics such as pH, ionic strength and salt valency on the extent of fouling caused by ferric hydroxide and manganese dioxide particles is anticipated to be important since these parameters could alter the particle size, charge and fractal dimensions as well as the membrane permeability. However, the impact of these parameters on ferric hydroxide and manganese dioxide particles characteristics has not been investigated, to the best of our knowledge. Furthermore, although the majority of LPMs currently in operation in the water industry are hollow fiber polymeric membranes or tubular ceramic membranes that are operated in a constant-flux mode, most of the publications focused on the fouling behavior of a simple flat-sheet membrane operating in a constant-pressure mode. However, these results are not expected to predict correctly the fundamental features of the filter cake properties as well as the rate and extent of fouling in full-scale plants. Consequently, understanding the characteristics and behavior of ferric hydroxide and manganese dioxide particles deposition on a tubular ceramic and hollow fiber polymeric UF/MF membranes while operating in a constant-flux mode is of interest for their application for iron and manganese control in drinking water.

Removal of Mn(II) through NGE process, sorption of Mn(II) onto manganese oxide coated media followed by catalytic oxidation of adsorbed manganese by chlorine, is an effective and economical method which attracted much attention from researchers over the past decades. Nevertheless, the process performance is strongly affected by the maintenance of available adsorption sites, which is governed by the manganese oxide coating level, chlorine concentration and pH. In addition to these parameters, HLR, temperature, calcium hardness, and initial Mn(II) concentration can further influence the process performance. However, their impacts have not been extensively documented. Moreover, in a continuous process, $MnO_{x(s)}$ coated sand has been solely packed in fixed-bed configuration comprising the following inconveniences:

- The adsorption sites cannot be used effectively due to the stationary state of the system;
- Susceptibility to clogging and rapid head loss buildup usually limit the process to low HLR with relatively high retention time;
- Frequent backwash is required, which results in a large amount of wastewater production;

- Poor fluid-solid contact and low HLR would result in relatively low mass transfer rate compared to fluidized bed, a situation which could limit the fixed bed operation to fairly low initial Mn(II) concentrations.

Accordingly, developing a process which can efficiently remove iron and manganese, from feed water containing high levels of these minerals, below the target limit of 0.02 mg/L and be operated at high HLR is of great interest. Operating at very high HLR would be beneficial for utilities since it reduces the process footprint as well as the capital cost. In this regard, this research project will evaluate the use of a hybrid process consisting of a PFB contactor followed by a UF membrane process.

3.2 Objectives and hypotheses

The main objective of this research project is to develop an integrated PFB-membrane hybrid process for improved iron and manganese control in drinking water (target limit of 0.02 mg Mn/L and 0.02 mg Fe/L in treated water).

On a more detailed level, the following specific objectives are defined:

1. Determine the characteristics (i.e., particle size distribution (PSD), ζ-potential and fractal dimension) of ferric hydroxide and manganese dioxide colloids/particles, which are generated during typical oxidation conditions prevailing in water of various physicochemical characteristics (i.e., pH, ionic strength and hardness);
2. Evaluate the performance of pre-oxidation-UF membrane process with respect to iron and manganese removal, and the extent of fouling under various water chemistry conditions;
3. Determine the fouling mechanisms and reversibility of the fouling in tubular ceramic and hollow fiber polymeric UF membranes;
4. Investigate the potential application of a PFB contactor to remove elevated concentrations of Mn(II) from groundwater down to below 0.02 mg/L while operating under high HLRs;
   - Evaluate the effects of key operational parameters such as feed manganese and chlorine concentrations, temperature, pH, hardness (Ca^{2+} concentration), and HLR (i.e., bed expansion) on PFB performance;
   - Assess the stability of the process over a long operational period;

5. Conduct a field pilot plant comparing the performances of a fixed vs. fluidized bed contactors for iron and manganese control on a natural groundwater during a long-term operation in order to demonstrate the feasibility of this process for small rural communities;

6. Compare the performance of a PFB-MF/UF membrane hybrid process with the conventional pre-oxidation-MF/UF membrane process (with respect to iron and manganese removal as well as fouling mitigation) under variable water chemistry conditions.

The objectives of this project are derived from the following research hypotheses:

1. Acidity (pH), ionic strength and hardness (Ca^{2+} concentration) have significant impact on the extent and reversibility of UF membrane fouling caused by oxidized iron and manganese species.

Originality: The influence of water chemistry conditions on the fouling of UF membranes caused by ferric hydroxide and manganese dioxide particles was never investigated.

2. The type of membrane (hollow fiber polymeric membrane vs. tubular ceramic membrane) has an impact on the characteristics of the cake layer and reversibility of fouling during UF of ferric hydroxide and manganese dioxide colloids/particles.

Originality: The influence of the two common membrane types, hollow fiber polymeric and tubular ceramic membrane, on UF fouling arising from ferric hydroxide and manganese dioxide colloids/particles was never investigated.

3. A PFB contactor can properly remove Mn(II) from feed water with elevated Mn(II) concentrations (typically > 1 mg/L). In the presence of adequate free chlorine residual, manganese removal through the PFB is not affected by the pH (6 - 8), HLR (20 - 60 m/h), and hardness (0 - 200 mg $CaCO_3$/L) of the feed water.

Originality: The performance of a PFB contactor for Mn(II) removal was never studied.

4. The PFB contactor can be operated continuously over a long time for iron and manganese control from natural groundwater while the head loss remains almost constant through the column.

Originality: The long-term rate of headloss accumulation in a PFB contactor for iron and manganese control in natural groundwater was never tested.

5. A hybrid membrane process combining a PFB and an UF membrane can properly reduce iron and manganese concentrations in groundwater to below 0.02 mg/L, for each of these minerals, while mitigates membrane fouling by more than 50%.

Originality: The novel integrated PFB-UF membrane process for iron and manganese control is proposed in this study, which has never been tested.

6. MF membrane is more susceptible to irreversible fouling than UF membrane due to the deposition of manganese dioxide colloids/particles inside the membrane pores or clogging of the pore mouth.

Originality: Comparison of MF and UF membrane fouling during filtration of ferric hydroxide and manganese dioxide colloids/particles has never been investigated.

3.3 Methodology

The experimental approach was conducted in four main parts:

1. Determine the characteristics of ferric hydroxide and manganese dioxide colloids/particles and the performance of ceramic and polymeric UF membranes with respect to iron and manganese control and membrane fouling (Obj. 1, 2 & 3) (Chapter 3 & 4);

2. Evaluate the performance of a lab-scale PFB contactor for manganese removal (Obj. 4) (Chapter 5);

3. Compare the performance of a field pilot-scale pyrolucite fixed vs. fluidized bed contactors for iron and manganese removal over long-term operation (Obj. 5) (Chapter 6);

4. Compare the performance of a PFB-MF/UF membrane hybrid process with the conventional pre-oxidation-MF/UF membrane process with respect to iron and manganese control and membrane fouling (Obj. 6) (Chapter 7).

The experimental protocol for each part is described in the following sections:

3.3.1 Characteristics of ferric hydroxide and manganese dioxide colloids/particles and the performance of ceramic and polymeric UF membrane

3.3.1.1 Characteristics of synthetic feedwater (SFW)

A fresh SFW was prepared prior to each experiment via addition of sodium chloride, calcium chloride dihydrate and sodium bicarbonate stock solutions to demineralized (DM) water to attain the final desired ionic strength (0.5, 1.0 and 10 mM), pH (6, 7 and 8) and hardness value (0, 100 and 317 mg $CaCO_3$/L). Table 3.1 summarizes the SFW compositions applied in this study, relevant to a typical natural water condition. Fe(II) (Fe(II) sulfate heptahydrate), Mn(II) (Mn(II) sulfate monohydrate) and oxidant ($KMnO_4$ or NaOCl) stock solutions were separately spiked into SFW.

Table 3.1. Characteristics of SFW.

Mn(II) (mg/L)	Fe(II) (mg/L)	Ca^{2+} hardness (mg $CaCO_3$/L)	Alkalinity (mg $CaCO_3$/L)	pH	Ionic strength (mM)	Temperature (ºC)
2.0	2.8	0 - 317	25	6 - 8	0.5 - 10	23 ± 1

3.3.1.2 Experimental set-up and procedure

The experimental setup consisted of oxidation and membrane filtration parts (Figure 3.1). In the oxidation part, Fe(II)/Mn(II) and NaOCl/$KMnO_4$ solutions were separately spiked into the SFW immediately before entering the oxidation column. The column was a 2-meter clear polyvinyl chloride (PVC) pipe with an inner diameter of 50.8 mm (2 in.) providing a retention time of 11.6 min for a flow of 350 mL/min. In all tests related to manganese removal, 2.0 mg Mn/L Mn(II) was oxidized by $KMnO_4$ to generate 5.3 mg/L particulate manganese dioxide, while for iron removal experiments, sodium hypochlorite was applied to oxidize 2.8 mg Fe/L Fe(II) to 5.3 mg/L ferric hydroxide particles. Effluent of oxidation column was collected after an hour of operation to analyze the characteristics of oxidized particles (i.e., PSD, ζ-potential and fractal dimension) and concentration of iron/manganese in water.

Table 3.2. Specifications of ceramic and polymeric UF membranes.

Manufacturer	Material	Surface area (cm^2)	MWCO[c] (kDa)	Permeability (LMH/bar)	pH stability	Temperature stability (ºC)	Pressure stability (kPa)
Norit (polymeric)	PES/PVP[a]	700	200	840	2-12	40	300
Atech (ceramic)	ZrO$_2$/Al$_2$O$_3$[b]	95	150	780	0-14	N.A.	1000

[a] Polyethersulfone/polyvinylpyrrolidone
[b] Zirconium dioxide/α-aluminum oxide
[c] Molecular weight cut off

Two UF membranes were operated in parallel in the membrane filtration part. The filtration experiments were conducted under dead-end constant-flux filtration mode. The specifications of each membrane are summarized in Table 3.2. Prior to each experiment, clean membrane resistance was determined by passing the DM water. Then, the particle-free SFW, under a specific pH, ionic strength and hardness, was filtered at the desired flux, until a steady pressure was obtained. The effluent from the oxidation column, was then introduced into the UF membranes an hour after initiation of the oxidation step. In all experiments, a constant flux of 200 LMH was applied for 150 min by a peristaltic pump (MasterFlex, Cole-Parmer Instrument) on each membrane. Permeate samples were taken at the initial and end of the experiment to measure the iron and manganese concentrations. The TMP was monitored every 15 s via a pressure transducer (Omega, PX409-030GUSB) applying a data acquisition software (TRH Central).
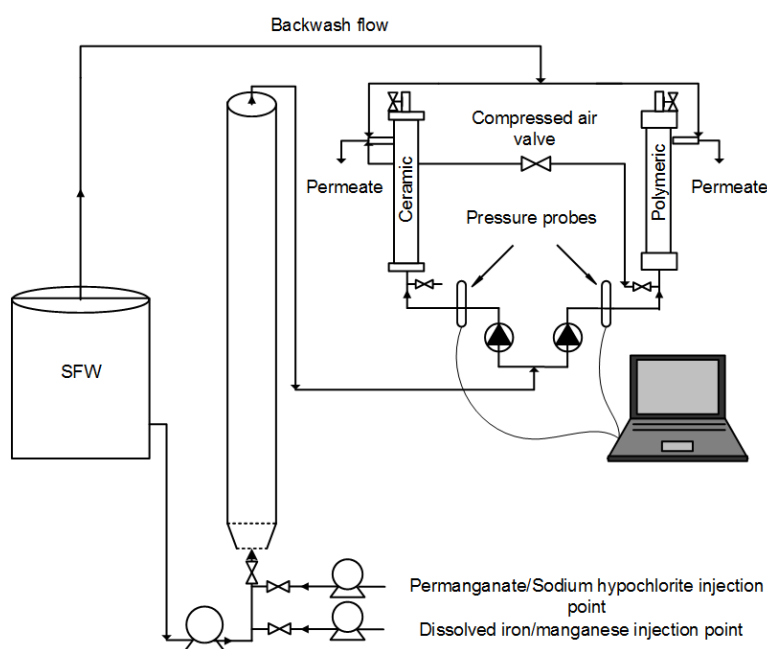
Figure 3.1. Schematic diagram of the bench-scale UF setup with peroxidation step.

At the end of each experiment, physical cleaning followed by a chemical cleaning were executed. Physical cleaning consisted of backwash with particle-free SFW and air scouring. Chemical cleaning was performed using a citric acid solution under elevated temperature. In this study, acid cleaning was found to be sufficient to recover the permeability of the membranes. Thus, the same membrane was used during the entire project.

3.3.1.3 Particle characterization

The size distribution of oxidized particles in membrane feed water were determined using DLS (Zetasizer Nano-ZS, Malvern, UK), LD (Mastersizer 3000, Malvern, UK) and serial membrane filtration techniques. DLS is well adapted to sub-micron colloids, while LD is well suited for determining the size of larger aggregates (> 1 µm) (Bowen, 2002). In fractionation through serial filtration technique, the iron and manganese concentrations were successively measured in filtrates from microfilters with pore sizes of 8 µm (CAT. NO. 09845D, Whatman[TM]), 3 µm (CAT. NO. SSWP04700, Millipore Corp.), 1.2 µm (CAT. NO. RAWP04700, Millipore Corp.), 0.45 µm (LOT NO. T41389, Pall Corp.) and 0.1 µm (LOT NO. T21020, Pall Corp.), as well as a 30 kDa (PVDF, Sterlitech Corp.) UF membrane. The Zetasizer Nano-ZS was also employed to determine electrophoretic mobility and ζ-potential of the particles using the Smoluchowski equation. Spatial structure of aggregates in terms of fractal dimension was also calculated from LD data obtained using the Malvern Mastersizer 3000. The samples were analyzed within 3 minutes of collection to diminish the possibility of further aggregation.

3.3.2 Performance of lab pilot-scale PFB contactor for manganese removal

3.3.2.1 Characteristics of synthetic groundwater (SGW)

Prior to each experiment, a volume of 200-400 L SGW was prepared using DM water. The alkalinity, hardness and Mn(II) concentration were adjusted using an appropriate amount of 0.5 M sodium bicarbonate, 0.5 M calcium chloride dihydrate and 0.1 M Mn(II) sulfate monohydrate stock solutions, respectively. Finally, the pH was adjusted by bubbling CO_2 and/or N_2 gas into the SGW. The following water quality and operational conditions were measured and controlled in each experiment: initial Mn(II) concentration (0.5 - 3.0 mg Mn/L), hardness (0 & 200 mg $CaCO_3$/L), temperature (9 & 23°C), pH (6.2 - 7.8) and HLR (24 - 63 m/h) (i.e., bed expansion (0 - 30%)). The characteristics of SGW applied in this study was summarized in Table 3.3.

Table 3.3. Characteristics of SGW.

Mn(II) (mg/L)	Ca^{2+} hardness (mg CaCO$_3$/L)	Alkalinity (mg CaCO$_3$/L)	pH	HLR (m/h)	Bed expansion	Temperature (°C)
0.5 - 3.0	0 & 200	200	6.2 - 7.8	24 - 63	0 - 30%	9 & 23

3.3.2.2 Experimental set-up and procedure

The PFB contactor had an inner diameter of 2.54 cm, which was filled up to 100 cm height with a commercially available pyrolucite (LayneOx™ brand). The physical properties of commercial pyrolucite are presented in Table 3.4. The column was covered with insulation material for experiments conducted at 9°C. Free chlorine concentration was controlled such that to provide an effluent free chlorine residual of 1 mg Cl$_2$/L by the addition of a diluted sodium hypochlorite solution. In order to determine the manganese removal profile, total and dissolved manganese concentrations were measured at different heights of the PFB (0, 5, 17.5, 25, 50, 75, 100, 110, and 150 cm from the bottom of the column). Mn(II) was defined as manganese filterable through 0.45 μm filter (CAT NO. HAWP02500, Millipore Corp.).

Table 3.4. Characteristics of commercial pyrolucite (LayneOx™ brand).

Effective size (D$_{10}$) (mm)	Mesh size	Uniformity coefficient (D$_{60}$/D$_{10}$)	Density (kg/m^3)	Bulk density (kg/m^3)	Porosity	Mn(II) uptake capacity (mg Mn/g media)
0.44	20×40	1.2	3850	2040	0.47	0.84

Short-term experiments were conducted for a period of 4 hours. Each experiment consisted of an hour acclimatization of the PFB with manganese-free SGW at the desired HLR that allowed cooling down the bed to 9°C. At time zero (t=0), a valve was switched to a drum containing Mn(II) and the first samples were collected. Additional samples were taken after 1, 2 and 4 hours of operation. At the end of each experiment, the PFB was expanded (up to around 50%) and rinsed with tap water for 10 min. In order to provide the same media condition for all tests, an overnight regeneration with 8-liter of recirculating chlorine solution (100 mg Cl$_2$/L) was conducted.

In order to determine the long-term stability of the PFB, assays were conducted for a period of 12 days. A schematic diagram of the experimental set-up is shown in Figure 3.2. In these experiments, SGW, which was renewed each 4 days, was continuously pumped into the bottom of the PFB. Free chlorine and Mn(II) stock solutions were injected into the water prior entering the column. Around

10% of the effluent water was discarded and the remainder was pumped into a granular activated carbon filter cartridge to remove the residual free chlorine and, then, returned back to the drum. pH, temperature, turbidity, and chlorine and manganese concentrations were controlled daily.
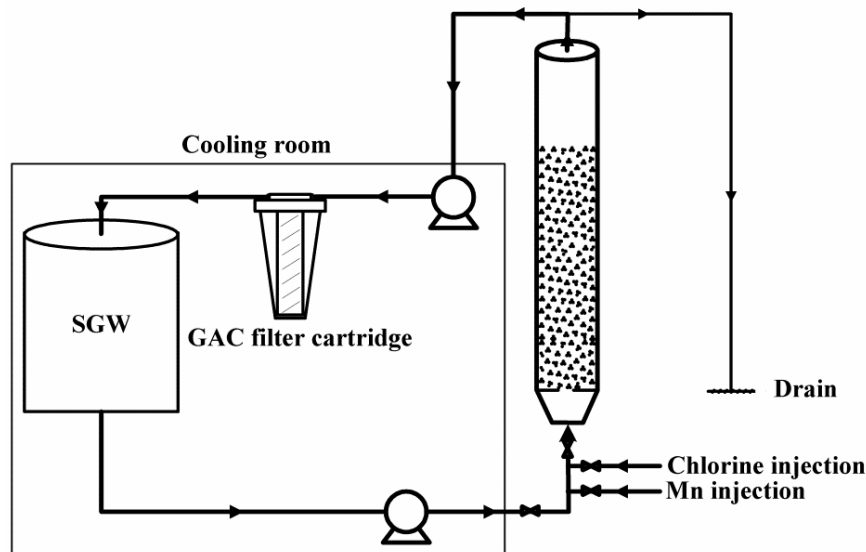
Figure 3.2. Schematic diagram of the long-term experimental plan.

3.3.3 Performance of pilot-scale pyrolucite fixed and fluidized bed contactors for iron and manganese removal

3.3.3.1 Characteristics of groundwater

The source water in this study was a natural groundwater supplying the community of Sainte-Marthe-sur-le-Lac, Quebec, Canada. However, in some experiments the feed water was enriched with Fe(II) or Mn(II) to determine the process performance under elevated concentration of these minerals. In this regard, Fe(II) sulfate heptahydrate or Mn(II) sulfate monohydrate stock solution was separately spiked into the natural groundwater before entering the columns. The feed water characteristics were regularly examined and summarized in Table 3.5.

Table 3.5. Characteristics of the groundwater tested in this study.

Iron (mg/L)	Manganese (mg/L)	Hardness (mg CaCO$_3$/L)	Alkalinity (mg CaCO$_3$/L)	pH	O$_2$ (mg/L)	DOC & TOC (mg C/L)	SUVA (L/mg/m)	Temperature (ºC)
0.01-0.18	0.09-0.35	200	170	7.0-7.2	1.9-2.9	3.3	1.9	8-12

3.3.3.2   Experimental set-up and procedure

The pilot plant was located at a groundwater treatment facility in Sainte-Marthe-sur-le-Lac, Quebec, Canada. A schematic of the pilot plant is shown in Figure 3.3. The columns were made of two identical clear PVC pipes with approximately 2.5 m length and 15.2 cm (6 in.) inner diameter, which were filled up to a height of 90 cm with the pyrolucite media (MangOx^{TM} brand). The characteristics of pyrolucite are listed in Table 3.6. The feed line was equipped with a static mixer to blend all the separately spiked solutions. In order to achieve an appropriate operation of the PFB, three different configurations of distributor plates were tested primarily: 1) a cap distributor plate (distributor A), 2) a shrouded perforated distributor plate filled with gravels of 10 mm in size and a 300 µm metal mesh on top of the plate (distributor B) and 3) an identical configuration as described for distributor B while the metal mesh on top of the plate was replaced by 15 cm gravels of 4-10 mm in size (distributor C). The best configuration was applied in the next part of the study.

Table 3.6. Characteristics of commercial pyrolucite (MangOx^{TM} brand).

Median diameter (D_{50}) (mm)	Uniformity coefficient (D_{60}/D_{10})	Mesh size	Specific gravity	Bulk density (kg/m^3)	Porosity	Manganese dioxide (% wt)
0.6	1.5	20×40	3.8	2000	0.47	86 %

Fluidized bed contactor. Natural groundwater was introduced into the bottom of the contactor at a flow rate of 30-45 m/h (12-18 gpm/ft^2) by a centrifuge pump (Natpro, Inc) and fluidized the media (bed expansion of 10-20%). Commercial bleach solution (4% (W/V) Cl$_2$/L) was continuously injected into the water prior entering the column at a flow rate that could maintain an effluent free chlorine residual of 1.0 mg Cl$_2$/L. Water samples were taken at different column heights (at distributor level and 7.5, 15, 30, 60, 100 and 110 cm above the distributor). Both total and dissolved (filterable through a 0.45 µm syringe filter (PVDF, CAT. NO. CS-GLPV3045)) iron and manganese concentrations were measured at each sampling point. A gauge pressure transducer (Omega, PX409-030GUSB) was mounted flush with the column wall right above the distributor plate for continuous recording of the pressure build-up within the bed over a 21 days of experimental period for each condition. At the end of each experiment, the fluidized bed was expended up to 40% for 20 min and the media was then fully regenerated with recirculation of 50-L NaOCl solution (1% (W/V) Cl$_2$/L) at the minimum fluidization condition for 24 hours.
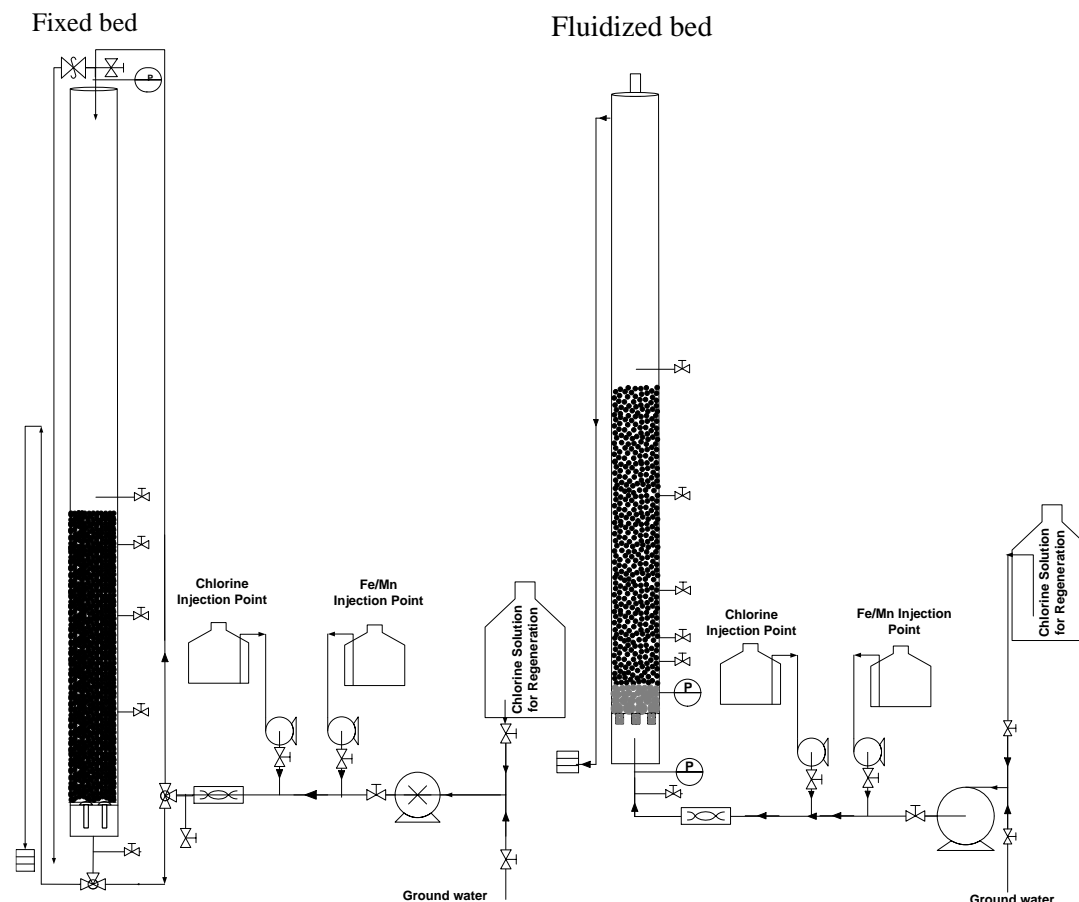
Figure 3.3. Schematic of pilot plant experimental set-ups. Left: Fixed bed. Right: Fluidized bed.

Fixed bed contactor. The fixed bed was identically operated to the fluidized bed. The differences could be listed as: (i) groundwater was fed to the top of the column with a gear pump (Natpro, Inc) providing a constant flow under all pressures over the 21 days of experimental cycle; (ii) the fixed bed was operated at HLR of 20 m/h; (iii) a pressure transducer (Omega, PX409-030GUSB) was installed on top of the contactor for continuous monitoring of the bed pressure drop, (iv) water samples were collected at 0, 6, 30, 60, and 90 cm from the top of the bed, (v) the fixed bed was backwashed when the upstream bed pressure raised to more than 0.5 bar. The backwashing step was executed for 20 min at 40% bed expansion using natural groundwater. In both columns, turbidity, pH, and free chlorine concentrations in the influent and effluent were also measured.

3.3.4 Performance of the PFB-MF/UF hybrid process compared to that of conventional pre-oxidation-MF/UF process

3.3.4.1 Characteristics of SFW

In this study, three different SFW characteristics, expected to have significant impact on the fouling of oxidized iron and manganese, were tested: 1) a soft water with negligible calcium concentration (hardness of 2 mg $CaCO_3$/L), 2) a moderately hard water with a calcium concentration of 40 mg/L (hardness of 100 mg $CaCO_3$/L) and 3) a moderately hard water (100 mg $CaCO_3$/L) in the presence of humic acids ($\approx$ 2 mg C/L). In the first step, an appropriate amount of sodium bicarbonate stock solution was added into the DM water to achieve the final alkalinity of 50 mg $CaCO_3$/L. For moderately hard water conditions, the calcium chloride dihydrate stock solution was added into the water. For experiments in the presence of humic acids, the concentration of humic acids was adjusted via addition of humic acids stock solution (Sigma-Aldrich, CAS NO. 68131-04) prepared with Milli-Q^{TM} water. Finally, the pH was adjusted at 7.0 by bubbling CO_2 and/or N_2 gas into the water. A fresh Fe(II) and Mn(II) stock solutions, 150 mg Fe^{2+}/L and 75 mg Mn^{2+}/L, were separately prepared and continuously spiked into the SFW prior entering the columns to achieve a final concentration of 2.6 and 1.3 mg/L in the feed water, respectively. Characteristics of the SFW are summarized in Table 3.7.

Table 3.7. Characteristics of the SFW tested in this study.

Iron (mg/L)	Manganese (mg/L)	Hardness (mg $CaCO_3$/L)	Alkalinity (mg $CaCO_3$/L)	pH	TOC (mg C/L)	SUVA (L/mg/m)	Temperature (ºC)
2.64 ± 0.12	1.29 ± 0.08	≈ 2 & 100	50	7.0	0.2 & 2.3	NA & 9.9	20

3.3.4.2 Experimental set-up and procedure

The experiments were conducted in a small pilot plant (Q = 0.5 m^3/d) located at Polytechnique Montreal. In the first set of the experiments, the MF and UF membranes were operated to establish the fouling behavior in the conventional peroxidation-MF/UF process. In the second set of the experiments, the MF/UF behavior was examined while using the PFB as a pretreatment process. A schematic of the PFB-MF/UF membrane experimental set-up is shown in Figure 3.4.
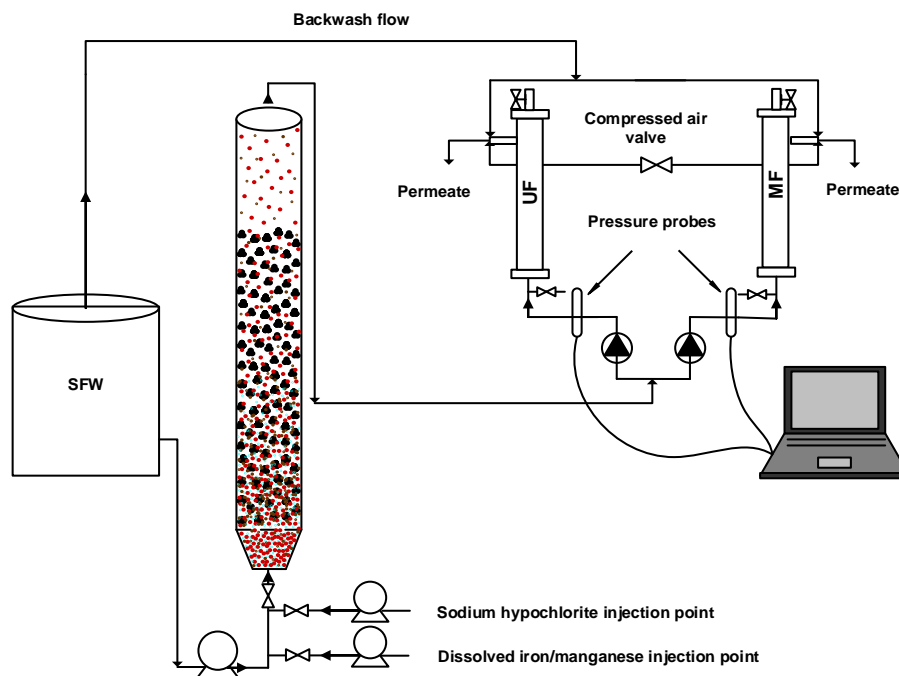
Figure 3.4. Schematic of the pilot-scale PFB- MF/UF hybrid process.

A fresh $KMnO_4$ (280 mg $KMnO_4$/L) or sodium hypochlorite (200 mg Cl_2/L) stock solutions were prepared for the pre-oxidation or PFB experiments, respectively, and spiked into the SFW immediately prior entering the columns. The oxidation column was a 2-meter clear PVC pipe with an inner diameter of 50.8 mm (2 in.) providing a retention time of 11.6 min for a total flow of 350 mL/min. The PFB column was a 2.5-meter clear PVC pipe with an inner diameter of 25.4 mm (1 in.), which was filled up to a height of 90 cm with pyrolucite media providing an empty bed contact time of 1.7 min for a total flow of 350 mL/min (HLR of 41 m/h (30% bed expansion)). In this process, the free chlorine dosage in the influent was adjusted such that to provide an effluent free chlorine residual concentration of 1.0 mg Cl_2/L. The PFB was operated for a period of 10 h for each experiment and the samples were taken at various heights of the bed (0, 9, 25, 50, 75, 100 and 120 cm from the bottom of the column). Total and dissolved (filterable through a 0.45 µm syringe filter (PVDF, CAT. NO. CS-GLPV3045, Chem Science Inc.)) iron and manganese concentrations were measured at each sampling point. Effluent from the oxidation or PFB columns were introduced to the MF/UF membranes after 1 and 4 h of operation, respectively.

Membrane experiments were conducted in dead-end, inside-out and constant flux configuration. Each membrane unit was equipped with a pressure transducer (Omega, PX409-030GUSB) that recorded the instantaneous pressure every 30 s using a data acquisition software (TRH Central).

Each MF/UF experiment successively consisted of: 1) filtration with DM water at the desired flux (150 or 300 LMH for the peroxidation-MF/UF process and 300 LMH for the PFB-MF/UF hybrid process), 2) filtration with particle-free SFW at the same flux, 3) filtration with the effluent of the columns for 6 h or until the TMP across the UF membrane increased to more than 170 kPa (25 psi), 4) physical cleaning (backwashing with particle-free SFW and air scouring), 5) determining the permeability of the particle-free SFW, 6) chemical cleaning (using oxalic acid and/or sodium hypochlorite solution), 7) rinsing with DM water, and 8) determining the clean water permeability of the membranes a day after the cleaning cycles. The same MF/UF membranes were used for all the experiments. Samples of membrane feed water and permeate were taken to measure the concentrations of iron, manganese, DOC and TOC.

3.3.4.3 Characterization of membrane fouling

Previous studies revealed that in many municipal and industrial solid-liquid separation via membrane filtration, the pressure increase profile in constant flux filtration mode can be described by the power-law compressible cake formation model (Sørensen and Sorensen, 1997; Chellam et al., 1998). Therefore, the constant flux blocking law model for compressible cake filtration (Eq. (1.21)) (Chellam and Xu, 2006) was applied in this study to describe the pressure increase behavior and the compressibility of the cake layer. The compressibility parameters, β and n', in this equation were estimated via fitting the experimental pressure data to Eq. (1.21) using a curve-fitting tool in Matlab (R2015a) with the smallest sum of squared residuals.

In addition, the resistance-in-series model (Eq. (2.1)) was also applied to provide further quantitative insight about the reversibility of the fouling and the effectiveness of cleaning methods.

$$J = \frac{\Delta P}{\mu\, R_t} = \frac{\Delta P}{\mu\,(R_m + R_{pr} + R_{cr} + R_{if})} \qquad (2.1)$$

where R_t is the total resistance (m^{-1}); R_{pr} is the physically reversible resistance (m^{-1}); R_{cr} is the chemically reversible resistance (m^{-1}); and R_{if} is the chemically irreversible fouling (m^{-1}).

These parameters were determined by:

R_m: measuring the particle-free SFW permeability of the membranes at the beginning of the experiment;

R_{pr}: the difference between the TMP of particle-free SFW after the physical cleaning step and the TMP at the end of filtration experiment;

R_{cr}: the difference between the stabilized TMP before and after the chemical cleaning step;

R_{if}: the difference between R_t and the sum of R_m, R_{pr}, and R_{cr}.

CHAPTER 4   ARTICLE 1 :   SIZE AND ZETA POTENTIAL OF OXIDIZED IRON AND MANGANESE IN WATER TREATMENT: INFLUENCE OF PH, IONIC STRENGTH AND HARDNESS

This chapter presents an article published in the Journal of Environmental Engineering, 142 (2016). The particle size distribution and ζ-potentials of ferric hydroxide and manganese dioxide, which were generated during typical oxidation conditions prevailing in waters of various physicochemical conditions (i.e., pH, ionic strength and hardness), were investigated in this study.

Size and Zeta Potential of Oxidized Iron and Manganese in Water Treatment: Influence of pH, Ionic Strength and Hardness

Seyedeh Laleh Dashtban Kenari[*] and Benoit Barbeau

Polytechnique Montreal, Department of Civil, Geological and Mining Engineering, NSERC-Industrial Chair on Drinking Water, Environment, C.P. 6079, Succursale Centre-Ville, Montreal, QC, H3C 3A7, Canada.

[*] Corresponding author: Tel: +1 514 340-4711 #2983; Fax: 514-340-5918;

E-mail: laleh.dashtban@polymtl.ca

ABSTRACT

Iron and manganese are commonly found in natural waters, particularly in groundwater. Due to the importance of particle size distribution (PSD) on the performance of removal processes, this research focuses on understanding the PSD and ζ-potentials of oxidized iron/manganese in water, as a function of pH, ionic strength and hardness. After rapid oxidation of dissolved iron/manganese, laser diffraction (LD), dynamic light scattering (DLS) and fractionation through serial membrane filtration techniques were used to define the PSD. For manganese dioxide, the ζ-potential was found to decrease as the pH decreased and as the ionic strength and hardness increased, resulting in a higher aggregate size. The aggregation rate of manganese dioxide strongly increased with hardness. On the other hand, ferric hydroxide PSD was not significantly altered by ionic strength or hardness at pH values relevant to typical natural waters. A combination of several techniques was found to be essential for providing a complete picture of the PSD. DLS and LD techniques were generally well adapted for nano-scale and micron-scale particles, respectively. The serial membrane filtration technique was suggested for water practitioners working toward the selection of an appropriate process for iron/manganese control in drinking waters.

KEYWORDS: Water treatment; Ferric hydroxide; Manganese dioxide; ζ-potential; Particle size distribution; Laser diffraction; Dynamic light scattering

4.1 Introduction

Iron and manganese naturally occur in both surface and ground waters as a result of weathering and leaching of metal-bearing minerals. Industrial wastewater has also been cited as a cause of water contamination by these minerals (United States Environmental Protection Agency (USEPA), 2004). Due to the more reducing redox conditions, groundwater commonly contains higher levels of dissolved iron (Fe(II)) and manganese (Mn(II)) than surface waters. The presence of iron and manganese in water mainly causes aesthetic and operating problems, including pipeline clogs, water discoloration, a metallic taste, odors, increased turbidity and the staining of laundry and plumbing fixtures, which may result in customer complains (World Health Organization (WHO), 2008). Furthermore, manganese has been claimed to be neurotoxic (Wasserman et al., 2006; Tuschl

et al., 2013). For these reasons, effective iron and manganese control is an important objective of drinking water treatment.

Among several methods that have been employed to control Fe(II) and Mn(II) in drinking water, one of the most common strategies is the chemical oxidation of dissolved species to particulate forms, ferric hydroxide and manganese dioxide, using an oxidant, followed by the removal of particles through depth media filtration. This is especially true in North America, where free chlorine is normally used to meet regulations on primary and secondary disinfection. Although Fe(II) is rapidly oxidized by free chlorine (Knocke et al., 1990), direct oxidation of Mn(II) by free chlorine is often unpractical because of the slow oxidation rate (Griffin, 1960; Knocke et al., 1990). Alternatively, potassium permanganate ($KMnO_4$), a powerful oxidizing agent, has been typically used for Mn(II) oxidation (Knocke et al., 1991; Phatai et al., 2010).

After Fe(II) and Mn(II) have been converted to solid forms via oxidation, the oxidized particles must be removed using a solid-liquid separation technique. Although a 0.45 µm filter is commonly being used in the laboratory to differentiate dissolved and particulate metals (American Public Health Association (APHA), American Water Works Association (AWWA) et al. 2005), the presence of very fine oxidized manganese was demonstrated in many research papers. The use of a 0.2 µm filter has been suggested by some authors (Reckhow et al., 1991; Sallanko et al., 2005), while 100 kilodalton (kDa) (Sallanko et al., 2005) or 30 kDa ultrafiltration (Carlson et al., 1997; Carlson and Knocke, 1999; Gregory and Carlson, 2001; Sallanko et al., 2005) was set as a limit for soluble, non-oxidized, manganese by others. In addition, iron and manganese colloidal oxides are commonly found on water purification membranes as foulants (Choo et al., 2005), even in reverse osmosis (RO) operations, where pre-treatment steps, such as manganese greensand or oxidation/filtration, have been applied to control iron and manganese levels in RO feed waters (Ning, 2009). Incomplete removal of colloidal iron and manganese particles in the pre-treatment steps may cause severe fouling problems for RO/NF plants.

Previous studies on inorganic minerals, namely bentonite and kaolinite (Vane et al., 1997), silica (Faibish et al., 1998), silicon carbide (Ramachandra Rao et al., 1999), titanium dioxide (Zhao et al., 2005) and aluminum salt (Duan et al., 2014), have illustrated the influence of pH, ionic strength and salt valency on the charge and size characteristics of these particles. Consequently, we hypothesize that the observed differences between the scientific literatures regarding the

fractionation of iron and manganese species are likely affected by the role of water chemistry on the surface charge and size of these particles. However, the importance of these parameters in water treatment systems has not been well documented.

Determining the particle size distribution (PSD) of oxidized iron and manganese is a key characteristic for developing an effective process to control these minerals. The objectives of this study are to (1) determine the ζ-potential and size distribution of ferric hydroxide and manganese dioxide, which are generated during typical oxidation conditions prevailing in waters of various physicochemical conditions, such as pH, ionic strength and hardness, and (2) to recommend a method to assess the PSD of iron and manganese oxides following the comparison of three techniques: laser diffraction (LD), dynamic light scattering (DLS) and fractionation through serial membrane filtration.

4.2 Materials and methods

4.2.1 Materials

All powdered chemicals were reagent grade (> 99% pure). NaCl, $CaCl_2.2H_2O$, $NaHCO_3$, $FeSO_4.7H_2O$ and $MnSO_4.H_2O$ were supplied by Fisher Scientific (Fair Lawn, NJ). Omni Trace® nitric acid (HNO_3, 67-70%) and $KMnO_4$ were purchased from EMD chemicals Inc. (Gibbstown, NJ). The concentration of $KMnO_4$ stock solution was adjusted to 130 mg/L. The commercial sodium hypochlorite (NaOCl, 8% (W/V) available chlorine) bleach solution was diluted to produce a stock solution (120 mg Cl_2/L). Ultrapure water (Milli-Q^{TM}) was used to prepare all stock solutions.

4.2.2 Synthetic water preparation

Synthetic waters were prepared at three ionic strengths (0.5, 1.0 and 10 mM), pHs (6, 7 and 8) and hardness values (0, 100 and 317 mg $CaCO_3$/L), which are relevant to typical natural water (river water and potable groundwater) conditions. All tests were conducted at $23 \pm 1°C$. Synthetic waters were prepared via addition of the following stock solutions to demineralized (DM) water. In all experiments, the alkalinity of synthetic water was first adjusted to 25 mg/L as $CaCO_3$, by addition of an appropriate amount of 0.5 M $NaHCO_3$ stock solution. Stock solutions of NaCl (0.5 M) and

$CaCl_2.2H_2O$ (0.5 M) were then used to regulate the salinity and hardness of the synthetic water. The pH of the synthetic water was finally adjusted by bubbling CO_2 and/or N_2 gas into the water.

Stock solutions containing 100 mg/L of Fe(II) or Mn(II) were prepared using $FeSO_4.7H_2O$ or $MnSO_4.H_2O$, respectively. These stock solutions served as sources of iron and manganese for the oxidation experiments (described later). To avoid oxidation of Fe(II) in the stock solution, ultrapure water was acidified to a pH of 3, and N_2 gas was then bubbled into the solution for 15 min prior to the addition of $FeSO_4.7H_2O$. This step was not needed for manganese, as preliminary tests confirmed that stable Mn(II) stock solution could be prepared by dissolution of $MnSO_4.H_2O$ in ultrapure water.

4.2.3 Experimental procedure

A 2-meter clear PVC pipe with a diameter of 50.8 mm (2 in.) was employed as a contactor column for oxidation of Fe(II)/Mn(II). The synthetic water was pumped into the column at a flow rate of 350 mL/min through a 1.27 mm (0.5 in.) inlet tube placed at the bottom of the column. Thus, the column provided an oxidation contact time of 11.6 min. $FeSO_4$ or $MnSO_4$ stock solutions and oxidation reagents were separately fed to the inlet tube after the synthetic water injection point. The last injection point was for the oxidants ($KMnO_4$ or Cl_2). To mix the reagents with the influent water, two small wire mesh screens (315 µm) were placed in the inlet tube, one after the oxidant injection point, and the other just prior to entering the column. The reason for conducting these experiments at the pilot- rather than the bench-scale was that UF membrane fouling was also studied. However, the UF results are beyond the scope of the current paper.

In all tests related to oxidized manganese characteristics, $KMnO_4$ was applied to oxidize 2.0 mg/L Mn(II) to 5.3 mg/L manganese dioxide (according to the stoichiometric reaction: $3Mn^{2+} + 2MnO_4^-$ $+ 2H_2O \Longrightarrow 5MnO_{2(s)} + 4H^+$) (Sommerfeld, 1999). However, in the case of Fe(II) oxidation, chlorination was used, as it is the most practical and cost effective method. NaOCl was injected to oxidize 2.8 mg/L Fe(II) to 5.3 mg/L ferric hydroxide (according to the stoichiometric reaction: $2Fe^{2+} + OCl^- + 5H_2O \Longrightarrow 2Fe(OH)_{3(s)} + Cl^- + 4H^+$) (Sommerfeld, 1999). After the oxidation step, the size distributions of particulate ferric hydroxide and manganese dioxide were analyzed for the various pH, ionic strength and hardness conditions. The samples were collected after the contact column reached a stable operating condition (one hour of operation). In total, seven conditions were tested for each metal while those with different pH and ionic strength were duplicated.

4.2.4 Particle size measurement techniques

Among different techniques for the particle size measurement, DLS and LD have become popular, as they rapidly measure the entire particle size distribution (Bowen, 2002). In addition to these methods, serial membrane filtration technique is the simplest option for general evaluation of particle size in suspensions although it is unable to provide detailed information about the PSD. Because the use of a single method is not recommended to characterize and identify the PSD (Bowen, 2002), oxidized iron and manganese were measured by applying these three analytical techniques. All samples were analyzed within 3 minutes of sample collection to reduce the possibility of further particle aggregation.

4.2.4.1 Light scattering

Two types of light scattering particle size analyzers: LD, also termed static light scattering, and DLS, also termed photon correlation spectroscopy, were used to measure the PSD of oxidized iron and manganese in water. In both techniques, a signal generated from the ensemble of particles in suspension is measured, and the scattered light intensities are interpreted using light scattering theory to determine a PSD that caused the observed scattering. Applying both techniques is necessary to cover a larger range of particle sizes. For both measurements, the real and imaginary parts of the refractive index for manganese dioxide were set to 2.4 (Malvern Instruments Ltd., 1997) and 0.01 (Gillespie Lindberg, 1992), respectively, while these values were defined to be approximately 2.2 (Malvern Instruments Ltd., 1997) and 0.07 (Sherman and Waite, 1985) for ferric hydroxide particles. In this study, both number size distribution and volume size distribution results are used for comparison. Volume distribution is proportional to the third power of the particle diameter (d^3), while the number distribution is proportional to d (Xu, 2000).

These methods have certain limitations which should be taken into account (Bowen, 2002; Dieckmann et al., 2009). To generate an accurate size distribution, the LD method must be applied to samples with relatively low concentration of particles in order to minimize the multiple scattering (CPS Instruments Europe). Accordingly, in LD experiments, the oxidized water samples were diluted with the equivalent synthetic water without Fe(II)/Mn(II), achieving a laser obscuration of 1 to 2%. The samples were then analyzed with a Mastersizer 3000 (Malvern Instruments Ltd., UK) which allows size determination from 0.01 µm to 3500 µm. However, a better accuracy is expected

for larger particles compared to submicron ones (Bowen, 2002). Ten consecutive measurements were performed to ensure the repeatability of the particle size over the course of an analysis.

The DLS experiments were conducted on a Zetasizer Nano-ZS (Malvern, UK). It was equipped with a He-Ne laser, which operated at a 633 nm wavelength, and a digital correlator. Although PSD from 0.4 nm to 10 µm can be measured with this equipment, it is better suited to analyze a narrow PSD ranging from approximately 1 to 500 nm (Bowen, 2002; Dieckmann et al., 2009). The samples were directly injected into the appropriate cell and measurements were executed at a fixed scattering angle of 173°. Three consecutive measurements were conducted to ensure repeatability.

4.2.4.2 Fractionation through serial membrane filtration

For this test, the concentrations of iron and manganese were successively measured in filtrates from microfilters with pore sizes of 8 µm (CAT. NO. 09845D, Whatman[TM]), 3 µm (CAT. NO. SSWP04700, Millipore Corp.), 1.2 µm (CAT. NO. RAWP04700, Millipore Corp.), 0.45 µm (LOT NO. T41389, Pall Corp., USA) and 0.1 µm (LOT NO. T21020, Pall Corp., USA), as well as a 30 kDa (PVDF, Sterlitech Corp., USA) ultrafiltration membrane. The samples were vacuum filtered through microfiltration membranes, while a 50 mL pressurized cell (Amicon 8200 device) was employed for the ultrafiltration membrane. The ultrafilter cell was pressurized to approximately 240 kPa (35 psi) using nitrogen gas. Prior to each experiment, the 30 kDa membrane was soaked overnight in ultrapure water. Then, 50 ml of ultrapure water was used to rinse the filter. The microfiltration membranes were rinsed by filtering 500 ml of ultrapure water before use.

The concentrations of iron and manganese were measured in filtrates by inductively coupled plasma-optical emission spectrometry (ICP-OES, model iCAP 6000), following heat and acid digestion with 0.5% HNO_3 (Omni Trace® grade, pH < 2) at 80 °C for 48 h. The pH analysis was performed with an UltraBasic pH meter (model UB-5 from Denver Instrument).

4.2.5 Zeta potential analysis

The Zetasizer Nano-ZS (Malvern, UK) was also employed to measure the ζ-potential of the particles using phase analysis light scattering. In this method, the ζ-potential is calculated from the measured electrophoretic mobility of the particle in a well-defined electrolyte using the Smoluchowski equation. All measurements were performed in triplicate. The results were averaged and the standard deviation is reported.

4.3 Results and discussion

The following sections present the experimental results obtained for the PSDs of iron and manganese after oxidation under various water conditions. The PSD results provided by the LD, DLS and serial filtration techniques are compared for oxidized manganese under various water qualities. A comparison with oxidized iron is then presented.

4.3.1 Effect of pH on particle size of oxidized manganese in water

The effect of pH on the PSD of manganese dioxide was evaluated in the absence of hardness using the serial membrane filtration technique (Figure 4.1). The size fractions of manganese dioxide differed depending on the pH conditions. Higher pH values produced more colloidal MnO_2. For example, at pH 8.0, almost all particles were found in the size fraction between 0.1 µm and 30 kDa, while approximately 75% of manganese dioxide particles were in the range of 0.1 µm to 0.45 µm at pH 7.0. At the lower pH of 6.0, more than 30% of particles were larger than 0.45 µm.
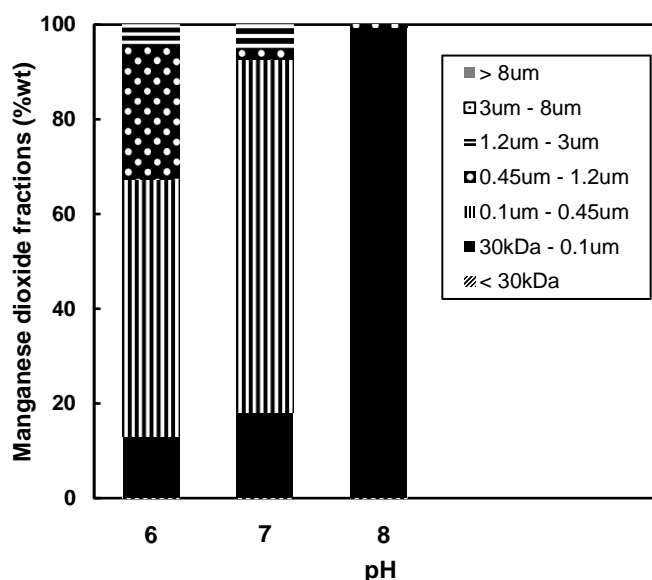
Figure 4.1. Size fractions of manganese after oxidation at different pH values using membrane filters.

The observed changes in manganese dioxide particle size are consistent with expectations. The average ζ-potentials measured for oxidized iron and manganese particles are summarized in Table 4.1 for each specific water condition investigated. Manganese dioxide particles are always negatively charged in natural waters because their isoelectric point (IEP), or point of zero charge,

is below pH 3 (Morgan and Stumm, 1964). As pH values increased from 6.0 to 8.0, the more negatively charged surfaces (from -36.4 ± 2.1 mV to -45.5 ± 2.1 mV) provide higher electric double layer (EDL) repulsions between the particles, which diminish particle aggregation. Although a slight aggregation of colloids was observed at pH 6.0, they were stable and highly dispersed considering the relatively high ζ-potential of -36.4 ± 2.1 mV. A visual inspection of the suspensions, which remained clear with no sediment, confirmed this conclusion.

Table 4.1. Comparison of apparent ζ-potential of ferric hydroxide and manganese dioxide particles under various water characteristics.

Particle type	pH	Ionic strength (mM)	Hardness (mg CaCO$_3$/L)	Conductivity (mS/cm)	ζ-potential (mv)
Manganese dioxide	6	0.5	0	0.061	-36.4 ± 2.1
	7	0.5	0	0.060	-42.9 ± 2.3
	8	0.5	0	0.057	-45.5 ± 2.1
	7	1	0	0.122	-41.6 ± 1.7
	7	10	0	1.220	-37.2 ± 0.6
	7	10	100	1.107	-12.8 ± 0.4
	7	10	317	0.945	-3.7 ± 0.1
Ferric hydroxide	6	0.5	0	0.068	6.6 ± 0.2
	7	0.5	0	0.068	1.6 ± 0.2
	8	0.5	0	0.067	-1.4 ± 0.3
	7	1	0	0.130	-0.9 ± 0.2
	7	10	0	1.263	1.4 ± 0.1
	7	10	100	1.155	4.9 ± 0.1
	7	10	317	0.967	7.5 ± 0.8

Figure 4.2A-C illustrates the number and volume size distribution of manganese dioxide at various pH levels, as measured using the DLS and LD techniques. In both methods, a monomodal distribution is observed under all pH conditions. As observed in the serial filtration experiments, the peak of the PSD shifts toward larger sizes as the pH is reduced from 8.0 to 6.0. As expected, the volume distribution is slightly skewed toward larger particle sizes, which contribute much more volume per particle.
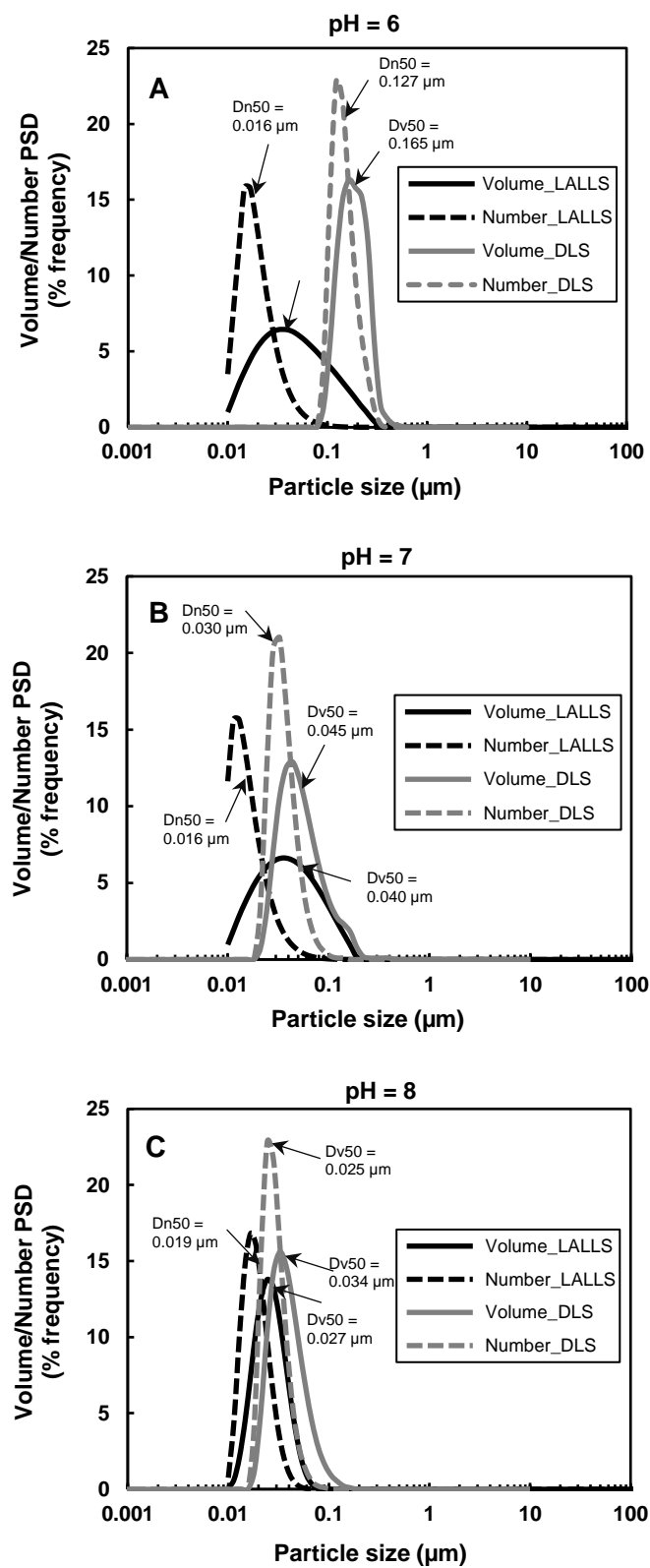
Figure 4.2. Comparison of PSD for manganese dioxide at different pH values measured by DLS and LD,

A) at pH = 6, B) at pH = 7, C) at pH = 8.

Under all pH conditions, LD illustrates the presence of very fine colloids, which were not detected by DLS. Based on the DLS method, the light scattered by colloids/particles in suspension is related to the diffusion coefficient, which can be further related to the hydrodynamic diameter of the particle (Weiner, 1992). In this regard, the diameter reported by DLS is the hydrodynamic diameter, which is quite similar to the geometric diameter of the particle. However, the highest discrepancy was found for small, highly charged particles, in which the EDL yields a larger allocated diameter (Bowen, 2002). Thus, the resultant particle size by DLS includes the stabilizer shell, which is more pronounced for sub-100 nm size particles, as previously stated (Safari et al., 2014). Another reason for the observed discrepancy between DLS and LD results may be related to the non-spherical particle shape assumed by LD, while DLS assumes spherical particles.

If one assumes that the particle density is independent of particle size, the volume distribution achieved by the two laser-based methods can be compared with the mass fractions obtained by the serial membrane filtration technique. Based on the DLS results, at pH 6.0 (Figure 4.2A), the curve illustrates a single band in the range of 91 to 531 nm, having a volume median particle size (Dv50) of 165 nm. At pH 7.0 (Figure 4.2B), the diameters of the particles range from 21 to 396 nm, with a Dv50 of 45 nm. For pH 8.0, a much narrower size distribution was observed, in the range of 18 to 142 nm, with a Dv50 of 34 nm (Figure 4.2C). The polydispersity index, an indication of the homogeneity of a sample, were always < 0.3, which suggests that the particle size values obtained by DLS were reliable. These results are generally consistent with the size ranges obtained via the serial membrane filtration technique (Figure 4.1), which reveals at pH 6.0 and 7.0, 67% and 93% of particles are in the range of 30 kDa and 450 nm , respectively, and at pH 8.0, 99% of particles are smaller than 100 nm.

On one hand, the DLS measurement overestimates the size of fine colloids (sub-100 nm), as confirmed by previous studies (Orts-Gil et al., 2011; Safari et al., 2014). However, on the other hand, the LD measurements had a lower sensitivity to size variations in nano-size ranges (Figure 4.2A-C). The results obtained by DLS and serial membrane filtration techniques are relatively comparable, and better encompass the size variations. Previous studies have similarly concluded that the DLS method gives rise to more accurate results for sub-500-nm particles, while the LD is better suited for particle size measurements in micron range (Bowen, 2002; Dieckmann et al., 2009). Although the discrepancies are often observed between the results from different particle size measurement techniques, applying several techniques is useful for acquiring

information regarding the particle size distribution, as limitations were consistently encountered with each method. Previous studies by Bowen (2002) and Dieckmann et al. (2009) also support this conclusion.

4.3.2 Effect of ionic strength on particle size of oxidized manganese in water

The influence of ionic strength (or salinity) on the colloidal manganese dioxide stability was investigated after oxidation of Mn(II) by $KMnO_4$. In these experiments, the ionic strength of water was adjusted using variable amounts of a 0.5 M NaCl stock solution. According to the serial filtration analysis (Figure 4.3), upon increasing the ionic strength by 20-fold, larger particles were observed. This indicates the occurrence of some aggregation, as a result of the reduction in the electrostatic forces stabilizing the colloidal particles. However, these aggregates are still in the nano-size range, and even at an ionic strength of 10 mM, more than 10% of manganese dioxide was smaller than 0.45 µm. The ζ-potential of manganese dioxide particles was measured as a function of ionic strength (Table 4.1). As indicated in Table 4.1, the ζ-potential becomes less negative, from -42.9 ± 2.3 to -37.2 ± 0.6, as the ionic strength increases from 0.5 mM to 10 mM, implying a partial screening of the negative charges by the cationic species, i.e., Na^+. However, these changes were not very pronounced in the presence of monovalent salt (NaCl) at concentrations typically occurring in natural waters.
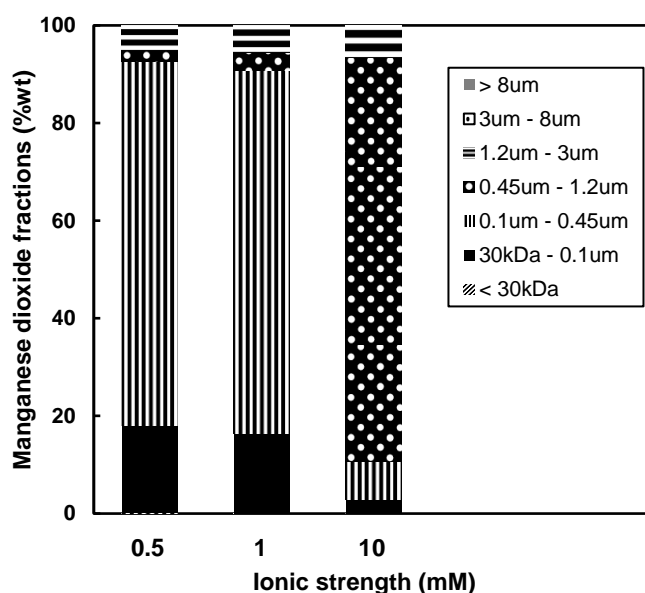
Figure 4.3. Size fractions of manganese after oxidation at different ionic strength using membrane filters.

The PSDs (by volume and number) of manganese dioxide particles measured by DLS and LD are presented in Figure 4.4A-C for increasing ionic strengths. A comparison between DLS and LD results shows that the DLS measurement overestimates the size of the smaller colloids. However, the size distribution curves obtained by LD at different ionic strengths overlap (except for the small peak in volume size distribution at an ionic strength of 10 mM), implying that the LD did not provide enough sensitivity in this size range to monitor the small particle growth achieved after increasing the ionic strength. This observation is coherent with the lower accuracy of LD for sub-micron particles (Bowen, 2002), especially when a blue light measurement is not performed (Mastersizer 3000 user manual 2011). Based on DLS results, the Dv50 values were 45 nm, 54 nm and 133 nm for ionic strengths of 0.5 mM, 1 mM and 10 mM, respectively. Likewise, the number size distribution obtained by DLS also shifted toward greater diameters as the ionic strength increased. The observed shift in number distribution confirms the growth in particle size because the number size distribution is sensitive to growth only when the size of a majority of the particle population increases. For all conditions tested, the polydispersity indices of the DLS measurement remain < 0.3.

At the high ionic strength of 10 mM, a bimodal volume size distribution was observed using both laser techniques, indicating a partial aggregation of manganese dioxide particles (Figure 4.4C). However, the greatest volume contribution originated from the nano-sized particles. In addition, the peak of micron-sized particles was undetected when data were presented as number size distributions, demonstrating a very low population of these particles.
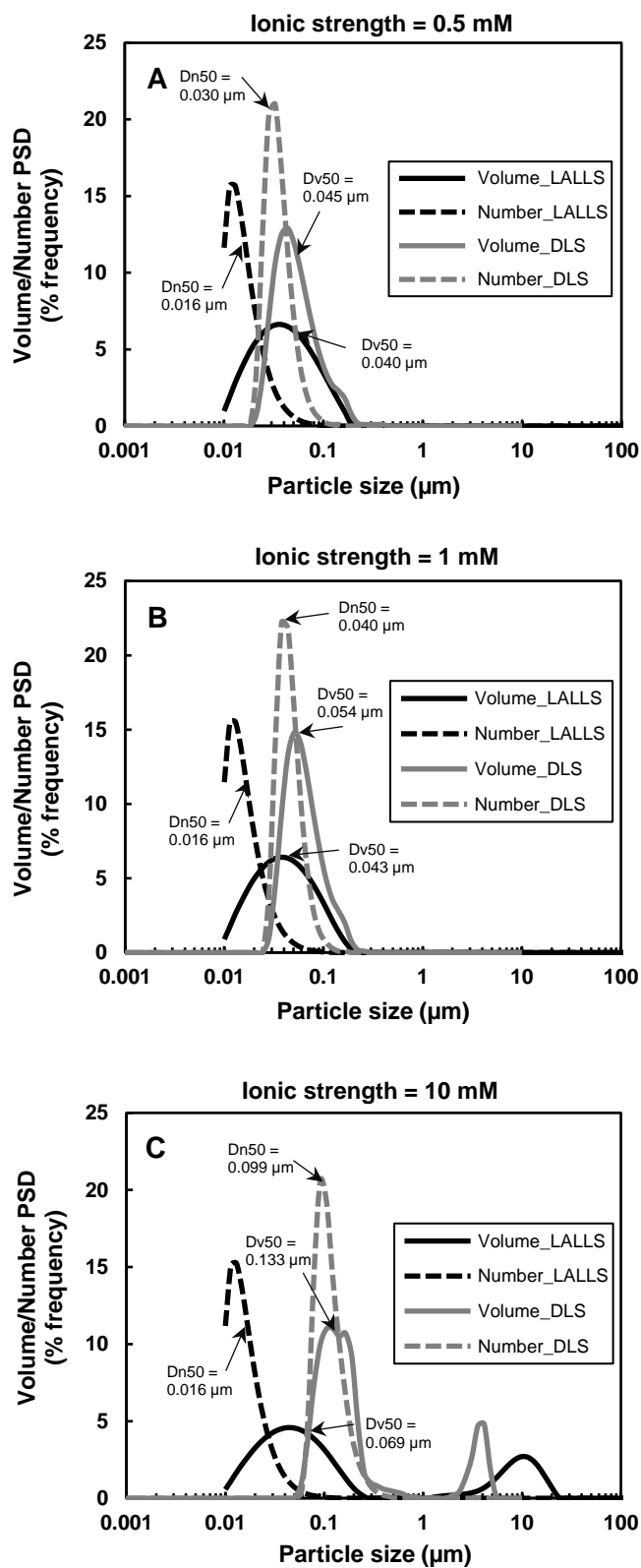
Figure 4.4. Comparison of PSD for manganese dioxide at different ionic strength measured by DLS and LD, A) at 0.5 mM, B) at 1 mM, C) at 10 mM.

4.3.3 Effect of hardness on particle size of oxidized manganese in water

For investigating the effect of hardness on the size fractions of manganese dioxide, oxidation of Mn(II) with $KMnO_4$ was conducted in waters with increasing concentrations of $CaCl_2$, at a constant ionic strength of 10 mM and pH 7.0. The concentrations of $CaCl_2$ in water were set at 0, 1 and 3.17 mM, corresponding to Ca^{2+} hardness values of 0, 100 and 317 mg $CaCO_3$/L.
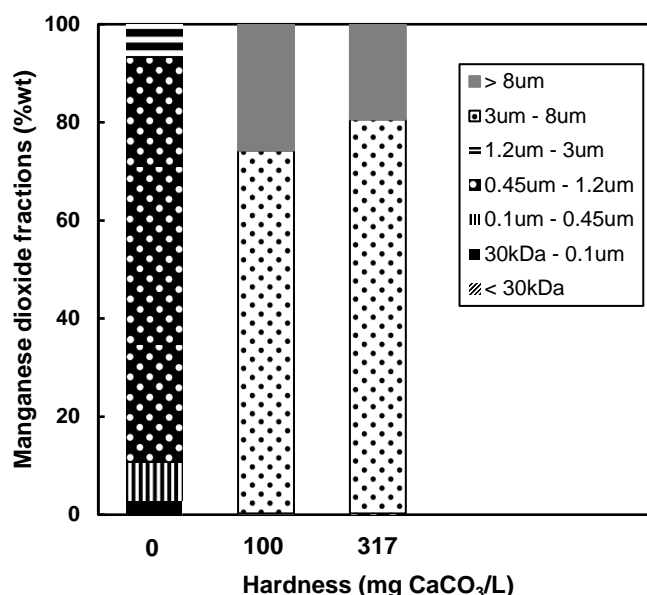
Figure 4.5. Size fractions of manganese after oxidation at different hardness of water using membrane filters.

As shown in Figure 4.5, comparing manganese dioxide particle diameters in NaCl and $CaCl_2$ electrolyte backgrounds, i.e., hardness values of 0, 100 and 317 mg $CaCO_3$/L, indicates that the particle size in moderately hard to very hard waters is several folds greater than for soft waters. The ζ-potential of manganese dioxide particles (Table 4.1), which decreased from -37.2 ± 0.6 to -12.8 ± 0.4 and -3.7 ± 0.1 by increasing the hardness of water from 0 to 100 and 317 mg $CaCO_3$/L, respectively, is coherent with this result. Thus, the dispersion of manganese dioxide particles is very sensitive to changes in the valency of the background salts, and agglomeration occurs due to the reduction in the energy barrier between two approaching particles. According to the serial filtration technique (Figure 4.5), the particles are typically present in the range of 0.45 to 1.2 µm in the absence of Ca^{2+} ions. Primary colloids, with sizes < 0.1 µm, and larger aggregates, with sizes > 1.2 µm, also contribute to the PSD. These observations are in general agreement with

the bimodal volume size distribution obtained by LD (Figure 4.6) in the absence of hardness, indicating an incomplete aggregation of the smaller colloids. However, the number size distribution suggests that the population of micron-sized aggregates is not significant. For the two higher hardness conditions, a monomodal distribution with a very large Dv50 shift, to several tens of microns, was measured which illustrates the agglomeration's growth with increased hardness. Based on LD results, the peaks of volume size distribution were found at diameters where nearly no particles were characterized by the number size distribution. The ranges obtained by the number size distribution (0.87 to 27.4 µm at a hardness value of 100, and 1.13 to 40.1 µm at a hardness value of 317 mg $CaCO_3$/L) are in good agreement with the serial filtration method as it reveals that the majority of particles were actually in the 3 to 8 µm diameter range. Thus, although the volume PSD is often used to characterize powders, the number-based PSD is less sensitive to analytical imprecision as it is proportional to d rather than d^3.
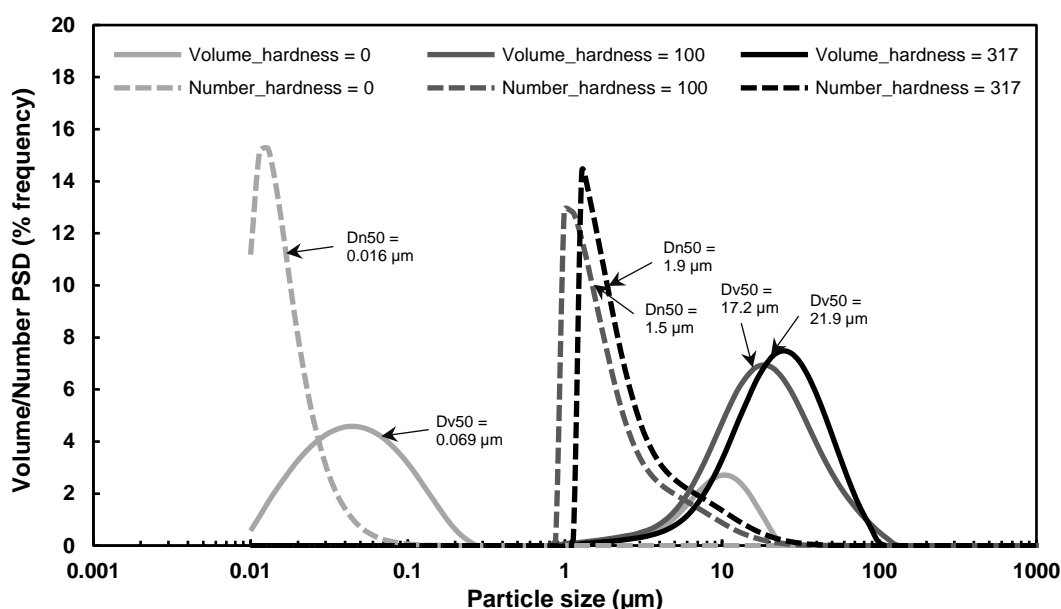
Figure 4.6. Comparison of PSD for manganese dioxide at different hardness (mg $CaCO_3$/L) of water measured by LD.

The DLS did not allow for measurement of the PSD at hardness values of 100 and 317 mg $CaCO_3$/L. This was due to the presence of large aggregates, with high polydispersity indices (> 0.8), and interference from sedimentation. As larger particles have a slower Brownian diffusion rate, a longer analysis time is needed, which may give rise to sedimentation. In addition, it is important to have a sufficient concentration of large particles to remain above the baseline. This is

typically difficult to achieve for particles larger than 500 nm, as particle-particle interactions at higher concentrations can have drastic effects on the analysis (Weiner, 1992). Nevertheless, this result confirms extensive aggregation of manganese dioxide colloids in hard waters, as observed with the other two methods.

4.3.4 Effect of pH, ionic strength and hardness on particle size of oxidized iron in water

In natural waters, iron commonly co-occurs with manganese. However, to better understand the characteristics of oxidized iron particles, Fe(II) was separately oxidized by sodium hypochlorite in synthetic waters having the same characteristics (pH, ionic strength and hardness) as previously mentioned. An Eh-pH stability diagram indicates that the dominant thermodynamically stable species are ferric hydroxides under a pH range of 6.0 to 8.0 and in the presence of an oxidant (Trudinger and Swaine, 1979).
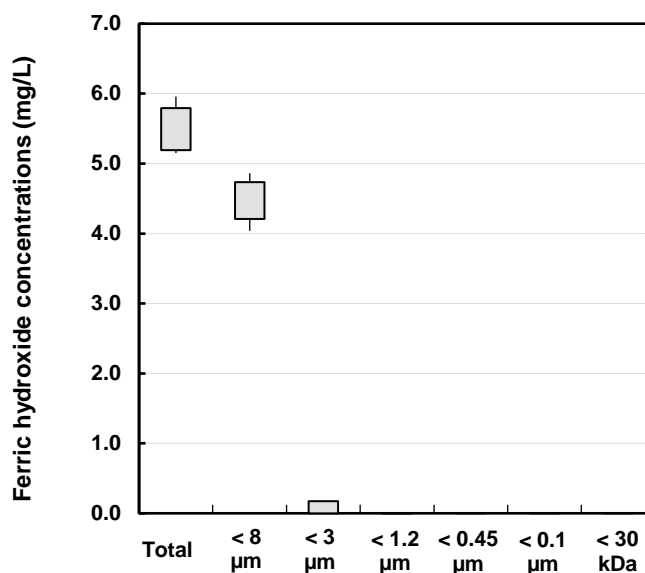
Figure 4.7. Size fractions of iron in water after oxidation with sodium hypochlorite at different pH, ionic strength and hardness.

Unlike manganese dioxide, the results obtained for ferric hydroxide particles using the serial filtration technique and based on various water characteristics do not significantly differ from one another. Likewise, no significant variation in the turbidity of the oxidized samples was observed (results not shown). As shown in Figure 4.7, all ferric hydroxide particles are on the micron scale,

and more than 80% (wt) are in the size range between 3 and 8 µm. These results are in general agreement with the nearly zero ζ-potential achieved for different water quality conditions, implying the rapid aggregation of ferric hydroxide particles. In Table 4.1, the IEP for ferric hydroxide was found to be between a pH of 7 and 8, a result coherent with previous reports, indicating pHs of 7.5-8.2 (Genz et al., 2004) and 7.5 (Kosmulski, 2009).

LD can potentially provide more informative results than the serial filtration technique regarding the ferric hydroxide PSD. Figure 4.8 compares the number and volume size distribution results obtained for various water characteristics (pH, ionic strength and hardness). Independent of the pH (Figure 4.8A) or ionic strength (Figure 4.8B) applied in this study, the PSDs were nearly identical. This result is consistent with observations for iron oxyhydroxide (Gilbert et al., 2007) and titanium dioxide (French et al., 2009) nanoparticles. In contrast, increasing the Ca^{2+} concentration (Figure 4.8C) led to a shift in the number size distribution toward larger particle diameters, indicating a higher aggregation rate. The ζ-potential for ferric hydroxide at pH 7 increased from 1.4 ± 0.1 to 4.9 ± 0.1 and 7.5 ± 0.8 mV by increasing the Ca^{2+} concentration from 0 to 1 and 3.17 mM, respectively. Therefore, the higher aggregate growth rate is not due to a charge neutralization mechanism. The bridging of Ca^{2+} cations between ferric hydroxide particles is most likely responsible for this phenomenon (Elimelech et al., 1995)

Increasing the Ca^{2+} hardness from 0 to 100 and 317 mg $CaCO_3$/L led to a significant shift in the volume size distributions. At a hardness value of 317 mg $CaCO_3$/L (Figure 4.8C), the entire volume size distribution is characterized by diameters larger than 240 µm, with a Dv50 of 1000 µm. However, results obtained via serial filtration reveal that the majority of particle diameters actually ranged between 3 and 8 µm (80%), which is in good agreement with the number size distribution obtained by LD (82%). Therefore, the use of the number PSD is recommended while using LD for characterizing agglomerating systems such as flocculation.
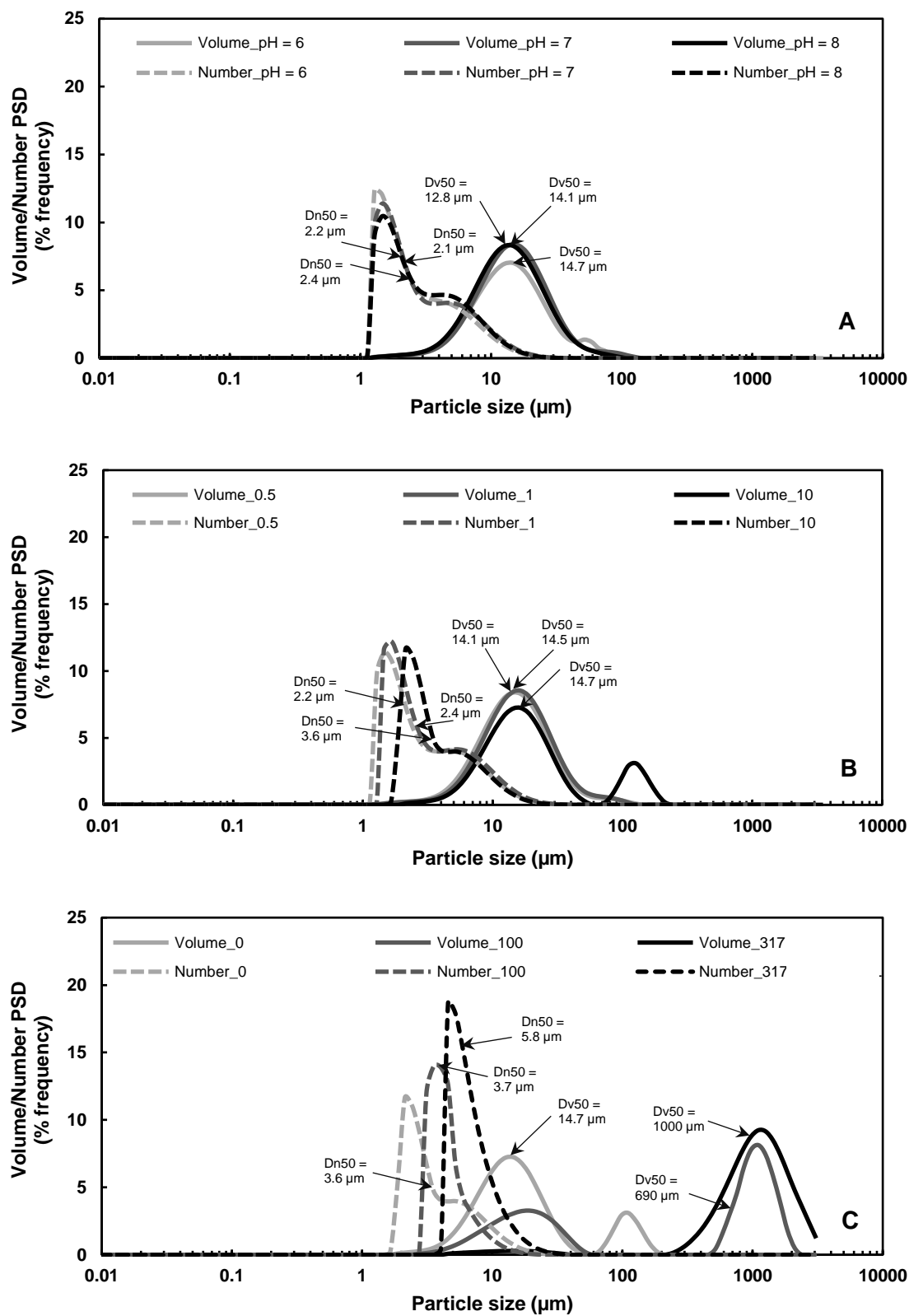
Figure 4.8. Comparison of PSD for ferric hydroxide at different water characteristics measured by LD, A) Effect of pH, B) Effect of ionic strength (mM), C) Effect of hardness (mg CaCO$_3$/L).

4.4 Conclusions

The present contribution comprises two parts: first, the effects of pH, salinity and hardness on the stability and size fractions of oxidized iron and manganese in water treatment systems were analyzed; second, the size results obtained using LD versus DLS, as well as fractionation through a series of membrane filters were compared.

- The pH, ionic strength and salt valency (i.e., Ca^{2+} vs. Na^+) affect the ζ-potential, and consequently, the size of manganese dioxide in water. Destabilization of colloidal manganese dioxide is mainly induced by charge neutralization. Under conditions relevant to water treatment, the sensitivity of the ferric hydroxide surface charge and particle size to pH and ionic strength is negligible.

- Among the studied parameters, the concentration of Ca^{2+} (hardness of water) strongly governs the destabilization of colloidal manganese dioxide, as micron-sized aggregates were formed in hard waters. Thus, the oxidative removal of manganese from groundwater with elevated Ca^{2+} should be easier than surface waters with low hardness values. In addition, the results imply that the addition of lime, rather than caustic soda, should be used for pH adjustment in systems practicing pH increases prior to coagulation followed by oxidation prior to filtration.

- The oxidative removal of manganese is more problematic than iron due to the formation of colloidal manganese as small as several tens of nanometers, especially in the case of soft waters with low salinity and high pH.

- For stabilized inorganic colloids, such as manganese dioxide in the absence of divalent cations, DLS detects nanoparticles, including the shell, which creates uncertainties regarding the onset of the PSD. This technique also suffers from the effect of polydispersity and the presence of aggregates. However, it is well adapted to sub-micron particles with narrow size ranges.

- Since it offers lower sensitivity and accuracy in the sub-micron ranges, the LD method is generally more suitable to characterize micron-sized particles. However, in agglomerating systems, the results must be interpreted with great care, and comparison with other methods is advised.

- Serial filtration technique is recommended as a simple option for general evaluation of particle size because (i) the availability of both laser based technique is not that common in the water industry and (ii) this method proved to be adequate to characterize the PSD.

Acknowledgments

CHAPTER 5 ARTICLE 2 : UNDERSTANDING ULTRAFILTRATION FOULING OF CERAMIC AND POLYMERIC MEMBRANES CAUSED BY OXIDIZED IRON AND MANGANESE IN WATER TREATMENT

This chapter presents an article published in the Journal of Membrane Science, 516 (2016). In this work, removal of iron and manganese and the associated fouling during the peroxidation-UF membrane process were investigated. The performance of ceramic versus polymeric UF membrane were subsequently compared applying constant flux blocking law model. In addition, the resistance-in-series model was adopted to quantitatively analyze the effectiveness of cleaning processes and reversibility of fouling.

Understanding Ultrafiltration Fouling of Ceramic and Polymeric Membranes Caused by Oxidized Iron and Manganese in Water Treatment

Seyedeh Laleh Dashtban Kenari[*] and Benoit Barbeau

Polytechnique Montreal, Department of Civil, Geological and Mining Engineering, NSERC-Industrial Chair on Drinking Water, Environment, C.P. 6079, Succursale Centre-Ville, Montreal, QC, H3C 3A7, Canada.

[*] Corresponding author: Tel: +1 514 340-4711 #2983; Fax: 514-340-5918;

E-mail: laleh.dashtban@polymtl.ca

ABSTRACT

Ultrafiltration (UF) with ceramic membrane has attracted growing attention in drinking water treatment. In this regard, a ceramic and a polymeric UF membrane process with in-line pre-oxidation has been applied for iron and manganese control in water. The effect of water chemistry including pH, ionic strength and hardness on the characteristics of oxidized iron and manganese aggregates, and subsequent UF fouling behavior were evaluated. The fouling of constant flux dead-end UF membranes was assessed using blocking law and resistance-in-series model analyses. Results suggest that the water chemistry did not have a notable impact on the overall iron and manganese removal efficiencies but did contribute to the extent of fouling caused by manganese dioxide aggregates. The resistance of the cake layer and its compressibility could be explained by the manganese dioxide aggregate properties, such as size, ζ-potential and fractal dimension, which were controlled by the water chemistry. However, the cake formed by ferric hydroxide aggregates induced very low and comparable resistance to the membranes under all conditions, in line with the similar aggregate properties. The fouling behavior of ceramic membrane was generally similar to that of polymeric one, however, the reversibility of the fouling differed from one another. Overall, this work provides further insight on the fouling of ferric hydroxide and manganese dioxide in water treatment.

KEYWORDS: Water treatment; Iron/manganese control; Constant flux dead-end ultrafiltration; Ceramic/polymeric membrane; Fouling resistance.

5.1 Introduction

Iron and manganese commonly occur in groundwater and some sources of surface water from weathering of metal-bearing minerals and rocks, leaching from soils rich in organic matter, contamination by industrial effluents and thermal stratification in lakes. Among different water sources, groundwater frequently contains high levels of dissolved iron and manganese arising from more reduced redox conditions. The presence of these metals in finished water creates aesthetic issues, such as colored water formation, increased turbidity, metallic taste, odor, and staining of laundry and plumbing fixture (World Health Organization (WHO), 2008). In this regard, the United States Environmental Protection Agency (United States Environmental Protection Agency

(USEPA), 2004) and Guidelines for Canadian Drinking Water Quality (Health Canada, 2010) have recommended an aesthetic objective limit of 0.3 and 0.05 mg/L for the concentrations of iron and manganese in drinking water, respectively. However, iron and manganese concentrations as low as 0.05 (World Health Organization (WHO), 2003) and 0.02 mg/L (Sly et al., 1990), respectively, may still cause aesthetic problems. In addition, manganese control in drinking water is receiving an increased attention due to its potential neurotoxicity (Wasserman et al., 2006; Tuschl et al., 2013). Manganese intake from water ingestion has been associated with intellectual impairment in children, even at low concentrations (<0.25 mg/L) (Bouchard et al., 2011). Thus, it is crucial to effectively control the concentration of manganese in drinking water.

A common treatment strategy for iron and manganese control in drinking water includes oxidation of dissolved iron and manganese followed by separation of oxidized particles from water. Traditional processes to remove particulate and colloidal matter from water are coagulation, flocculation, sedimentation and granular media filtration, which have drawbacks of operating in successive steps heterogeneous reactions that require significant contact time and, therefore, process footprint. Furthermore, oxidized manganese is not always effectively removed by such treatment technologies (Carlson et al., 1997) due to its propensity to form negatively charged colloids (Morgan and Stumm, 1964; Dashtban Kenari and Barbeau, 2016a). Alternatively, compact membrane processes, such as microfiltration (MF) and ultrafiltration (UF), are increasingly used in water treatment facilities for filtration of dilute suspensions containing fine particles and colloids based on size exclusion (Crittenden et al., 2012). Management of membrane fouling is an important limitation of this technology. As opposed to surface water systems where organic fouling is dominant, management of inorganic fouling caused by iron/manganese is of importance for many UF/MF groundwater systems.

Several factors impact membrane fouling including membrane types and material properties, operating conditions, process configuration, cleaning strategies and feed solution characteristics (Crittenden et al., 2012; Lee and Kim, 2014). In recent years, application of ceramic membranes has been receiving growing attention due to their inherent advantages over conventional polymeric membranes. Namely, ceramic membranes offer superior chemical, thermal and mechanical stability allowing much more aggressive physical and chemical cleaning approaches which can prolong their life expectancy. In addition, the higher integrity and reliability of ceramic membranes would reduce the repetitive testing, repair and replacement of membrane modules leading to

savings in operation cost (Pendergast and Hoek, 2011). In spite of the high potential of ceramic membrane application for iron/manganese removal, their fundamental fouling behavior caused by ferric hydroxide and manganese dioxide particles has not yet been documented.

Regarding feed water characteristics, it is expected that membrane performance during filtration of metal oxide colloids and particles will be considerably impacted by pH, ionic strength and salt valency as these parameters are known to have an impact on particle-particle and particle-membrane interactions (Lee et al., 2003; Santiwong et al., 2008). Moreover, changes in pH, ionic strength and salt valency may alter water permeability of MF/UF membranes, even though salt rejection is negligible in these systems (Huisman and Dutre, 1997; Faibish et al., 1998; Zhao et al., 2005; Manttari et al., 2006). Consequently, understanding the behavior and characteristics of ferric hydroxide and manganese dioxide particles deposition on UF/MF membranes is of interest for their application for iron and manganese control in drinking water.

This study aimed to investigate the removal of iron/manganese oxides and the associated fouling during the operation of pre-oxidized dead-end UF ceramic or polymeric membranes. Characteristics (such as size, ζ-potential and fractal dimension) of ferric hydroxide and manganese dioxide aggregates achieved under various water chemistry conditions, were assessed against the fouling behaviors that they produced on UF membranes. The performance of ceramic versus polymeric UF membrane with respect to the extent of fouling and iron/manganese removal were then compared. Constant flux blocking law model was applied to determine the specific resistance and the compressibility of the filter cake. Finally, the resistance-in-series model was applied to quantitatively analyze the advantage of ceramic membrane with respect to the cleaning processes effectiveness and reversibility of fouling.

5.2 Materials and methods

5.2.1 UF membranes

Although the majority of membranes that have been using in industries are hollow fiber polymeric membranes and tubular ceramic membranes, most of the publications focused on the fouling behavior of a simple disc-type membrane. These results could not well predict the rate and extent of fouling in full-scale plant (Carroll and Booker, 2000). In this study, two types of UF membranes, which are relevant for industrial applications, were selected. A hollow fiber polymeric membrane,

UFC M5, composed of a blend of polyvinylpyrrolidone and polyethersulfone with a nominal molecular weight cut off (MWCO) of 200 kDa was used (Norit X-Flow, Enschede, The Netherlands). The membrane contains 93 fibers with an inner diameter of 0.8 mm, a length of 300 mm and an effective filtration area of 700 cm^2. This membrane is resistant to temperature up to 40°C and pressure up to 300 kPa and its tolerance to pH ranges from 2 to 12. A single-channel tubular ceramic UF membrane with an outer diameter of 10 mm, an inner diameter of 6 mm, a length of 500 mm and a filtration area of 95 cm^2 was purchased from Atech Innovations GmbH (Gladbeck, Germany). This asymmetric membrane is made of zirconium dioxide and a support of α-aluminum oxide with open pores which provides maximum permeability and high mechanical stability. According to the manufacturer, the nominal MWCO of the membrane is 150 kDa. The membrane is resistant to a pressure up to 1 MP, and pH of 0-14. The initial permeability of the ceramic and the polymeric membranes were measured as 780 and 840 LMH/bar, respectively, using demineralized (DM) water at pH 6 and 20°C. The specifications of the ceramic and polymeric membranes are summarized in Table 5.1.

The pore size of the membranes was estimated from the Stokes-Einstein equation (Kawakatsu et al., 1993). Accordingly, the pore size of 150-kDa ceramic membrane and 200-kDa polymeric membrane are approximately 17 nm and 19 nm, respectively.

Table 5.1. Specifications of ceramic and polymeric membranes utilized in this study.

Manufacturer	Material	Surface area (cm^2)	MWCO[c] (kDa)	Permeability (LMH/bar) at 20°C	pH stability[d]	Temp. Stability[d] (^{o}C)	Pressure Stability[d] (kPa)
Norit (polymeric)	PES/PVP[a]	700	200	840	2-12	40	300
Atech (ceramic)	ZrO$_2$/Al$_2$O$_3$[b]	95	150	780	0-14	N.A.	1000

[a] Polyethersulfone/polyvinylpyrrolidone
[b] Zirconium dioxide/α-aluminum oxide
[c] Molecular weight cut off
[d] Reported by manufacturer
N.A.: Not available

5.2.2 Preparation of synthetic feedwater (SFW)

A fresh SFW was prepared prior to each experiment via addition of appropriate amount of sodium chloride, calcium chloride dihydrate and sodium bicarbonate stock solutions to demineralized (DM) water to achieve the final desired ionic strengths (0.5, 1.0 and 10 mM), pHs (6, 7 and 8) and hardness values (0, 100 and 317 mg CaCO$_3$/L). The pH of the SFW was then adjusted by bubbling

CO_2 and/or N_2 gas into the water. The stock solutions were prepared using Milli-Q water. Dissolved manganese stock solution (100 mg Mn^{2+}/L) was prepared by dissolution of manganese (II) sulfate monohydrate into Milli-Q water while Milli-Q water was first acidified to a pH of 3 and N_2 gas was bubbled into the water for 15 min prior to the dissolution of iron (II) sulfate heptahydrate (100 mg Fe^{2+}/L). All chemicals were analytical grade reagents.

Although iron and manganese are commonly co-occurring in natural waters, they have been studied separately to better assess the fouling characteristics of each mineral. Table 5.2 summarizes the SFW conditions applied in this study, relevant to typical natural water conditions.

Table 5.2. Characteristics of ferric hydroxide and manganese dioxide particles at various water chemistry conditions.

Particle type	Experiment no.	pH	Ionic strength (mM)	Hardness (mg $CaCO_3$/L)	ζ -potential (mV)	$D_n[1,0]$[a] (μm)	Df[b]
	A1	6	0.5	0	-36.4 ± 2.1	0.128	1.67
	A2	7	0.5	0	-42.9 ± 2.3	0.036	1.63
	A3	8	0.5	0	-45.5 ± 2.1	0.030	1.21
Manganese dioxide	A4	7	1.0	0	-41.6 ± 1.7	0.047	1.61
	A5	7	10	0	-37.2 ± 0.6	0.118	1.70
	A6	7	10	100	-12.8 ± 0.4	2.56	2.79
	A7	7	10	317	-3.7 ± 0.1	3.36	3.03
	B1	6	0.5	0	6.6 ± 0.2	3.49	1.70
	B2	7	0.5	0	1.6 ± 0.2	3.79	1.61
	B3	8	0.5	0	-1.4 ± 0.3	3.81	1.68
Ferric hydroxide	B4	7	1.0	0	-0.9 ± 0.2	4.15	1.59
	B5	7	10	0	1.4 ± 0.1	4.43	1.62
	B6	7	10	100	4.9 ± 0.1	5.33	1.59
	B7	7	10	317	7.5 ± 0.8	7.28	1.71

[a] Average diameter (number)
[b] Fractal dimension

5.2.3 Experimental procedure

The experimental setup consisted of two steps, as shown schematically in Figure 5.1: oxidation and membrane filtration. In the oxidation step, dissolved iron or manganese and oxidant (potassium permanganate or sodium hypochlorite) solutions were separately spiked into the SFW prior entering the oxidation column. The oxidation column was a 2-meter clear PVC pipe with an inner diameter of 50.8 mm (2 in.) that provided a retention time of 11.6 min for a total flow of 350 mL/min. In all tests related to manganese removal from water, potassium permanganate (stock solution 130 mg/L) was applied to oxidize 2.0 mg Mn/L dissolved manganese to 5.3 mg/L particulate manganese dioxide, while for iron removal experiments, sodium hypochlorite (stock solution 120 mg Cl_2/L) was injected to oxidize 2.8 mg Fe/L dissolved iron to 5.3 mg/L ferric hydroxide particles. Water samples were collected after an hour of operation to ensure a steady state condition had been reached. The samples were taken to analyze the characteristics of oxidized particles, such as size, ζ-potential and fractal dimension, as well as concentration of iron/manganese in water.
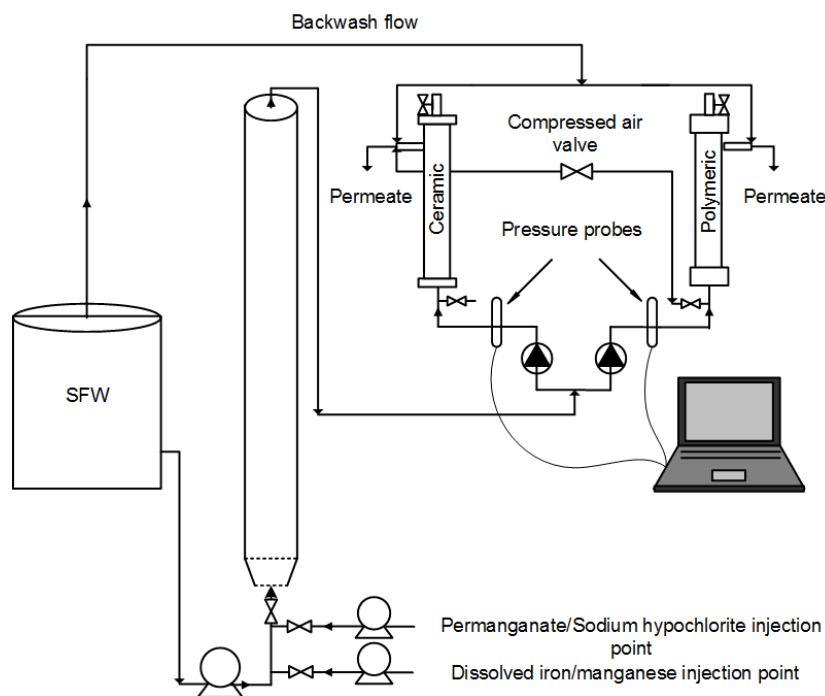
Figure 5.1. Schematic diagram of the bench-scale UF setup with peroxidation step.

The membrane filtration part consisted of two UF membranes operated in parallel. The experiments were conducted under dead-end constant-flux filtration mode, similar to that of most water and waste-water treatment plants. The flow direction was inside-out for both membranes.

Preliminary tests with DM water revealed that the intrinsic resistance of both membranes was independent of applied pressure over the range employed in this study. However, the permeability results indicated that the intrinsic membrane resistance and subsequently the initial permeability of both membranes were a function of water characteristics, i.e. pH, ionic strength and salt valency, as indicated in previous studies (Huisman and Dutre, 1997; Faibish et al., 1998; Zhao et al., 2005; Manttari et al., 2006). Prior to the filtration experiment, the clean membrane resistance was determined by filtering DM water. Then, the particle-free SFW, under the specific pH, ionic strength and hardness, was passed through the membranes, at the desired flux, until a steady pressure was obtained. The feed suspension, i.e. the effluent from the oxidation column, was then introduced into the UF membranes an hour after initiation of oxidation. In all fouling experiments, a constant (and high) flux of 200 LMH was maintained for 150 min by a peristaltic pump (MasterFlex, Cole-Parmer Instrument) on each membrane. Permeate samples were taken at the initial and end of filtration experiment to measure the concentration of iron and manganese in water. The TMP was continuously recorded every 15 s via a pressure transducer (Omega, PX409-030GUSB) using a data acquisition software (TRH Central). At the end of each experiment, physical cleaning followed by a chemical cleaning were carried out. All filtration experiments were duplicated and performed at $23 \pm 1^{\circ}C$.

5.2.4 Membrane cleaning procedures

Before starting the experiments, virgin membranes were first cleaned with citric acid solution (2 wt% for the ceramic membrane and 1 wt% for the polymeric one) at a flux of 100 LMH for 30 min. Then, the membranes were rinsed with DM water and cleaned again with sodium hypochlorite solution (500 mg Cl_2/L for the ceramic membrane and 200 mg Cl_2/L for the polymeric one) at the same flux of 100 LMH for another 30 min. After these cleaning steps, the membranes were rinsed thoroughly with DM water, and the clean water permeability of the membranes was calculated by measuring the TMP at increasing water fluxes.

Physical cleaning was performed at the end of each filtration experiment. Backwashing was first conducted for both membranes using particle-free SFW for 3 min at a flux of 400 LMH (twice the

operating flux). After this step, the physical cleaning of the ceramic membrane was further enhanced by backwashing with air scouring for 5 s at 400 kPa, while forward flushing with air was limited to 200 kPa for polymeric membrane to maintain its integrity, as suggested by the supplier. Chemical cleaning was performed as follow: for the ceramic membrane, 1.0 L of 2 wt% citric acid at 50°C was recirculated for 30 min, while the polymeric one was cleaned by recirculating 1.0 L of 1 wt% citric acid at 30°C for 30 min. The pH of citric acid solutions were adjusted to 1 and 2 using 0.1 N HCl for the ceramic and polymeric membranes, respectively. In this investigation, acid cleaning was always found to be sufficient to recover the clean water permeability of the membranes.

5.2.5 Particle characterization

The size distribution of ferric hydroxide and manganese dioxide particles and/or aggregates in membrane feed water were determined using dynamic light scattering (Zetasizer Nano-ZS, Malvern, UK) or static light scattering (Mastersizer 3000, Malvern, UK) techniques. Dynamic light scattering is better suited for sub-micron colloids, while static light scattering instrument is well adapted to determine the size of larger aggregates (> 1 µm). Due to the higher sensitivity of membrane filtration process to smaller particles, number-based size distribution was used to interpret the results. The average aggregate size was calculated as the mean of this size distribution (D[1,0]). Ten consecutive measurements were taken to ensure the repeatability of the analysis.

The Zetasizer Nano-ZS was also employed to determine electrophoretic mobility and ζ-potential of the particles and/or aggregates in water using the Smoluchowski equation. Triplicate measurements were performed for each sample.

Spatial structure of aggregates in terms of fractal dimension, Df, was also estimated in this study. For Euclidean objects, the fractal dimension is 1 for a straight line, 2 for a sheet and 3 for a solid sphere, while fractal aggregates show non-Euclidean dimensionality and take non-integer values of fractal dimension. The high fractal dimensions, values approaching 3, indicate compact nearly spherical aggregates, whereas more amorphous and less compact aggregates have low fractal dimensions, values approaching 1 (Jefferson and Jarvis, 2006).

The fractal dimensions of aggregates were calculated from static light scattering data obtained using the Malvern Mastersizer 3000. In this apparatus, a stirred sampling unit is used to introduce

the suspension flow into the measurement cell. The stirrer speed in the sampling unit was kept around 1000 rpm to minimize the breakage of aggregates while maintaining the circulation of the suspensions (Tang et al., 2000). More details regarding these techniques can be found in our previous report (Dashtban Kenari and Barbeau, 2016a).

Based on Rayleigh-Gans-Debye theory, there exists a relationship between the measured scattered light intensity of aggregates, $I(q)$, and the scattering wave vector, q (nm^{-1}), as indicated in the following equations (Guan et al., 1998):

$$I(q) \alpha q^{-Df} \tag{4.1}$$

$$q = \frac{4\pi n}{\lambda} \sin(\theta/2) \tag{4.2}$$

where n is the refractive index of the medium; λ is the wavelength of the incident beam (nm); and θ is the scattering angle. Accordingly, the curves of scattering intensities as a function of wave vector display a linear relationship on a log-log plot over the fractal regime or the so-called power law regime. Thus, the fractal dimension can be estimated from the absolute slope of this linear region. It is worth mentioning that, knowing the aggregate size distribution for each experimental condition, the fractal dimension was calculated in the linear region corresponding to that specific size ranges since there may exist several linear regions over the tail of this log-log curve (Sorensen, 2001). A typical example of fractal dimension calculations under low and high ionic strengths of water are shown in Figure 5.2.

All analyses related to the characteristics of aggregates were made within 3 minutes of sample collection to reduce the possibility of further aggregation. Experiments conducted under different pH and ionic strengths were performed in duplicate.
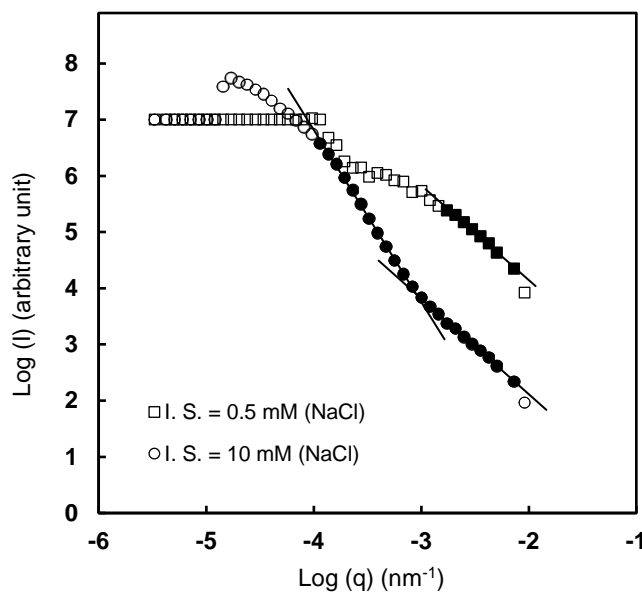
Figure 5.2. Typical results of static light scattering for fractal dimension calculation.

5.2.6 Iron and manganese analysis

Total iron and manganese concentrations were measured with an inductively coupled plasma-optical emission spectrometry (ICP-OES, model iCAP 6000). Prior to the analysis, particulate iron and manganese were dissolved using heat and acid digestion method; 0.5% HNO_3 (Omni Trace® grade, pH < 2) at 80°C for 48 h. Triplicate analyses were performed on each sample and the average concentrations were recorded. The pH measurements were carried out with an UltraBasic pH meter (model UB-5 from Denver Instrument). The pH meter and the ICP-OES were calibrated on the day of experiment.

5.2.7 Membrane fouling characterization

Generally, membrane fouling of inorganic particles and colloids consist in the accumulation of materials at the surface and/or in the pores of a membrane, which triggers a reduction in membrane permeability.

5.2.7.1 Constant flux blocking law model for compressible cake layer

In dead-end filtration of colloidal and particulate suspension having dimensions larger than the pore size of the membrane, cake filtration mechanism can fully describe the pressure increase and membrane fouling. The characteristics of deposited cake layer, such as its hydraulic permeability

and compressibility, are mainly dependent on the type of foulant and water chemistry condition (Shirazi et al., 2010). According to the Darcy's law, the flow through the clean and fouled membrane, Q (m^3/s), can be written as:

$$Q = \frac{\Delta P_0 A_0}{\mu R_m} \tag{4.3}$$

$$Q = \frac{\Delta P A_0}{\mu (R_c + R_m)} \tag{4.4}$$

where ΔP_0 and ΔP are initial and final transmembrane pressures (kPa), respectively; A_0 is the membrane surface area (m^2); R_m is the intrinsic membrane resistance (m^{-1}); R_c is the cake layer resistance (m^{-1}); and μ is the viscosity of the fluid (kPa.s). The cake layer resistance can be expressed in terms of the average specific cake resistance, α_{ave} (m/kg), as follows:

$$R_c = \alpha_{ave} c_b V_s \tag{4.5}$$

where c_b is the bulk concentration (kg/m^3); and V_s is the volume of permeate per unit membrane area (m^3/m^2). Eq. (4.6) was derived from the combination of Eqs. (4.3), (4.4) and (4.5) that expresses the increase in TMP at constant flux during incompressible cake filtration, in which the specific cake resistance remains constant throughout the experiment.

$$\Delta P = \frac{Q\mu(\alpha c_b V_s + R_m)}{A_0} = \Delta P_0 + \frac{Q\mu\alpha c_b}{A_0} V_s \tag{4.6}$$

However, the filter cake of many natural materials, such as clays, microbial cells and flocculated colloidal maters, is compressible to some degree (Chellam and Xu, 2006; Singh and Song, 2006). During water and waste water treatment, the specific cake resistance, α (m/kg), often increases according to a power law (Chellam and Xu, 2006; Sorensen and Sorensen, 1997; Chellam et al., 1998):

$$\alpha = \beta \Delta P^{n'} \tag{4.7}$$

where β (m/kg/kPa$^{n'}$) and n' are empirical constants. β is related principally to the size and shape of the particles, and the dimensionless parameter n' is the cake compressibility coefficient varying from zero for an incompressible cake to nearly 1 for a highly compressible cake. Substituting Eq. (4.7) in Eq. (4.6) gives rise to the following equation (Huisman and Dutre, 1997):

$$\Delta P = \Delta P_0 + \frac{Q\mu c_b}{A_0} \beta \Delta P^{n'} V_s \tag{4.8}$$

In order to determine the compressibility parameters, experimental pressure data were directly fitted to Eq. (4.8) using a curve-fitting tool in Matlab (R2015a) with a trust region method resulting in the smallest sum of squared residuals.

5.2.7.2 Resistance-in-series model for quantifying membrane fouling

The reversibility of fouling was quantified by the resistance-in-series model (Eq. (4.9)), as follows:

$$J = \frac{\Delta P}{\mu R_t} = \frac{\Delta P}{\mu(R_m + R_{pr} + R_{cr} + R_{if})} \tag{4.9}$$

where J is the flux (m/s); R_t is the total resistance (m^{-1}); R_{pr} is the physically reversible resistance (the portion of fouling that can be recovered by backwash and air scouring) (m^{-1}); R_{cr} is the chemically reversible resistance (m^{-1}); and R_{if} is the chemically irreversible fouling (m^{-1}).

R_m was calculated before each experiment by measuring the particle-free SFW permeability of the membranes. R_{pr} was obtained after physical cleaning step by measuring the stabilized TMP of particle free SFW at the operating flux and temperature. The difference between this TMP and the TMP at the end of filtration was used for R_{pr} determination. R_{cr} was calculated from the difference between the stabilized TMP before and after the chemical cleaning step. The R_{if} was back-calculated from the difference between R_t and the sum of R_m, R_{pr}, and R_{cr}.

5.3 Results and discussion

This section presents iron and manganese removal performance and UF fouling under different water chemistry relevant of typical natural water conditions.

5.3.1 Iron and manganese removal performance in oxidation and UF hybrid process

Analysis of the initial and final filtration samples showed that the rejection of iron and manganese under different water chemistry conditions using both ceramic and polymeric UF membranes were higher than 99.5%. The concentration of these minerals were reduced below the target value of 0.02 mg/L in the filtrate. The complete iron and manganese removal achieved through the filtration of oxidized suspensions indicates that: (1) iron and manganese were completely oxidized by sodium hypochlorite and potassium permanganate, respectively, during the retention time provided

by the column, (2) there were negligible colloidal iron and manganese of size less than the nominal pore size of the membranes, as confirmed by particle size analysis presented in Table 5.2.

5.3.2 Characterization of manganese dioxide fouling in UF membranes

In the following sections, the effects of pH, ionic strength and hardness on the fouling behavior of ceramic and polymeric membranes with manganese dioxide suspension are evaluated.

5.3.2.1 Effect of pH

Figure 5.3 illustrates the impact of pH (for ionic strength = 0.5 mM) on fouling of ceramic (Figure 5.3a) and polymeric (Figure 5.3b) membranes. For both types of membranes, normalized TMP (P/P_0) showed a slight non-linear, concave upward increase as a function of cumulative permeate volume. Figure 5.3 also indicates that the pressure profiles are well described by the constant flux power law compressible cake model (Eq. (4.8)) (solid lines in Figure 5.3), further confirming the dominant role of cake formation. For both types of membranes, increasing pH from 6.0 to 7.0 induced a significant increase of fouling. On the other hand, a further increase of pH from 7.0 to 8.0 reduced the rate of fouling back to its original rate observed at pH 6.0. To facilitate the comparison of the experimental results, the average values of specific cake resistance under different conditions were also calculated (Table 5.3), via Eq. (4.5) using experimental R_c, V_S and c_b values, and the same trend was observed. These results can be explained by the changes in the hydraulic properties of the cake layer formed by manganese dioxide of different size, ζ-potential and fractal dimension (Table 5.2). Although substantial aggregation did not occur under these conditions due to the high repulsive forces between the manganese dioxide particles (ζ-potential values ranged from -36.4 ± 2.1 to -45.5 ± 2.1 mV), the size distribution results revealed a partial aggregation of particles even at pH 8.0, in which colloids of around 100 nm were also found (Dashtban Kenari and Barbeau, 2016a). The lowest cake resistance was observed at pH 6.0 due to the formation of much larger manganese dioxide aggregates (average size of 128 nm) compared to that of formed at pH 7.0 (average size of 36 nm) and 8.0 (average size of 30 nm). Cake porosity is higher when it is composed of larger particles and/or aggregates (Lee et al., 2003; Xu et al., 2011). However, although the size of colloidal manganese dioxide was slightly smaller at pH 8.0 compared to pH 7.0, the average specific cake resistance was much lower at pH 8.0. At pH 8.0, the larger thickness of the electrostatic double layer (higher negative surface charge) increases the distance

between the deposits resulting in production of cake with higher permeability and lower fouling resistance (Faibish et al., 1998; Singh and Song, 2006). This is mainly important for colloids smaller than 100 nm (Faibish et al., 1998; Bowen and Jenner, 1995). The modification of cake characteristics is also revealed by the measurements of the fractal structure of the aggregates. While pH 6.0 and 7.0 produced similar fractal numbers (1.67 and 1.63, respectively), the fractal dimension at pH 8.0 was very low (1.21) indicative of the formation of less compact aggregates. This fractal dimension was much lower than expected according to the reaction limited regime for charged aggregates ($D_f \approx 2.2$) (Jefferson and Jarvis, 2006). González et al. (2004) indicated that a very low fractal dimension of 1.2 can be found for very small clusters with long-range repulsion forces. This is likely due to the very slow aggregation rate of highly negative charged particles.

In addition to cake resistance, the compressibility of the filter cake is another important parameter to consider for the design of a membrane filtration process. Filter cake compressibility is generally a function of particle size, shape and fractal dimension, surface charge and degree of aggregation (Lee et al., 2003; Singh and Song, 2006; Tiller and Yeh, 1987). The compressibility parameters of the cake formed from manganese dioxide under different water chemistry conditions, obtained via non-linear optimization of pressure data using Eq. (4.8), are presented in Table 5.3. Moderate and similar compressibility coefficients (ranged from 0.27 to 0.31) were found for manganese dioxide colloids under different pH conditions and very low salt concentration (ionic strength of 0.5 mM) most likely due to the repulsive electrostatic double layer interactions between the negatively charged colloidal manganese dioxide (ζ-potential varied from -36.4 ± 2.1 to -45.5 ± 2.1 as the pH increased from 6.0 to 8.0). The slight increase in cake compressibility at the lower pH of 6.0 is coherent with the larger aggregate sizes measured for this condition. Thus, these results shows that the compressibility of colloidal manganese dioxide is not only influenced by the thickness of the electric double layer but also, to a lower extent, by the size of aggregates.

Figure 5.3. Effect of pH on constant flux/dead-end UF of manganese dioxide suspensions using (a) a ceramic membrane and (b) a polymeric membrane. Ionic strength = 0.5 mM, T = 23°C. Instantaneous normalized pressures from experimental data are shown as discrete points. Solid lines represent the model fits using the constant flux blocking law model for compressible cake (Eq. (4.8)).

A general comparison between the Figure 5.3a and b reveals that the TMP increase pattern and the fouling behavior were quite similar in ceramic and polymeric UF membranes under different pH conditions. Only slightly more fouling and higher average specific cake resistances (Table 5.3) were observed with the polymeric membrane compared to the ceramic one. The differences between the average specific cake resistances of the two membranes were found to be 13%, 7% and 3% under the pH of 6.0, 7.0 and 8.0, respectively. This nearly identical fouling resistance was expected since the membrane material should not noticeably affect the behavior of cake formation mechanism in dead-end filtration (Huisman et al., 1999; Bacchin et al., 2006). The slight difference between the ceramic and polymeric membranes was likely due to the hydrodynamic effects arising from the different configuration of these membranes, a longer tubular ceramic membrane with a larger inner diameter versus a shorter hollow fiber polymeric membrane with a smaller inner diameter (Carroll and Booker, 2000; Krawczyk and Jonsson, 2014). The compressibility coefficients for manganese dioxide cakes (Table 5.3) were also nearly identical in the two membranes, which further confirms that the cake compressibility is predominantly controlled by the aggregate properties that is, in turn, governed by water chemistry condition.

Table 5.3. Summary of the blocking law model parameters and average specific cake resistances for the ceramic and polymeric membranes.

Particle type	Experiment no.	α_{ave}[a] (m/kg)		n'[b]		β[c] (m/kg/kPa$^{n'}$)	
		Ceramic	Polymeric	Ceramic	Polymeric	Ceramic	Polymeric
Manganese dioxide	A1	4.95E+14	5.67E+14	0.307	0.311	1.20E+14	1.33E+14
	A2	9.19E+14	9.83E+14	0.291	0.287	2.05E+14	2.26E+14
	A3	5.87E+14	5.72E+14	0.269	0.265	1.61E+14	1.65E+14
	A4	9.95E+14	1.03E+15	0.285	0.274	2.26E+14	2.52E+14
	A5	4.39E+14	4.75E+14	0.127	0.121	2.50E+14	2.74E+14
	A6	1.01E+14	2.20E+14	N.A.	N.A.	N.A.	N.A.
	A7	7.76E+13	1.64E+14	N.A.	N.A.	N.A.	N.A.
Ferric hydroxide	B1	3.18E+13	2.75E+13	N.A.	N.A.	N.A.	N.A.
	B2	2.53E+13	3.16E+13	N.A.	N.A.	N.A.	N.A.
	B3	2.58E+13	2.71E+13	N.A.	N.A.	N.A.	N.A.
	B4	2.75E+13	2.92E+13	N.A.	N.A.	N.A.	N.A.
	B5	2.50E+13	2.67E+13	N.A.	N.A.	N.A.	N.A.
	B6	2.79E+13	2.49E+13	N.A.	N.A.	N.A.	N.A.
	B7	2.91E+13	2.46E+13	N.A.	N.A.	N.A.	N.A.

[a] Cake-averaged specific resistance
[b] Compressibility coefficient
[c] Empirical constant
N.A.: Not available

5.3.2.2 Effect of ionic strength

The results of parallel filtration experiments with the ceramic and polymeric membranes under different ionic strength are shown in Figure 5.4. The pressure data (discrete points) were once again in excellent agreement with the constant flux blocking law model (solid lines). At a pH of 7.0, doubling the ionic strength of water from 0.5 to 1 mM slightly increased the normalized TMP at the end of the filtration experiment for both membranes. In spite of a small increase in the average size of manganese dioxide colloids with increasing the ionic strength from 0.5 to 1 mM, the resistance of the deposited cake layer slightly increased due to the compression of electrostatic double layer (ζ-potential slightly decreased) (Faibish et al., 1998; Bowen and Jenner, 1995). However, when ionic strength was raised from 1 to 10 mM, the normalized TMP at the end of filtration significantly decreased. The average specific cake resistances decreased identically (54 and 56%) for both membranes. The reduction in hydraulic resistance gained from the higher ionic

strength (10-fold increase) was associated with the larger aggregate dimensions: their average size increased by more than 100% (Table 5.2). As the ionic strength increased, the compression of electrostatic double layer (ζ-potential reduced from -42.9 ± 2.3 to -37.2 ± 0.6 mV by increasing the ionic strength from 0.5 to 10 mM, respectively) enhanced the degree of colloid aggregation. Consequently, the increase in the size of manganese dioxide aggregates resulted in the formation of more permeable cake layer with greater inter-aggregate porosity.
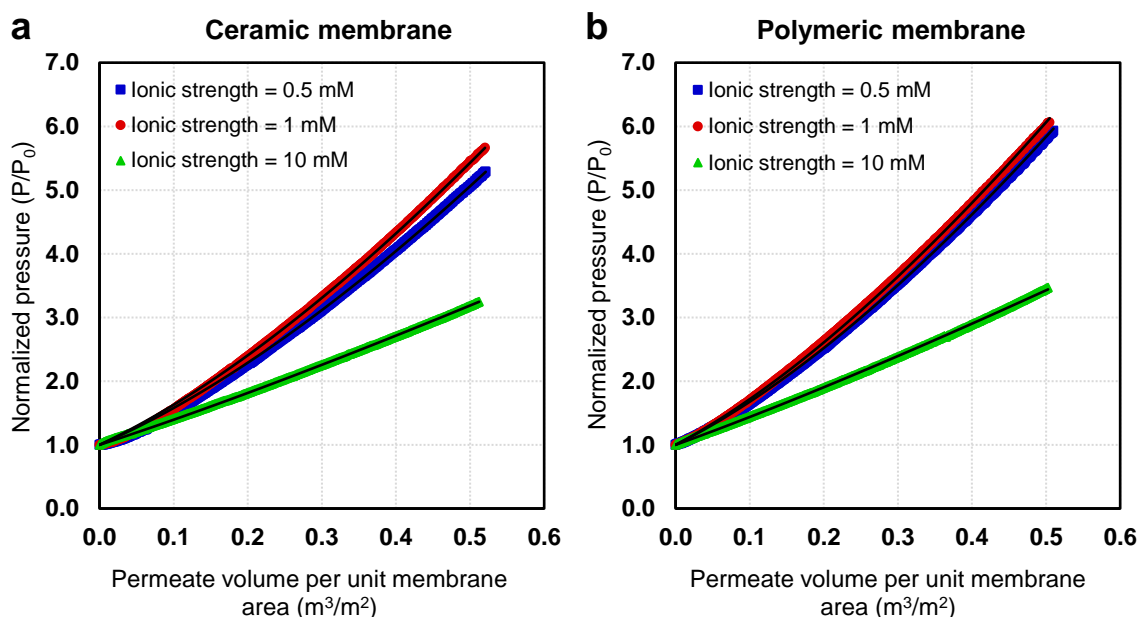
Figure 5.4. Effect of ionic strength (pH = 7.0) on constant flux/dead-end UF of manganese dioxide suspensions using (a) a ceramic membrane and (b) a polymeric membrane. Instantaneous normalized pressures from experimental data are shown as discrete points. T = 23°C. Solid lines represent the model fits using the constant flux blocking law model for compressible cake (Eq. (4.8)).

The fractal dimensions obtained for manganese dioxide aggregates slightly increased by rising the ionic strength, in agreement with previous studies on silica colloids (Singh and Song, 2006) and titanium dioxide nanoparticles (Chowdhury et al., 2013). This result explains the lower compressibility coefficients observed at higher ionic strengths (or salinity) (Table 5.3). As the ionic strength increased, the compression of electrostatic double layer reduced the inter-particle distance that can be filled subsequently at higher TMP. This was particularly considerable when the ionic strength increased by 10-fold giving rise to a decrease of 55% in the compressibility of the filter cake. As a result, the pressure increased almost linearly with permeate volume (Figure 5.4).

Therefore, the compressibility of the cake formed by colloidal manganese dioxide is substantially associated with ionic strength.

5.3.2.3 Effect of hardness

The fouling behavior of colloidal manganese dioxide has also been studied at constant ionic strength (10 mM) but increasing hardness conditions (0, 100 and 317 mg CaCO$_3$/L). As shown in Figure 5.5, the presence of calcium ions (Ca^{2+}) notably alleviated the fouling of both membranes. As more calcium was spiked (hardness increased from 100 to 317 mgCaCO$_3$/L), increment of normalized TMP further declined but to a much lesser extent. According to the ζ-potential values, at high hardness conditions most of the surface charges of colloids were neutralized, thus, the electrostatic double layer was almost completely suppressed resulting in aggregation of destabilized colloids. As a consequence the mean size of aggregates increased from 0.118 µm to more than 2 µm giving rise to a more permeable cake layer. In addition, when the double layer repulsion is neutralized, a settling aggregate becomes stagnant as soon as it reaches an already deposited aggregate on the top layer of the cake which hinders its movement into a neighboring void space resulting in a porous cake of higher permeability.

In these experiments the pressure data were not fitted to the blocking law model for compressible cake (Eq. (4.8)) since the TMP did not increase high enough over the course of filtration to estimate a reliable value of cake compressibility coefficient (longer filtration time would have been required). However, Figure 5.5 clearly implies the compressibility of the cake formed under hardness of 100 and 317 mg CaCO$_3$/L because a very slow gradual increase of the pressure in the early stage of filtration was followed by a more rapid growth of the pressure at later times. A similar trend has been observed for both membranes even though the extent of fouling was a slightly higher for polymeric membrane than the ceramic one.

Interestingly, although the size of aggregates increased with the hardness of water, the fractal dimension of aggregates also increased. The fractal dimension approached 3 for the aggregates generated at the hardness of 317 mgCaCO$_3$/L implying the formation of compact, nearly spherical aggregates. This could be related to the adsorption of calcium ions onto negatively charged manganese dioxide particles which can result in a tight adhesion of the calcium saturated particles (Pantina and Furst, 2006). In other word, the particles act as hard spheres that can pack firmly into aggregates. These results also reveal that the filter cakes formed of large aggregates have high

permeability and low resistance, regardless of their compactness or intra-aggregate porosity. The compressibility of the cake layer is related to the collapse of the clusters and, thus, a reduction of the inter-aggregate porosity.
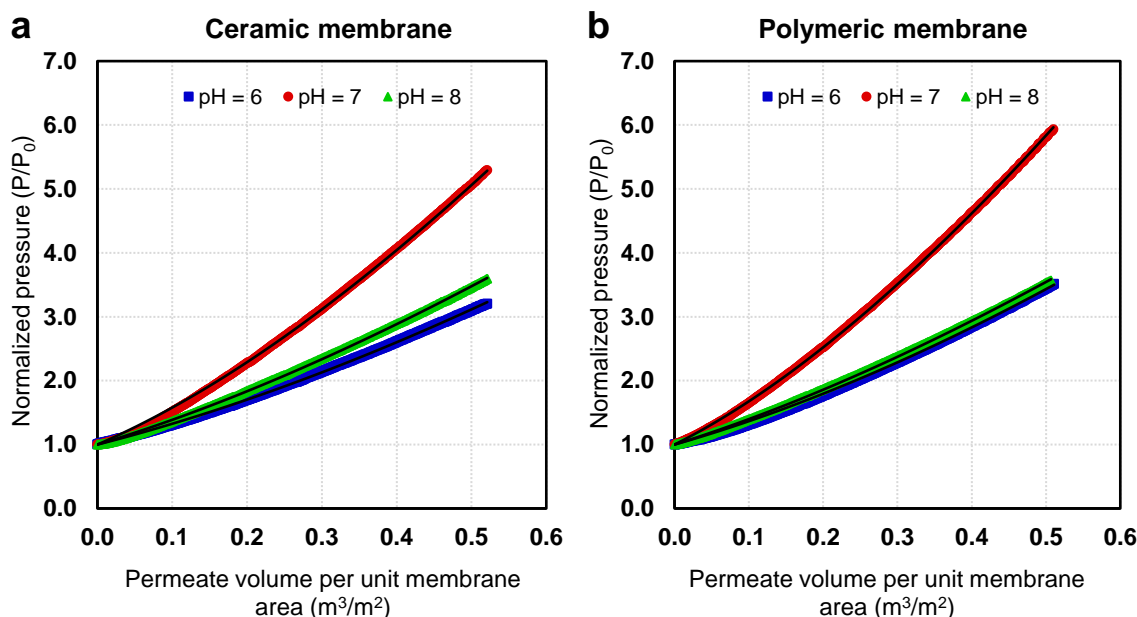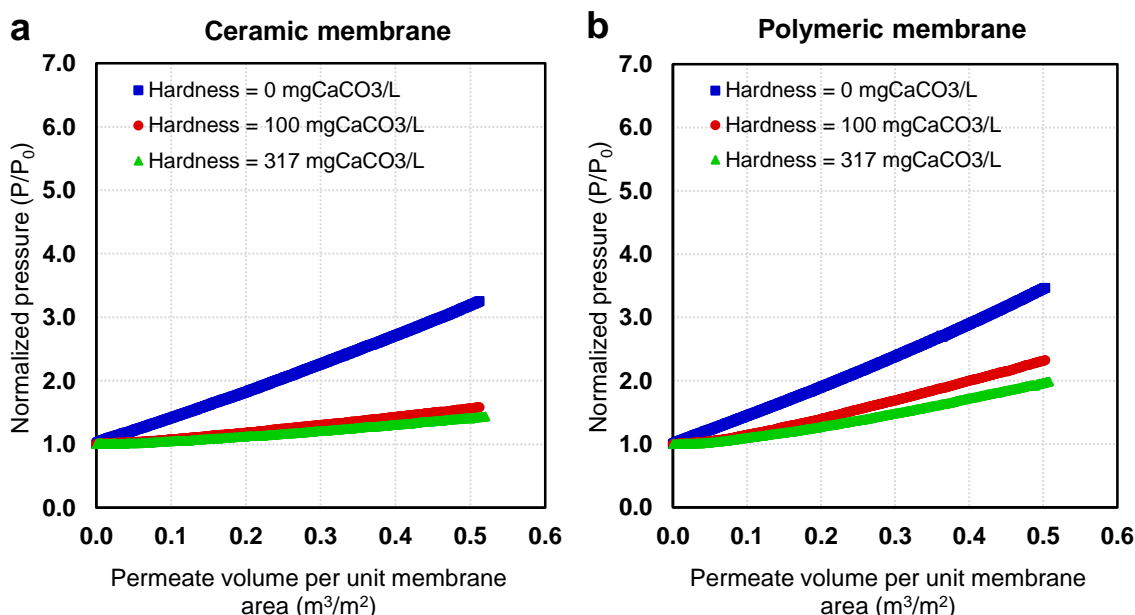

Figure 5.5. Effect of calcium hardness (IS = 10 mM) on constant flux/dead-end UF of manganese dioxide suspensions using (a) a ceramic membrane and (b) a polymeric membrane. T = 23°C. Instantaneous normalized pressures from experimental data are shown as discrete points.

In conclusion, hardness of water clearly has a major impact on the resultant filtration behavior of manganese dioxide suspensions with higher hardness giving rise to a superior membrane performance regardless of the fractal nature of the aggregates.

5.3.3 Characterization of ferric hydroxide fouling in UF membranes

An identical experimental design was conducted using ferric hydroxide suspensions. Figure 5.6 presents the normalized TMP changes observed during the first 150 min filtration ($\cong 0.5$ m^3/m^2) under different water chemistry conditions for both ceramic (Figure 5.6a) and polymeric (Figure 5.6b) membranes. As the mean size of ferric hydroxide aggregates (Table 5.2) were much higher than the pore size of the UF membranes, the solid suspensions accumulating on the membrane resulted in a pressure increase due to cake formation. The results of the normalized pressure profiles demonstrated a very low fouling tendency of ferric hydroxide suspensions, regardless of the membrane types and water chemistry conditions. The relatively similar hydraulic

resistance of the cake layer under different water chemistry is due to the very similar characteristics of ferric hydroxide aggregates independently of pH (from 6.0 to 8.0), ionic strengths (from 0.5 to 10 mM) or hardness (0 to 317 mgCaCO$_3$/L). Ferric hydroxide aggregates exhibited the following characteristics: mean size (3.49 to 7.28 µm), ζ-potential (-1.4 ± 0.3 to 7.5 ± 0.8 mV) and fractal dimension (1.59 to 1.71). The nearly zero ζ-potential of ferric hydroxide under different water quality conditions is in line with its high degree of aggregation as all aggregates were present in micron size range (Dashtban Kenari and Barbeau, 2016a). Thus, the very low average specific cake resistances were related to both the large size of aggregates and their low fractal dimension.

In conclusion, unlike manganese dioxide, the specific resistance of the cake formed by ferric hydroxide aggregates is not strongly dependent on water chemistry since ferric hydroxide aggregates are easily destabilized under natural water conditions (the isoelectric point lays in the pH range of 7.0 to 8.0) with low concentration of natural organic matter (e.g. ≈ 0.5 mg/L in these experiments).

Comparing the results of Figure 5.5 and Figure 5.6 implies that the fouling resistances of ferric hydroxide aggregates under all tested conditions were even lower than that of manganese dioxide aggregates under hard water condition. This is likely due to the more compact nature of the manganese dioxide aggregates forming the cake layer (the fractal dimension of 3.03 vs. 1.59-1.71 for manganese dioxide and ferric hydroxide aggregates, respectively).

Future studies should assess membrane fouling during the filtration of waters containing both iron and manganese species since these minerals more commonly co-occur in natural waters. This will be particularly relevant under soft water conditions where colloidal manganese dioxide lower than 100 nm size would be present in conjunction with micron size ferric hydroxide aggregates. We speculate that positively charged ferric hydroxide aggregates may promote aggregation of colloidal manganese dioxide, and thus, alleviate the total membrane fouling.
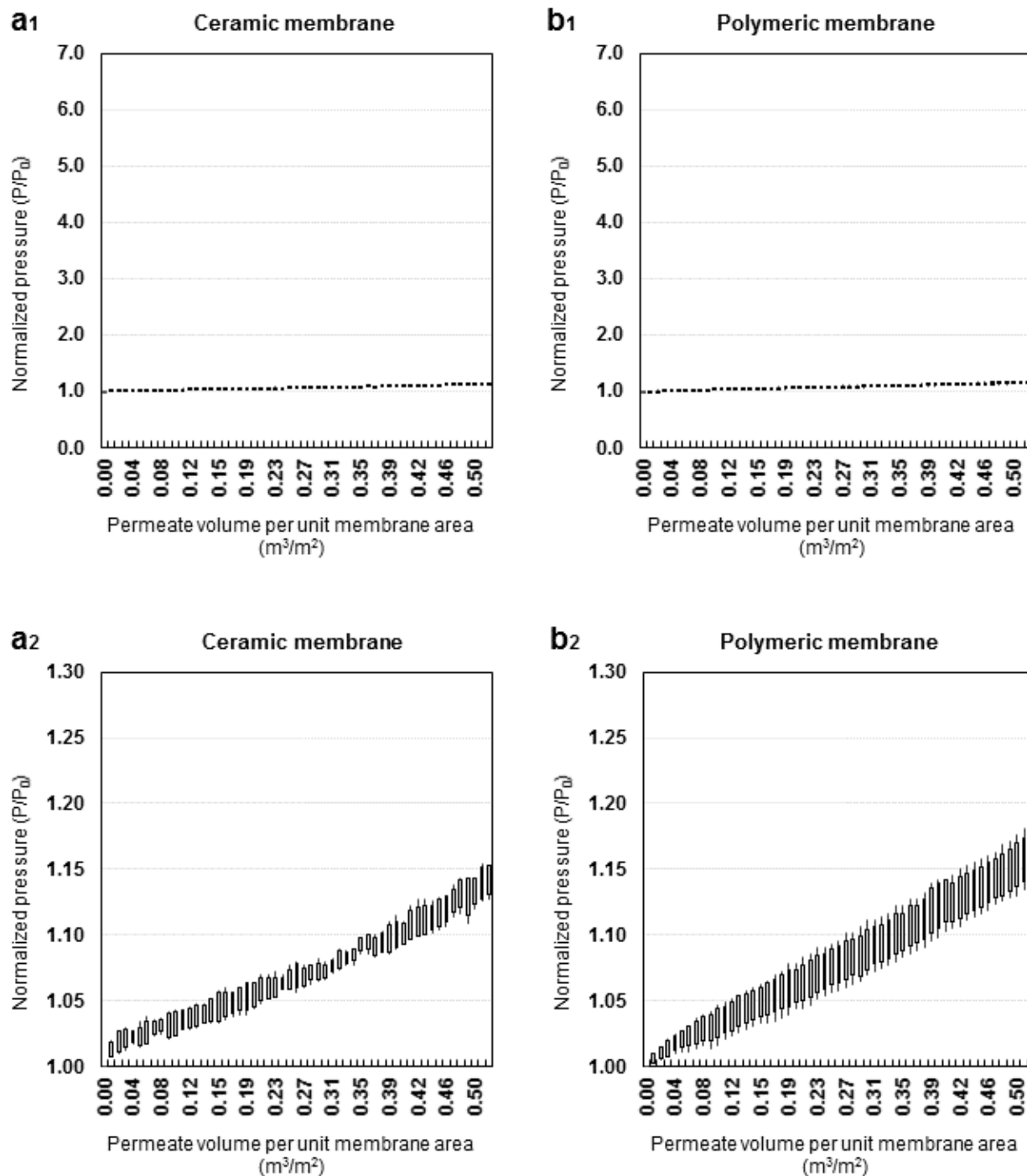
Figure 5.6. Constant flux/dead-end UF of ferric hydroxide suspensions under different pH, ionic strength and harness conditions using a ceramic membrane (a1 & a2) and a polymeric membrane (b1 & b2). Instantaneous normalized pressures from experimental data are shown as wisker-boxes points. Figures a1 and b1 use an identical Y-axis scale than the equivalent Mn figures (Figure 5.3, Figure 5.4, and Figure 5.5) while Figures a_2 and b_2 present a blow-up Y-axis scale.

5.3.4 Resistance-in-series model analysis

The resistance-in-series model analysis was applied in order to quantify the effectiveness of physical and chemical cleaning procedures for the ceramic and polymeric membranes. Figure 5.7 shows the results of this analysis for filtration of manganese dioxide under different pH (Figure 5.7a), ionic strength (Figure 5.7b), and hardness (Figure 5.7c) conditions. The difference between polymeric and ceramic membranes was evident when the contribution of physically and chemically reversible fouling to total fouling of the membrane was examined. A large portion of the ceramic membrane resistance was physically removable while physically reversible fouling, R_{pr}, did not contribute significantly to the polymeric membrane resistance. For instance, at pH 6.0, 7.0 and 8.0 (Figure 5.7a) physical cleaning alone recovered 97%, 99% and 84% of the ceramic membrane fouling, while only 22%, 10% and 2% of the polymeric membrane fouling was recovered, respectively. Such a difference most likely resulted from the possibility of applying more aggressive physical cleaning condition to the ceramic membrane than the polymeric one. For the polymeric membrane in the absent of calcium ions, chemically reversible fouling, R_{cr}, was the main contributor to membrane fouling. Under such conditions the low-permeable cake formed on the surface of the membrane was not completely removed by the physical cleaning procedure. Chemically irreversible fouling, R_{if}, was negligible for both membranes as the original permeability was fully recovered after chemical cleaning, an evidence that irreversible adsorption of iron and manganese did not occur during filtration. In conclusion, these results suggest that ceramic membranes would offer a better performance for the removal of manganese oxides due to the higher efficacy of physical cleaning.

Figure 5.8 shows the resistance-in-series model analysis results for the filtration of ferric hydroxide suspensions. A very low and comparable fouling resistances were observed under all conditions tested, as discussed earlier. In addition, similar to the filtration of manganese dioxide under high hardness conditions, R_m accounted for a significant portion of the total resistance as the membranes had a small pore sizes of 150 and 200 kDa, while the suspended particles were in micron size ranges.
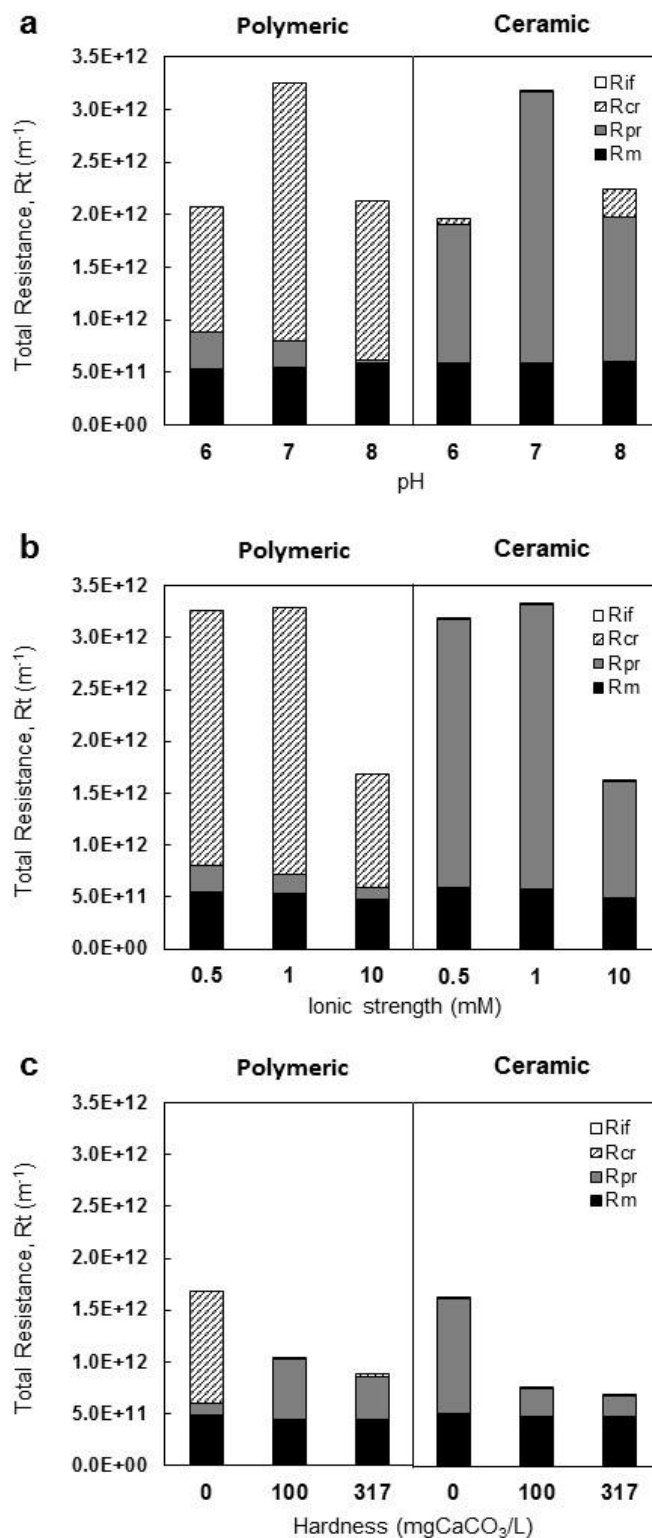
Figure 5.7. Resistance-in-series model analysis for the constant flux/dead-end UF of manganese dioxide suspension under different (a) pH, (b) ionic strength, and (c) hardness conditions by the ceramic and polymeric membranes. T = 23°C.
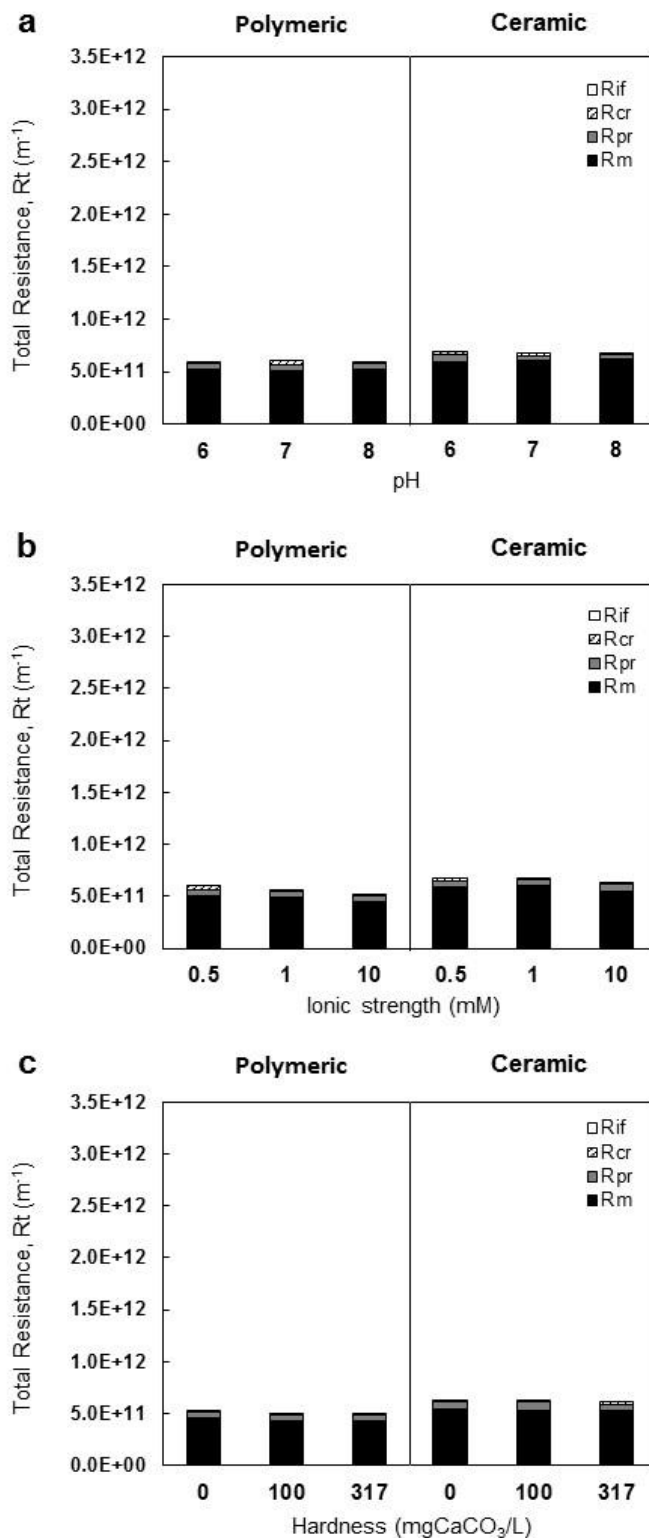
Figure 5.8. Resistance-in-series model analysis for the constant flux/dead-end UF of ferric hydroxide suspension under different (a) pH, (b) ionic strength, and (c) hardness conditions by the ceramic and polymeric membranes. T = 23ºC.

5.4 Conclusions

The present study investigated the performance of the sequential process of oxidation and dead-end UF for the control of iron and manganese in drinking water.

- UF in conjunction with pre-oxidation properly controlled the concentration of iron and manganese in water below the target value of 0.02 mg/L under all tested conditions.
- The influence of water chemistry, such as pH, ionic strength and hardness, on the characteristics of ferric hydroxide and manganese dioxide aggregates plays a major role on the fouling of UF membranes.
- Cake formation was the most significant contributor to fouling. The specific resistance of the deposited cake layer and its compressibility is mainly governed by the size, ζ-potential, and fractal dimension of the resultant aggregates rather than the type of membrane material and its configuration.
- Manganese dioxide aggregates are prone to severely foul UF membranes under soft water condition while ferric hydroxide aggregates only caused minimal fouling resistance to the membrane irrespective to the water chemistry condition.
- For manganese dioxide smaller than 100 nm, the hydraulic resistance of the cake layer and, in turn, the extent of fouling is mainly governed by the thickness of electrostatic double layer surrounding the colloids rather than the size of colloids.
- The oxidation of manganese followed by UF process can only be recommended for groundwater containing high level of hardness.
- Membrane filtration results consistently demonstrated that the ceramic tubular membrane and the polymeric hollow fiber membrane, utilized herein, are almost similarly fouled under identical water chemistry. However, physical cleaning was considerably more effective for the ceramic membrane compared to the polymeric one.

Future work should consider the influence of natural organic matter on UF fouling of iron and manganese suspensions as well as consider the cake characteristics produced by a mixture of both metals, a common case observed in natural waters.

Acknowledgement

CHAPTER 6   ARTICLE 3 :   PYROLUCITE FLUIDIZED BED REACTOR (PFBR): A ROBUST AND COMPACT PROCESS FOR REMOVING MANGANESE FROM GROUNDWATER

This chapter presents an article published in Water Research, 49 (2014). It reports the potential application of a pyrolucite fluidized bed reactor to remove elevated concentration of manganese from groundwater down to below 20 µg/L while operating under high hydraulic loading rates. The effects of key operational parameters on the performance of pyrolucite fluidized bed reactor and the long-term stability of process were evaluated.

Pyrolucite Fluidized-Bed Reactor (PFBR): A Robust and Compact Process for Removing Manganese from Groundwater

Seyedeh Laleh Dashtban Kenari[*] and Benoit Barbeau

Polytechnique Montreal, Department of Civil, Geological and Mining Engineering, NSERC-Industrial Chair on Drinking Water, Environment, C.P. 6079, Succursale Centre-Ville, Montreal, QC, H3C 3A7, Canada.

[*] Corresponding author: Tel: +1 514 340-4711 #2983; Fax: 514-340-5918;

E-mail: laleh.dashtban@polymtl.ca

ABSTRACT

The purpose of this paper is to introduce a pyrolucite fluidized-bed reactor (PFBR) as a potential drinking water process to treat groundwater containing high levels of dissolved manganese (Mn(II)) (0.5-3 mg/L) and reduce its concentration to < 0.02 mg/L in treated water. A pilot-scale study was conducted under dynamic conditions using synthetic groundwater (SGW), to elucidate the effect of operational conditions and groundwater composition on manganese (Mn) removal achieved by the PFBR. Results demonstrated almost complete Mn removal (close to 100%) in less than 1 min under all tested operational conditions (influent Mn concentration of $0.5 - 3$ mg/L, calcium (Ca^{2+}) hardness of $0 - 200$ mg $CaCO_3$/L, pH of $6.2 - 7.8$, temperature of 9 & 23°C and high hydraulic loading rate (HLR) of $24 - 63$ m/h (i.e., bed expansion of $0 - 30\%$)). Improved Mn removal profile was achieved at higher water temperature. Also, the results showed that adsorption of Mn(II) onto pyrolucite and subsequent slower surface oxidation of sorbed Mn(II) was the only mechanism responsible for Mn removal while direct oxidation of Mn(II) by free chlorine did not occur even at high concentrations of Mn(II) and free chlorine and elevated temperatures. Higher average mass transfer coefficient and consequently adsorption rate was achieved at elevated HLR. Increasing effluent free chlorine residuals from 1.0 to 2.0-2.6 mgCl2/L allowed increasing the operation time needed for media regeneration from 6 days to > 12 days. Turbidity was maintained around 0.2 NTU during the entire test periods indicating good capture of MnO_x colloids within the PFBR.

KEYWORDS: Drinking Water; Groundwater; Treatment; Manganese; Pyrolucite; Fluidized-Bed Reactor.

6.1 Introduction

Groundwater often contains significant levels of soluble manganese (Mn(II)) due to the favourable redox condition prevailing in many aquifers. In Canada, approximately 26% of the population, mostly living in small rural communities, relies on groundwater as a drinking water resource. Presence of Mn in finished water may cause organoleptic and operational problems including discoloration of water, unpleasant metallic taste and odour, increased turbidity and biofouling of pipelines as well as staining of laundry and plumbing fixtures (World Health Organization (WHO), 2008). Thus, the United States Environmental Protection Agency (USEPA), (2004) has

recommended a secondary maximum contaminant level (SMCL) (or guideline in the case of Health Canada) of 0.05 mg/L for Mn in drinking waters. However, a concentration as low as 0.02 mg/L may still result in adverse aesthetic impacts (Sly et al., 1990). In addition, although Mn is considered an essential trace mineral for human beings, a chronic exposure to low levels Mn intake from water (< 250 µg/L) has been associated with significant intellectual impairments in children (Bouchard et al., 2011).

As opposed to Europe where biological Mn removal is widespread, a traditional treatment strategy to control Mn level in North America involves oxidation of Mn(II) to an insoluble species (Mn(IV)) using a strong oxidant ($KMnO_4$ or less commonly ClO_2 or O_3) followed by rapid sand filtration (Knocke et al., 1990b). However, oxidation of Mn(II) by strong oxidants is highly dependent upon the pH, temperature, initial dissolved Mn concentration and reaction time (Van Benschoten et al., 1992). In addition, application of ClO_2 has been limited to waters with very low oxidant demand due to the production of undesired inorganic species, i.e. chlorite and chlorate (Gopal et al., 2007). The use of ozonation or $KMnO_4$ always brings the risk of permanganate escaping in treated water and resulting in pink water formation (Gregory and Carlson, 2003). Furthermore, it is difficult to effectively remove Mn oxides ($MnO_{x(s)}$) through depth filtration (Carlson et al., 1997) due to its tendency to form negatively charged colloids (Morgan and stumm, 1964).

Due to the propensity of $MnO_{x(s)}$ oxides to adsorb Mn(II) (Griffin, 1960; Morgan and Stumm, 1964), another process, termed Natural Greensand Effect (NGE), was introduced to control Mn(II). Removal of Mn(II) is achieved through sorption of Mn(II) onto $MnO_{x(s)}$ surface followed by catalytic oxidation of adsorbed Mn(II) by free chlorine. It is an effective and economical method that gained widespread usage over the past decades. Nevertheless, the process performance is strongly impacted by the maintenance of available adsorption sites, which is governed by the $MnO_{x(s)}$ coating level, chlorine concentration and pH (Knocke et al., 1990a). In addition to these parameters, hydraulic loading rate (HLR), temperature, calcium (Ca^{2+}) hardness, and initial Mn(II) concentration can also influence the process performance.

$MnO_{x(s)}$-coated sand, such as Mn greensand, has been essentially used in packed bed contactors at a relatively low HLR to remove low feed water Mn(II) concentrations (mostly < 0.5 mg/L) (Hargette and Knocke, 2001; Yang et al., 2008; Buamah et al., 2009; Piispanena and Sallanko, 2010). For higher Mn concentrations, rapid head loss buildup leading to frequent backwashing is

an important limitation of a packed bed configuration. This constraint has recently been addressed with the development of post-filtration adsorption contactors (Zuravnsky, 2006) which use a larger media (2.0-6.4 mm) than conventional greensand (0.3-0.4 mm). HLR as high as 32 - 50 m/h (16-20 gpm/ft^2) were successfully tested. However, this process is targeting application on conventionally treated surface waters exhibiting low Mn concentrations (< 0.1 mg/L).

In order to use adsorptive contactors on groundwaters having high Mn concentrations, we are putting forth the hypothesis that a pyrolucite (a natural Mn media consisting of 70 to 80% Mn dioxide (MnO_2) by weight) fluidized bed configuration will be advantageous over the packed bed contactor. Efficient removal of copper ions in FBR containing $MnO_{x(s)}$ coated sand has been reported (Lee et al., 2004). It was anticipated that the combination of pyrolucite and FBR could potentially offer a robust process which is less sensitive to water quality for enhanced Mn removal. Firstly, pyrolucite has a very high density (around 4,000 kg/m^3), which translates into the possibility to operate at very high HLR, and high specific adsorption sites. Secondly, the intrinsic turbulence found in fluidized beds provides more efficient utilization of the adsorption sites and better performance compared to fixed-bed contactors (USEPA, 2000). Finally, this configuration will offer the possibility to use a fine granular media (0.4 mm), a condition which is favorable for adsorption due to the increased surface area since it solves the issue of head loss accumulation.

The primary goal of the current research effort is to investigate the potential use of a pyrolucite FBR (PFBR) to remove high concentrations of Mn(II) from groundwater down to below 20 µg/L while operating at high HLR. The specific objectives of this paper are, first, to evaluate the effects of key operational parameters such as feed Mn concentration, temperature, pH, hardness (Ca^{2+} concentration), and HLR (i.e., bed expansion) on PFBR performance and, secondly, to assess the stability of the PFBR with respect to Mn removal over a long period of operation.

6.2 Material and Methods

The following sections detail the experimental procedures as well as the operational and analytical methods used to evaluate the performance of a small pilot-scale PFBR with respect to Mn removal.

6.2.1 Synthetic Groundwater (SGW) Preparation

All assays were conducted at pilot-scale (20 LPH) using a SGW. Before each assay, a volume of 200-400 L of SGW was prepared using deionized water. The required alkalinity and hardness were provided using an appropriate amount of 0.5 M $NaHCO_3$ and 0.5 M $CaCl_2$ solutions, respectively. The concentration of Mn(II) in water was controlled by the addition of 0.1 M $MnSO_4.H_2O$ stock solution. The pH of the SGW was adjusted by bubbling CO_2 and/or N_2 gas into the water prior to conduct the assay. SGW were not deoxygenated as preliminary assays indicated that performance was not significantly impacted by the presence of dissolved oxygen in the feed waters.

6.2.2 Lab-Pilot Experimental Set-up and Pyrolucite Characteristics

The FBR column had a cross-sectional area of 5.07 cm^2 corresponding to an inner diameter of 2.54 cm, which was filled up with a 100 cm of a commercially available pyrolucite (LayneOx™ brand). The physical properties of pyrolucite media are presented in Table 6.1. Short-term (four-hour) Mn(II) uptake capacity of media was determined at pH=7, 23°C, 1 mg/L Mn concentration and alkalinity and hardness of 200 mgCaCO$_3$/L according to the procedure outlined by Tobiason et al. (2008). Mn uptake capacity result of new media was 0.84 mg Mn/g media and increased to 0.93 $\pm$ 0.01 after regeneration (indicates regeneration condition).

Table 6.1. Summary of pyrolucite media characteristics.

Effective Size (D_{10}) (mm)	Mesh Size	Uniformity Coefficient (D_{60}/D_{10})	Density (kg/m^3)	Bulk Density (kg/m^3)	Porosity (ε)	Mn Dioxide (% wt)	Mn Uptake Capacity (mg Mn/g media)
0.44	20 × 40	1.2	3850	2040	0.47	70 – 80%	0.84

6.2.3 Operation of the Experimental set-up

As assays were conducted both at 22°C and 9°C, the column was covered with insulation material for experiments conducted at 9°C in order to provide constant temperature throughout the PFBR. Free chlorine concentration was controlled by the addition of dilute bleach (NaOCl) solution which was prepared daily using a 6% (W/V) NaOCl stock solution. The SGW and dilute NaOCl solution were mixed ahead of a screen located at the bottom of the reactor. For most experiments, an effluent free chlorine residual of 1 mgCl$_2$/L was targeted. Unless mentioned otherwise, the PFBR was operated at a bed expansion of 10% corresponding to an hydraulic loading rate (HLR) of 40 m/h (16 gpm/ft^2).

In order to determine the Mn removal profile within the PFBR, total and dissolved Mn concentrations were measured at different heights of the PFBR (0, 5, 17.5, 25, 50, 75, 100, 110, and 150 cm from the bottom of the column). Dissolved Mn was defined here as Mn filterable through 0.45 μm Millipore filter (CAT NO. HAWP02500). The PFBR was operated for periods of 4 hours (short term assays) or 12 days (long term assays). Samples were collected at increasing operation time. At each sampling time, turbidity and free chlorine concentration in the influent and effluent water were analyzed. Additionally, in each experiment, alkalinity, pH and temperature of influent and effluent waters were measured.

Each experimental trial first consisted in acclimatizing the PFBR for an hour with Mn-free SGW at the desired HLR. This step also allowed cooling down the PFBR to 9°C. At time zero, the valve was switched to the drum containing the desired level of Mn. Then, the first samples were collected at time zero (t = 0h) from each sampling port along the PFBR column. Additional water samples were collected at 1, 2 and 4 hours after initiation of the experiment (t = 0h). At the end of each experiment, the PFBR was expanded (up to around 50%) and the media was rinsed with tap water for around 10 min. In order to provide the same media condition for all tests, an overnight regeneration of the media with 8-liter of recirculating chlorine solution (100 mg Cl_2/L) was conducted.

6.2.4 Experimental Matrix

The experimental plan was developed to test the water quality and operational variables expected to explain PFBR performance. Accordingly, four water quality characteristics and one operational parameters were measured and controlled in each experimental condition: the influent dissolved Mn concentration (0.5 – 3 mg Mn/L), Ca^{2+} hardness (0 – 200 mg $CaCO_3$/L), pH (6.2 – 7.8), temperature (9 – 23°C), and HLR (24 – 63 m/h) (i.e., bed expansion (0 – 30%)). The reference groundwater characteristics was chosen as pH=7, 9°C, HLR of 40 m/h, alkalinity and hardness of 200 mg$CaCO_3$/L and Mn concentration of 1 mg/L. The experimental matrix was realized by changing one test variable at a time.

6.2.5 PFBR Stability Experiments

In order to determine the long-term performance of the PFBR for Mn removal, assays were conducted for a period of up to 12 days. A schematic diagram of the experimental set-up used to

achieve this objective is shown in Figure 6.1. During these experiments, 400 L SGW was continuously pumped to the bottom of the PFBR. The SGW was renewed after 4-day of operation. As shown in Figure 6.1, free chlorine and Mn were injected from the stock solutions into the water prior entering the column. Around 10% of the effluent water from the PFBR was discarded. The remainder water was pumped to a GAC filter cartridge to remove the residual free chlorine and then returned back to the drum. The pH, temperature, alkalinity, turbidity, and chlorine and Mn concentrations were monitored and controlled daily.
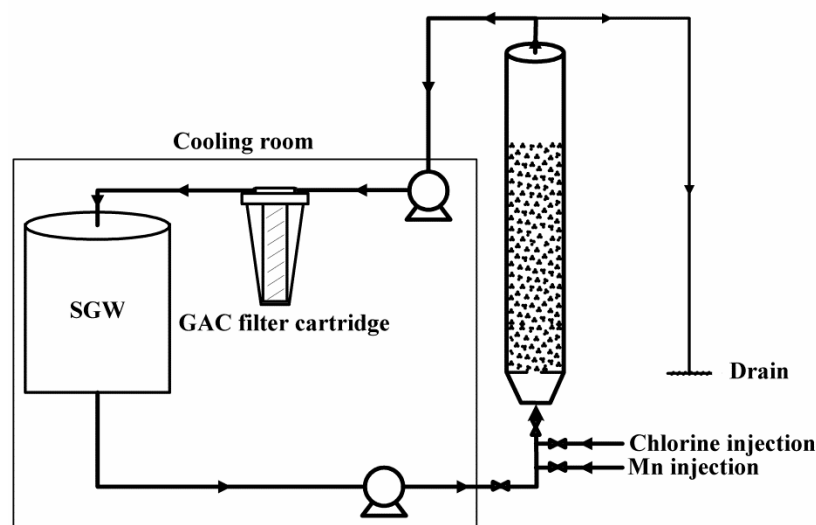
Figure 6.1. Schematic diagram of the long-term experimental plan.

6.2.6 Analytical Methods

Samples collected for total and dissolved Mn analysis were acidified to 0.5% HNO_3 and stored at 4°C. Mn analysis was performed using an Inductively Coupled Plasma-Optical Emission Spectrometry (ICP-OES, model iCAP 6000) from Thermo Instruments Inc. with a 1 µg/L Mn detection limit. A calibration curve was run at the beginning of each set of analysis. A standard and a blank were measured for quality assurance after every 20 unknown samples.

The DPD (N, N-diethyl-p-phenylenediamine) colorimetric method, Standard Method 4500-Cl-G, (American Public Health Association (APHA), American Water Works Association (AWWA) 2005) was used to measure the free chlorine residual concentration. A spectrophotometer (Hach, model DR 5000) was used for the analysis. Alkalinity was measured by titration with 0.02 N sulfuric acid (Method 2320 (American Public Health Association (APHA), American Water Works

Association (AWWA) 2005). Solution pH and turbidity were measured with an UltraBasic pH meter, model UB-5 from Denver Instrument and a Hach 2100 N turbidimeter, respectively.

6.3 Results and Discussion

The following section describes the Mn removal efficiency of the pilot-scale PFBR during the 4-hour experimental period. In all experiments, the difference between the total and dissolved (0.45 µm filterable) Mn was very low (less than 3%), and hence, only total Mn concentrations will be presented in all figures.

6.3.1 Short-term (4h) PFBR performance

A 4-hour operation cycle was chosen to evaluate the impacts of influent water characteristics on PFBR performance. In all figures, the percentage of Mn removal versus empty bed contact time was plotted. Each contact time refers to a specific height of the PFBR. For instance, at an HLR of around 40 m/h (10% expansion of PFBR), 0, 9, 17, 25, 50, 75, 100 and 110 cm from the bottom of PFBR refer to 0, 8, 15, 23, 45, 67, 89 and 98 s of contact time, respectively.

Figure 6.2 and Figure 6.3 show the performance of the PFBR over four increasing times during the 4-h cycle for increasing initial Mn concentrations of 0.5, 1, 2 and 3 mg/L at 9 and 23°C, respectively. The results demonstrate extremely high Mn removal performance as $> 99.9\%$ of Mn was removed in less than 1 min even at high initial Mn level of 3.3 mg/L (concentration of Mn in the effluent was always less than 5 µg/L). In addition, Mn removal profiles can be considered stable at lower initial Mn concentrations. However, at higher Mn levels, especially at 9°C, unstable Mn removal profile was observed. This is conceivable since the adsorption reaction is very fast, while the subsequent autocatalytic oxidation of sorbed Mn(II) by chlorine is slower to some extent (Knocke et al., 1990a). In addition, although Mn(II) uptake capacity increases by increasing feed Mn(II) concentration, Tobiason et al. (2008) showed that breakthrough occurs earlier at higher Mn(II) concentrations. Higher chlorine concentration might be required for continuous removal of Mn while operating at high initial Mn levels.
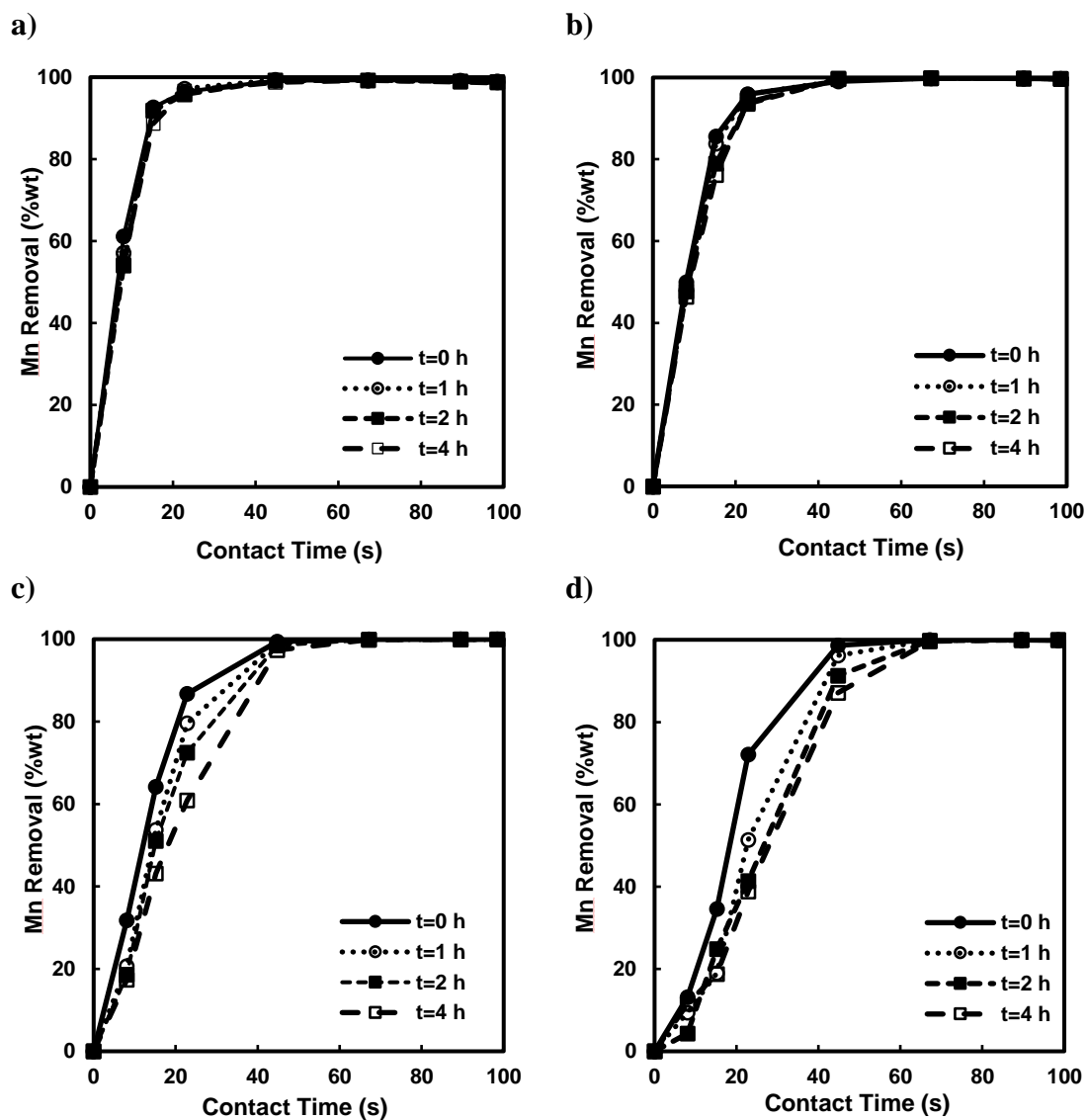
Figure 6.2. Mn removal performance over the height of PFBR as a function of time. Influent SGW: Mn0 = a) 0.5, b) 1.0, c) 2.3-2.4, d) 3-3.2 mg/L, T= 9±1°C, pH = 7.0±0.1, chlorine = 1-1.3 mg/L, alkalinity and hardness = 200 mg CaCO$_3$/L.
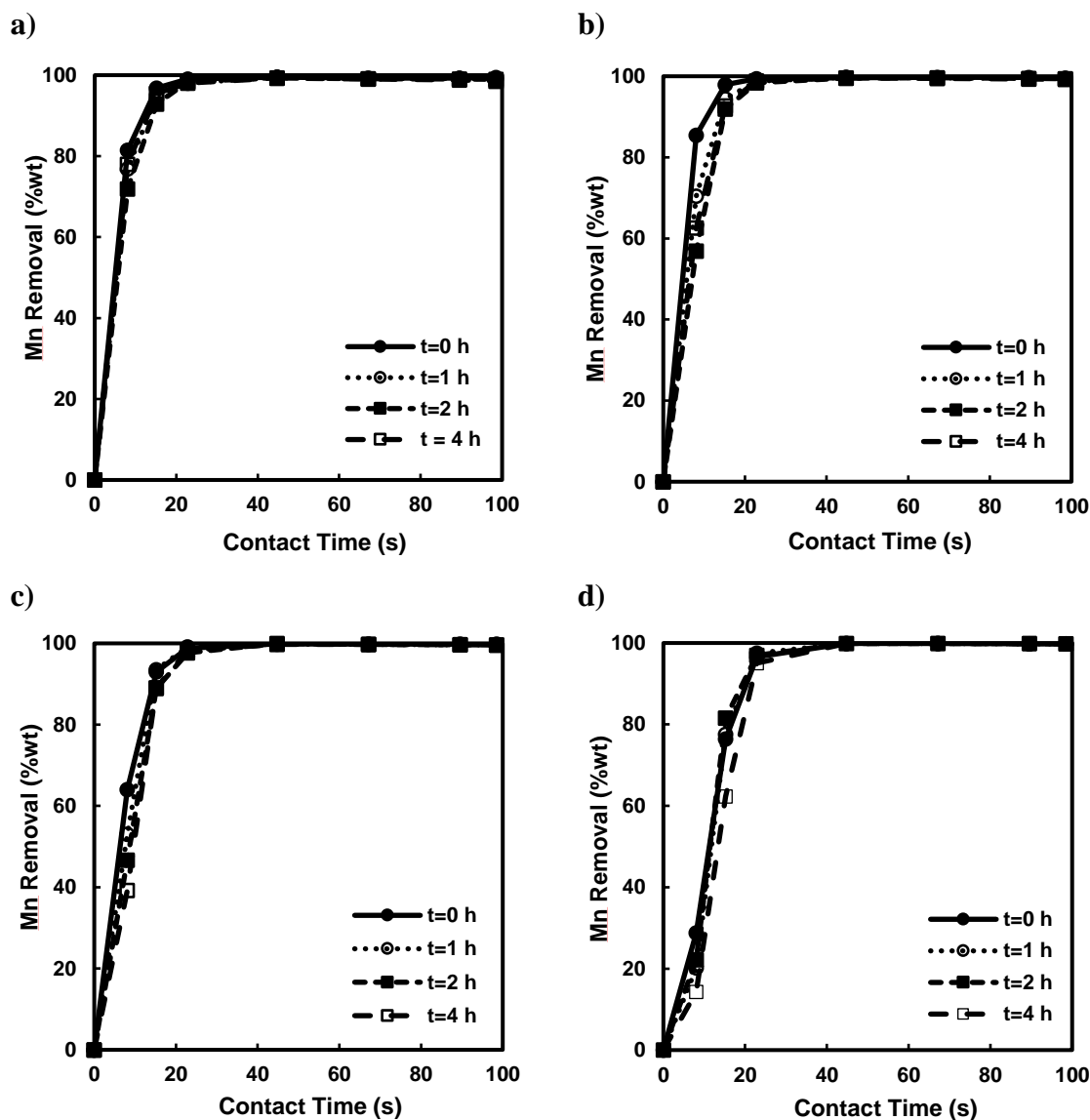
Figure 6.3. Mn removal performance over the height of PFBR as a function of time. Influent SGW: Mn0 = a) 0.5, b) 1.0-1.1, c) 2.3-2.4, d) 3.2-3.3 mg/L, T= 23±1°C, pH = 7.0±0.1, chlorine = 1.2-1.4 mg/L, alkalinity and hardness = 200 mg CaCO₃/L.

Since adsorption onto $MnO_{2(s)}$ is an endothermic process (Ren et al., 2011), Mn(II) uptake capacity of pyrolucite media is expected to increase at elevated temperatures. In addition to its effect on Mn(II) sorption, temperature can also negatively affect Mn removal in continuous regeneration process by increasing solution oxidation of Mn(II) by free chlorine at elevated temperatures (23°C versus 9°C). Under such scenario, the process performance would be expected to decline due to the formation of colloidal MnO_x, especially at higher feed Mn(II) concentrations for which condition it might be difficult to capture colloidal MnO_x within the PFBR. However, as can be seen in

Figure 6.2 and Figure 6.3, improved Mn removal profile was achieved at higher temperature as a result of higher Mn(II) adsorption capacity of pyrolucite. In conclusion, an increase in temperature slightly improved PFBR performance which is coherent with an improved adsorption/oxidation of Mn(II). The very short contact time (less than 1 min) between Mn(II) and free chlorine is most likely preventing significant solution oxidation of Mn(II) by free chlorine. This is in agreement with the identical concentration of dissolved and total Mn measured in each sampling point along the PFBR.

It has been shown that the adsorption of Mn(II) onto $MnO_{x(s)}$ is highly dependent on pH (Morgan and Stumm, 1964). The point of zero charge (pH_{zpc}) of $MnO_{x(s)}$ on coated sand was shown to be about 1.26 (Hu et al., 2004). As the solution pH increases, the oxide surface charge becomes increasingly negative. This leads to an increase in Mn(II) adsorption rate as well as an increase in the adsorption capacity of $MnO_{x(s)}$ as more sites become available for Mn(II) uptake (Knocke et al., 1990a). Representative data plotted in Figure 6.4 indicate that the ability of the PFBR to effectively remove Mn was relatively insensitive to the SGW pH level occurring over a range of 6.2 to 7.8. This can be attributed to the fact that fewer Mn(II) uptake rate at a lower pH conditions can be compensated by larger amount of oxide surface (i.e., active sites) (Knocke et al., 1990a). Thus, it can be concluded that high level of adsorption sites on the pyrolucite media plays a key role in Mn removal efficiency of PFBR. As shown by Zuravnsky (2006) and Knocke et al. (2010), pyrolucite media offers a higher capability for Mn(II) adsorption than $MnO_{x(s)}$-coated sand. This was attributed to both a higher specific concentration of $MnO_{2(s)}$ on the media (mg Mn/g media) and a higher amount of available active sites on its surface (Zuravnsky, 2006). In addition, improved contact between the SGW and pyrolucite media is found in the PFBR as opposed to packed bed contactors (USEPA, 2000). This probably offers a more efficient utilization of available adsorption sites.

The impact of calcium hardness was tested with the hypothesis that higher calcium may modify surface media zeta potential and compete for negative adsorption sites. This hypothesis was supported by results from Merkle et al. (1997) who found that high Ca^{2+} concentrations (above 60 mg Ca/L) hindered the adsorption of Mn(II) by oxide coated media,. In this study, no significant difference of performance was noted (results not shown) and a constant Mn(II) removal profile was achieved within the PFBR across a fairly wide range of Ca^{2+} concentration (0 to 80 mg Ca^{2+}/L corresponding to 0 to 200 mg $CaCO_3$/L). This result confirms the previous discussion regarding

the high level of available adsorption site provided by PFBR which makes the process to be relatively insensitive to these changes.
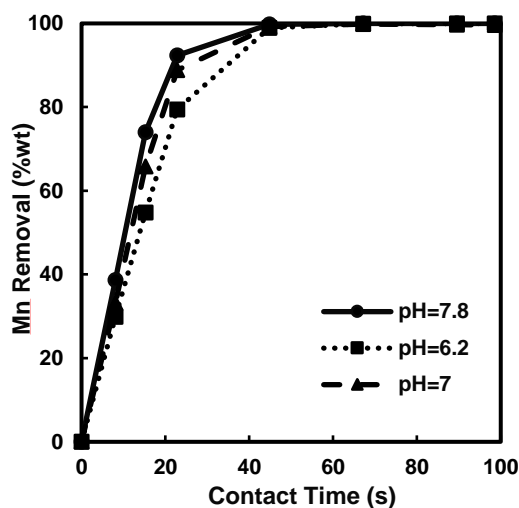
Figure 6.4. Effect of pH on Mn removal performance over height of PFBR. Influent SGW: Mn0 = 1.0-1.1 mg/L, T= 9±1°C, chlorine = 1.2-1.4 mg/L, hardness = 200 mg CaCO$_3$/L, alkalinity = 50 mg CaCO$_3$/L.

Designing a process which can effectively remove Mn while operating at high HLR is of great importance for reducing the required process footprint and consequently the unit costs for Mn control. A FBR provides the ability to operate at HLR of 40-60 m/h, a largely higher range than in fixed bed contactors (typically 10-20 m/h). Representative data shown in Figure 6.5a compare Mn removal profiles at HLR of 24 (i.e., minimum fluidization velocity), 40 (i.e., 10% expansion), 50 (i.e., 20% expansion) and 63 m/h (i.e., 30% expansion) under relatively high initial Mn concentration (2.2 to 2.4 mg/L). As can be seen, although the hydraulic detention time in the PFBR is very short at the highest HLR of 63 m/h (less than 75 seconds), 100% of Mn was removed during the 4 hours experimental scenario.

Concentrations of total and dissolved Mn at any given location within the PFBR were almost identical. Also, chlorine demand over the PFBR was lower (0.2-0.3 mg Cl$_2$/L) than the expected required chlorine for oxidation of Mn(II) (Knocke et al., 1990a). These observations demonstrate that adsorption of Mn(II) onto pyrolucite and subsequent slower surface oxidation of sorbed Mn(II) was responsible for Mn removal while direct oxidation of Mn(II) did not occur even at the highest initial Mn(II) concentrations (2.2 to 2.4 mg/L). If direct oxidation of Mn(II) by free chlorine had been important, it should have led to the formation of particulate Mn within the FBR and increased

turbidity in the PFBR effluent. However, none of these phenomena were observed during our experiments (even after 12 days of operation).

a)

b)
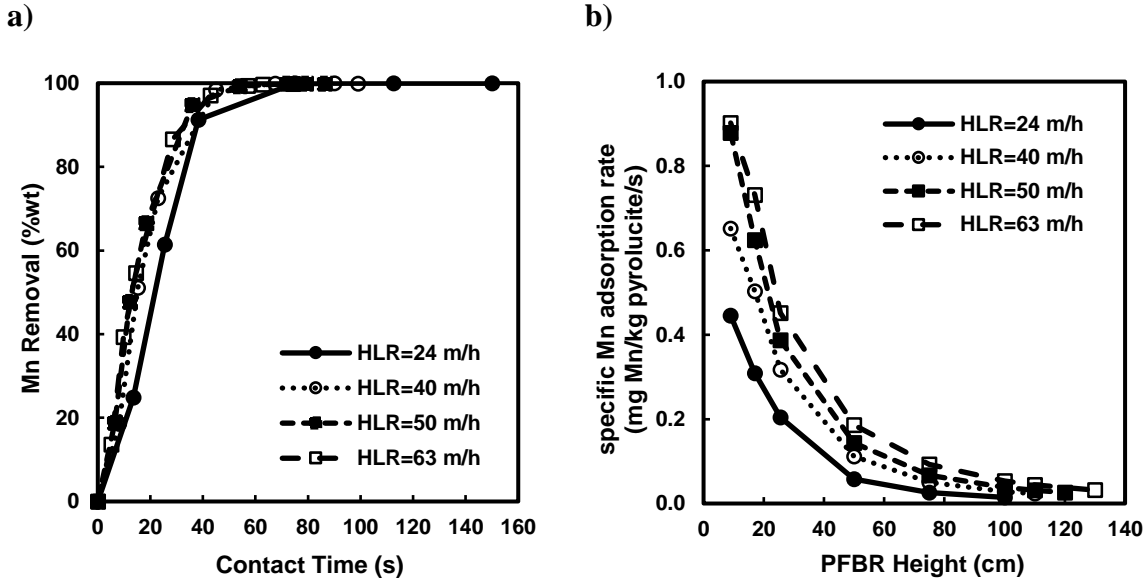
Figure 6.5. Effect of HLR on a) Mn removal performance and b) specific Mn adsorption rate over height of PFBR. Influent SGW: Mn0 = 2.2-2.4 mg/L, T= 9±1°C, pH = 7.0±0.1, chlorine = 1.2-1.4 mg/L, hardness and alkalinity = 200 mg CaCO$_3$/L.

Dwivedi and Upadhyay (1977) showed that Eq. (5.1) can properly correlate liquid-phase fixed and fluidized bed data for particle-fluid mass transfer with an average deviation of 18% in the range of Reynolds number from 0.01 up to 15000.

$$\varepsilon J_d = \frac{0.765}{Re^{0.82}} + \frac{0.365}{Re^{0.386}} \tag{5.1}$$

where ε is void fraction, J_d is Chilton-Colburn mass transfer factor $((k_f/U)Sc^{2/3})$, and Re is the particle Reynolds number (Ud_p/υ). Accordingly, the average mass transfer coefficient (k_f) can be expressed as follows (Eq. (5.2)):

$$k_f = \left(\frac{0.765}{Re^{0.82}} + \frac{0.365}{Re^{0.386}}\right) * \left(\frac{U}{\varepsilon\, Sc^{2/3}}\right) \tag{5.2}$$

where U is superficial fluid velocity (m/s) and Sc is the dimensionless Schmidt number (υ/D).

Bošković-Vragolović et al. (2009) applied an adsorption method as a suitable procedure for mass transfer studies. They concluded that Eq. (5.2) satisfactorily fits the experimental data obtained

from diluted solution fluid-to-solid mass transfer in their FBR. This is consistent with Dwivedi and Upadhyay (1977) conclusion.

Eq. (5.2) depicts that k_f is proportional to fluid velocity. However, it is worth mentioning that an increase in FBR fluid velocity also results in an increase in bed voidage (or porosity) which is inversely proportional to k_f. Bošković-Vragolović et al. (2009) computed k_f values at different fluid velocities in both fixed-bed and FBR. Their results showed that the highest k_f can be achieved at minimum fluidization velocity, in which the adsorbent concentration is maximum (ε is minimum). From their results, it seems that after minimum fluidization velocity higher HLR cannot compensate the resulting increase in voidage and hence the k_f decrease.

Surprisingly, the result obtained in this study, as depicted in Figure 6.5b, shows that specific Mn adsorption rate, over the height of PFBR, is higher at elevated HLR. Consistently, the calculated k_f at different HLR (Table 6.2) using Eq. (5.2) reveals that k_f slightly increases at higher HLR (14% for the highest HLR). Such difference with Bošković-Vragolović et al. (2009) data is probably due to the high specific gravity of the pyrolucite media relative to the glass particles used by these authors. A high specific gravity prevents excessive expansion of the PFBR at high HLR. For example, Table 6.2 indicates that an increased HLR from 24 to 63 m/h represents a 2.6-fold increase. Meanwhile, bed porosity is only increased by 25%. Consequently, the increased HLR can compensate the detrimental effect on k_f of working with a higher porosity. These results show that, unlike the packed-bed pyrolucite contactor (Zuravnsky, 2006; Tobiason et al., 2008), Mn removal performance in PFBR not only does not reduce at elevated HLR but also a slight increase can be achieved (Figure 6.5a and b).

Table 6.2. The average mass transfer coefficient at different HLR.

HLR (m/h)	Re	ε	$k_f \times 10^5$ (m/s)
24	2.17	0.47	9.58
40	3.62	0.52	10.47
50	4.53	0.56	10.58
63	5.71	0.59	10.93

6.3.2 Long-Term Stability of the PFBR

Additional experiments were performed over a period of 12 days to determine the stability of the PFBR with respect to Mn removal. These assays were duplicated using two different effluent free chlorine residuals. The presence of sufficient free chlorine residual is critical for both the maintenance of available sorption sites and to increase the mass transfer gradient between the interface of the media and the bulk water (Knocke et al., 1990a). Figure 6.6 shows Mn concentration in the PFBR inlet and outlet during the 12-day experiments, while free chlorine residuals were kept at 1.0 (Figure 6.6a) and 2.0-2.6 $mgCl_2/L$ (Figure 6.6b) in treated water, respectively. For experiments conducted using a free chlorine residual of 1.0 $mgCl_2/L$ in the effluent, the process failed to adequately remove Mn (i.e. < 20 µg/L in the effluent) after 6 days of operation (Figure 6.6a). However, increasing the effluent concentration to 2.0-2.6 $mgCl_2/L$ led to Mn concentration steadily reduced to below the limit value of 20 µg/L in the effluent (almost 100% removal performance) (Figure 6.6b) for the entire test period. As shown in Figure 6.6a and b, chlorine demand over the PFBR was increased at higher influent chlorine concentration (from < 0.2 $mgCl_2/L$ to 0.2-0.9 $mgCl_2/L$). This confirms the higher stability of the PFBR at effluent free chlorine of 2.0-2.6 mg/L as most of the occupied sites were continuously regenerated (the theoretical chlorine demand to oxidize Mn(II) to Mn(IV) is 1.0-1.3 $mgCl_2/L$ for this influent Mn(II) concentration, however, the oxidation state of Mn on the surface of media may vary between Mn(III) to Mn(IV) (Cerrato et al., 2011)). For some systems, such free chlorine residual might be too high to be considered applicable and depends on the required needs with respect to primary and secondary disinfection. Nevertheless, regenerating the media after 6 days of operation appears a realistic operational constraint for a small groundwater system operator. Finally, these operational cycles were achieved for a relatively high influent Mn concentration of 0.8-1.3 mg/L. It is expected that lowering influent Mn condition will lead to longer duration before regeneration. Similarly, a deeper PFBR might also be an option to extend the duration of operation before regeneration.

Finally, it is important to point out that over this time period (12 days), the turbidity in the PFBR effluent was constantly at 0.2 NTU which implies that no post-filtration would be needed after the PFBR. Additional assays are scheduled to be conducted using an industrial pilot under natural groundwater conditions to address the longer-term fate of the Mn removed within the PFBR.

a)   b)
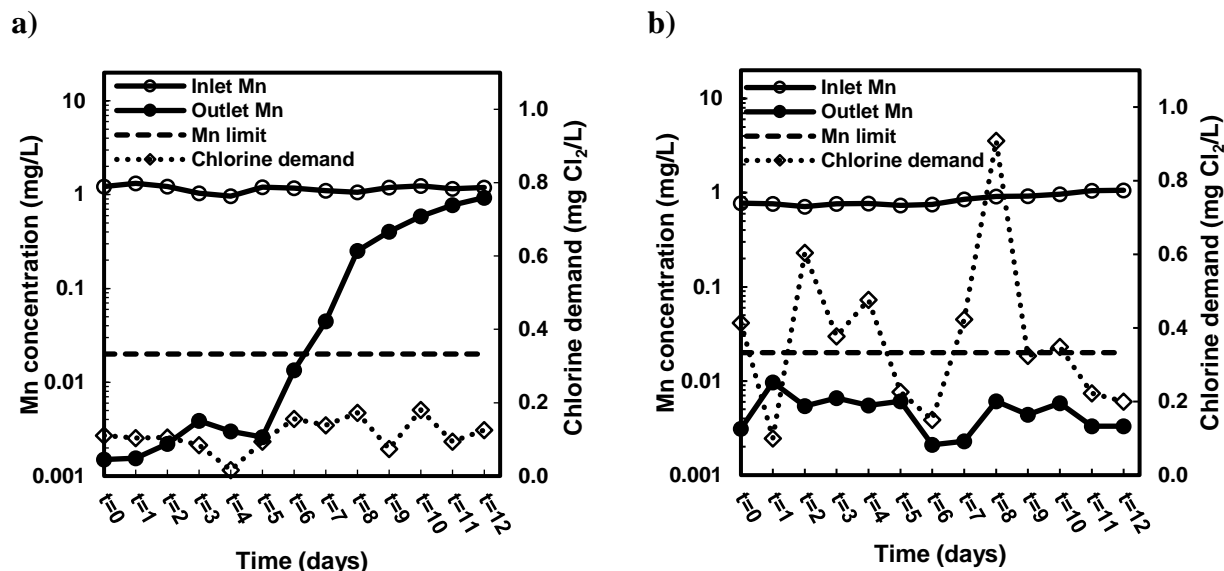
Figure 6.6. Stability of the PFBR for Mn control at effluent free chlorine concentrations of a) 1.0 mg/L b) 2.0-2.6 mg/L. Mn0 = 0.8-1.3 mg/L, T= 10±2ºC, pH = 7.0±0.1, HLR ≈ 40 m/h (10% expansion), alkalinity = 150-200 mg CaCO$_3$/L and hardness = 200 mg CaCO$_3$/L.

6.4 Conclusions

The potential application of a PFBR for Mn removal from groundwater containing high level of Mn(II) was evaluated under various synthetic groundwater (SGW) composition and operational conditions. The following conclusions were drawn from this research study:

- High performance of a PFBR with respect to dissolved Mn removal was demonstrated under different operating conditions and SGW composition. Close to 100% Mn removal was achieved within a short contact time (< 1 min).

- Low influent pH values (down to 6.2) and high Ca^{2+} concentrations (up to 80 mg/L or 200 mg CaCO$_3$/L) did not have significant detrimental effect on Mn removal throughout the PFBR.

- Providing sufficient contact time was found to be a key design parameter in this process rather than the SGW composition.

- High specific gravity of pyrolucite allowed the process to be operated at high HLR without any concern of reduction in adsorption rate.

- Maintenance of an appropriate effluent free residual chlorine in the effluent of PFBR plays a major role in the long-term stability of this process.

Future assays should evaluate the impact of natural organic matter as well as test if dissolved iron can be removed simultaneously with Mn in the PFBR.

Acknowledgements

CHAPTER 7   ARTICLE 4 :   COMPARISON OF PYROLUCITE FIXED AND FLUIDIZED BEDS FOR IRON AND MANGANESE CONTROL IN GROUNDWATER: A PILOT-SCALE STUDY

This chapter presents a manuscript submitted to the Journal of Environmental Chemical Engineering. It reports the results obtained from an extensive experimental campaign aimed at investigating the performances of pilot-scale pyrolucite fixed and fluidized bed contactors for iron and manganese control in groundwater under different conditions.

Comparison of Pyrolucite Fixed and Fluidized Beds for Iron and Manganese Control in Groundwater: A Pilot-Scale Study

Seyedeh Laleh Dashtban Kenari[a*], Jaber Shabanian[b], and Benoit Barbeau[a]

[a] Polytechnique Montreal, Department of Civil, Geological and Mining Engineering, NSERC-Industrial Chair on Drinking Water, Environment, C.P. 6079, Succursale Centre-Ville, Montreal, QC, H3C 3A7, Canada.

[b] Polytechnique Montreal, Department of Chemical Engineering, C.P. 6079, Succursale Centre-Ville, Montreal, Quebec, H3C 3A7, Canada.

[*] Corresponding author: Tel: +1 514 340-4711 #2983; Fax: 514-340-5918;

E-mail: laleh.dashtban@polymtl.ca

ABSTRACT

Iron and manganese removal is a common water treatment goal in groundwater systems. Pilot-scale pyrolucite fixed and fluidized bed contactors were tested in parallel to examine the iron and manganese removal from a natural groundwater which was supplemented with iron/manganese in order to challenge both processes. The design of the distributor plate located at the bottom of the pyrolucite fluidized bed (PFB) had crucial impact on the release of particulate manganese from the filter media. Using an optimal distributor plate, the PFB contactor provided effective manganese removal (< 0.02 mg/L) at very high hydraulic loading rate (45 m/h). The fixed bed was also effective at 20 m/h. Under elevated iron concentration (0.18 ± 0.02 mg/L), the pyrolucite fixed bed alone provided almost complete iron and manganese removal while requiring frequent backwash of the filter bed (3 d). However, under such condition, the PFB failed to properly control the iron and manganese concentrations below the target limit of 0.02 mg/L as manganese and iron were found to be carried over in the effluent. Further study should address the potential implementation of a cost-effective post-filtration process, downstream of the PFB, which would finalize the iron and manganese removal from the PFB effluent.

KEYWORDS: Iron/manganese removal; fixed bed; fluidized bed; groundwater; pyrolucite.

7.1 Introduction

Nearly 30% of Canadian and 44% of the US population, mostly living in small rural communities, relies on groundwater as a source of drinking water. Groundwater commonly contains high levels of dissolved iron and manganese due to the presence of reduced redox conditions. Although the presence of iron and manganese in drinking water is principally regarded as an aesthetic and operating issues, recent studies have disclosed that manganese intake from water ingestion, even at low levels, may lead to intellectual impairment in children (Bouchard et al., 2011) and other neurological disorders (Wasserman et al., 2006; Tuschl et al., 2013). The United States Environmental Protection Agency (USEPA 2004) and Guidelines for Canadian Drinking Water Quality (Health Canada, 2014) recommended an aesthetic drinking water objective of 0.3 and 0.05 mg/L for iron and manganese, respectively. However, the concentrations of iron and manganese as low as 0.05 mg/L (World Health Organization, 2003) and 0.02 mg/L (Sly et al., 1990) may still

result in discoloration of water. As a consequence, Health Canada (2016) has recently proposed an aesthetic objective limit of 0.02 mg/L and a health-based value of 0.1 mg/L for total manganese in drinking water. The implementation of these guidelines (still pending at the time of preparing this article) is expected to reinforce the importance of proper operation and design of manganese removal processes.

The oxidation and filtration method that is conventionally utilized in North America for iron and manganese control in groundwater has some constraints, which can be listed as follows: (i) multiple hours of contact time is required for substantial oxidation of manganese by free chlorine even at pH 8.0 (Knocke et al., 1990b; Allard et al., 2013); (ii) oxidation of manganese by stronger oxidants than chlorine, such as potassium permanganate and ozone, depends on the pH, temperature, initial dissolved manganese concentration, and contact time (Knocke et al., 1990b; Van Benschoten et al., 1992); (iii) application of these strong oxidants always rises the risk of pink water formation, especially in water sources with high concentration of natural organic matter (NOM) (Gregory and Carlson, 2003); (iv) manganese oxides can be difficult to capture by granular media filtration (Carlson et al., 1997) owing to the formation of stabilized colloids with a high negative charge (Dashtban Kenari and Barbeau, 2016a); and (v) colloidal manganese is prone to severely foul microfiltration (MF) or ultrafiltration (UF) membranes (Dashtban Kenari and Barbeau, 2016b).

Natural greensand effect (NGE) process has proved to be a reliable technique for successful manganese control (Knocke et al., 1990a; Knocke et al., 2010; Dashtban Kenari and Barbeau, 2014). In this process, manganese removal is based on the adsorption of dissolved ion onto the $MnO_{x(s)}$ surface followed by catalytic oxidation of the adsorbed manganese. Thus, the performance of this process is substantially affected by the maintenance of available sorption sites, which is governed by the $MnO_{x(s)}$ coating level, pH, and the concentration of oxidant. The dual functions of filter media in NGE process allow two modes of operation: intermittent regeneration (IR) and continuous regeneration (CR) (Knocke et al., 1990a). In IR operation mode, the filter media adsorbs dissolved manganese until available sorption sites are exhausted and breakthrough take place. The filter media is then regenerated by potassium permanganate or free chlorine to restore its adsorption capacity. In CR mode, free chlorine is continuously injected into water prior entering the filtration column and the exhausted adsorption sites are continuously regenerated in order to keep them active. However, since the adsorption rate is much faster than the oxidation rate of adsorbed manganese by free chlorine (Knocke et al., 1990a), all the adsorption sites may not be fully

regenerated and exhaustion might occur after a long operation unless sufficient chlorine residual is maintained throughout the column (Dashtban Kenari and Barbeau, 2014).

Catalytic filtration of manganese has been particularly implemented in fixed bed contactors containing $MnO_{x(s)}$-coated sand, such as manganese greensand, at relatively low hydraulic loading rates (HLRs) (6-12 m/h) (Hargette and Knocke, 2001; Yang et al., 2008; Piispanen and Sallanko, 2010). The conventional fixed bed contactors for adsorption of manganese have several disadvantages, such as a relatively high hydraulic retention time, high energy expenses due to rapid head loss build-up, and a large amount of wastewater production during backwash. Alternatively, pyrolucite fluidized bed (PFB) adsorptive contactors could offer a number of promising benefits in comparison with the fixed bed contactors containing $MnO_{x(s)}$-coated sand such as: (i) pyrolucite media, which is a natural manganese sand consisting of more than 80% manganese dioxide, offers high available adsorption sites; (ii) high specific gravity of pyrolucite (around 4.0) allows operating the fluidized bed at very high HLRs without any concerns about the particle entrainment from the bed; (iii) the adsorption sites can be efficiently exploited in fluidized state due to the better fluid-solid contact which offers a higher adsorption rate; and (iv) the fluidized bed contactor permits the application of pyrolucite media with high specific surface area (all granules are smaller than 0.8 mm in size) that is favorable for adsorption kinetic while simultaneously eliminates the head loss accumulation problem that is common for the fixed bed contactors. In an earlier study by our group (Dashtban Kenari and Barbeau, 2014), we demonstrated that high levels of dissolved manganese in synthetic groundwater could be successfully controlled by a PFB contactor. However, the long-term stability of the process was not explored using natural groundwater. In addition, it is unknown if the PFB contactor performance for manganese removal is impacted by the presence of iron in water. Finally, it is unclear if a proper treatment performance of a PFB contactor can be achieved for iron removal or not while, unlike manganese, dissolved iron is readily oxidized by free chlorine (Knocke et al., 1990b).

This study aimed at shedding light on the performance of a pilot-scale PFB contactor for dissolved iron and manganese removals during long-term operation of a pilot system fed by a natural groundwater. In parallel, a pilot-scale fixed bed contactor was operated as a control. Both contactors were operated under variable iron and manganese concentrations and HLRs. This study also addresses the operational challenges that can be encountered for pyrolucite fixed and fluidized bed contactors.

7.2 Materials and methods

7.2.1 Materials: chemicals, source water and pyrolucite filter media

Chemicals

All powdered reagents employed in this study were of commercial purity grade. Iron (II) sulfate heptahydrate, manganese (II) sulfate monohydrate, potassium iodide, and sodium arsenite were purchased from Fisher Scientific (Fair Lawn, NJ). Omni Trace® nitric acid (67-70%) and potassium permanganate were supplied from EMD chemicals Inc. (Gibbstown, NJ). All stock solutions were prepared using ultrapure water (Milli-Q^{TM}).

Source water

The source water tested during this investigation was a natural groundwater supplying the community of Sainte-Marthe-sur-le-Lac, Quebec, Canada. In some experiments the feed water was artificially enriched with dissolved iron or manganese to determine the process performance under elevated concentration of these species. In this regard, iron (II) sulfate heptahydrate or manganese (II) sulfate monohydrate stock solution was separately spiked into the natural groundwater prior entering the contactors. In order to prevent the precipitation of ferric hydroxide in the stock solution (4 g Fe^{2+}/L), the pH of Milli-Q^{TM} water was adjusted at 3.0 with hydrochloric acid and the solution was subsequently deoxygenated by bubbling nitrogen gas for 15 min prior to dissolution of iron (II) sulfate heptahydrate in water. Preliminary assays confirmed the stability of manganese (II) stock solution (6 g Mn^{2+}/L). Therefore, it was simply prepared by dissolving manganese (II) sulfate monohydrate in Milli-Q^{TM} water. The characteristics of the feed water was regularly examined and are summarized in Table 7.1.

Table 7.1. Characteristics of the groundwater tested in this study.

Iron (mg/L)	Manganese (mg/L)	Hardness (mg CaCO$_3$/L)	Alkalinity (mg CaCO$_3$/L)	pH	DO[1] (mg/L)	DOC[2] & TOC[3] (mg C/L)	SUVA[4] (L/mg/m)	Temperature (ºC)
0.01-0.18	0.09-0.35	200	170	7.0-7.2	1.9-2.9	3.3	1.9	8-12

[1]Dissolved oxygen
[2]Dissolved organic carbon
[3]Total organic carbon
[4]Specific ultraviolet absorbance

Pyrolucite filter media

Commercially available pyrolucite (MangOx^{TM} brand, high purity: 86% manganese dioxide by wt) was utilized as a filter media in both types of contactor. The physical characteristics of pyrolucite are presented in Table 7.2. The virgin pyrolucite was conditioned with potassium permanganate prior to its use in the pilot plant.

Table 7.2. Characteristics of commercial pyrolucite.

Median diameter (D$_{50}$) (mm)	Uniformity coefficient (D$_{60}$/D$_{10}$)	Mesh size	Specific gravity	Bulk density (kg/m^3)	Porosity	Manganese dioxide (% wt)
0.6	1.5	20 * 40	3.8	2000	0.47	86 %

7.2.2 Pilot plant configuration

The pilot plant was located at a groundwater treatment facility in Sainte-Marthe-Sur-le-Lac, Quebec, Canada. The configuration of the pilot plant with fixed and fluidized bed contactors is shown in Figure 7.1. The columns were made of two identical transparent clear polyvinyl chloride (PVC) pipes with approximately 2.5 m length and 15.2 cm (6 in.) inner diameter. Both columns were filled up to an initial fixed bed height of 90 cm with the commercially available pyrolucite. The feed line was equipped with a static mixer to blend all the individually spiked solutions with the natural groundwater. The volumetric flow rate was adjusted with a rotameter.

In order to achieve an appropriate operation of the PFB contactor, we first examined different configurations of influent distributor plate. Designing a proper distributor was shown to be critical to the successful operation of the PFB contactor. The best configuration identified during these preliminary tests was then used for the rest of the study. Configurations of these plates are briefly described as follows and are presented in Figure 7.2:

i)   Distributor A: A cap distributor plate containing two caps each having forty slits of 0.2 mm width and 25 mm long. The plate was made from PVC.

ii) Distributor B: A shrouded perforated distributor plate made from PVC with a total thickness of 5 cm. The bottom layer of the plate, which was responsible for creating enough pressure drop to evenly distribute liquid across the bed cross-section, was 1.2 cm thick and consisted of seven holes of 4 mm in diameter. Six of these holes were evenly arranged in a circular path of 10 cm diameter while the last one was located at

the center of the plate. The shroud layer (installed on top of the bottom pressure drop controlling layer) was 3.8 cm thick with an identical number of holes centered with those placed on the bottom layer, yet with a larger diameter (3 cm). This configuration could assist in reducing particle attrition due to the jet formation, especially if the shroud is long enough to embed the expanding jet velocity profile (Pell 1990). The shroud layer was filled with large gravel (about 10 mm in size) to further help in breaking the liquid jet formed by the bottom layer of the distributor plate. The perforated distributor plate was provided with a 300 µm metal mesh to prevent particles accumulating inside the shroud or the plenum chamber/windbox.

iii)   Distributor C: An identical configuration as described for Distributor B. However, the 300 µm metal mesh on top of the perforated distributor plate was replaced by a 15 cm gravel layer of 4-10 mm in size.
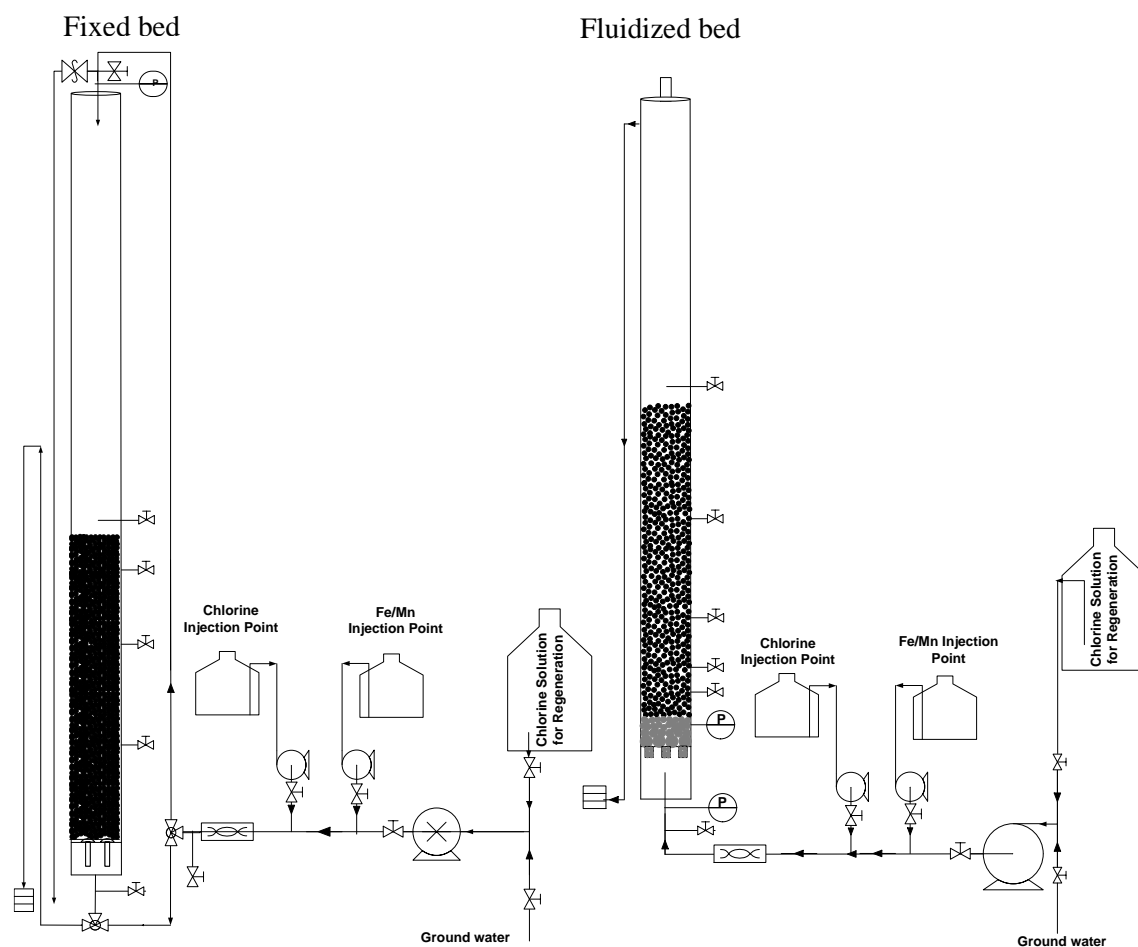
Figure 7.1. Schematic of pilot plant experimental set-ups. Left: Fixed bed. Right: Fluidized bed.

Distributor A	Distributor B	Distributor C
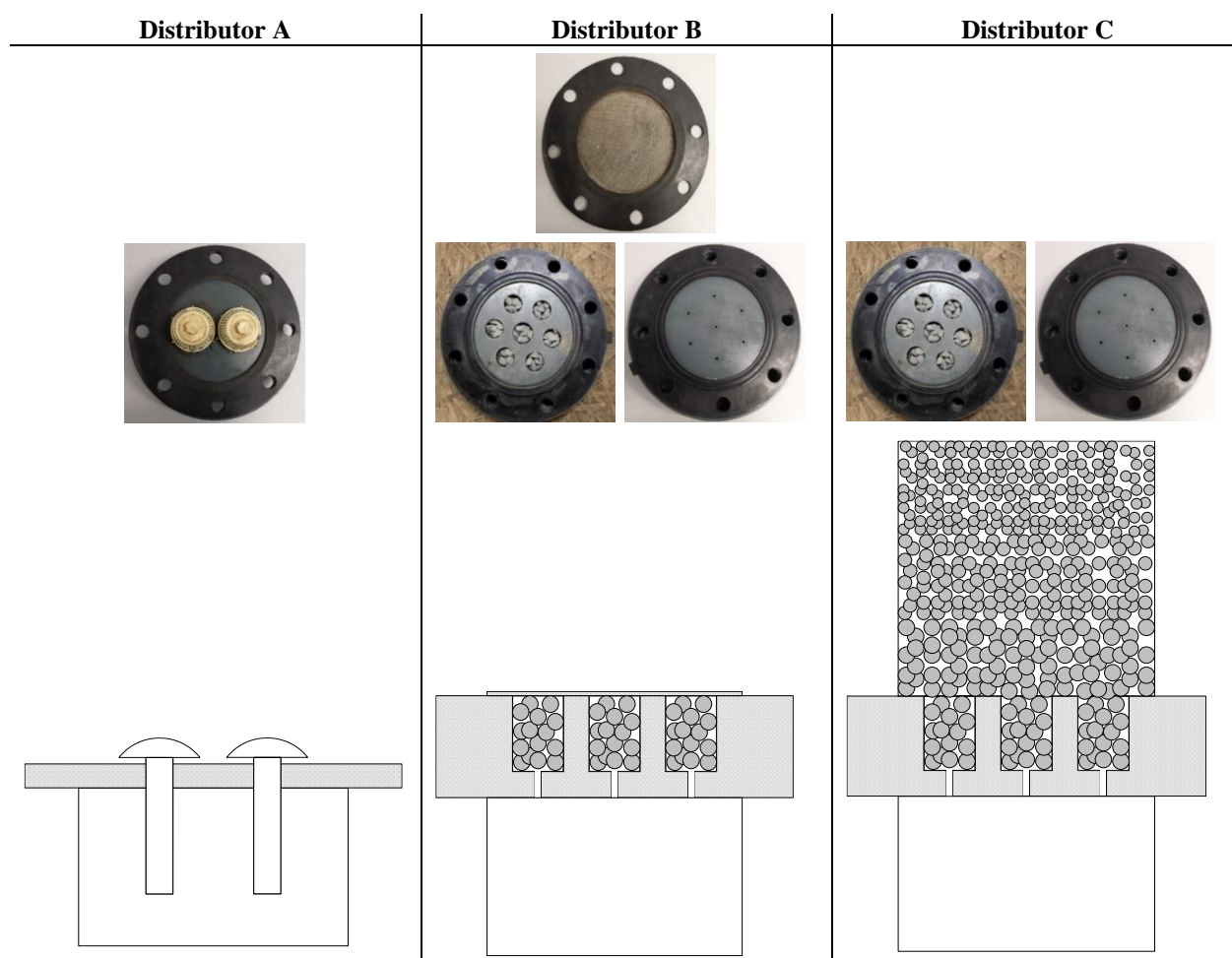
Figure 7.2. Schematic drawing of various distributors for fluidized bed contactor.

7.2.3 Pilot plant operation

Fluidized bed contactor

Natural groundwater was introduced into the bottom of the column at a flow rate of 30-45 m/h (12-18 gpm/ft^2) using a centrifuge pump (Natpro, Inc.) which fluidized the pyrolucite media to a bed expansion of 10-20%. Commercial bleach solution (4% (W/V) Cl_2/L) was continuously injected into the water prior entering the column. The flow of this solution was accurately adjusted to maintain an effluent free chlorine residual of 1.0 mg Cl_2/L. In order to determine iron and manganese removal profile along the fluidized bed, water samples were taken at different heights of the column (at distributor level and 7.5, 15, 30, 60, 100 and 110 cm above the distributor). Both dissolved and total iron and manganese concentrations were measured at each sampling point. Dissolved species were defined as iron and manganese filterable through a 0.45 µm syringe filter

(PVDF, CAT. NO. CS-GLPV3045). A gauge pressure transducer (Omega, PX409-030GUSB) was mounted flush with the wall of the fluidized bed and right above the distributor plate for continuous monitoring of the pressure build-up within the bed over a total 21 days of experimental period for each condition explored in this research. The first samples that were collected after one hour of initiation of the experiment are ascribed to the time zero (t = 0). At the end of each experiment, i.e., after 21 days of operation, the fluidized bed was expended up to 40% for 20 min to remove the loosely-attached particles to the pyrolucite media. In order to maintain an identical condition for all experiments while preserving the same pyrolucite media in the bed, the media was then fully regenerated with recirculation of 50-L sodium hypochlorite solution (1% (W/V) Cl_2/L) at the minimum fluidization condition for 24 hours.

Fixed bed contactor

The fixed bed was similarly operated to the fluidized bed. The differences in operation could be listed as: (i) groundwater was fed to the top of the pressurized column with the help of a gear pump (Natpro, Inc.), which provided a constant flow under all pressures over the 21 days of experimental cycle; (ii) the fixed bed was operated at a HLR of 20 m/h; (iii) a pressure transducer (Omega, PX409-030GUSB) was installed on the top of the column for continuous monitoring of the fixed bed pressure drop, (iv) water samples were collected at various depths of 0, 6, 30, 60, and 90 cm from the top of the bed, (v) the fixed bed was backwashed for 20 min at 40% bed expansion using raw water when the upstream bed pressure reached more than 0.5 bar.

In both columns, turbidity, pH, and free chlorine concentrations in the influent and effluent waters were also measured. Peristaltic pumps (MasterFlex, Cole-Parmer) were used to dose iron/manganese and sodium hypochlorite stock solutions into the inlet line. Both contactors were operated for a period of 21 days under each experimental condition.

7.2.4 Analytical methods

Iron and manganese concentrations were analyzed with an inductively coupled plasma-optical emission spectrometry (ICP-OES, model iCAP 6000) from Thermo Instruments Inc. Water samples were acidified to 0.5% nitric acid (pH < 2) after the sample collection. Before the analysis, the samples were further digested by incubation in a water bath at 80 °C for 48 hours to completely

dissolve the particulate iron and manganese. The instrument was calibrated at the beginning of each set of analysis. The average of three measurements was recorded for each sample.

Total organic carbon (TOC) and dissolved organic carbon (DOC) concentrations were determined by a TOC meter (Sievers 5310 C). For DOC measurements, the samples were pre-filtered through a 0.45 µm filter (LOT NO. T41389, Pall Corp., USA), which had been pre-rinsed with 1 L of Milli-Q^{TM} water.

The free chlorine concentration in the influent and effluent of the columns were regularly checked employing a Hach® chlorine test. The test kits, i.e., powder pillows, contain DPD colorimetric reagent, which is commonly employed to monitor the free chlorine concentration in potable water (0.02-2.00 mg Cl_2/L). To eliminate the interference of particulate manganese dioxide, potassium iodide and sodium arsenite solutions were added into the water before the analysis. The dissolved oxygen concentration, pH, and oxidation/reduction potential of the natural groundwater were determined by a Hach® HQ40d portable multiparameter meter with a specific electrode used for each measurement. The instrument was calibrated on the day of experiment. The turbidity was determined using a Hach® 2100 N turbidimeter.

7.3 Results and discussion

The experimental results obtained in this study are presented and discussed in three sections. First, the effect of distributor on the performance of the fluidized bed is evaluated. Subsequently, the performance of the pyrolucite fixed and fluidized bed contactors with respect to iron and manganese removal are compared under different conditions. Finally, the analysis of head loss accumulation is presented for both processes.

7.3.1 Effect of distributor in fluidized bed contactor

The minimum fluidization velocity (U_{mf}) of the pyrolucite particles in the fluidized bed contactor was determined using the conventional method (Kunii and Levenspiel 1991) of measuring bed pressure drop variations as a function of superficial fluid velocity. The pyrolucite media was operating in the fixed bed state at superficial fluid velocities below U_{mf} while it expanded and operated in the fluidized state at fluid velocities beyond U_{mf}. Figure 7.3 illustrates the results of the measured pressure drop across the bed when it was equipped with Distributor C and the

fluidizing velocity was progressively decreased from a fully fluidized state to a fixed bed. Similar U_{mf} values were obtained for the other two configurations of distributor plate. From this figure, the pyrolucite media became fluidized at a superficial fluid velocity of 24 m/h. The PFB contactor was operated at a flow rate within the range of 30-45 m/h in this study to (i) ascertain the pyrolucite media was adequately fluidized within the column and (ii) to prevent (additional) attrition of pyrolucite media due to an enhanced jetting effect close to the distributor plate.

The overall performance of a fluidized bed contactor is largely determined by hydrodynamic properties, i.e., fluid-particle contact, which, in turn, is influenced by the design of the distributor plate (Werther, 1978). The distributor plate in a fluidized bed contactor is intended to uniformly distribute the fluidizing agent across the entire bed cross-section, minimize weeping of solids into the windbox, and to support the weight of the bed material while minimizing the attrition of the bed material (Pell, 1990, Karri and Knowlton, 1999). Accordingly, different configurations of distributor plate were primarily examined to find the best configuration yielding an appropriate operation of the PFB contactor.
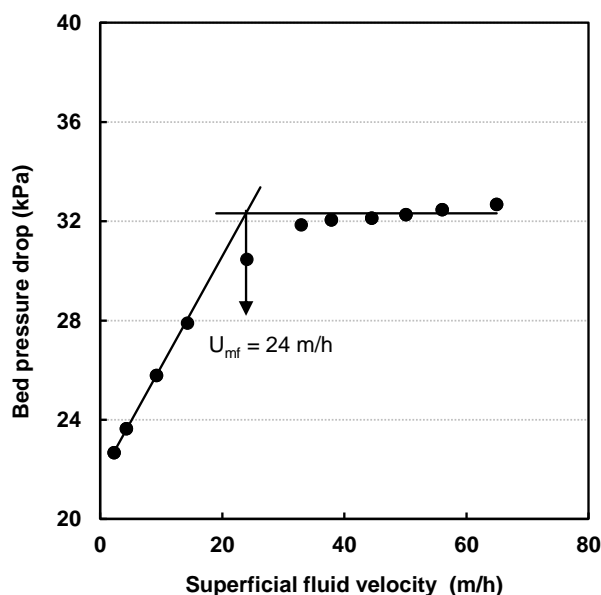
Figure 7.3. Bed pressure drop profile in the pyrolucite fluidized bed contactor during decreasing superficial fluid velocity (Distributor C). T= 8°C.

In order to compare the performance of PFB contactor with different distributor plates, the superficial fluid velocity was adjusted to result in a 10% bed expansion under each condition to yield an identical bed inventory. The visual observations indicated that the required superficial fluid

velocity (or HLR) to achieve the bed expansion criterion for Distributors A, B, and C were 40, 30, and 32 m/h, respectively. This reveals that Distributor A was less effective in void development in the bed, which, in turn, could decrease the quality of fluid-particle contact. Yet, a good fluid-particle contact quality enhances the adsorption rate of dissolved manganese onto the pyrolucite media in the fluidized bed contactor.

The evolutions of normalized **dissolved** manganese concentrations with respect to the inlet condition for different distributor configurations were plotted against the height of the PFB contactor in Figure 7.4. It shows that the PFB contactor presented identical removal performance when it was equipped with either of Distributor B or C. Comparing the removal performance of PFB contactor when equipped with Distributors B and C with the Distributor A indicates that the PFB contactor was more effective in the former cases, particularly in the first 15 cm above the distributor plate (58% vs. 27% and 90% vs. 62% removals at 7.5 cm and 15 cm above the distributors, respectively, in the first day of operation (Figure 7.4a)). The difference was even more pronounced after four days of operation (Figure 7.4b). This observation reveals that Distributor A could not adequately distribute water over the whole cross-section of the bed above the distributor plate and properly utilize the adsorption capacity of the pyrolucite media.
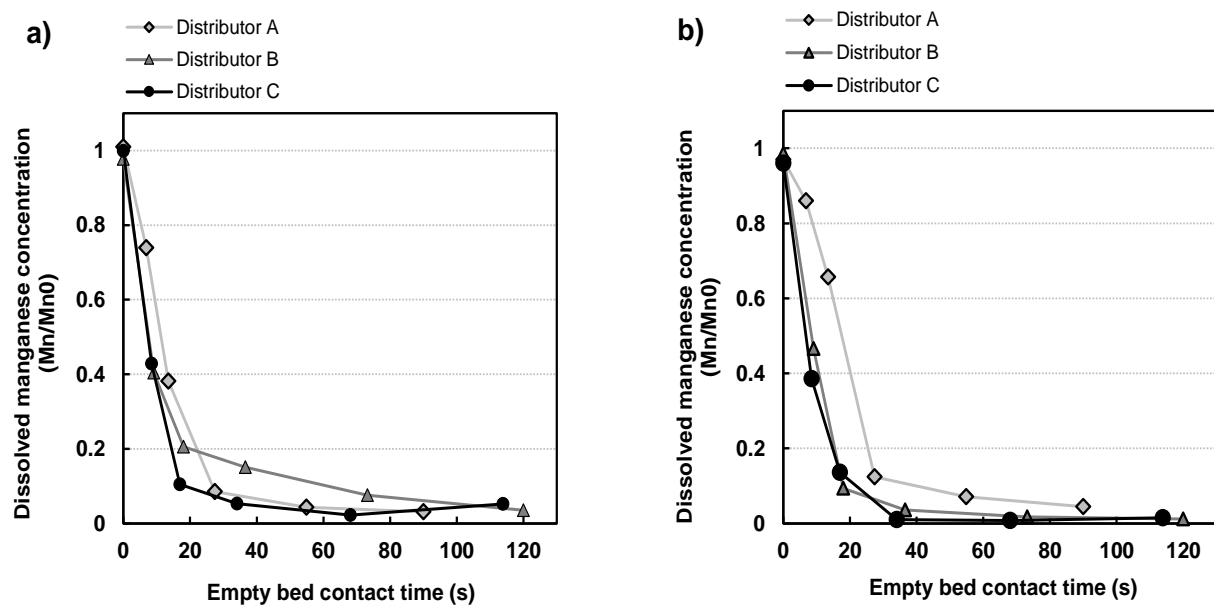
Figure 7.4. Effect of distributor configuration on the performance of pyrolucite fluidized bed contactor for dissolved manganese (Mn) removal. Initial Mn (Mn0) = 0.09-0.15 mg/L, T = 8-12°C and pH = 7.0-7.2.

Figure 7.5 illustrates the evolutions of normalized **particulate** manganese concentrations with respect to the inlet condition along the axis of the PFB contactor for different distributor configurations. It shows that a considerable amount of particulate manganese was released, particularly in the jetting zone above the distributor plate, when employing Distributor A. In this case, the turbidity of the effluent water progressively increased from 0.5 NTU to around 30 NTU after 12 days of operation. Distributor B, however, resulted in the release of a lower amount of particulate manganese while the best performance was achieved by using Distributor C. These observations can be explained by the reduction in the jetting effect caused by the distributor plate, which can greatly contribute in separation of loosely bounded manganese on the surface of pyrolucite media in the contactor. This argument is supported by the presence of significantly more particulate manganese in the fluidizing liquid as the treatment process proceeded when employing Distributors A and B. The loosely bounded manganese originates from dissolved manganese that adsorbed on the surface of pyrolucite media and subsequently oxidized during the process.

According to the observations made in this part of the study, Distributor C was adopted in the PFB contactor for the next part of the study.
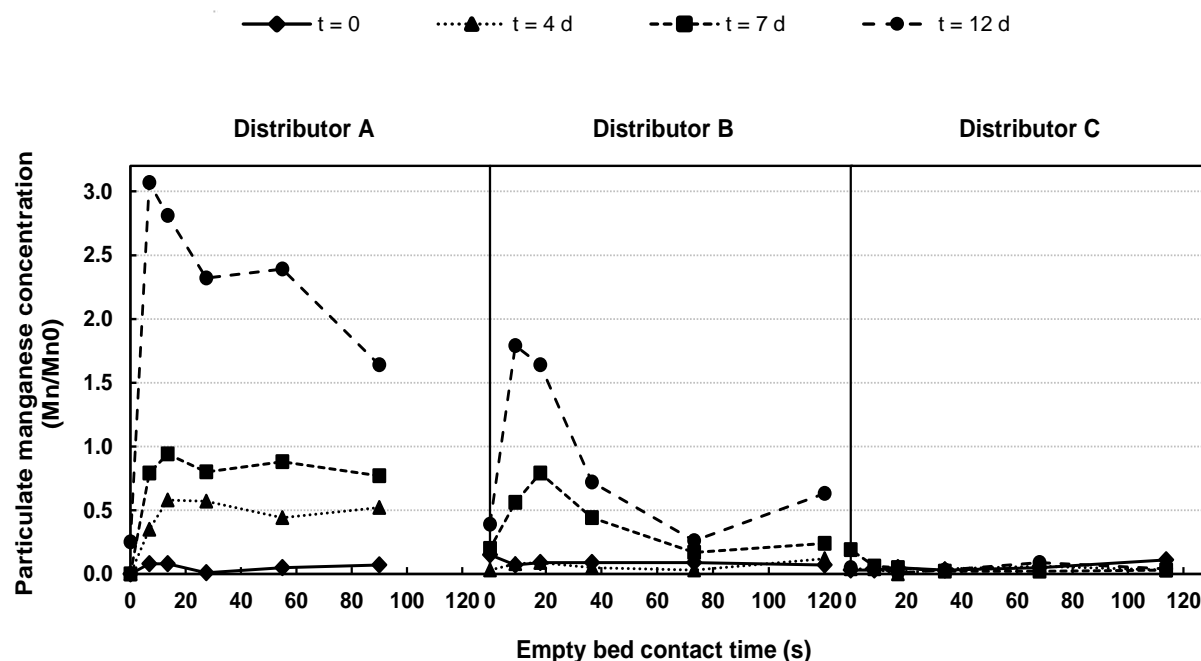
Figure 7.5. Effect of distributor configuration on the release of particulate manganese (Mn) along the height of pyrolucite fluidized bed contactor. Initial Mn (Mn0) = 0.09-0.15 mg/L, T = 8-12°C and pH = 7.0-7.2.

7.3.2 Iron and manganese removal performance in pilot plant

7.3.2.1   Experiments with un-spiked natural groundwater

The supplied groundwater naturally contained 0.01 ± 0.00 mg Fe/L and 0.09 ± 0.01 mg Mn/L which were both present in dissolved form. Since the concentration of iron in the raw water was very low, the removal of iron under this water condition will not be presented. Figure 7.6 shows the evolution of soluble and total manganese concentrations along the axis of the fixed and fluidized bed contactors (expressed as empty bed contact time). The reported concentrations are normalized with respect to the total manganese concentration in the influent. The PFB contactor was effective in removing manganese, even at a very high HLR of 45 m/h, with almost 100% efficiency for the influent dissolved manganese removal across the column (Figure 7.6a_1 and b_1). Although the PFB contactor led to a slightly lower total manganese removal, i.e., 85-95% (referred to Figure 7.6 a_2 and b_2), than the dissolved one, the concentration of total manganese in the effluent water was always below the target limit of 0.02 mg/L. One may postulate that this lower efficiency was only the result from the presence of particulate manganese in the influent water. However, Figure 7.6 indicates that no significant particulate manganese ($< 8\%$) was present in the influent water. More than 92% of the initial manganese was dissolved. The abrasive forces resulting from the intensified particle-particle collisions in the fluidized bed released loosely bonded manganese into the fluidizing liquid, which was also responsible for the lower total manganese removal efficiencies. Figure 7.6a_2 and b_2 support this argument since the PFB contactor was slightly less effective for total manganese removal at a higher HLR. Higher momentum transfer from the fluidizing fluid to the particles and, hence, more attrition effect, are expected at a higher HLR. However, in general, the ability of the PFB contactor to effectively remove manganese was insensitive to the HLR values (or hydraulic detention times). This result is consistent with our previous finding during the short-term (4 h) operation of the PFB contactor (Dashtban Kenari and Barbeau, 2014).

The results presented in Figure 7.6c_1 and c_2 indicate that the total and dissolved manganese removal efficiencies of the pyrolucite fixed bed contactor was about 100% while the effluent manganese concentration was always lower than 0.005 mg/L. The higher performance of the fixed bed compared to the fluidized bed contactor for the total manganese removal can be explained by the stationary state of the fixed bed, which can better retain all particulates that are formed within the

column. However, the concentration of total manganese in the effluent water was satisfactory ($<$ 0.02 mg Mn/L) for both processes.

Scrutinizing Figure 7.6 further reveals that the dissolved and total manganese profiles were stable under all operating conditions because the concentration curves obtained during 5 sampling campaigns over 21 days of experiment overlapped on each other. This result also confirms that the free chlorine residual concentration of 1 mg Cl_2/L maintained in the effluent was adequate for continuous regeneration of the pyrolucite adsorption sites under natural groundwater condition tested here.

Figure 7.6. Evolutions of normalized manganese (Mn) concentrations as a function of empty bed contact time. Pyrolucite fluidized bed at (a) hydraulic loading rate (HLR) of 32 m/h (10% bed expansion), (b) 45 m/h (20% bed expansion), and (c) fixed bed at HLR of 20 m/h. Groundwater conditions: Initial Mn (Mn_0) $= 0.09 \pm 0.01$ mg/L, Initial iron $= 0.01 \pm 0.00$ mg/L and T= 8°C.

7.3.2.2   Experiments with manganese-spiked natural groundwater

In these experiments, the natural groundwater was spiked to achieve a dissolved manganese concentration of 0.35 ± 0.03 mg Mn/L. Figure 7.7a and b illustrate the normalized manganese removals as a function of empty bed contact time in the fluidized and fixed bed contactors, respectively. Both contactors were effective in removing total and dissolved manganese ($> 95\%$) over the 21 days of experiment. The target total manganese concentration of 0.02 mg/L was not exceeded during the entire test period. Thus, an elevated manganese concentration in the raw water did not significantly decrease the performance of the overall process, implying the very high adsorption capacity of pyrolucite media. Similarly to the experiments with un-spiked groundwater, more than 92% of manganese was in dissolved form in the influent water and remained in this form inside the contactor which indicates that the removal mechanism in both contactors was predominantly governed by sorption of the dissolved manganese onto the pyrolucite surface with subsequent surface catalyzed oxidation of adsorbed manganese by chlorine.

Under a more stressed manganese loading condition (concentrations around 0.35 mg/L), stable manganese removal profiles were not observed within both contactors. Comparing Figure 7.6 and Figure 7.7 reveals that an increase in the concentration of soluble manganese impacted the shape of adsorption profile, particularly, closer to the end of an experimental cycle. Figure 7.7 also exhibits that although effective manganese removal was achieved across the 21-day experimental cycle, both contactors would have eventually breakthrough due to the saturation of available adsorption sites. Under this scenario, the contactors would need to be stopped and regenerated more aggressively with a strong chlorine or permanganate solution to regenerate the adsorption sites. Following this step, the same treatment cycle would be repeated. The experimental results presented in Figure 7.7 imply that even though the rate of oxidation of dissolved manganese on the $MnO_{x(s)}$ surface by chlorine is rapid (Knock et al., 1990 b), it was slower than its adsorption rate. It is likely that increasing the free chlorine concentration above 1 mg Cl_2/L would extend the operation cycle duration before regeneration. Nevertheless, this free chlorine concentration allows to operate the FBR for 21 days and the fixed bed for around 60 days.

Figure 7.7. Evolutions of normalized manganese (Mn) concentrations as a function of empty bed contact time. (a) Pyrolucite fluidized bed at hydraulic loading rate (HLR) of 45 m/h (20% bed expansion) and (b) fixed bed at HLR of 20 m/h (b). Groundwater conditions: Initial Mn (Mn_0) = 0.35 ± 0.03 mg/L, Initial iron = 0.01 ± 0.00 mg/L and T= 8°C.

7.3.2.3 Experiments with iron-spiked natural groundwater

To evaluate the effect of iron concentration on the performance of both processes, the natural groundwater was supplemented with a ferrous iron feed such that a total concentration of 0.18 ± 0.02 mg/L was achieved in the influent water. The concentration of manganese in the groundwater was 0.11 ± 0.01 mg/L over this experimental cycle. All iron and manganese species were presented in dissolved form before the chlorine injection point. The performance of the fixed

and fluidized bed contactors to remove manganese and iron are plotted in Figure 7.8 and Figure 7.9, respectively. Results demonstrate that more than 90% of dissolved iron and manganese were removed steadily over 21 days while using the PFB contactor. However, the PFB contactor performance for the removal of total iron and manganese varied from 50-80% and 60-80%, respectively. The effluent concentrations fluctuated between 0.04-0.08 mg/L for iron and 0.02-0.04 mg/L for manganese. Thus, an elevated iron concentration led to a significant decrease in manganese removal. In addition, comparing Figure $7.8a_1$ and Figure $7.6a_1$ shows that as the adsorption of manganese progressed in the presence of a higher iron concentration, the adsorption capacity of pyrolucite media for manganese diminished. Although preliminary results, using a synthetic feed water prepared with demineralized water had shown an almost instantaneous oxidation of dissolved iron by free chlorine, results in natural waters revealed that a complete oxidation of iron did not occur over the 90 s of detention time in the PFB contactor. This was principally a result from a higher DOC content of the natural groundwater (3.3 mg C/L) in comparison with the synthetic water (< 0.2 mg/L). The formation of NOM-iron complexes can slow down the kinetic of iron oxidation with chlorine (Reckhow et al., 1991). As a result, the dissolved iron may have competed with dissolved manganese for the pyrolucite adsorption sites (Hu et al., 2004). In addition, as the ferric hydroxide coating develops on the media grains, the previously available adsorption sites become inaccessible under this layer. In broad agreement with these results, previous studies demonstrated that the availability of adsorption sites on the exterior surface of MnO_x (s)-coated media is a crucial parameter for the removal of dissolved manganese from water (Merkle et al., 1997; Knocke et al., 2010).

Comparing Figure $7.9a_1$ and a_2 reveals that the mechanism of iron removal in the PFB contactor was partially governed by adsorption of dissolved species onto the pyrolucite media. Nonetheless, the partial solution oxidation of dissolved iron by free chlorine was not negligible. Previous experiments under a very low iron concentration (0.01 ± 0.00 mg/L) indicated that, unlike iron, solution oxidation of dissolved manganese by free chlorine is not significant. Thus, the presence of 20-40% particulate manganese observed in treated water during this experiment was presumably related to the presence of manganese adsorbed onto the ferric hydroxide precipitates and carryover from the PFB contactor. This hypothesis is supported by the fact that ferric hydrous oxides can serve as sorption media for dissolved iron (Sharma et al., 1999) and manganese (Buamah et al.,

2008). Therefore, the sole application of a PFB contactor is not recommend for groundwater treatment applications where elevated iron concentrations are present in the influent.
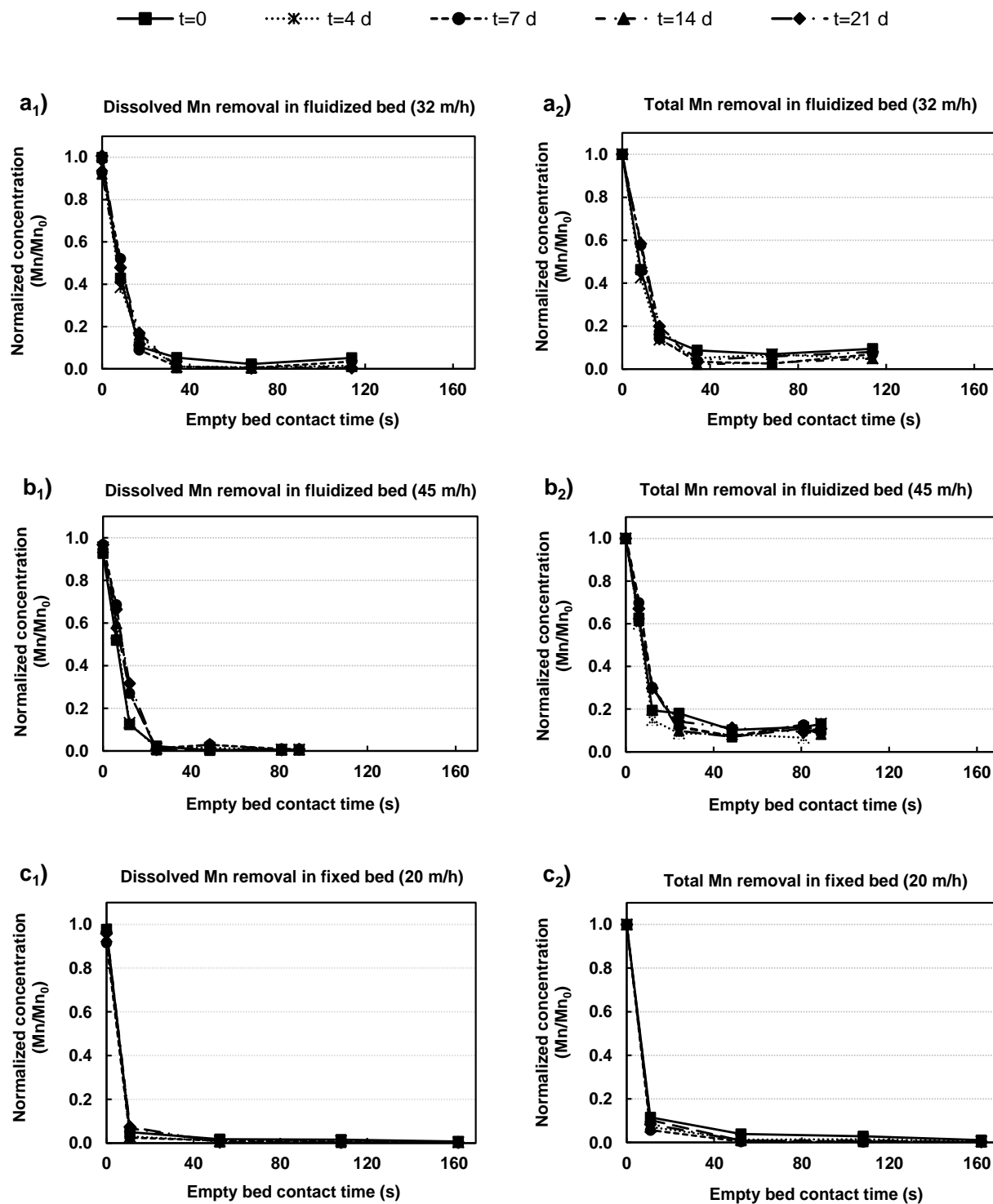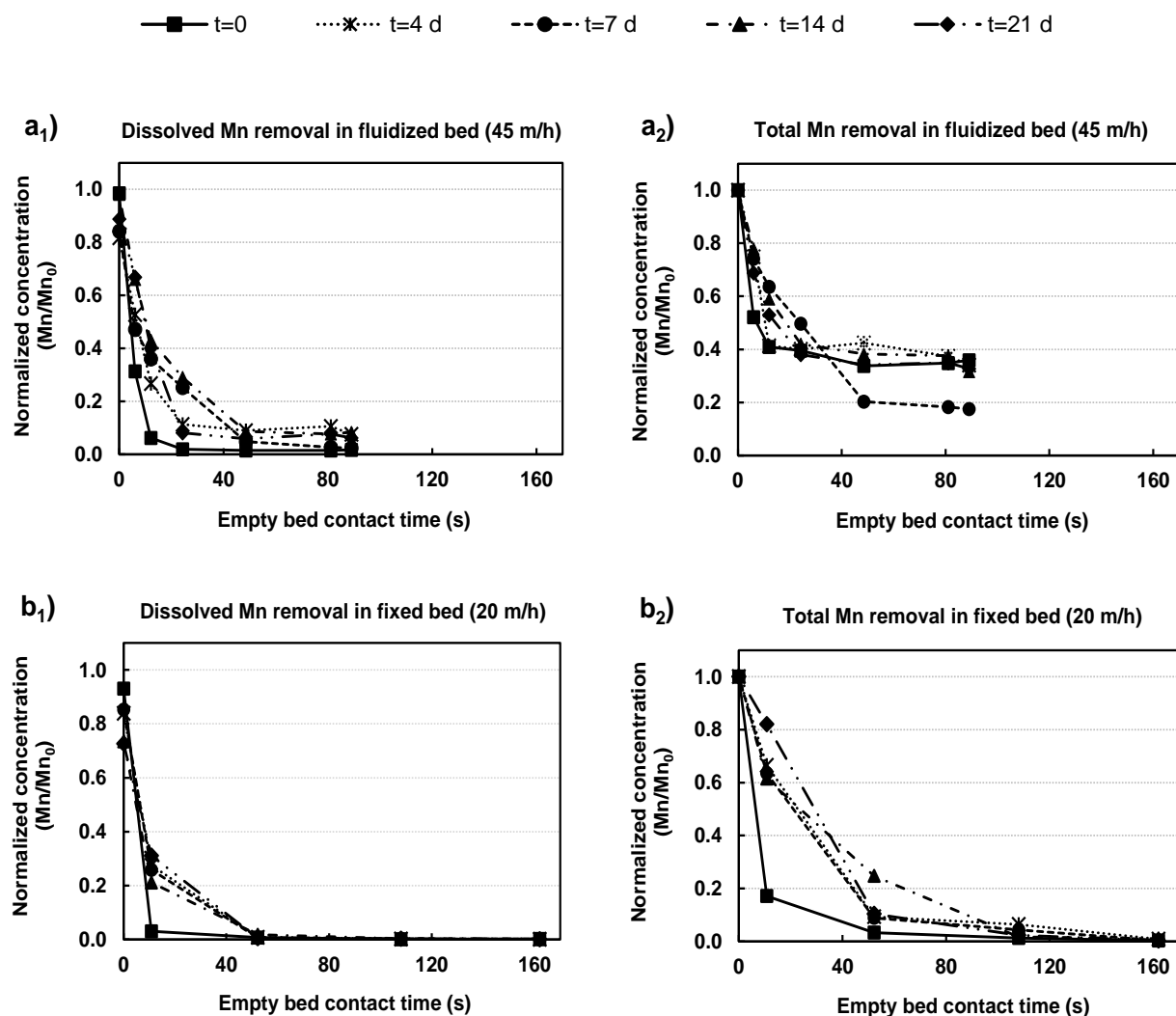

Figure 7.8. Evolutions of normalized manganese (Mn) concentrations as a function of empty bed contact time. (a) Pyrolucite fluidized bed at hydraulic loading rate (HLR) of 45 m/h (20% bed expansion) and (b) fixed bed at HLR of 20 m/h. Groundwater conditions: Initial Mn (Mn_0) = 0.11 ± 0.01 mg/L, Initial iron = 0.18 ± 0.02 mg/L and T= 9°C.

The performance of the fixed bed contactor for iron and manganese removal is shown in Figure 7.8b and Figure 7.9b, respectively. The concentrations of iron and manganese species in the treated water (< 0.005 mg/L) were well below the target limit of 0.02 mg/L. However, similar to the PFB contactor, a steady state removal performance was not experienced in the fixed bed contactor and the adsorption capacity of the pyrolucite media decreased as the filtration process approached the

end of a filtration cycle. This is likely due to the deposition and build-up of ferric hydroxide on the pyrolucite media, which covered some available adsorption sites, over the course of a filtration cycle. Unlike the PFB contactor, 60-90% of the iron was oxidized by chlorine before reaching the filter media due to the approximate 5 min detention time available in the column above the pyrolucite media. Thus, the mechanism of iron removal in the fixed bed contactor mainly comprised of an initial formation of ferric hydroxide in the water phase and its subsequent capture by the filter media.

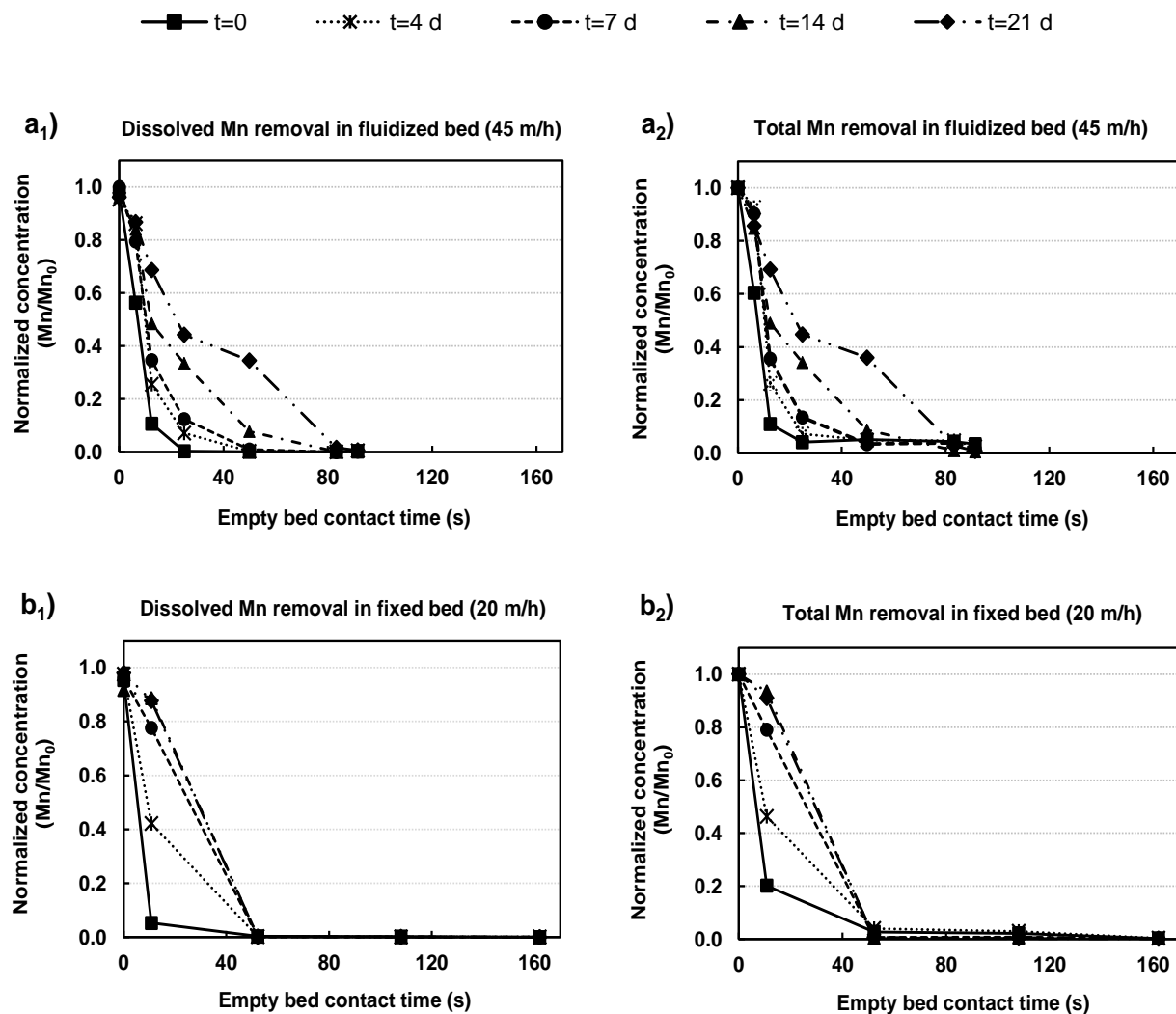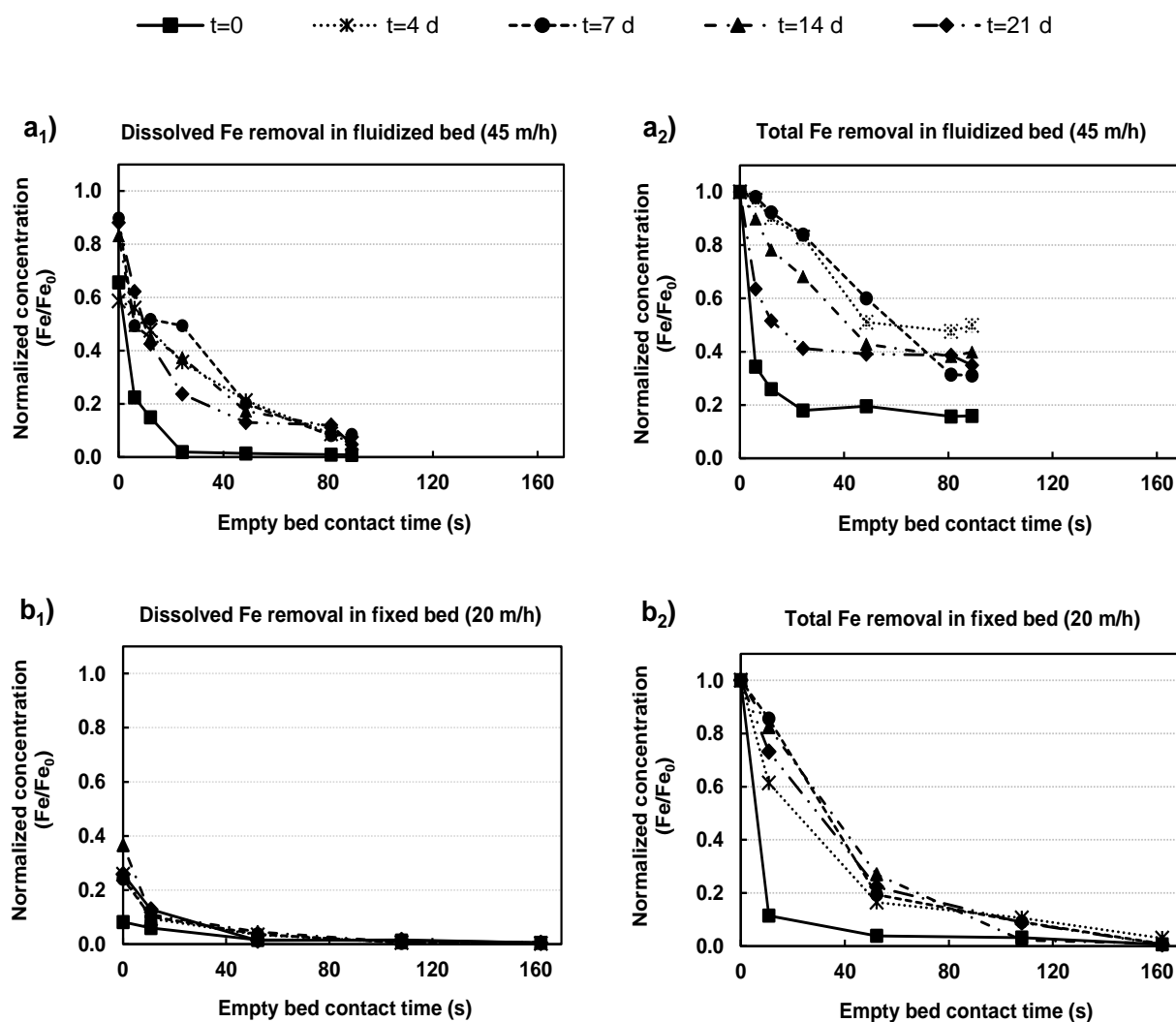Figure 7.9. Evolutions of normalized iron (Fe) concentrations as a function of empty bed contact time. (a) Pyrolucite fluidized bed at hydraulic loading rate (HLR) of 45 m/h (20% bed expansion) and (b) fixed bed at HLR of 20 m/h. Groundwater conditions: Initial Fe (Fe$_0$) = 0.18 ± 0.02 mg/L and T= 9°C.

7.3.3 Evolutions of head losses in the fixed and fluidized bed contactors

Head losses were continuously monitored over the 21 days of experimental period for both processes (Figure 7.10a). The fixed bed contactor exhibited increase in the head loss over the filtration period which varied largely depending on the influent water characteristics. On the other hand, the head loss across the PFB was stable (33 kPa) and independent of the influent water characteristics. As expected, the total head loss across the fluidized bed was comprised of the apparent weight of the pyrolucite media per cross-section unit of the column and the water head in the column, which are independent of the superficial fluid velocity and change in influent water quality conditions.

Under very low iron concentration, the very low turbidity of the influent water (Figure 7.10b) allowed for the operation of the fixed bed contactor at a high HLR (20 m/h) with no concern about excessive head loss build-up. As a result, when the manganese concentration was 0.09 ± 0.01 or 0.35 ± 0.03 mg/L in the influent water, the fixed bed contactor was required to be backwashed once or twice over the 21 days. The increased head loss is most likely due to the accumulation of precipitated $MnO_{x(s)}$ (less than 10% solution oxidation of manganese was observed) on the contactor media and partial blockage of the void spaces. Under an elevated iron concentration in the influent water, a substantial head loss developed across the fixed bed and, thus, the filtration cycle was significantly shortened (around 3 days) owing to the retention of more particulate materials (60-90% of iron were oxidized before reaching the filter media) in the pyrolucite filter media. The higher turbidity (0.3 NTU) of the influent groundwater spiking with iron compare to the assays without spiking (0.1 NTU) also have contributed in shortening the filtration cycles.
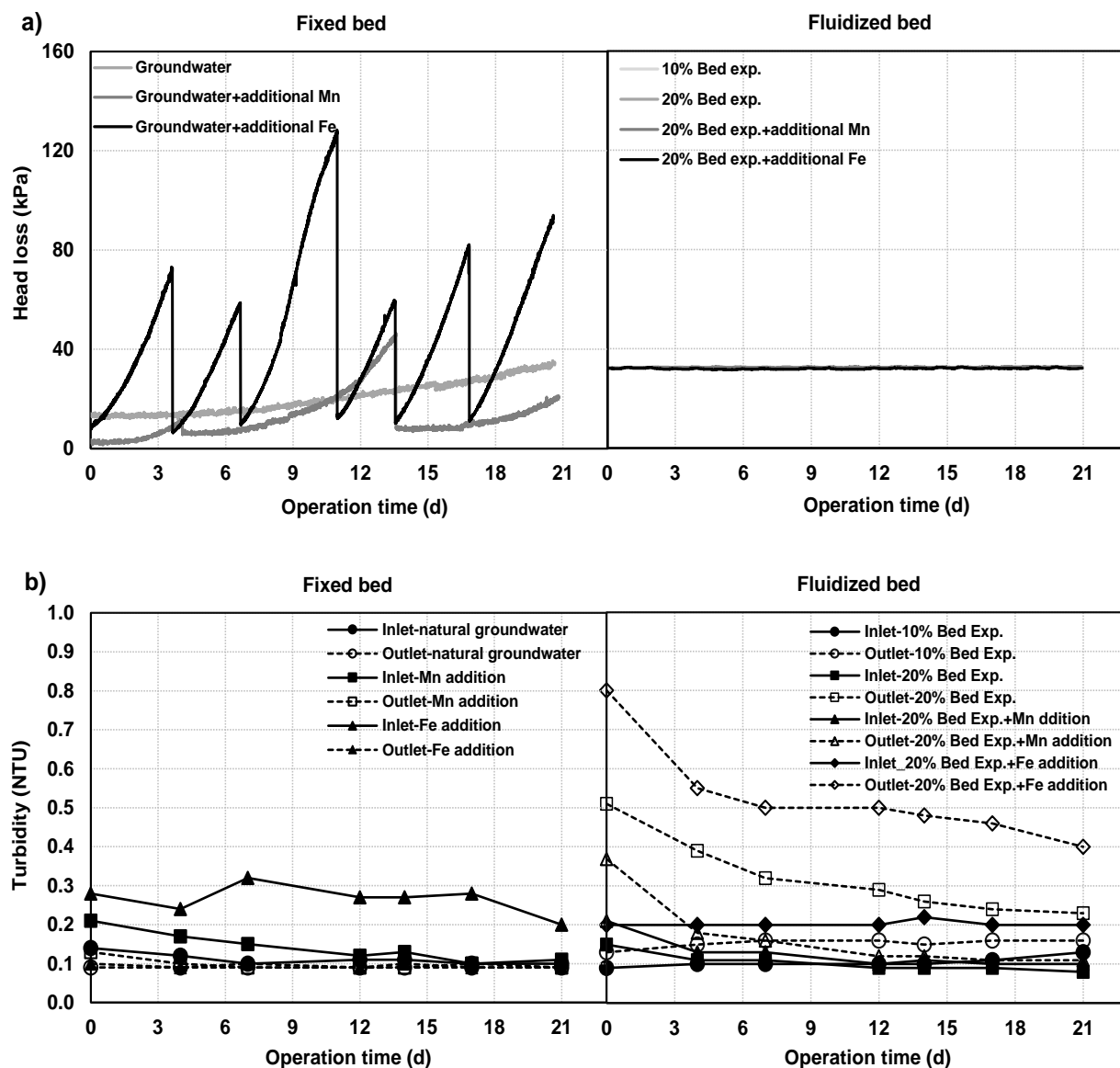
Figure 7.10. Evolution of (a) head loss and (b) turbidity in fixed and fluidized bed contactors under different experimental conditions. T= 9°C.

Figure 7.10b illustrates that the fixed bed contactor was able to maintain the turbidity of the treated water at 0.1 NTU while the turbidity of the PFB effluent water varied between 0.1 and 0.5 NTU. However, even the turbidity of 0.5 NTU, which was only experienced under an elevated iron concentration, is still satisfactory for the water treatment utilities.

In conclusion, although the pyrolucite fixed bed contactor controls efficiently the concentration of iron and manganese in the treated water under an elevated iron concentration, it gives rise to a considerably larger energy consumption and wastewater production (with a typical turbidity

between 40 NTU and 70 NTU measured during this assay). On the other hand, the PFB only needs to be backwashed prior to a regeneration. No regeneration was needed during the 21 days period investigated. Combining a PFB contactor with a downstream process with the capability of operating at very high loading rate would however be required under influent conditions with elevated iron concentrations. In addition, despite the fact that both contactors were highly efficient to remove manganese under very low iron concentrations, the PFB offers the important advantage of operating at high HLR values allowing for the use of smaller contactor footprints and, thus, a decreases in capital costs. As stated earlier, the PFB also greatly reduces the production of wastewaters which is an important design constraint due to the manganese discharge limits imposed in many regulations. On a final note, the adsorbed manganese accumulating on the PFB media is expected to increase the pyrolucite media size over time. However, this phenomenon is expected to be marginal as an influent manganese concentration (0.1 mg/L) that would be removed entirely in a 45 m/h PFB would only increase by 3% the mass content of manganese dioxide in the reactor after one year of operation. This would represent a theoretical increase in media size of 7 µm.

7.4 Conclusions

The main purpose of this research was to assess the long-term fate of iron and manganese in a PFB contactor supplied by natural groundwater. Accordingly, the results of a pilot-scale experiments under different operating conditions with varying iron and manganese concentrations were described here. The following conclusions were derived from this research study:

- Selection of an appropriate distributor plate for the PFB contactor was crucial for an efficient process performance. Among different configurations of distributor plate that were tested, a shrouded perforated distributor plate with 15 cm of gravel on top of it proved to be optimal.

- The PFB contactor has a strong adsorption capacity for dissolved iron and manganese. However, the adsorption capacity and long-term stability of the process were influenced by the initial concentration of these species.

- The PFB contactor proved effective at promoting a high degree of total manganese removal under a wide range of influent manganese concentrations as long as iron levels were low. It also minimized wastewater production while providing a high treatment performance and a small footprint. Consequently, this process is recommended for water treatment facilities

with manganese treatment objectives and negligible iron in the influent water. Under elevated iron concentrations in the influent water, a downstream process after the PFB contactor is required to achieve acceptable iron and manganese removal.

- The pyrolucite fixed bed contactor demonstrated its ability to effectively control iron and manganese under all conditions tested. However, fairly rapid head loss build-up was observed across the pyrolucite fixed bed media operated at 20 m/h under elevated iron concentrations (3 days filtration cycle).

- The concentration of iron in the groundwater mainly controlled the head loss build-up rate through the fixed bed. On the other hand, the head loss in the PFB contactor remained relatively constant, regardless of the influent water quality.

- In both fixed and fluidized bed contactors, manganese was principally removed by the sorption uptake of dissolved manganese onto the pyrolucite media followed by the catalytic oxidation of the adsorbed species on the surface of pyrolucite particles. A similar mechanism could be inferred for a part of iron removal in the PFB contactor while the role of pyrolucite fixed bed in the iron removal was mainly via the capture of particulate and/or colloidal ferric hydroxide that formed following solution oxidation of soluble iron by chlorine.

Future studies should focus on the development of a high rate post-filtration technique that is stable and cost effective for the removal of the residual particles from the effluent of the PFB contactor for waters containing both iron and manganese species.

Acknowledgments

CHAPTER 8 ARTICLE 5 : INTEGRATED PYROLUCITE FLUIDIZED BED-MEMBRANE HYBRIDE PROCESS FOR IMPROVED IRON AND MANGANESE CONTROL IN DRINKING WATER

This chapter presents the article published in Water Research, 113 (2017). In this chapter an integrated pyrolucite fluidized bed-membrane hybrid process was proposed for iron and manganese control in drinking water. Consequently, the performance of the hybrid process with respect to treated water quality and membrane fouling under variable water chemistry conditions was investigated.

Integrated Pyrolucite Fluidized Bed-Membrane Hybrid Process for Improved Iron and Manganese Control in Drinking Water

Seyedeh Laleh Dashtban Kenari[*] and Benoit Barbeau

Polytechnique Montreal, Department of Civil, Geological and Mining Engineering, NSERC-Industrial Chair on Drinking Water, Environment, C.P. 6079, Succursale Centre-Ville, Montreal, QC, H3C 3A7, Canada.

[*] Corresponding author: Tel: +1 514 340-4711 #2983; Fax: 514-340-5918

E-mail: laleh.dashtban@polymtl.ca

ABSTRACT

Newly developed ceramic membrane technologies offer numerous advantages over the conventional polymeric membranes. This work proposes a new configuration, an integrated pyrolucite fluidized bed (PFB)-ceramic MF/UF hybrid process, for improved iron and manganese control in drinking water. A pilot-scale study was undertaken to evaluate the performance of this process with respect to iron and manganese control as well as membrane fouling. In addition, the fouling of commercially available ceramic membranes in conventional pre-oxidation-MF/UF process was compared with the hybrid process configuration. In this regard, a series of experiments were conducted under different influent water quality and operating conditions. Fouling mechanisms and reversibility were analyzed using blocking law and resistance-in-series models. The results evidenced that the flux rate and the concentration of calcium and humic acids in the feed water have a substantial impact on the filtration behavior of both membranes. The model for constant flux compressible cake formation well described the rise in transmembrane pressure. The compressibility of the filter cake substantially increased in the presence of 2 mg/L humic acids. The presence of calcium ions caused significant aggregation of manganese dioxide and humic acid which severely impacted the extent of membrane fouling. The PFB pretreatment properly alleviated membrane fouling by removing more than 75% and 95% of iron and manganese, respectively.

KEYWORDS: Iron/manganese removal; Ultrafiltration/Microfiltration; Ceramic membrane; Fouling; Pyrolucite fluidized bed, Cake compressibility.

8.1 Introduction

Iron and manganese naturally co-occur in both surface and ground waters mainly as a result of weathering and leaching of metal-bearing minerals and rocks. Among different water sources, groundwater more commonly contains significant levels of iron and manganese. The United States Environmental Protection Agency (USEPA) (2004) and the Canadian Drinking Water Quality Guidelines (Health Canada, 2014) established an aesthetic objective limit of 0.3 and 0.05 mg/L for the concentrations of iron and manganese in drinking water, respectively, due to adverse aesthetic issues. However, concentrations of iron and manganese above 0.05 (World Health Organization, 2003) and 0.02 mg/L (Sly et al., 1990), respectively, may still give rise to aesthetic problems.

Consequently, Health Canada (2016) has recently proposed an aesthetic objective limit of 0.02 mg/L for total manganese in drinking water. The impact of manganese in drinking water is receiving more attention due to its potential neurotoxicity. Several epidemiological studies suggest that exposure to manganese in drinking water is associated with neurological effects in children including intellectual impairment and poor neurobehavioral function (e.g., memory, hyperactivity and attention) (Bouchard et al., 2011; Oulhote et al., 2014), even for fairly low concentrations of manganese in treated water. Health Canada (2016) recently proposed a health-based maximum acceptable concentration of 0.1 mg/L using animal studies showing neurotoxic effects of manganese in rats. Consequently, it is expected that effective manganese control will become an important goal for drinking water utilities following the introduction of a health-based regulation.

A traditional treatment strategy includes oxidation of dissolved iron and manganese to particulate forms, ferric hydroxide and manganese dioxide, using a strong oxidant, such as potassium permanganate, chlorine dioxide or ozone, followed by depth filtration (Knocke et al., 1990b). Unlike iron, which can be readily oxidized by a weak oxidant, such as oxygen, oxidation of manganese by strong oxidants is dependent upon the pH, temperature, initial dissolved manganese concentration and contact time (Knocke et al., 1990b). In addition, since oxidized manganese forms colloidal species under low ionic strength conditions (Morgan and Stumm, 1964; Dashtban Kenari and Barbeau, 2016a), it is not effectively removed by sand filtration. Alternatively, application of low-pressure membranes, microfiltration (MF) and ultrafiltration (UF), is becoming more attractive in drinking water production. However, membrane fouling by manganese dioxide, which leads to a severe decrease in permeability during filtration (Choo et al., 2005; Dashtban Kenari and Barbeau, 2016b), is the major obstacle to widespread application of membranes for this application. Thus, developing a compact pretreatment process, which can properly alleviate the fouling of the membrane, is of great interest.

Generally, membrane fouling mechanisms can be described by pore blocking and/or cake layer formation models, depending, amongst other factors, on the ratio of the particle size to the pore size of the membrane. Pore blocking mainly occurs when the size of particles is comparable to or smaller than the pore size of the membrane while cake formation is the predominant fouling mechanism during the filtration of particles with much larger diameter than the membrane pore size (Shirazi et al., 2010; Muthukumaran and Baskaran, 2014). Thus, the membrane pore size may not only affect the treated water quality but also the fouling behavior and, in turn, the economic

viability of treatment plant. In addition, membrane material, water characteristics and operating conditions are other major factors influencing membrane filtration performance. Newly developed tubular ceramic membranes offer superior chemical resistance, physical integrity and thermal stability compared with the conventional hollow fiber polymeric membranes. Likewise, our earlier study revealed that tubular ceramic membrane requires less frequent chemical cleaning compared with the hollow fiber polymeric membrane due to the possibility to implement more aggressive physical cleaning (Dashtban Kenari and Barbeau, 2016b).

Considering the propensity of manganese dioxide to adsorb dissolved metal ions (Morgan and Stumm, 1964), a process, termed Natural Greensand Effect, is often used to remove dissolved manganese from water (Knocke et al., 1990a) through sorption of dissolved manganese onto manganese dioxide coated sand followed by auto-catalytic oxidation of the adsorbed species. Manganese dioxide coated sand has been primarily employed in packed bed contactors at relatively low hydraulic loading rates (HLRs) (6-12 m/h) (Hargette and Knocke, 2001; Yang et al., 2008; Piispanena and Sallanko, 2010). The possibility of using higher HLRs (up to 49 m/h) have been demonstrated for the removal of traces of manganese (0.09 mg/L) from surface waters using post-contactors with large size (2.0-2.4 mm) pyrolucite (a natural manganese dioxide ore) media (Knocke et al., 2010; Bierlein et al., 2015). In addition, Dashtban Kenari and Barbeau (2014) studied the performance of pyrolucite fluidized bed (PFB) for manganese removal under different water quality conditions. This process revealed a promising performance for manganese removal (influent concentration = 2.2-2.4 mg Mn/L) at much higher HLRs (up to 60 m/h) than the packed bed configuration (typically 10-20 m/h). An increased HLR reduces the process footprint and therefore capital costs. However, the fate of iron removal in this process has not been investigated.

In order to come up with a novel process, which can properly reduce the concentration of iron and manganese to below 0.020 mg/L and overcome the problems encountered in the abovementioned processes, it is proposed to use a PFB as a pretreatment for MF/UF membranes. Consequently, the principal objective of this study was to investigate the performance of a PFB-MF/UF membrane hybrid process with respect to treated water quality and membrane fouling under variable water chemistry conditions. We also compared the performance of this hybrid process with a reference treatment process excluding the presence of the PFB pretreatment (i.e. pre-oxidation and membrane filtration). Considering the significance of operating conditions on fouling, this study also dealt with the effect of flux rate and membrane pore size (MF vs. UF) on the fouling behavior of oxidized

iron and manganese in dead-end constant flux membrane systems. The blocking law model was applied to analyze the fouling mechanisms and determine the compressibility of the filter cake. Finally, the resistance-in-series model was employed to provide a quantitative insight concerning the effectiveness of membrane cleaning procedures.

8.2 Materials and methods

8.2.1 Pyrolucite filter media and MF/UF membranes

Pyrolucite filter media

Commercially available pyrolucite (MangOx^{TM} brand) with high purity (86% MnO_2 by wt), was employed as a catalytic media in the upflow adsorption fluidized bed. This media has been shown to offer a higher capacity for Mn(II) adsorption than $MnO_{x(s)}$-coated sand (Knocke et al., 2010, Zuravnsky, 2006), which was attributed to a higher specific concentration of $MnO_{2(s)}$ (mg Mn/g media) and a higher amount of available active sites on its surface (Zuravnsky, 2006). Characteristics of the pyrolucite media are presented in Table 8.1. In order to provide a more uniform bed expansion, the media was sieved and only the grains with size ranging from 0.25 to 0.60 mm (55% (wt) of the total grains) was used in the fluidized bed.

Table 8.1. Characteristics of commercial pyrolucite.

Effective size (D_{10}) (mm)	Mesh size	Uniformity coefficient (D_{60}/D_{10})	Specific gravity	Bulk density (kg/m^3)	Manganese dioxide (% wt)
0.43	20×40	1.5	3.8	2000	86 %

MF/UF membranes

Single channel tubular ceramic membranes, MF and UF, with an inner diameter of 6.0 mm, an outer diameter of 10 mm and a length of 500 mm were employed (Atech Innovations GmbH, Gladbeck, Germany). The filtration area of both membranes was 95 cm^2. The MF membrane had a nominal pore size of 0.1 µm and the UF membrane had a nominal molecular weight cut off (MWCO) of 150 kDa (equivalent to a pore size of approximately 17 nm). Both membranes are made of an active layer of zirconium dioxide and a support of α-aluminum oxide. Clean water permeabilities of the virgin membranes were determined by passing demineralized (DM) water (at pH 6 and 20ºC) through the membrane under different flow rates. Accordingly, the initial hydraulic

permeability of MF and UF membranes were 1740 and 820 LMH/bar, respectively. Although the permeability of the UF membrane is lower than that of MF one, their use may be beneficial due to the increasingly stringent regulations for drinking water quality as it removes a wider range of substances, including colloids and viruses. Primary disinfection of viruses is an important goal of many groundwater systems.

8.2.2 Preparation of synthetic feedwater (SFW)

In this paper, water chemistry conditions expected to have significant impact on the fouling of oxidized iron and manganese were tested. Dashtban Kenari and Barbeau (2016b) revealed that hardness of water plays a significant role on the characteristics of manganese dioxide aggregates and subsequent membrane fouling. In addition, the role of natural organic matter (NOM), as a common constituent of all water sources, is of great importance in the proposed PFB-MF/UF hybrid process because it may not only impact the fouling of membranes (Zularisam et al., 2006; Shao et al., 2011), but also slow down the oxidation kinetic of dissolved iron and manganese (Knocke et al., 1990b). Humic substances, the major fraction of NOM (Zularisam et al., 2006; Shao et al., 2011) and key membrane foulants during water treatment (Gray et al., 2007; Huang et al., 2007), were selected as a model compound to include in our tests. Considering the potential impact of hardness and NOM on the characteristics of ferric hydroxide and manganese dioxide aggregates and their subsequent influence on the fouling of membranes, three different SFW characteristics were tested in this study: 1) soft water with negligible calcium concentration (hardness of 2 mg $CaCO_3$/L), 2) moderately hard water with a calcium concentration of 40 mg/L (hardness of 100 mg $CaCO_3$/L) and 3) moderately hard water (100 mg $CaCO_3$/L) in the presence of humic acids ($\approx$ 2 mg C/L).

The SFW was prepared via addition of an appropriate amount of sodium bicarbonate (Fisher Scientific, Fair Lawn, NJ, USA) stock solution into the DM water to achieve the final alkalinity of 50 mg $CaCO_3$/L. For moderately hard water conditions, the calcium chloride dihydrate (Fisher Scientific, Fair Lawn, NJ) stock solution was added into the water, so as to provide a hardness of 100 mg $CaCO_3$/L. For experiments in the presence of humic acids, the concentration of humic acids in the SFW was adjusted at around 2 mg C/L via addition of humic acids (Sigma-Aldrich, CAS NO. 68131-04, St. Louis, MO) stock solution prepared with Milli-Q^{TM} water. According to Shao et al. 2011, 87% of the humic acids in solution have a size between 30 kDa and 0.45 µm at pH 7.0.

The solution was then vacuum filtered through a 30 µm filter (CAT. NO. NY3004700, Millipore Corp.) to remove ash particles. The filtered solution was stored in cooling room at 4°C for up to 4 weeks. In the final step, the pH of SFW was adjusted at 7.0 by bubbling CO_2 and/or N_2 gas into the water.

A fresh iron (II) and manganese (II) stock solutions, 150 mg Fe^{2+}/L and 75 mg Mn^{2+}/L, were separately prepared and their concentration in the SFW were respectively set at 2.6 and 1.3 mg/L for all experiments (i.e., very challenging conditions). Manganese (II) stock solution was simply prepared by dissolving manganese (II) sulfate monohydrate (Fisher Scientific, Fair Lawn, NJ) in Milli-Q^{TM} water while prior to the dissolution of iron (II) sulfate heptahydrate (Fisher Scientific, Fair Lawn, NJ), Milli-Q^{TM} water was acidified to a pH of 3, and N_2 gas was bubbled for 15 min to avoid oxidation of iron (II) in the stock solution. Characteristics of the SFW tested in this study are summarized in Table 8.2.

Table 8.2. Characteristics of the synthetic water tested in this study.

Iron (mg/L)	Manganese (mg/L)	Hardness (mg CaCO$_3$/L)	Alkalinity (mg CaCO$_3$/L)	pH	TOC (mg C/L)	SUVA (L/mg/m)	Temperature (°C)
2.64 ± 0.12	1.29 ± 0.08	2 or 100	50	7.0	0.2 or 2.3	NA or 9.9	20

8.2.3 Experimental procedure

The experiments were carried out in a small pilot plant (Q = 0.5 m^3/d) located at Polytechnique Montreal. In the first set of experiments, the MF and UF membranes were employed to establish the fouling behavior in a conventional configuration involving pre-oxidation followed by membrane filtration. In the second set, the filtration behavior was examined while using the PFB as a pretreatment process. A simple schematic of the PFB-MF/UF membrane experimental setup is illustrated in Figure 8.1.

A fresh potassium permanganate (EMD chemicals Inc., Gibbstown, NJ) or sodium hypochlorite (commercial bleach, 8% (W/V) available chlorine) stock solutions (280 mg KMnO$_4$/L and 200 mg Cl$_2$/L, respectively) were prepared prior the experiment for the pre-oxidation or PFB experiments, respectively. Iron (II) and manganese (II) as well as oxidants were separately spiked into the SFW immediately prior entering the columns. Mixing was achieved by injecting the solutions ahead of screens located at the inlet line and bottom of the columns. The oxidation column was a 2-meter

clear PVC pipe having an inner diameter of 50.8 mm (2 in.), which provided a detention time of 11.6 min for a total flow of 350 mL/min. The PFB column was a 2.5-meter clear PVC pipe with an inner diameter of 25.4 mm (1 in.). Pyrolucite was added into the column up to a height of 90 cm which provided an empty bed contact time of 100 s for a total flow of 350 mL/min (at a HLR of 41 m/h (30% bed expansion)). In this process, the free chlorine dosage in the column influent was adjusted to provide an effluent free chlorine concentration of 1.0 mg Cl_2/L. The PFB was operated for a period of 10 h for each experiment. In order to determine iron and manganese removal profiles within the column, water samples were taken at different heights (0, 9, 25, 50, 75, 100 and 120 cm from the bottom of the column) after 2, 4 and 10 h of operation. Total and dissolved iron and manganese concentrations were measured at each sampling point. The dissolved metals were defined as iron and manganese filterable through a 0.45 µm syringe filter (PVDF, CAT. NO. CS-GLPV3045, Chem Science Inc., Dorval, QC). Effluents from the oxidation or PFB columns were fed into the MF/UF membranes after 1 and 4 h of operation, respectively.
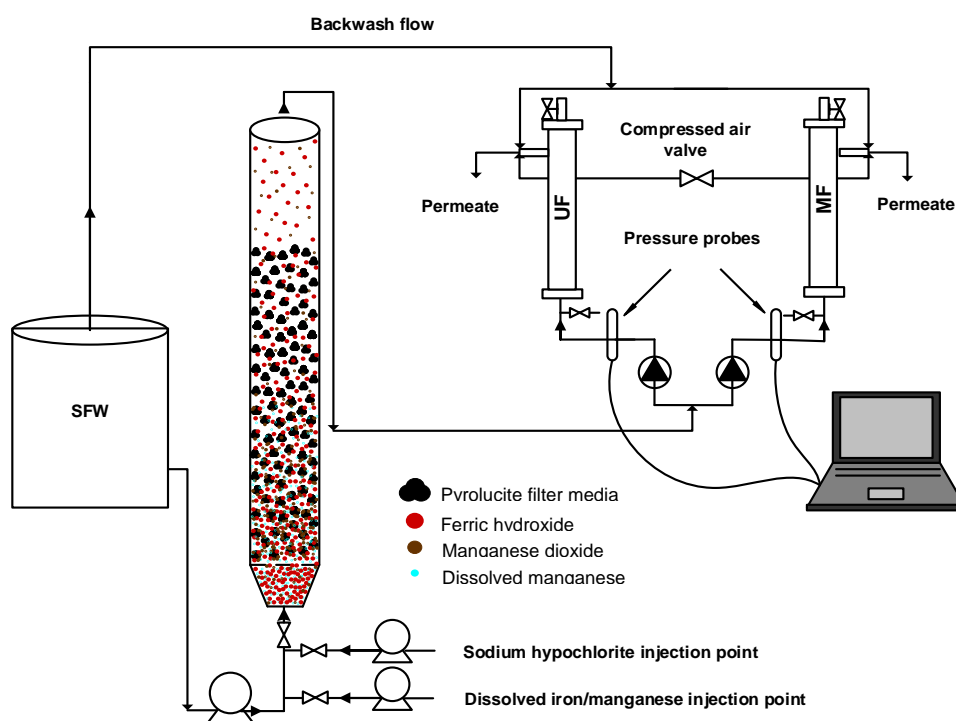
Figure 8.1. Schematic of the pilot-scale pyrolucite fluidized bed (PFB)-microfiltration (MF)/ultrafiltration (UF) hybrid process. SFW: Synthetic feed water.

Membrane experiments were conducted in dead-end, inside-out and constant flux configuration driven by peristaltic pumps. Before launching the MF/UF experiments, the DM water was passed

through the membranes at the desired flux until a steady transmembrane pressure (TMP) had been reached. Afterwards, the particle-free SFW with the desired characteristics was filtered at the same flux and the initial permeability of the membrane was determined. Then, the particle-free SFW was replaced by the outlet of the column. The experiments related to the pre-oxidation-MF/UF process were conducted at different flux rates of 150 and 300 LMH while the filtration behavior was only assessed at a flux of 300 LMH for the PFB-MF/UF hybrid process. Fluxes were regularly checked during the experiment by measuring the permeate flow rate and were found to vary by less than 1.5%. Each membrane unit was equipped with a pressure transducer (Omega, PX409-030GUSB). The instantaneous pressure data was collected every 30 s using a data acquisition software (TRH Central, Santa Ana, CA). Samples of membrane feed water and permeate were taken to measure the concentrations of iron and manganese as well as DOC and TOC for the tests including humic acids. The membrane runs were stopped after 6 h of operation or after the TMP across the UF membrane increased to more than about 170 kPa (25 psi). All experiments were carried out at 20°C.

The same MF/UF membrane was utilized for all the experiments. Following the filtration, the membranes were first physically and then chemically cleaned so that the initial permeability of the membranes was completely recovered. The physical cleaning procedure first consisted in backwashing with particle-free SFW for 3 min at twice the operating flux; then the cleaning step was enhanced by backwashing with air scouring for 5 s at 400 kPa; and finally, the membranes were again backwashed with particle-free SFW for 3 min to completely remove the detached particles. The chemical cleaning was conducted by recirculating 1.0 L of 2% (W/W) oxalic acid (Fisher Scientific, Fair Lawn, NJ) at 50°C and pH 1-2 for 30 min. For the experiments containing humic acids, an alkaline/oxidizing cleaning step was also carried out after the acid cleaning step by recirculating 1.0 L of 500 mg Cl_2/L sodium hypochlorite solution at 50°C and pH 11-12 for 30 min. After these cleaning steps, the membranes were thoroughly rinsed with DM water. The clean water permeabilities of the membranes were checked with DM water a day after the cleaning cycles. In addition, the permeability of particle-free SFW was also calculated after each cleaning step to determine the physically and chemically reversible fouling of the membranes (Dashtban Kenari and Barbeau, 2016b).

8.2.4 Analytical methods

Serial filtration was applied to determine the size distribution of iron and manganese suspensions in the membrane feed water. Accordingly, a series of disc type MF and UF membranes with nominal pore sizes of 30 µm (CAT. NO. NY3004700, Millipore Corp.), 8 µm (CAT. NO. SCWP04700, Millipore Corp.), 3 µm (CAT. NO. SSWP04700, Millipore Corp.), 1.2 µm (CAT. NO. RAWP04700, Millipore Corp.), 0.8 µm (CAT. NO. AAWP04700, Millipore Corp.), 0.45 µm (LOT NO. T41389, Pall Corp.), 0.22 µm (CAT. NO. GSWP04700, Millipore Corp.) and 0.1 µm (LOT NO. T21020, Pall Corp.), and MWCO of 30 kDa (PVDF, Sterlitech Corp.) were used. Prior each experiment, the MF membranes were first flushed with approximately 500 mL of Milli-Q^{TM} water and the 30 kDa UF membrane was immersed in Milli-Q^{TM} water for 24 h. The membrane feed solution was vacuum filtered successively through the MF membranes. The filtrate was then passed through the 30 kDa membrane using a 50 mL Amicon 8200 cell which was pressurized to approximately 240 kPa (35 psi) with nitrogen gas.

Iron and manganese concentrations were measured by inductively coupled plasma-optical emission spectrometry (ICP-OES, model iCAP 6000), following heat and acid digestion with 0.5% HNO_3 (Omni Trace®, EMD chemicals Inc., Gibbstown, NJ) (pH < 2) at 80 ˚C for 48 h. The average of triplicate analysis of each sample is reported. The pH measurements were carried out using a Hach (HQ40d) portable pH meter.

DOC and TOC concentrations were analyzed using a TOC meter (Sievers 5310 C, GE Water). For DOC measurements, the samples were pre-filtered through the 0.45 µm filter which was previously rinsed with 1 L of Milli-Q^{TM} water. UV_{254} absorbance was measured on 0.45 µm pre-filtered samples using a Hach spectrophotometer (DR 5000) with a 1 cm path length quartz cell.

8.2.5 Characterization of membrane fouling

8.2.5.1 Constant flux blocking law model

In several municipal and industrial solid-liquid separations by membranes, the pressure increase profile in constant flux filtration mode can be described by the power-law compressible cake formation model (Sorensen and Sorensen, 1997; Chellam et al., 1998). A previous study (Dashtban Kenari and Barbeau, 2016b) highlighted the importance to account for cake compressibility while modeling cake fouling caused by manganese and ferric oxides. In this regard, the constant flux

blocking law model for compressible cake filtration (Eq. (7.1)) (Chellam and Xu, 2006; Dashtban Kenari and Barbeau, 2016b) was applied to describe the pressure increase behavior and the compressibility of the filter cake.

$$\Delta P = \Delta P_0 + \frac{Q\mu c_b}{A_0} \beta \Delta P^{n'} V_s \tag{7.1}$$

where ΔP_0 and ΔP are initial and final TMP (kPa), respectively; A_0 is the Surface area of the clean membrane (m^2); Q is the flow through the membrane (m^3/s); μ is the viscosity of the fluid (kPa.s); c_b is the bulk concentration (kg/m^3); β (m/kg/kPa$^{n'}$) and n' are empirical constants (n' is the cake compressibility coefficient ($0 \leq n' \leq 1$)); and V_s is the volume of permeate per unit membrane area (m^3/m^2).

The compressibility parameters were determined by fitting the experimental pressure data to Eq. (7.1) using a curve-fitting tool in Matlab (R2015a) with a trust region method resulting in the smallest sum of squared residuals.

1.1.1. Resistance-in-series model

The resistance-in-series model (Eq. (7.2)) was applied to quantify the contribution of irreversible fouling and effectiveness of different cleaning procedures.

$$J = \frac{\Delta P}{\mu R_t} = \frac{\Delta P}{\mu (R_m + R_{pr} + R_{cr} + R_{if})} \tag{7.2}$$

where J is the flux through the membrane (m/s); R_t is the total resistance (m^{-1}); R_m is the intrinsic membrane resistance (m^{-1}), R_{pr} is the physically reversible resistance (m^{-1}); R_{cr} is the chemically reversible resistance (m^{-1}); and R_{if} is the chemically irreversible fouling (m^{-1}).

R_m was determined prior each experiment by measuring the particle-free SFW permeability of the membranes. R_{pr} was obtained via the difference between the TMP of particle-free SFW after the physical cleaning step and the TMP at the end of filtration. R_{cr} was calculated from the difference between the stabilized TMP before and after the chemical cleaning step. R_{if} was back-calculated from the difference between R_t and the sum of R_m, R_{pr}, and R_{cr}.

In addition, to facilitate the comparison of the experimental results, the foulants (ferric hydroxide, manganese dioxide and humic acids) resistance, R_f, under different conditions were illustrated as a function of V_s. The R_f was defined as the difference between the R_t and the R_m, as follows:

$$R_f = R_f - R_m = \frac{\Delta P - \Delta P_0}{\mu J} \tag{7.3}$$

8.3 Results and discussion

This section first presents iron and manganese removal performances in pre-oxidation-MF/UF and PFB-MF/UF processes. The fouling behavior of MF and UF membranes is then illustrated under different water chemistry conditions. Finally, the results of the resistance-in-series model analysis are presented.

8.3.1 Iron and manganese removal performance

Figure 8.2 illustrates the concentration of iron and manganese as a function of empty bed contact time which refers to a specific height of the bed. From this figure, stable removal profiles were observed over the 10-h operation for both iron and manganese under soft water (Figure 8.2a), moderately hard water (hardness=100 mg $CaCO_3$/L) (Figure 8.2b) and moderately hard water including 2 mg/L humic acids (Figure 8.2c). Accordingly, 76%-89% iron and 95%-97% manganese removal were achieved through the PFB in around 100 s contact time, regardless of the influent water quality. The lower removal of iron is explained by mechanistic differences. Due to the very slow oxidation rate of manganese by chlorine, nearly all manganese remained dissolved throughout the PFB. Thus, manganese removal involved a very fast adsorption of dissolved manganese onto the pyrolucite media and subsequent autocatalytic oxidation of adsorbed manganese by chlorine. Unlike manganese, iron is oxidized almost instantaneously to particulate ferric oxides which removal is dependent on the attachment of particulate ferric hydroxide onto the pyrolucite media. Due to the shear exerted on the pyroluctite media in the fluidized bed (30% bed expansion), it is only partly effective in retaining the particulate species. Therefore, lower rejection was observed for iron than for manganese. It is worth mentioning that although a PFB alone can remove almost all dissolved manganese from water in the absence of iron (Dashtban Kenari and Barbeau, 2014), its performance to remove manganese declines in the presence of iron. This is likely due to the carryover of oxidized manganese species with the particulate ferric hydroxide. These results indicate the need to provide a downstream process which can properly reduce the concentration of these species below the target value of 0.020 mg/L.
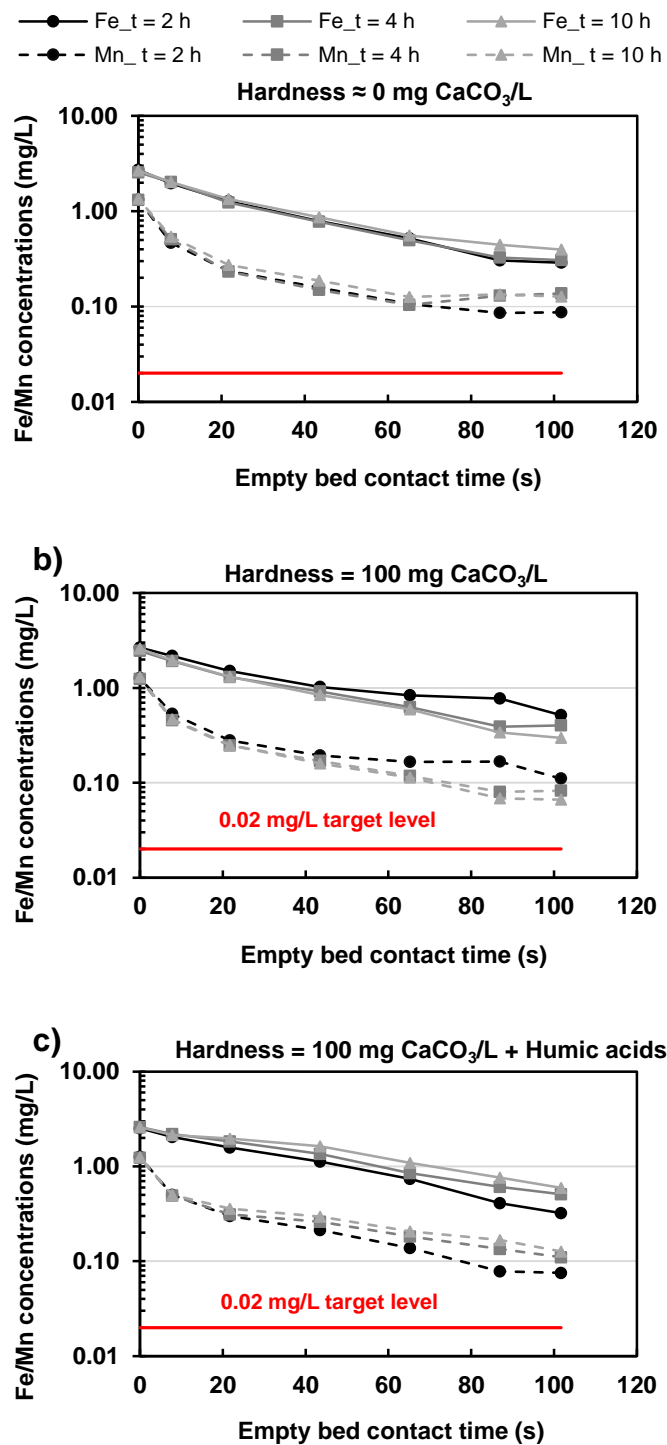
Figure 8.2. Iron (Fe) and manganese (Mn) concentrations for increasing empty bed contact times inside the pyrolucite fluidized bed (PFB). Assays conducted under various water quality conditions: a) hardness ≈ 0 mg $CaCO_3/L$, b) hardness $= 100$ mg $CaCO_3/L$ and c) hardness $= 100$ mg $CaCO_3/L$ + Humic acids. Alkalinity $= 50$ mg $CaCO_3/L$, T $= 20$°C, pH $= 7.0$ and hydraulic loading rate (HLR) $= 41$ m/h.
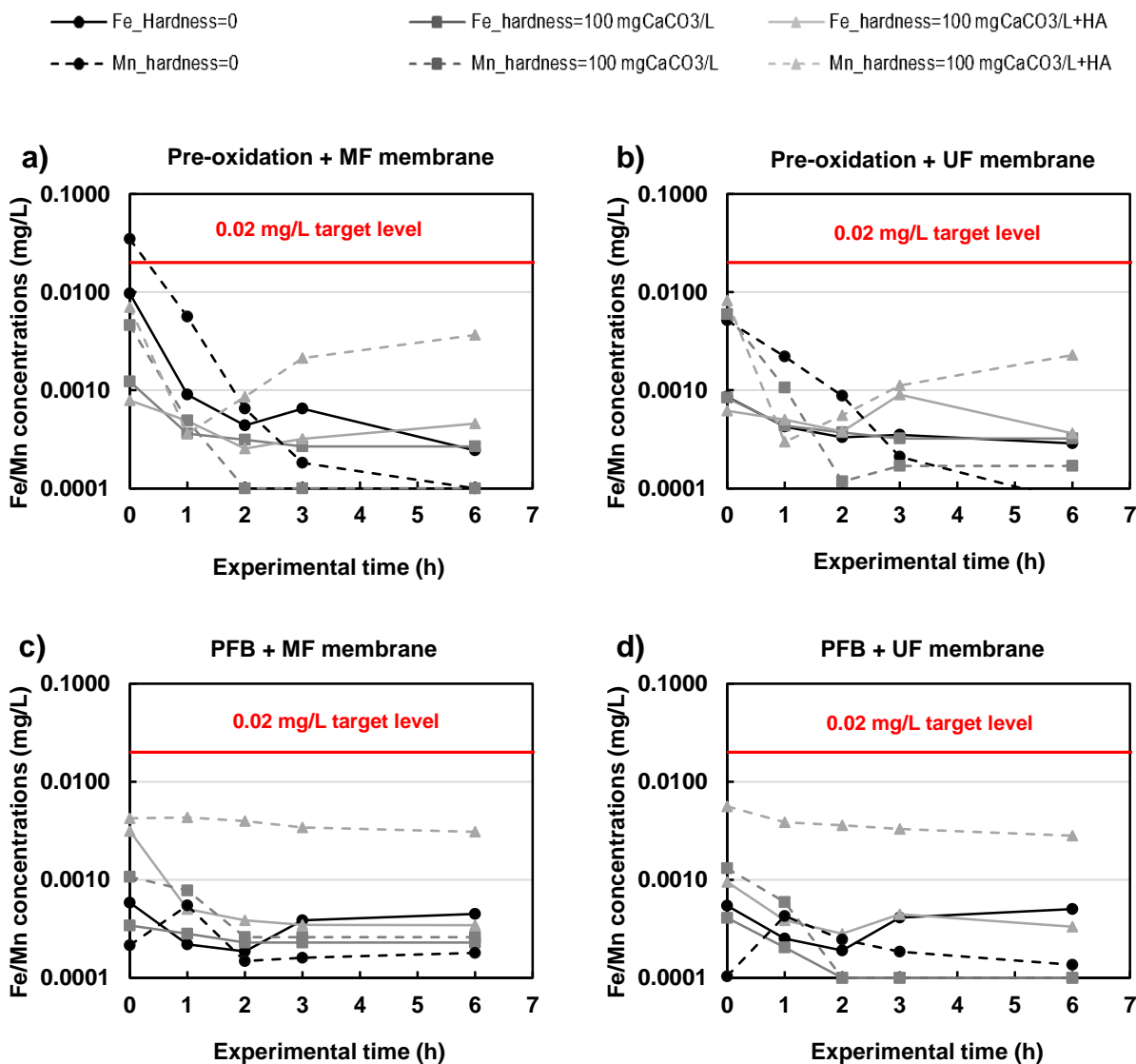
Figure 8.3. Iron (Fe) and manganese (Mn) concentrations in the permeate of the two process configurations tested under various water quality conditions at different experimental time: a) pre-oxidation + microfiltration (MF), b) pre-oxidation + ultrafiltration (UF), c) pyrolucite fluidized bed (PFB) + MF and d) PFB + UF. T = 20°C, pH = 7.0 and flux = 300 LMH.

Figure 8.3 illustrates the iron and manganese concentrations in the permeate water over the 6-h MF/UF filtration run under different water quality conditions. Figure 8.3a and b reveal that the pre-oxidation-MF/UF membrane process could properly reduce the concentration of iron and manganese below 0.010 mg/L, except at the initial stage of the filtration process using pre-oxidation-MF membrane under soft water condition (manganese concentration = 0.035 mg/L). This result is explained by the presence of colloidal manganese dioxide with less than 100 nm size (the

nominal pore size of MF membrane) under such condition (Dashtban Kenari and Barbeau, 2016a). At the latter filtration time, the cake layer accumulated on the surface of the membrane retained these fine colloids. From Figure 8.3c and d, the PFB-MF/UF hybrid process could effectively reduce the concentration of iron and manganese in the finished water to below 0.005 mg/L over the entire filtration run under all conditions tested.

8.3.2 Comparison of membrane fouling for the pre-oxidation-MF/UF process vs. the PFB-MF/UF hybrid process

The following sections compare the fouling behaviors of MF/UF membranes for two pretreatment options under different water quality conditions.

8.3.2.1 Soft water condition (hardness = 2 mg CaCO$_3$/L)

Figure 8.4a and b present the rise in TMP and the foulant resistances as a function of V_S under a water condition with negligible hardness. For the pre-oxidation-MF/UF process, the slight non-linear, concave upward increase of TMP as a function of cumulative permeate volume (Figure 8.4a) indicates that the majority of the membrane fouling was caused by the cake layer formed on the surface of the membranes. Excellent agreement of the experimental data with the constant flux power law compressible cake model (cf. solid lines in Figure 8.4a) was observed which further confirms the dominant role of cake formation on fouling. The slight concave downward curve during the very early stage of filtration suggests the presence of pore blocking mechanisms in the first few minutes of the experiment. Serial fractionation of membrane feed water (Figure 8.5a) revealed the presence of fine colloids (< 100 nm) that are smaller than the nominal pore size of the MF membrane. These small colloids may deposit into the inner channels of the membrane pores and, thus, diminish the pore diameters. Likewise, the concentrations of iron and manganese in the permeate water indicated that some colloids passed through the MF membrane at the initiation of the experiments. Thus standard pore blocking or pore constriction is possibly one of the mechanisms responsible for the initial pressure increase in the MF membrane. After this initial stage, the fine particles were retained within the cake layer and removed before reaching the membrane surface. For UF membrane, the sharp increase of TMP measured at the initiation of filtration, especially at higher flux, is possibly related to the blockage of the pore mouth by the colloids. The higher hydraulic resistance of the UF membrane probably enhanced attachment of

colloids on the membrane surface and blockage of the pore mouth. Consequently, fouling mechanisms included the initial pore blockage for the first few minutes, and the subsequent formation of a cake layer on the membrane surface. However, the contribution of pore blocking to the overall fouling of the membrane was negligible.

Figure 8.4. Comparison of membrane fouling for the pre-oxidation-microfiltration (MF)/ultrafiltration (UF) process and the pyrolucite fluidized bed (PFB)-MF/UF hybrid process under soft water condition (hardness ≈ 0 mg $CaCO_3$/L): (a) instantaneous transmembrane pressure (TMP) from experimental data and the model fits using the constant flux blocking model for compressible cake (solid lines) (Eq. (1)) and (b) foulant resistance. T = 20°C and pH = 7.0.

In pre-oxidation-MF/UF process, the steep TMP increase over the entire filtration cycle was consistent with the fact that more than 75% of aggregates were in submicron range in the membrane feed water (Figure 8.5a). The presence of colloids led to the formation of a more compact and less porous cake layer (Lee et al., 2003). Fitting the experimental data to the Eq. (7.1) permitted to determine the compressibility of the cake layer. Table 8.3 summarizes the compressibility coefficients of the deposited cake layer under different experimental conditions. The results

demonstrated that the mixture of ferric hydroxide and manganese dioxide aggregates in soft water was only slightly compressible ($n' < 0.25$ (Tiller et al., 1987)) and the compressibility coefficients were approximately comparable, regardless of the operating condition or membrane type. The mixture of large and small aggregates can result in the formation of a dense cake layer (Madaeni, 2001) which hardly compresses further in the process since small colloids already occupy the void between the large rigid metal oxide aggregates.

Table 8.3. Compressibility coefficients (n') for the deposited cake layer in pre-oxidation-microfiltration (MF)/ultrafiltration (UF) process.

Experimental conditions	Flux (LMH)	n'	
		MF	UF
Hardness ≈ 0 mg CaCO₃/L	150	0.173	0.246
	300	0.163	0.157
Hardness ≈ 100 mg CaCO₃/L	150	0.347	0.283
	300	0.342	0.353
Hardness ≈ 100 mg CaCO₃/L + humic acids	150	0.593	0.614
	300	0.520	0.607

As can be seen from Figure 8.4b, at the lower flux of 150 LMH, the R_f of the MF membrane was virtually identical to that of the UF membrane indicating the similar fouling mechanisms and properties of the cake layer. When the flux was increased to 300 LMH, the R_f of the MF and UF membrane increased by 3% and 21%, respectively. This increase in the R_f of the UF membrane was attributed to the higher compaction of the cake layer achieved at higher TMP.

Comparing membrane fouling for the pre-oxidation-MF/UF process vs. the PFB-MF/UF hybrid process revealed that the use of a PFB prior the membrane modules substantially reduced the extent of membrane fouling, an effect caused by the removal of iron and manganese within the PFB. Particularly, it removed more than 95% of manganese, which has been evidenced to induce severe fouling to the membranes (Dashtban Kenari and Barbeau, 2016b), and 85% of iron. Furthermore, from Figure 8.5a, all the oxidized aggregates in the effluent of the PFB were larger than 3 µm resulting in cake layer formation which exerted minimal fouling to the membranes. Consequently, the R_f of the MF and UF membrane decreased by 95% and 98%, respectively. The negligible fouling of the MF/UF membrane in the downstream of PFB after 6 h of operation at a high flux

rate of 300 LMH implies that this hybrid process could continuously operate for several days without any physical or chemical cleaning.

Another interesting result that is worth nothing here is the size distribution of ferric hydroxide and manganese dioxide aggregates. According to Figure 8.5a, the majority of aggregates corresponded to a size between 0.45 and 0.8 µm, which accounted for 60 % of the total mass of aggregates. However, our previous results on water containing only manganese had shown that more than 90% of manganese dioxide aggregates had a size smaller than 0.45 µm under the same condition (Dashtban Kenari and Barbeau, 2016a). We conclude that the presence of positively charged ferric hydroxide aggregates (Dashtban Kenari and Barbeau, 2016a) promoted the aggregation of negatively charged colloidal manganese dioxide. In addition, these species may adsorb or attach to one another resulting in a unique size distribution, as illustrated in Figure 8.5a.

169
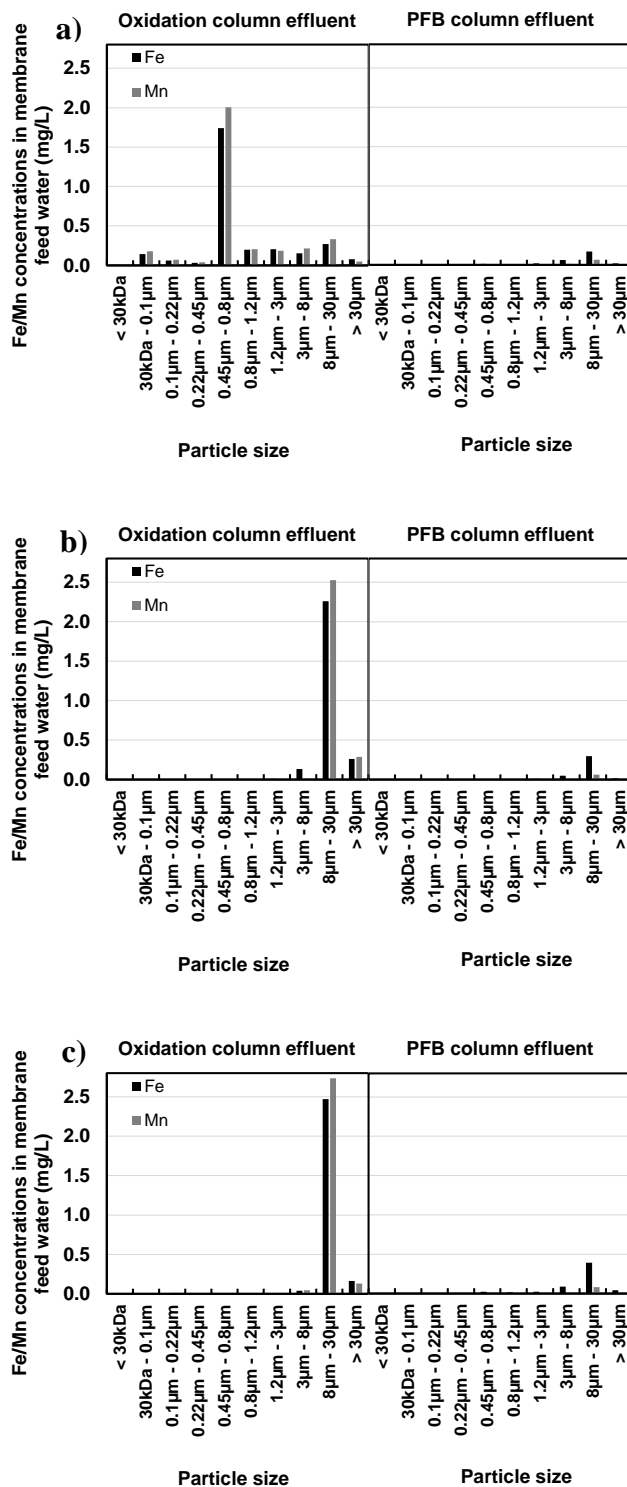
Figure 8.5. Particle size distribution of oxidized iron (Fe) and manganese (Mn) aggregates in the membrane feed water using the serial filtration technique. a) Hardness ≈ 0 mg CaCO$_3$/L, b) Hardness = 100 mg CaCO$_3$/L, and c) Hardness = 100 mg CaCO$_3$/L + humic acid ≈ 2 mg/L, T = 20°C and pH = 7.0.

8.3.2.2   Moderately hard water condition (hardness = 100 mg CaCO₃/L)

Figure 8.6 illustrates the rise in TMP and the foulant resistance in MF and UF of water containing iron and manganese under moderately hard water condition. Comparing Figure 8.6 and Figure 8.4 reveals that increasing hardness from 0 to 100 mg CaCO$_3$/L had a significant impact on fouling of both MF and UF membranes in the pre-oxidation-MF/UF configuration. The reduction in membrane fouling under higher hardness condition was associated with the much larger aggregates size. High calcium concentration increases aggregation of colloidal particles via charge neutralization, electrostatic double layer compression and bridging phenomenon (Zhang et al., 2009). As shown in Figure 8.5b, about 87% of iron and manganese species (by mass) had a size ranging from 8 to 30 µm which is significantly larger than the pore size of the membranes. Figure 8.6a also illustrates the fitting of the experimental data to the compressible cake formation model (solid lines). The excellent agreement of the model with the experimental data confirms that cake filtration dominated the fouling process during these experiments. As presented in Table 8.3, the deposited filter cake under this condition was moderately compressible, i.e. approximately twice higher than the cake formed under soft water condition. This is mainly related to the much larger aggregate size with nearly neutral surface charge (Dashtban Kenari and Barbeau, 2016a), which increases the void space between the aggregates. This void space can be eventually occupied by the forthcoming aggregates resulting in compression of the filter cake.

At the lower flux of 150 LMH, the TMP build-up in MF membrane showed a similar trend as for the UF membrane over the entire filtration cycle such that the foulant resistance curves once again overlapped (Figure 8.6b). Under this condition, relatively low fouling was observed for both membranes. Rising the flux to 300 LMH increased the drag force, and thus resulted in the formation of more compact cakes with greater resistances. As a consequence, higher foulant resistance was observed under this condition especially for the UF membrane.

Although, the extent of fouling in pre-oxidation-MF/UF process was substantially lowered under moderately hard compared to soft water condition, the fouling was still high at the elevated flux of 300 LMH and required frequent cleaning. The pretreatment with PFB properly mitigated the membrane fouling and enhanced the performance of both membranes. Thus, the use of PFB pretreatment is of benefit, even under hard water condition, as it removed a large portion of iron and manganese species and reduced total suspended solids concentration.
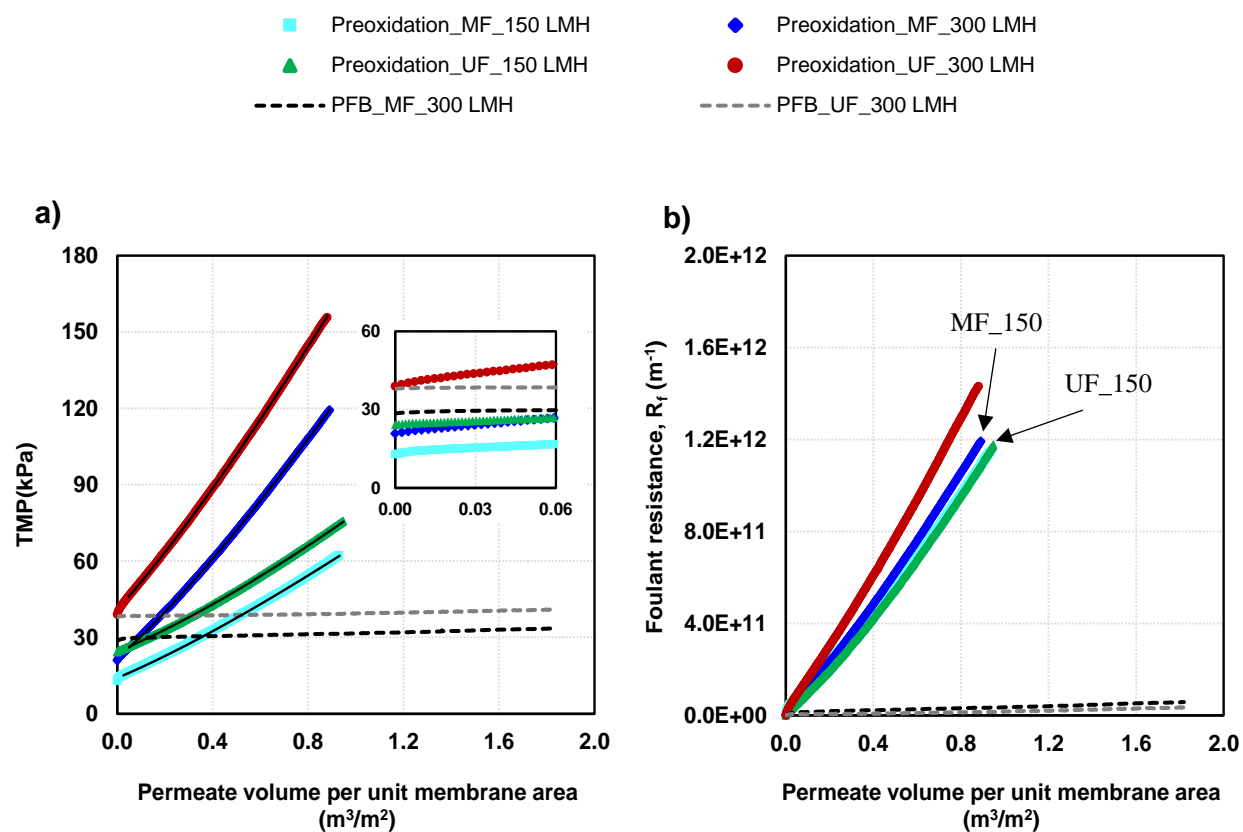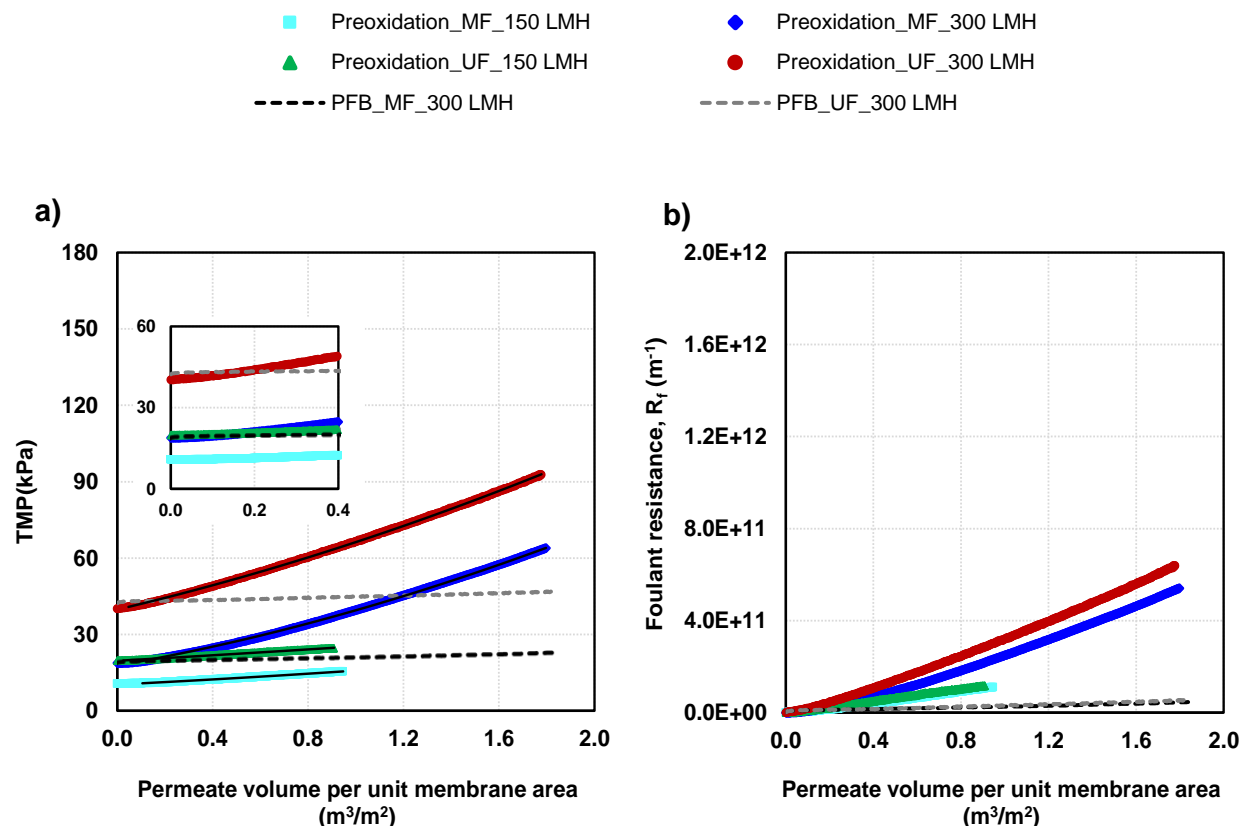
Figure 8.6. Comparison of membrane fouling in pre-oxidation-microfiltration (MF)/ultrafiltration (UF) process and pyrolucite fluidized bed (PFB)-MF/UF hybrid process under moderately hard water condition (hardness = 100 mg $CaCO_3$/L): (a) instantaneous transmembrane pressure (TMP) from experimental data and the model fits using the constant flux blocking model for compressible cake (solid lines) (Eq. (1)) and (b) fouling resistance. T = 20°C and pH = 7.0.

8.3.2.3 Moderately hard water containing humic acids

The filtration behavior in both processes under hardness of 100 mg $CaCO_3$/L containing 2 mg C/L humic acids is depicted in Figure 8.7. Comparing Figure 8.6 with Figure 8.7, we observed that in the presence of humic acids, fouling of both membranes progressed much more rapidly presumably due to the relatively high concentration of calcium ions, which resulted in rejection of almost all humic acids by both membranes. Under very low calcium concentrations, the majority of the NOM passes through the MF/UF membranes without causing significant membrane fouling (Katsoufidou et al., 2005; Shao et al., 2011). However, under moderately hard water condition (40 mg Ca^{2+}/L or 1 mM), the ionic strength increased and, thus, the net charge surrounding the humic acid (which is negatively charged at a pH greater than 4.7 (Stevenson, 1982)) decreased resulting in the reduction

in intra- and inter-molecular electrostatic repulsion. In addition, calcium ions can also bind to the carboxylic acid functional groups of humic acids (Zularisam et al., 2006; Shao et al., 2011). These led to the aggregation of humic acid and, thus, their deposition on the membrane surface. Consequently, the removal of humic acids as well as the fouling of the membranes increased although a significant influence of humic acids on ferric hydroxide or manganese dioxide aggregates size was not observed (Figure 8.5c). Previous studies also indicated that membrane fouling caused by humic acids is more severe under high calcium concentrations due to the higher retention of aggregated molecules on the membrane surface (Katsoufidou et al., 2005; Shao et al., 2011).
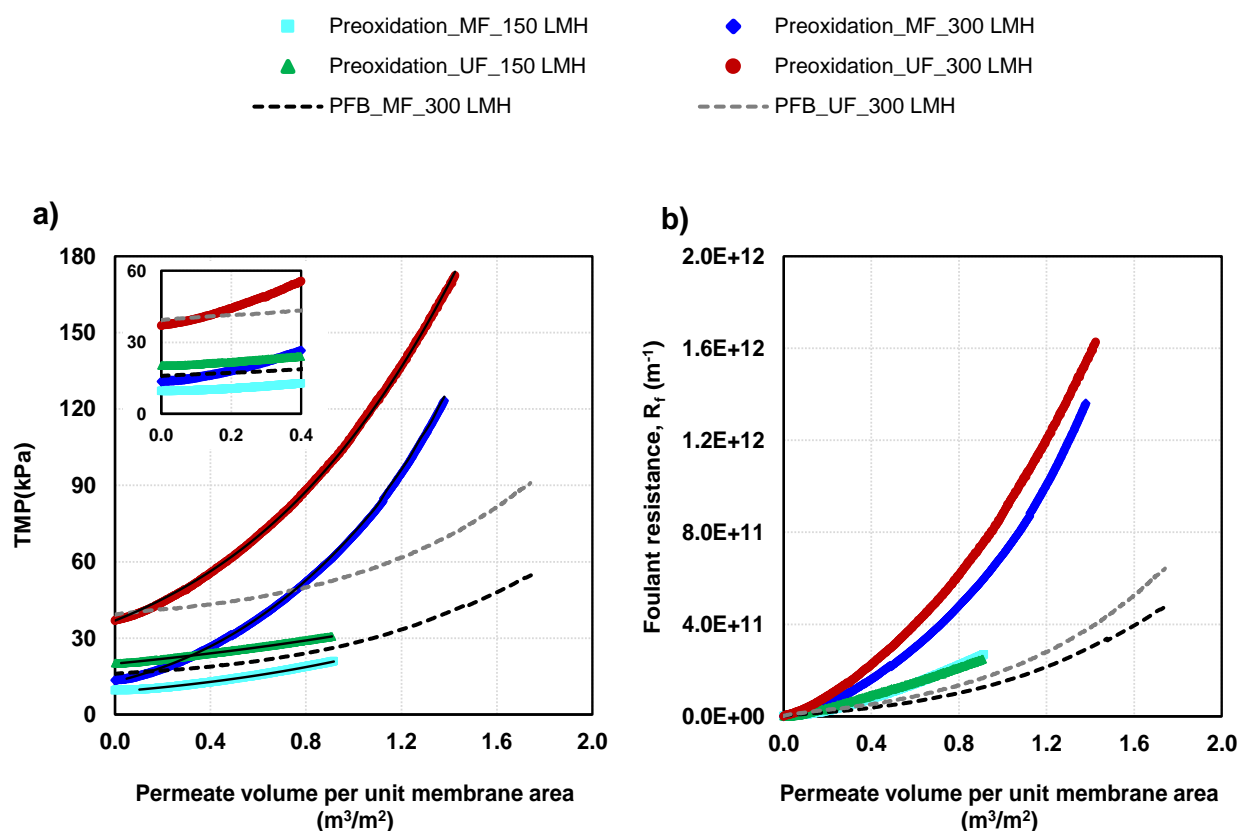
Figure 8.7. Comparison of membrane fouling in pre-oxidation-microfiltration (MF)/ultrafiltration (UF) process and pyrolucite fluidized bed (PFB)-MF/UF hybrid process under moderately hard water condition (hardness = 100 mg CaCO$_3$/L) and $\approx$ 2 mg/L humic acid: (a) instantaneous transmembrane pressure (TMP) from experimental data and the model fits using the constant flux blocking model for compressible cake (solid lines) (Eq. (1)) and (b) fouling resistance. T = 20°C and pH = 7.0.

Figure 8.7 illustrates a concave-upward behavior of TMP versus volume filtered. Under all conditions, the TMP gradually increased at shorter times while the fouling exacerbated at longer time scales. The increased fouling rates at longer time scales are due to the compressibility of the cake layer, which resulted in a greater increase in the hydraulic resistance. Figure 8.7a also shows the fitting of the experimental TMP to the model for compressible cake formation (solid lines). As observed, the model correctly predicts the fouling behavior at the later stages of filtration. The data at the initiation of the experiment was excluded from the model fitting due to the retardation in the development of the filter cake, especially at the lower flux. In addition, the filter cake may exhibit a retardation effect during the compression as the compressibility coefficient progressively increased until an equilibrium has been reached (Hwang and Hsueh, 2003). This especially occurs during the initial stages of filtration of soft aggregates. From Table 8.3, fairly high and comparable compressibility coefficients (0.52-0.61) were attained in the pre-oxidation-MF/UF process under all conditions tested. Thus, the compressibility coefficients for oxidized suspensions containing organic compounds were much higher than those for the oxidized iron and manganese species alone, presumably due to break-up and/or deformation of soft organic aggregates (Vela et al., 2008) which bound particles one to another and concurrently filled some of the spaces between them.

At the higher flux, the increased drag force gave rise to the formation of more compact cakes with greater resistances. For example, R_f after 0.9 m^3/m^2 increased from 2.44E+11 to 7.37E+11 as flux augmented from 150 to 300 LMH for UF membrane. At the lower flux of 150 LMH, the foulant resistance was almost independent of membrane type (Figure 8.7b). As the flux increased to 300 LMH, the difference between the required TMP for UF and MF membrane increased giving rise to a more significant difference between the fouling of these membranes. As a consequence, a more compact cake layer with greater resistance was formed on the UF membrane.

As depicted in Figure 8.7, using PFB as a pretreatment step resulted in a dramatic reduction in membrane fouling. As a result, the fouling of MF and UF membrane after a V_s of 1.3 m^3/m^2 decreased by 78% and 76%, respectively. However, the fouling of both membranes are much higher than in the previous conditions (Figure 8.4 and Figure 8.6) while the concentrations of oxidized iron and manganese in the membrane feed water did not change significantly. Thus, humic acids (and their interaction with manganese/iron) were the main contributor to the fouling of membranes under this condition. The fouling was initially similar for both MF and UF membranes,

but as the filtration progressed, the fouling of UF membrane became much larger than that of the MF membrane due to the higher compaction of foulant under higher TMP.

8.3.3 Resistance-in-series model analysis

The "resistance-in-series" analysis was applied to provide further quantitative insight into the reversibility of ceramic MF/UF membrane fouling. Figure 8.8 presents the results of this analysis in pre-oxidation-MF/UF process and PFB-MF/UF hybrid process under very low hardness value (Figure 8.8a), hardness of 100 mg $CaCO_3$/L (Figure 8.8b), and hardness of 100 mg $CaCO_3$/L with 2 mg/L humic acids (Figure 8.8c). Chemically irreversible fouling was negligible under all conditions implying that adsorption of foulants within the membrane pores did not take place.

In pre-oxidation-MF/UF configuration, R_{cr} largely contributed to the total fouling of the membranes under soft water condition (Figure 8.8a). For instance, at the flux of 300 LMH, R_{cr} accounted for 34% and 50% of the MF and UF membranes fouling, respectively. Deposition of colloids and pore blocking at the early stage of filtration as well as the formation of a cohesive and compact cake layer was the likely cause of the physically irreversible fouling. Correspondingly, frequent acid cleaning would be essential for the successful operation of this process. On the other hand, the PFB-MF/UF hybrid process could be continuously operated for several days without requiring substantial cleaning.

Under moderately hard water conditions (Figure 8.8b and c), the majority of fouling was physically reversible, further confirming the dominant role of cake formation mechanism and rejection of contaminants by size exclusion. At the flux of 150 LMH, the intrinsic membrane resistance was the main contributor to the total resistance of the membranes. However, at the flux of 300 LMH, both membranes were severely fouled in the presence of humic acids. Although the fouling was physically reversible, the extent of the fouling would be expected to impact the economic viability of the pre-oxidation-MF/UF process. Comparison between Figure 8.8b and c reveals that the humic acids were the main contributor to fouling under hard water conditions. Since the PFB cannot remove humic acids from water, almost all humic aggregates (> 90% DOC removal) were accumulated on the membrane surface resulting in higher resistance than in the absence of humic acids, which was quantitatively comparable to the foulant resistance (R_f/V_s) for the pre-oxidation-MF/UF process operated at the flux of 150 LMH. It is likely that the more compressed humic acids
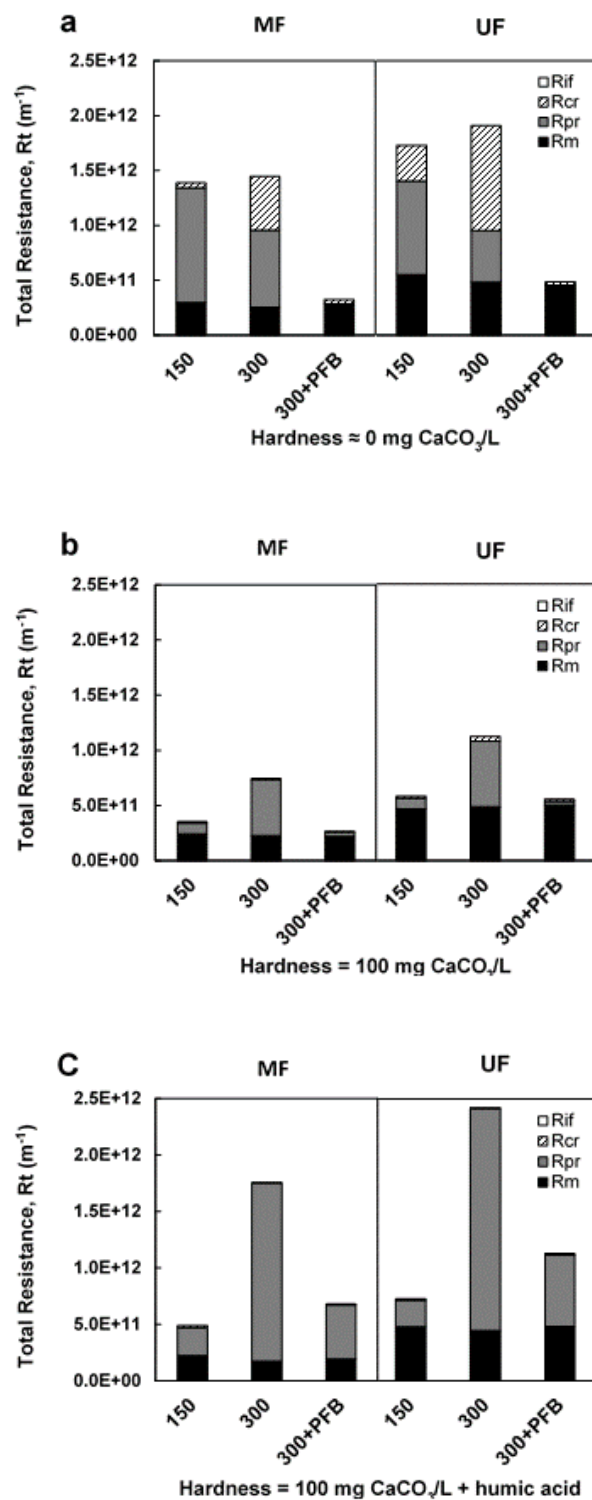
Figure 8.8. Resistance-in-series analysis for the constant flux/dead-end microfiltration (MF)/ultrafiltration (UF) of ferric hydroxide and manganese dioxide suspensions under (a) hardness $\approx$ 0 mg $CaCO_3$/L, (b) hardness = 100 mg $CaCO_3$/L, and (c) hardness = 100 mg $CaCO_3$/L + 2 mg/L humic acids. T = 20°C.

cake developed at the higher flux of 300 LMH compensated for the lower concentrations of oxidized iron and manganese measured in the PFB-MF/UF effluent.

8.4 Conclusions

The main goal of this study was to develop a more robust process for iron and manganese control in drinking water. The performance of a PFB pretreatment for mitigating MF/UF membrane fouling was investigated. The following conclusions can be drawn:

- Both pre-oxidation-MF/UF and PFB-MF/UF hybrid processes reduced the concentration of iron and manganese in finished water to below the target limit of 0.020 mg/L (except at the initial stage of the pre-oxidation-MF process under soft water condition).

- Severe fouling of both membranes were observed in pre-oxidation-MF/UF process under all conditions tested, especially under soft water or in the presence of humic acids at high flux.

- In pre-oxidation-MF/UF process under soft water condition, the fouling behavior was governed by initial pore blockage followed by cake filtration during the later stage. However, the initial pore blocking step was negligible compared to the total fouling of the membranes. Under moderately hard water conditions, cake formation was the predominant fouling mechanism during the entire filtration period. The dominant role of cake formation was confirmed by the excellent fit of the experimental data to the blocking law model for compressible cake.

- The PFB pretreatment properly alleviated the membrane fouling by removing more than 75% and 95% of iron and manganese, respectively. The PFB-MF/UF hybrid process, in the absence of humic acids, could be continuously operated for several days without any chemical/physical cleaning.

- With the pre-oxidation-MF/UF process under soft water condition, chemically reversible resistance largely contributed to the total resistance of the membranes. Under all other conditions, fouling was physically reversible.

- As the filtration flux increased, the fouling became more severe for the UF than the MF membrane due to the higher operation pressure of the former which led to higher compaction of the deposited cake layer on the membrane surface.

Acknowledgments

CHAPTER 9   GENERAL DISCUSSION

This chapter highlights the main findings of this research project. The general objective was to develop a robust and compact process for iron and manganese control, which can consistently guaranty the desired target limit in treated water (0.02 mg Mn/L and 0.02 mg Fe/L). To achieve this goal, we investigated: 1) the characteristics of oxidized iron and manganese in water treatment; 2) the fouling of UF membranes caused by oxidized iron and manganese; 3) the application of PFB for manganese removal; 4) a pilot-scale demonstration of fixed vs. fluidized pyrolucite beds for iron and manganese control; and 5) the performance of a PFB-MF/UF hybrid process for improved iron and manganese control. The main findings of each part is discussed in sections 8.1 to 8.5.

9.1 Characteristics of oxidized iron and manganese in water treatment

Following oxidation of Fe(II)/Mn(II), LD, DLS and fractionation through serial membrane filtration techniques were used to define the PSD of oxidized species. The results indicated that the pH of water has a significant impact on the size of manganese dioxide colloids/particles. Increasing the pH from 6.0 to 8.0 substantially reduced the size of manganese dioxide while almost all colloids were found in the size fraction between 0.1 µm and 30 kDa. This result was in line with the measured ζ-potential of these colloids. Since the point of zero charge of manganese dioxide is below pH 3.0 (Morgan and Stumm, 1964), it is always negatively charged in natural waters. When pH increased from 6.0 to 8.0, the more negatively charged surface (ζ-potential of -36.4 ± 2.1 mV to -45.5 ± 2.1 mV) provides higher EDL repulsion between the colloids, therefore reducing the aggregation of colloids. A monomodal PSD is observed under all pH conditions using the DLS and LD measurement techniques with a shift toward larger sizes as the pH is reduced from 8.0 to 6.0. In these experiments, LD always demonstrated the presence of very fine colloids, which were not detected by DLS, because the latter measures the hydrodynamic diameter, which is larger than the geometric diameter for small highly charged colloids. This difference is particularly considerable for sub-100 nm size colloids, as previously stated by Safari et al. (2014). In these experiments, the DLS results were fairly similar to the results obtained via the serial membrane filtration technique. This result is consistent with the previous findings, which suggest that the DLS method provides

more accurate results for sub-500 nm particles, while the LD is best suited for micron size particles (Bowen, 2002; Dieckmann et al., 2009).

The fractal dimensions of aggregates were also calculated from LD data. While manganese dioxide aggregates have quite similar fractal dimensions (1.67 and 1.63, respectively) at pH 6.0 and 7.0, the fractal dimension at pH 8.0 was very low (1.21), which is indicative of very small clusters with long-range repulsion forces (González et al., 2004).

Increasing the ionic strength from 0.5 to 10 mM (pH = 7 and hardness $\approx$ 0) resulted in significant increase in the size of manganese dioxide, indicating partial aggregation of colloids due to the reduction in the electrostatic forces (the ζ-potential changed from -42.9 ± 2.3 to -37.2 ± 0.6). However, these aggregates are still mainly present in the sub-micron range. A comparison between DLS and LD results reveals that the DLS measurement overestimates the size of fine colloids. However, the LD method did not provide enough sensitivity in the sub-micron range to show the small particle size growth achieved by increasing the ionic strength. This explains why the number size distribution obtained by DLS shifted toward greater diameters indicating the growth in particle size (the number size distribution is sensitive to growth only when the size of a majority of the particles increases). This result is in agreement with the lower accuracy of the LD method for sub-micron particles (Bowen, 2002). The fractal dimensions of manganese dioxide aggregates slightly increased by increasing the ionic strength, consistent with previous studies on silica colloids (Singh and Song, 2006) and titanium dioxide nanoparticles (Chowdhury et al., 2013).

At a constant ionic strength (10 mM and pH = 7), the size of manganese dioxide aggregates was dramatically influenced by calcium ion. Under soft water conditions, the particles were typically present in the range of 0.45 to 1.2 µm while under moderately hard water and very had water conditions, all particles were larger than 3 µm (according to the serial filtration technique). Accordingly, the ζ-potential of manganese dioxide decreased from -37.2 ± 0.6 to -12.8 ± 0.4 and -3.7 ± 0.1 by increasing the hardness of water from 0 to 100 and 317 mg $CaCO_3$/L, respectively. Thus, aggregation occurred due to the charge neutralization and compaction of EDL. Under hard water condition where significant aggregation occurred, the number size distribution measured with the LD method was in good agreement with the serial filtration technique while the volume PSD overestimated the size of aggregates as it is proportional to d^3. The DLS did not allow for measurement of the PSD under hard water condition due to the presence of large aggregates, with

high polydispersity indices (> 0.8), and interference from sedimentation. The fractal dimensions of manganese dioxide aggregates increased with the hardness of water due to the adsorption of calcium ions onto negatively charged colloids/particles, which can result in a tight adhesion of the calcium saturated aggregates (Pantina and Furst, 2006). As a result, the fractal dimension approached 3 for the aggregates generated at the hardness of 317 mg $CaCO_3$/L indicating the formation of compact, nearly spherical aggregates.

Unlike manganese dioxide, characteristics of ferric hydroxide aggregates did not significantly differ under different water chemistry conditions tested. All particles were on the micron scale, and more than 80% (by wt) were in the size range between 3 and 8 µm (according to the serial filtration technique). Likewise, the nearly zero ζ-potential of particles under different conditions implies the rapid aggregation of ferric hydroxide particles. The number size distributions obtained by LD was in good agreement with serial filtration results while the volume size distribution overestimated the size of aggregates. Thus, the number PSD is suggested while using LD for characterizing agglomerating systems such as flocculation. The fractal dimensions of these aggregates under all conditions were between 1.59 and 1.71, implying the high intra-aggregate porosity of these suspensions.

In conclusion, for sub-micron aggregates the DLS is in good agreement with serial filtration technique while for micron size aggregates, the LD and serial filtration techniques are coherent.

9.2 Fouling of UF membranes caused by oxidized iron and manganese

Iron and manganese removal efficiencies through the pre-oxidation and UF process were more than 99.5% under different water chemistry conditions using both ceramic and polymeric membranes (concentration of each mineral was < 0.02 mg/L in the filtrate). These results imply that Fe(II) and Mn(II) were completely oxidized by $KMnO_4$ during the retention time provided by the column and all particles/colloids were larger than the nominal pore size of the membranes.

A constant flux power law compressible cake model adequately described the pressure profiles under all conditions, indicating the dominant role of cake formation. Accounting for cake compression was important to adequately model the results. During UF of manganese dioxide aggregates, increasing pH from 6.0 to 7.0 (ionic strength = 0.5 mM and hardness ≈ 0) caused a

significant increase in membrane fouling while further increase of pH from 7.0 to 8.0 reduced the rate of fouling, as the fouling at pH 6.0 and 8.0 were nearly identical. Even though substantial aggregation was not found under these conditions due to the high repulsive forces between the colloids, the PSD evidenced some partial aggregation of colloids even at pH 8.0. The lowest cake resistance at pH 6.0 was attributed to the formation of much larger manganese dioxide aggregates compared to that of formed at pH 7.0 and 8.0. However, although the size of colloids was slightly smaller at pH 8.0 than pH 7.0, the average specific cake resistance was much lower at pH 8.0, because at this pH, the larger thickness of the EDL increased the distance between the deposits giving rise to the formation of a cake layer with higher permeability and lower resistance (Faibish et al., 1998; Singh and Song, 2006). The low resistance of the cake layer at pH 8.0 can also be related to the very low fractal dimension of the aggregates (1.21) which indicates the high intra-aggregate porosity of the deposited cake layer. Moderate and fairly comparable compressibility coefficients (0.27 to 0.31) were found for colloidal manganese oxides under different pH condition, most probably due to the repulsive EDL interactions between the negatively charged colloids. The slightly higher compressibility coefficient at pH 6.0 is in line with the larger aggregate size measured under this condition.

Increasing the ionic strength of water from 0.5 to 1 mM (pH = 7 and hardness ≈ 0) slightly increased the normalized TMP and the average specific resistance of the cake layer formed by manganese dioxide aggregates due to the slight compression of the EDL (Faibish et al., 1998; Bowen and Jenner, 1995). However, when ionic strength was raised from 1 to 10 mM, the normalized TMP and the average specific cake resistance diminished. The reduction in hydraulic resistance was associated with the larger aggregate dimensions (average size increased by more than 100%). Increasing the ionic strength by 10-fold compressed the EDL and enhanced the aggregation of colloids. Consequently, larger manganese dioxide aggregates formed more permeable cake layer with greater inter-aggregate porosity. The compressibility of the cake layer was reduced by increasing the ionic strength because the EDL compression diminished the inter-particle distance which could then be filled subsequently at higher TMP.

Hardness of water significantly controlled the fouling caused by manganese dioxide aggregates. Under a constant ionic strength (10 mM), increasing the hardness from nearly 0 to 100 mg $CaCO_3$/L notably alleviated the fouling of UF membranes. An additional increase in hardness, from 100 to 317 mg $CaCO_3$/L, further declined the normalized TMP rate, but to a much lesser extent. Under

hard water conditions, most of the surface charges of colloids were neutralized (according to ζ-potential), thus, the EDL was almost completely suppressed giving rise to aggregation of destabilized colloids. As a result, the mean size of aggregates increased from 0.118 µm to more than 2 µm resulting in the formation of a more permeable cake layer. This cake layer was highly compressible since we noted that a very slow increase of the pressure in the early stage of the filtration was followed by a more rapid growth at the later time. Due to the very high fractal dimensions of aggregates (close to 3) under hard water condition, the compressibility of the cake layer is related to the collapse of the clusters and, consequently, to the reduction of the inter-aggregate porosity.

The TMP increase pattern and the fouling were quite similar in ceramic and polymeric UF membranes under different conditions tested. The slightly higher fouling of polymeric membrane was likely caused by the hydrodynamic effects arising from the different configuration of these membranes (a longer tubular ceramic membrane with a larger inner diameter vs. a shorter hollow fiber polymeric membrane with a smaller inner diameter) (Carroll and Booker, 2000; Krawczyk and Jonsson, 2014). The compressibility coefficients of the cake layer were also comparable in both membranes, confirming the fact that the cake compressibility is predominantly controlled by the aggregate properties, not the type of the membrane. In general, the compressibility of manganese dioxide aggregates is mainly influenced by the ionic strength of water, the thickness of the EDL and the size of aggregates. The difference between polymeric and ceramic membranes was evident when the contribution of physically and chemically reversible fouling was determined. For ceramic membranes, almost all fouling resistance was physically removable while chemically reversible fouling mainly contributed to the fouling of polymeric membranes, especially in soft water condition. In the absent of calcium ion, the low-permeable cake formed on the surface of the membrane was not completely removed by the physical cleaning procedure applied for polymeric membrane. These results suggest that ceramic membranes would be a better choice for the removal of manganese oxides due to the possibility to implement of more aggressive physical cleaning.

During UF of ferric hydroxide aggregates, a very low fouling rate, regardless of water chemistry conditions, was observed. The relatively similar hydraulic resistance of the cake layer under different condition is in line with the similar characteristics of the ferric hydroxide aggregates, independent of pH (from 6.0 to 8.0), ionic strengths (from 0.5 to 10 mM) or hardness (0 to 317 mg $CaCO_3$/L). Since the mean size of these aggregates (3 to 7 µm) were much higher than the

membranes pore size (150 or 200 kDa), the aggregates accumulated on the membrane surface resulting in a cake formation with very low average specific resistances. Chemically irreversible fouling was negligible for both membranes under all conditions, an evidence that irreversible adsorption of iron and manganese did not occur during filtration. It is expected that this type of fouling would only be discernable after long-term operation.

In conclusion, unlike manganese dioxide aggregates, the specific resistance of the cake formed by ferric hydroxide aggregates is not substantially dependent on the pH, ionic strength or hardness of water because ferric hydroxide aggregates are easily destabilized under natural water conditions (the point of zero charge lays in the pH range of 7.0 to 8.0). The fouling resistance of ferric hydroxide aggregates were even lower than that of manganese dioxide aggregates under hard water condition. This might be due to the less compact nature of the ferric hydroxide aggregates, forming a cake with high inter- and intra-aggregate porosity (the fractal dimension of 1.59-1.71 vs. 3.03 for ferric hydroxide and manganese dioxide aggregates, respectively). In addition, the intrinsic membrane resistance was the main contributor to the total resistance of both polymeric and ceramic membranes while filtering iron oxides as the former had pore sizes in the range of 150 and 200 kDa, while the suspended particles were in the micron size range.

9.3 Application of PFB for manganese removal

Short-term (4 h) performance of PFB contactor for Mn(II) removal was evaluated under different conditions. The results demonstrate almost complete manganese removal (concentration of manganese in treated water was always less than 5 µg/L) in less than 1 min under all conditions tested. The removal profiles were stable under low initial Mn(II) concentrations (< 1.0 mg/L). However, under elevated Mn(II) concentrations (what values), an unstable Mn removal profile was observed, especially at 9°C. This is conceivable due to a faster adsorption reaction than the subsequent autocatalytic oxidation of adsorbed Mn(II) by chlorine (Knocke et al., 1990a). Moreover, although Mn(II) uptake capacity increases with feed Mn(II) concentration, breakthrough occurs earlier under higher Mn(II) concentrations (Tobiason et al., 2008). Improved Mn(II) removal profile under elevated temperature (23°C vs. 9°C) is related to a higher Mn(II) adsorption capacity of pyrolucite under such condition since the adsorption onto $MnO_{2(s)}$ is an endothermic process (Ren et al., 2011). In addition, the oxidation rate of adsorbed Mn(II) increased with temperature, resulting in a faster recovery of the adsorption sites. However, the solution phase

oxidation of Mn(II) by free chlorine did not occur due to the very short contact time (less than 1 min) within the PFB. Although the adsorption capacity of $MnO_{x(s)}$ reduces as pH declines (Knocke et al., 1990a), changing the pH from 7.8 to 6.2 did not have a notable impact on manganese removal profile throughout the PFB. This can be attributed to the inherent advantage of PFB, which provides a larger amount of active sites for Mn(II) uptake. Zuravnsky (2006) and Knocke et al. (2010) also demonstrated that pyrolucite media offers a higher Mn(II) uptake capability than $MnO_{x(s)}$-coated sand. In addition, improved solid-liquid contact between water and pyrolucite media in the fluidized bed contactor, as opposed to a fixed bed contactor, offers a more effective utilization of available sorption sites. The same result was achieved under different water hardness (0 vs. 200 mg $CaCO_3$/L). Although the presence of high amount of calcium ion was expected to deteriorate the Mn(II) removal profile (Merkle et al., 1997), quite similar removal profiles were observed at hardness of 0 and 200 mg $CaCO_3$/L. The identical total and dissolved manganese concentration at each sampling point demonstrates that the solution oxidation of manganese within the PFB did not occur. Chlorine demand within the PFB was lower (0.2-0.3 mg Cl_2/L) than the expected chlorine required for oxidation of Mn(II). Since SGW was prepared with DM water, chlorine was only consumed to oxidize the adsorbed Mn(II). Thus, manganese removal mechanism within the PFB includes adsorption of Mn(II) onto pyrolucite and subsequent slower surface oxidation of adsorbed Mn(II) by free chlorine.

Developing a process which can provide efficient manganese removal while operating at high HLR is of great interest owing to the reduction in the process footprint and capital costs. The PFB contactor can be operated at HLR of 40-60 m/h, a much higher range than the fixed bed contactors (typically 10-20 m/h). Although hydraulic retention time within the PFB contactor was very short at the HLR of 63 m/h (less than 75 seconds), 100% Mn(II) removal efficiency was achieved during the 4 hr experimental cycles (initial Mn(II) = 2.2 to 2.4 mg/L). The Mn(II) removal profiles overlapped under HLR of 24 to 63 m/h, indicating the consistent removal performance under different HLR. On the other hand, the specific Mn(II) adsorption rate (mg Mn(II)/kg pyrolucite/s), over the height of PFB, is higher at elevated HLR. Likewise, determining the average mass transfer coefficient as an indication of adsorption rate (Bošković-Vragolović et al., 2009) revealed that mass transfer coefficient slightly increased at higher HLR. This is a very important finding which shows that, unlike the results obtained by Bošković-Vragolović et al. (2009), a PFB can be operated at very high HLRs without reduction in mass transfer coefficient as well as adsorption rate. This

discrepancy is likely related to the very high specific gravity of the pyrolucite media relative to the glass particles used by these authors. The high specific gravity prevents excessive expansion of the PFB at high HLR, thus, the increased HLR can compensate the detrimental effect of increased porosity on mass transfer coefficients. In addition, unlike the pyrolucite fixed bed (Zuravnsky, 2006; Tobiason et al., 2008), Mn(II) removal performance through the PFB slightly increased with HLR.

Long-term (12 d) stability experiments showed that the process operated with a free chlorine residual of 1.0 mg Cl_2/L in the effluent failed to adequately remove manganese (i.e., < 20 µg/L in the effluent) after 6 days of operation (feed Mn(II) = 0.8-1.3 mg/L). However, increasing the effluent free chlorine residual to 2.0-2.6 mg Cl_2/L led to a stable removal performance of almost 100% for the entire test period. Chlorine consumption within the PFB was increased under higher chlorine concentration (from < 0.2 mg Cl_2/L to 0.2-0.9 mg Cl_2/L), implying the higher stability of the PFB under such condition as most of the occupied sites were continuously regenerated. For some utilities, such free chlorine residual might be too high to be considered applicable depending on the required dosage to fulfil primary and secondary disinfection. Nonetheless, further regeneration of pyrolucite after 6 days of operation appears a realistic operational constraint for a small groundwater system operator. On the other hand, these operational cycles were achieved for a relatively high influent manganese concentration (0.8-1.3 mg/L). Operational cycles would be much longer under lower influent manganese condition. Likewise, a deeper PFB could also extend the duration of operation prior to regeneration. Finally, it is important to mention that the turbidity of the PFB effluent was constantly at 0.2 NTU over the entire test period, implying that post-filtration would not be needed after the PFB (as long as no iron is present in the feed water).

9.4 Pilot-scale study on fixed vs. fluidized pyrolucite beds for iron and manganese control

In this study, a pilot-scale pyrolucite fixed and fluidized bed contactors were operated in parallel on the Ste-Marthe-sur-le-Lac groundwater (DOC = 3.3 mg C/L, alkalinity = 170 mg $CaCO_3$/L, hardness = 200 mg $CaCO_3$/L, temperature = 8-12°C). Three models of distributors plate (located at the bottom of the FBR) were tested. The required HLR to achieve 10% bed expansion for Distributors A, B, and C were 40, 30, and 32 m/h, respectively, implying that the Distributor A was

less effective in void development in the bed, thus, could decrease the quality of fluid-particle contact. Yet, a good fluid-particle contact quality enhances the adsorption rate in the fluidized bed contactor. Likewise, the results revealed that the PFB contactors equipped with Distributors B and C were more efficient than Distributor A for Mn(II) removal, particularly in the first 15 cm above the distributor plate. The differences became more pronounced as the experiment progressed. Therefore, Distributor A could not well distribute water over the whole cross-section of the bed above the distributor plate and appropriately utilize the adsorption capacity of the media. Measuring the particulate manganese concentration through the height of PFB shows that a significant amount of manganese was released in the jet zone above the distributor plate, when using Distributor A and B. The best performance was obtained using Distributor C, because the reduction in the jet effect caused by this distributor eliminated separation of loosely bounded manganese from the surface of the pyrolucite media. Thus, PFB contactor was equipped with distributor C for further experiments. Any full-scale implementation of the FBR should pay close attention to the design of the distributor plates.

For the experiments under very low feed iron concentration (0.01 ± 0.00 mg Fe/L), the PFB efficiently removed manganese (manganese concentration in the effluent water was always < 0.02 mg/L), even at a very high HLR of 45 m/h, over the entire 21 days experimental cycle (feed manganese $= 0.09 \pm 0.01$ mg Mn/L). Although almost 100% of Mn(II) was removed, 5-15% particulate manganese was observed in the effluent, especially at the higher HLR of 45 m/h, due to the presence of particulate manganese in the feed water as well as the abrasive forces resulting from the intensified particle-particle collisions in the fluidized bed. However, the concentration of total manganese in the effluent water was always below the target limit of 0.02 mg/L. In parallel, the pyrolucite fixed bed contactor efficiently removed manganese ($\approx$ 100% removal performance) under the same feed water condition but a lower HLR (20 m/h). The concentration of manganese in the effluent was always lower than 0.005 mg/L due to the stationary state of the fixed bed, which can better retain all particulates formed within the column. Dissolved and total manganese profiles were stable over 21 days of experiment for both fixed and fluidized beds, implying that the free chlorine residual concentration of 1 mg Cl_2/L in the effluent was adequate for continuous regeneration of the adsorption sites. Under higher feed manganese concentration (0.35 ± 0.03 mg Mn/L), both contactors were effective in removing manganese ($> 95\%$) over the 21 days of experiment (effluent manganese concentration < 0.02 mg/L) implying the very high adsorption

capacity of pyrolucite media. More than 92% of manganese was in dissolved form in the feed water and remained dissolved inside the contactors indicating that the removal mechanism was predominantly governed by sorption of Mn(II) onto the pyrolucite surface with subsequent surface catalyzed oxidation of adsorbed manganese by chlorine. Under this condition, stable manganese removal profiles were not observed within the contactors implying that they would have eventually breakthrough owing to the saturation of the available adsorption sites. Increasing the free chlorine concentration above 1 mg Cl_2/L would likely extend the operation cycle duration before further regeneration.

Under elevated feed iron concentration (0.18 ± 0.02 mg/L), more than 90% of Fe(II) and Mn(II) were removed over 21 days using the PFB contactor (initial Mn(II) concentration $= 0.11 \pm 0.01$ mg/L). However, the PFB contactor performance for total iron and manganese removal varied from 50-80% and 60-80%, respectively. Thus, an elevated iron concentration caused a significant decrease in manganese removal. Unlike instantaneous oxidation of Fe(II) by free chlorine in SGW, complete oxidation of Fe(II) did not occur in natural groundwater over the 90 s retention time available in the PFB contactor. This is most likely related to the higher DOC content of the natural groundwater (3.3 mg C/L) than the SGW (< 0.2 mg/L). Consequently, Fe(II) may have competed with Mn(II) for the adsorption sites (Hu et al., 2004). In addition, as the ferric hydroxide coating developed on the media grains, the previously available sorption sites became inaccessible under this layer. Iron removal in the PFB contactor was governed by two mechanisms: 1) adsorption of Fe(II) onto the pyrolucite media and 2) solution oxidation of Fe(II) and subsequent attachment of oxidized particles on the media grains. The presence of 20-40% particulate manganese in treated water was presumably related to the adsorption of Mn(II) onto the ferric hydroxide particles and carryover from the PFB contactor. This hypothesis is supported by the fact that ferric hydrous oxides can serve as adsorbent for Mn(II) (Buamah et al., 2008). In conclusion, the application of a PFB contactor as a standalone process is not recommend for groundwater treatment with elevated iron concentrations. In fixed bed contactor, the concentrations of iron and manganese in the treated water (< 0.005 mg/L) were well below 0.02 mg/L. However, a steady state removal performance was not experienced due to the deposition and build-up of ferric hydroxide on the pyrolucite media, which covered some available adsorption sites. Unlike the PFB contactor, 60-90% of Fe(II) was oxidized by chlorine prior reaching the filter media due to the 5 min retention time available in the column above the media. Thus, the iron removal mechanism in the fixed bed contactor mainly

comprised of water phase oxidation of Fe(II) and subsequent capture of oxidized particles by the filter media.

The pressure drop across the PFB was constant and stable (33 kPa) over the 21 d experimental cycle, regardless of water quality. It can be estimated from the apparent weight of the pyrolucite media per cross-section unit of the column and the water head in the column. Under very low iron concentration (0.01 ± 0.00 mg Fe/L), the very low turbidity of the influent water (≈ 0.1 NTU) allowed for the operation of the fixed bed contactor at a high HLR (20 m/h) while only one and two backwashes were required over the 21 days for the feed manganese concentration of 0.09 ± 0.01 or 0.35 ± 0.03 mg/L, respectively. The accumulation of oxidized manganese (less than 10% solution oxidation of manganese was observed) and partial blockage of the void spaces were presumably responsible for the increased head loss under these conditions. Under an elevated feed iron concentration (0.18 ± 0.02 mg/L), a substantial head loss accumulated across the bed, thus, the filtration cycle was significantly shortened (around 3 days) due to the retention of more particulate materials (60-90% of iron was oxidized before reaching the filter media (turbidity = 0.3 NTU) within the filter. In summary, even though the pyrolucite fixed bed contactor effectively controls the concentration of iron and manganese under an elevated iron concentration, it consumes more energy and produces more wastewater. On the other hand, combining a PFB contactor with a downstream process with the capability of operating at very high loading rate while providing other treatment goals (such as disinfection with UF) would be a great option. In addition, although both contactors were highly effective for manganese control under very low iron concentrations, the PFB offers the advantage of operating at high HLR, which reduces the contactor footprint, capital cost as well as wastewater production.

On a final note, the accumulation of adsorbed manganese on the PFB media is expected to increase the size of pyrolucite over time. However, complete manganese removal from this natural groundwater with around 0.1 mg Mn/L in a 45 m/h PFB would only increase the mass content of manganese dioxide in the contactor by 3% after one year of operation. This represent a theoretical increase in media size of 7 µm.

9.5 Performance of a PFB-MF/UF hybrid process for improved iron and manganese control

Stable iron and manganese removal profiles were observed over the 10-h operation of PFB under different conditions (soft water, moderately hard water and moderately hard water including humic acids). As a result, 76%-89% iron and 95%-97% manganese removal were achieved in around 100 s of contact time, irrespective of water quality. The difference in iron and manganese removal performance can be explained by mechanistic differences. Manganese removal involves a very fast adsorption of Mn(II) onto the pyroluite and subsequent catalytic oxidation of adsorbed manganese by chlorine. However, iron removal involved instantaneous oxidation of Fe(II) by free chlorine followed by partial attachment of particulates onto the pyroluite. The observed lower rejection for iron is related to the shear exerted on the pyroluctite in the fluidized bed (30% bed expansion), which reduced the attachment of particulate species. These findings further indicate the need to apply a downstream process which can properly reduce the concentration of these species below 0.020 mg/L. Application of MF/UF process downstream of a PFB effectively reduced the iron and manganese concentrations in treated water to below 0.005 mg/L under all conditions tested. In comparison, pre-oxidation-MF/UF process could also reduce the iron and manganese concentrations below 0.010 mg/L, except at the initial stage of the filtration using MF membrane under soft water condition (manganese concentration = 0.035 mg/L). This is related to the presence of colloidal manganese dioxide with less than 100 nm in size (nominal pore size of MF membrane). As filtration proceeded, the cake layer accumulated on the membrane retained these fine colloids.

Under soft water condition (hardness = 2 mg $CaCO_3$/L), the fouling in the pre-oxidation-MF/UF process can be explained by an initial pore blocking mechanism (in the first few minutes of the filtration) followed by cake formation in the later filtration times. However, the contribution of pore blocking to total fouling was negligible. Excellent agreement of the experimental data, after the first few minutes of filtration, with the constant flux power law compressible cake model further confirmed the dominant role of cake formation. Serial fractionation of the membrane feed water revealed the presence of fine colloids (< 100 nm), which may deposit into the inner channels of the membrane pores or block the pore mouth at the initial stage of filtration. At later time scales, these colloids were retained within the cake layer before reaching the membrane surface. The severe fouling of the membranes under this condition, was consistent with the presence of more than 75%

submicron aggregates in the feed water. Deposition of these colloids led to the formation of a more compact and less porous cake layer. The results revealed that the mixture of oxidized iron and manganese in soft water condition was only slightly compressible ($n' < 0.25$ (Tiller et al., 1987)), because the blend of large and small aggregates forms a dense cake layer (Madaeni, 2001), which hardly compresses as the process proceeds since small colloids already occupies the void space between large aggregates. Interestingly, the presence of positively charged ferric hydroxide aggregates promoted the aggregation of negatively charged colloidal manganese dioxide under soft water condition. Moreover, these species may adsorb or attach to one another resulting in a unique size distribution. Increasing hardness from 2 to 100 mg $CaCO_3$/L significantly reduced the fouling of both MF and UF membranes in this process due to the generation of much larger aggregates (about 87% (wt) of aggregates had a size ranging from 8 to 30 µm). Under such condition, the power law compressible cake formation model well described the TMP increase behavior over the entire filtration cycle confirming the dominant role of cake filtration. The deposited cake layer under this condition was moderately compressible ($n' = 0.28$-0.35) mainly due to the generation of large aggregates and high void spaces between the deposited aggregates which can be eventually occupied by the forthcoming aggregates. In the presence of 2 mg C/L humic acids, fouling of the membranes progressed more rapidly presumably due to the rejection of almost all humic acids by both membranes for the relatively high hardness of 100 mg $CaCO_3$/L. Under such condition, the reduction in the net charge surrounding the humic acids as well as binding of the carboxylic acid functional groups of humic acids by calcium ions (Zularisam et al., 2006; Shao et al., 2011) led to the aggregation of humic acids and, thus, their deposition on the membrane surface. Constant flux compressible cake formation model correctly predicted the concave-upward behavior of TMP under this condition. Fairly high compressibility coefficients (0.52-0.61) were obtained under this condition, presumably due to break-up and/or deformation of soft organic aggregates (Vela et al., 2008).

Under all water quality conditions and flux of 150 LMH, the fouling resistance of the MF membrane was identical to that of the UF one indicating similar fouling mechanisms and cake layer properties. Rising the flux to 300 LMH increased the drag force and resulted in the formation of more compact cakes with greater resistances. When the flux was increased to 300 LMH, the fouling resistance of UF membrane was higher than of the MF membrane, which can be attributed to the formation of more compact cake layer at the higher operational TMP found in the tested UF

membranes. Under elevated flux, the difference between the required TMP for UF and MF membrane increased resulting in a substantial difference between the fouling of these membranes. The compressibility coefficients under all water quality conditions were approximately comparable, irrespective of the operating condition or membrane type.

Comparing the fouling of the pre-oxidation-MF/UF process vs. the PFB-MF/UF hybrid process revealed that the application of a PFB prior MF/UF membrane substantially reduced the extent of membrane fouling (more than 90%) in the absence of humic substances, because more than 95% of manganese and 75% of iron were removed inside the PFB. In addition, all the oxidized aggregates in the effluent of the PFB were larger than 3 µm resulting in cake layer formation which exerted minimal fouling on the membranes. The negligible fouling of the PFB-MF/UF hybrid process after 6 h of operation at a high flux of 300 LMH implies that the hybrid process could continuously operate for several days without any physical or chemical cleaning. Under elevated humic acids concentration, although the application of a PFB as a pretreatment process significantly reduced the membrane fouling (78%), the fouling was much higher than in the absence of humic acids because the PFB does not have significant impact on the removal of organic matter.

According to the resistance-in-series model, adsorption of foulants within the membrane pores did not take place under all conditions and the chemically irreversible fouling was negligible. In the pre-oxidation-MF/UF configuration under soft water condition, chemically reversible fouling largely contributed to the fouling of the membranes, especially UF, confirming pore blocking at the early stage of filtration as well as the formation of a cohesive and compact cake layer. Under moderately hard water conditions, the majority of fouling was physically reversible, confirming the dominant role of cake formation. However, the extent of fouling would be expected to impact the economic viability of the pre-oxidation-MF/UF process. In contrast, the PFB-MF/UF hybrid process could be continuously operated for several days without any cleaning, unless in the presence of humic substances. Humic acids were the main contributor to fouling under hard water conditions.

As a conclusion, the PFB-MF/UF was found to be an effective option to treat groundwater supplies with elevated iron and manganese concentrations. Considering the higher costs of UF/MF membranes compared to pressure filters, it is anticipated that this treatment option would be especially of interest for water utilities requiring to perform parasite removal (i.e. groundwater

under the direct influence) which requirement could be addressed by the use of low pressure membranes. In all cases, the design engineer should consider selecting a very high operating flux in order to benefit (from an economic standpoint) to the maximum of the fouling reduction offered by the use of the FBR.

CHAPTER 10   CONCLUSION AND RECOMMENDATIONS

The main purpose of this research project was to develop a robust process for iron and manganese control in drinking water. In order to better elucidate the potential applicability of the proposed process, its performance was compared with the most common treatment processes (greensand filtration as well as oxidation and membrane filtration) which has been for this purpose. The following conclusions were derived from different parts of this research:

➤ **Characteristics of ferric hydroxide and manganese dioxide aggregates under different water chemistry conditions and UF membrane fouling during filtration of these suspensions:**

- Characteristics of manganese dioxide aggregates (size, ζ-potential and fractal dimension) and, subsequently, UF membrane fouling caused by these aggregates are significantly influenced by pH, ionic strength and salt valency (i.e., Ca^{2+} vs. Na^+) of water. Unlike manganese dioxide, the sensitivity of the ferric hydroxide characteristics to pH, ionic strength and hardness is negligible under conditions relevant to water treatment.

- The pre-oxidation-UF process properly controlled iron and manganese concentrations below the target value of 0.02 mg/L under all tested conditions. However, removal of manganese dioxide from water is more problematic than ferric hydroxide due to the formation of colloids as small as several tens of nanometers, especially under soft water condition with low salinity and high pH. Under such conditions, colloidal manganese dioxide is prone to severely foul UF membranes. In contrast, ferric hydroxide aggregates caused similar and low fouling to the membrane irrespective of the water chemistry conditions tested.

- Among the studied parameters, water hardness strongly controls the destabilization of colloidal manganese dioxide, as micron-sized aggregates were generated under hard water conditions. The deposited cake layer under this condition had high inter-aggregate porosity and low fouling resistance. These results also imply that the addition of lime, rather than caustic soda, is a more favorable option for pH adjustment followed by oxidation prior to filtration.

- Fouling mechanism can be described by a power law compressible cake formation model, indicating the dominant role of cake filtration as a fouling mechanism. The specific

resistance of the cake layer and its compressibility is mainly governed by the characteristics of aggregates rather than the type of membrane material (ceramic vs. polymeric) and its configuration (tubular vs. hollow fiber). For colloids smaller than 100 nm, the hydraulic resistance of the cake layer is mainly governed by the thickness of the EDL rather than the size of colloids.

- Under identical condition, the ceramic tubular membrane and the polymeric hollow fiber membrane tested were almost similarly fouled. The main difference is related to the reversibility of fouling as physical cleaning was considerably more effective for the ceramic membrane than the polymeric one due to the potential implementation of more aggressive physical cleaning.

- For stabilized inorganic colloids, DLS detects nanoparticles including the shell resulting in uncertainties regarding the onset of the PSD. This technique also suffers from the polydispersity and the presence of large aggregates. However, it is well adapted to measure sub-micron particles with narrow size ranges. In contrast, the LD method is generally more suitable for micron-sized aggregates but offers low sensitivity and accuracy for particles in the sub-micron ranges. However, in agglomerating systems, such as flocculation, the results must be interpreted with great care, and comparison with other methods is suggested.

- Serial filtration technique is recommended as a simple option for general evaluation of manganese dioxide and ferric hydroxide aggregates, because (i) the availability of DLS and LD techniques is not that common in the water industry and (ii) this method proved to be sufficient for PSD characterization.

➢ **The potential application of a PFB contactor for manganese removal from groundwater containing high level of Mn(II):**

- Almost complete Mn(II) removal ($\approx 100\%$) was achieved in less than 1 min under different operating conditions and SGW composition.

- The manganese removal mechanism consists of rapid adsorption of Mn(II) onto pyrolucite media followed by slower autocatalytic oxidation of adsorbed Mn(II) in the presence of free chlorine.

- Mn(II) removal profiles within the PFB contactor was consistent irrespective to the pH (6.2-7.8) and hardness (0-200 mg $CaCO_3$/L) of the feed water.

- High specific gravity of pyrolucite allowed the process to be operated at high HLR (e.g., 63 m/h) without any concern regarding a reduction of the adsorption rate.

- Maintenance of an adequate free chlorine residual in the effluent of PFB plays a key role in the long-term stability of this process.

> **The performance of pilot-scale pyrolucite fixed and fluidized beds for iron and manganese control in natural groundwater:**

- Efficient performance of a pilot-scale PFB contactor is strongly controlled by the type of distributor plate. Among different configurations of distributor plates tested herein, a shrouded perforated distributor plate with a 15 cm layer of gravel (4-10 mm) on top proved to be optimal.

- Although the PFB contactor has a strong adsorption capacity for Fe(II) and Mn(II), the long-term stability of the process was influenced by the initial concentration of these species.

- The PFB contactor proved effective for manganese removal under a wide range of feed manganese concentrations as long as iron levels were very low. It also minimized wastewater production (only produced during regeneration) while providing a high treatment performance and a small footprint. As a result, this process is suggested for water treatment utilities targeting only manganese removal with negligible iron in the influent water. Under elevated iron concentrations, a downstream process after the PFB contactor is needed to achieve the desired removal performance (concentration < 0.02 mg/L for both metals).

- The pyrolucite fixed bed contactor successfully removed iron and manganese under all conditions tested. However, fairly rapid head loss build-up was observed across the column operated at 20 m/h under elevated iron concentrations (3 days filtration cycle). Actually, the iron concentration in groundwater mainly controlled the head loss build-up rate through the fixed bed. In contrast, the head loss through the PFB contactor remained constant, irrespective to the influent water quality.

- In both contactors (fixed vs fluidized), manganese was essentially removed by the adsorption of Mn(II) onto the pyrolucite media followed by the autocatalytic oxidation of the adsorbed Mn(II) on the surface of the media. A similar mechanism could be deduced

for the removal of a large portion of iron in the PFB contactor while iron was mainly removed via solution oxidation of Fe(II) by chlorine followed by the capture of particulate and/or colloidal ferric hydroxide by pyrolucite fixed bed.

> **The performance of a PFB pretreatment for mitigating MF/UF membrane fouling:**
> - The comparison between the pre-oxidation-MF/UF and PFB-MF/UF hybrid processes revealed that both processes could reduce the concentration of iron and manganese in treated water to below the target limit of 0.020 mg/L (except at the initial stage of the pre-oxidation-MF process under soft water condition).
> - In pre-oxidation-MF/UF process, severe fouling of both membranes were observed under all conditions tested, especially under soft water or in the presence of humic acids at high flux. Under soft water condition, the mechanism of membrane fouling can be described as initial pore blocking followed by cake filtration during the later stage while the contribution of initial pore blocking to the overall fouling of the membranes was negligible. Under moderately hard water conditions, cake filtration was the predominant fouling mechanism during the entire filtration run. The dominant role of cake formation was inferred from the excellent fit of the experimental data to the constant flux blocking law model for compressible cake formation.
> - The application of PFB as a pretreatment process gave rise to significant fouling mitigation by removing more than 75% and 95% of iron and manganese, respectively. In the absence of humic acids, the PFB-MF/UF hybrid process could be continuously operated for several days (more than a week) without any cleaning.
> - Under all conditions tested, fouling was physically reversible except for the pre-oxidation-MF/UF process operated under soft water condition, during which chemically reversible resistance largely contributed to the total resistance of both membranes.
> - Under high filtration flux, the fouling was more severe for the UF than the MF membrane due to the higher operation pressure of the former leading to higher compaction of the cake layer on the membrane surface.

This work also sparked new ideas for future research. It would be interesting to:

- Evaluate the PFB performance for removal of other heavy metals that are frequently present in groundwater such as chromium(III), arsenic(III) and arsenic(V) ions in conjunction with iron and manganese.
- Develop a phenomenological model that can predict the Mn(II) removal profile within the PFB via NGE process or the regeneration interval for practical applications.
- Evaluate the long-term performance (one year) of the PFB-MF/UF hybrid process in a pilot-scale study using natural groundwater.

BIBLIOGRAPHY

Aguiar, A.O., Duarte, R.A. and Ladeira, A.C.Q. (2013). The application of MnO_2 in the removal of manganese from acid mine water. Water, Air, & Soil Pollution, 224(9), 1690.

Allard, S., Fouche, L., Dick, J., Heitz, A. and von Gunten, U. (2013). Oxidation of manganese(II) during chlorination: Role of bromide. Environmental Science & Technology, 47(15), 8716-8723.

Al-Rashdi, B.A.M., Johnson, D.J. and Hilal, N. (2013). Removal of heavy metal ions by nanofiltration. Desalination, 315, 2-17.

American Public Health Association (APHA), American Water Works Association (AWWA). (2005). Standard methods for the examination of water and wastewater (21th Ed.). Washington, DC, USA: American Public Health Association.

American Water Works Association (AWWA). (2005). M53-Microfiltration and ultrafiltration membranes for drinking water. Manual of water supply practices (1th Ed.). Denver, CO, USA: American Water Works Association.

Azizi, A., Morina, M., Hajdini, S. and Latifi, L. (2013). Oxidation and removal of iron and manganese in water treatment plant in Velekince, Gjilan, Kosovo. Journal of International Environmental Application and Science, 8(2), 166-170.

Bacchin, P., Aimar, P. and Field R.W. (2006). Critical and sustainable fluxes: theory, experiments and applications. Journal of Membrane Science, 281(1-2), 42-69.

Barbeau, B., Carrière, A. and Bouchard, M.F. (2011). Spatial and temporal variations of manganese concentrations in drinking water. Journal of Environmental Science and Health, Part A, 46(6), 608-616.

Barlokova, D. and Ilavsky, J. (2009). Iron and manganese removal from small water resources. Proceedings of the International Symposium on Water Management and Hydraulic Engineering, Ohrid, Macedonia, 1-5 September.

Bazilio, A.A., Kaminski, G.S., Larsen, Y., Xuyen, M. and Tobiason, J.E. (2016). Full-scale implementation of second-stage contactors for manganese removal. Journal of the American Water Works Association, 108(12), E606-E614.

Bernat, X., Pihlajamäki, A., Fortuny, A., Bengoa, C., Stüber, F., Fabregat, A., Nyström, M. and Font, J. (2009). Non-enhanced ultrafiltration of iron(III) with commercial ceramic membranes. Journal of Membrane Science, 334(1-2), 129-137.

Bierlein, K.A., Knocke, W.R., Tobiason, J.E., Subramaniam, A., Pham, M. and Little, J.C. (2015). Modeling manganese removal in a pilot-scale postfiltration contactor. Journal of the American Water Works Association, 107(2), E109-E119.

Bošković-Vragolović, N., Garić-Grulović, R., Grbavčić, Ž. and Pjanović, R. (2009). Mass transfer and fluid flow visualization in packed and fluidized beds by the adsorption method. Russian Journal of Physical Chemistry A, 83(9), 1550-1553.

Bouchard, M.F., Sauvé, S., Barbeau, B., Legrand, M., Brodeur, M.E., Bouffard, T., Limoges, E., Bellinger, D.C. and Mergler, D. (2011). Intellectual impairment in school-age chlidren exposed to manganese from drinking water. Environmental Health Perspectives, 119(1), 138-143.

Bowen, P. (2002). Particle size distribution measurement from millimeters to nanometers and from rods to platelets. Journal of Dispersion Science and Technology, 23(5), 631-662.

Braghetta, A., DiGiano, F.A. and Ball, W.P. (1997). Nanofiltration of natural organic matter: pH and ionic strength effects. Journal of Environmental Engineering, 123(7), 628-641.

Bruins, J.H., Petrusevski, B., Slokar, Y.M., Huysman, K., Joris, K., Kruithof, J.C. and Kennedy, M.D. (2015a). Biological and physico-chemical formation of Birnessite during the ripening of manganese removal filters. Water Research, 69, 154-161.

Bruins, J.H., Petrusevski, B., Slokar, Y.M., Kruithof, J.C. and Kennedy, M.D. (2015b). Manganese removal from groundwater: Characterization of filter media coating. Desalination and Water Treatment, 55(7), 1851-1863.

Buamah, R., Petrusevski, B., de Ridder, D., van de Wetering, T.S.C.M. and Shippers, J.C. (2009). Manganese removal in groundwater treatment: practice, problems and probable solutions. Water Science & Technology: Water Supply, 9(1), 89-98.

Buamah, R., Petrusevski, B. and Schirppers, J.C. (2008). Adsorptive removal of manganese(II) from the aqueous phase using iron oxide coated sand. Journal of Water Supply: Research and Technology-AQUA, 57(1), 1-11.

California Department of Public Health (CDPH). (2010). Drinking water notification levels and response levels: An overview (pp. 14).

Camel, V. and Bermond, A. (1998). The use of ozone and associated oxidation processes in drinking water treatment. Water Research, 32(11), 3208-3222.

Carlson, K.H. and Knocke, W.R. (1999). Modeling manganese oxidation with $KMnO_4$ for drinking water treatment. Journal of Environmental Engineering, 125(10), 892-896.

Carlson, K.H., Knocke, W.R. and Gertig, K.R. (1997). Optimizing treatment through Fe and Mn fractionation. Journal of the American Water Works Association, 89(4), 162-171.

Carroll, T. and Booker, N.A. (2000). Axial features in the fouling of hollow-fibre membranes. Journal of Membrane Science, 168(1-2), 203-212.

Casale, R.J., LeChevallier, M.W. and Pontius, F.W. (2002). Manganese control and related issues. American Water Works Association Research Foundation, Denver, CO, USA (pp. 214).

Cavanagh, J.E., Weinberg, H.S., Gold, A., Sangaiah, R., Marbury, D., Glaze, W.H., Collette, T.W., Richardson, S.D. and Thruston, A.D. (1992). Ozonation byproducts: Identification of bromohydrins from the ozonation of natural waters with enhanced bromide levels. Environmental Science & Technology, 26(8), 1658-1662.

Cerrato, J.M., Hochella, M.F., Knocke, W.R., Dietrich, A.M. and Cromer, T.F. (2010). Use of XPS to Identify the Oxidation State of Mn in Solid Surfaces of Filtration Media Oxide Samples from Drinking Water Treatment Plants. Environmental Science & Technology, 44(15), 5881-5886.

Cerrato, J.M., Knocke, W.R., Hochella, M.F., Dietrich, A.M., Jones, A. and Cromer, T.F. (2011). Application of XPS and solution chemistry analyses to investigate soluble manganese removal by MnOx(s)-coated media. Environmental Science & Technology, 45(23), 10068-10074.

Chang, Y.-Y., Song, K.-H., Yu, M.-R. and Yang, J.-K. (2012). Removal of arsenic from aqueous solution by iron-coated sand and manganese-coated sand having different mineral types. Water Science and Technology, 65(4), 683-688.

Chellam, S., Jacangelo, J.G. and Bonacquisti, T.P. (1998). Modeling and experimental verification of pilot-scale hollow fiber, direct flow microfiltration with periodic backwashing. Environmental Science & Technology, 32(1), 75-81.

Chellam, S. and Xu, W. (2006). Blocking laws analysis of dead-end constant flux microfiltration of compressible cakes. Journal of Colloid and Interface Science, 301(1), 248-257.

Choo, K.H., Han, S.C., Choi, S.J., Jung, J.H., Chang, D., Ahn, J.H. and Benjamin, M.M. (2007). Use of chelating polymers to enhance manganese removal in ultrafiltration for drinking water treatment. Journal of Industrial and Engineering Chemistry, 13(2), 163-169.

Choo, K.-H., Lee, H. and Choi, S.-J. (2005). Iron and manganese removal and membrane fouling during UF in conjunction with prechlorination for drinking water treatment. Journal of Membrane Science, 267(1-2), 18-26.

Chowdhury, I., Walker, S.L. and Mylon, S.E. (2013). Aggregate morphology of nano-TiO2: Role of primary particle size, solution chemistry, and organic matter. Environmental Science: Processes Impacts, 15, 275-282.

Coffey, B., Gallagher, D. and Knocke, W. (1993). Modeling soluble manganese removal by oxide-coated filter media. Journal of Environmental Engineering, 119(4), 679-694.

Côté, P., Mourato, D., Güngerich, C., Russell, J. and Houghton, E. (1998). Immersed membrane filtration for the production of drinking water: case studies. Desalination, 117(1-3), 181-188.

CPS Instruments Europe. (2015). Comparison of particle sizing methods. <http://www.cpsinstruments.eu/pdf/Compare%20Sizing%20Methods.pdf> (Aug. 13, 2015).

Crittenden, J.C., Trussell, R.R., Hand, D.W., Howe, K.J. and Tchobanoglous G. (2012). MWH's water treatment: principles and design (3ed Ed.). Hoboken, NJ, USA: John Wiley & Sons, Inc.

Dashtban Kenari, S.L. and Barbeau, B. (2014). Pyrolucite fluidized-bed reactor (PFBR): A robust and compact process for removing manganese from groundwater. Water Research, 49(1), 475-483.

Dashtban Kenari, S.L. and Barbeau, B. (2016a). Size and zeta potential of oxidized iron and manganese in water treatment: Influence of pH, ionic strength, and hardness. Journal of Environmental Engineering, 04016010.

Dashtban Kenari, S.L. and Barbeau, B. (2016b). Understanding ultrafiltration fouling of ceramic and polymeric membranes caused by oxidized iron and manganese in water treatment. Journal of Membrane Science, 516, 1-12.

Dieckmann, Y., Colfen, H., Hofmann, H., and Petri-Fink, A. (2009). Particle size distribution measurements of manganese-doped ZnS nanoparticles. Analytical Chemistry, 81(10), 3889-3895.

Dion, L.-A., Bouchard, M.F., Sauvé, S., Barbeau, B., Tucholka, A., Major, P., Gilbert, G., Mergler, D. and Saint-Amour, D. (2016). MRI pallidal signal in children exposed to manganese in drinking water. NeuroToxicology, 53, 124-131.

Duan, J., Wang, J., Guo, T. and Gregory, J. (2014). Zeta potentials and sizes of aluminum salt precipitates – Effect ofanions and organics and implications for coagulation mechanisms. Journal of Water Process Engineering, 4, 224-232.

Dwivedi, P.N. and Upadhyay, S.N. (1977). Particle-fluid mass transfer in fixed and fluidized beds. Industrial & Engineering Chemistry Process Design and Development, 16(2), 157-165.

El Araby, R., Hawash, S. and El Diwani, G. (2009). Treatment of iron and manganese in simulated groundwater via ozone technology. Desalination, 249(3), 1345-1349.

Eley, M. and Nicholson, K. (1993). Chemistry and adsorption-desorption properties of manganese oxides deposited in Forehill Water Treatment Plant, Grampian, Scotland. Environmental Geochemistry and Health, 15(2), 85-91.

Elimelech, M., Gregory, J., Jia, X., and Williams, R. (1995). Particle Deposition and Aggregation: Measurement, Modeling, and Simulation. Woburn, MA, USA: Butterworth-Heinemann.

Ellis, D., Bouchard, C. and Lantagne, G. (2000). Removal of iron and manganese from groundwater by oxidation and microfiltration. Desalination, 130(3), 255-264.

Elzo, D., Huisman, I., Middelink, E. and Gekas, V. (1998). Charge effects on inorganic membrane performance in a cross-flow microfiltration process. Colloids and Surfaces A: Physicochemical and Engineering Aspects, 138(2–3), 145-159.

Escobar, I.C., Hoek, E.M., Gabelich, C.J. and DiGiano, F.A. (2005). Committee report: recent advances and research needs in membranes fouling. Journal of the American Water Works Association, 97(8), 79-89.

Faibish, R.S., Elimelech, M. and Cohen, Y.K. (1998). Effect of interparticle electrostatic double layer interactions on permeate flux decline in crossflow membrane filtration of colloidal suspensions: an experimental investigation. Journal of Colloid and Interface Science, 204(1), 77-86.

Ficek, K.J. and Boll, J.E. (1980). Potassium permanganate: an alternative to prechlorination. Aqua 32(7), 153-156.

French, R.A., Jacobson, A.R., Kim, B., Isley, S.L., Lee Penn, R. and Baveye, P.C. (2009). Influence of ionic strength, pH, and cation valence on aggregation kinetics of titanium dioxide nanoparticles. Environmental Science & Technology, 43(5), 1354-1359.

Gao, W., Liang, H., Ma, J., Han, M., Chen, Z.-L., Han, Z.-S. and Li, G.-B. (2011). Membrane fouling control in ultrafiltration technology for drinking water production: A review. Desalination, 272(1-3), 1-8.

Genz, A., Kornmuller, A. and Jekel, M. (2004). Advanced phosphorus removal from membrane filtrates by adsorption on activated aluminum oxide and granulated ferric hydroxide. Water Research, 38(16), 3523-3530.

Gilbert, B., Lu, G. and Kim, C.S. (2007). Stable cluster formation in aqueous suspensions of iron oxyhydroxide nanoparticles. Journal of Colloid and Interface Science, 313(1), 152-159.

Gillespie, J.B. and Lindberg, J.D. (1992). Ultraviolet and visible imaginary refractive index of strongly absorbing atmospheric particulate matter. Applied Optics, 31(12), 2112-2115.

González, A.E., Martinez-López, F., Moncho-Jordá, A. and Hidalgo-Álvarez, R. (2004). Simulations of colloidal aggregation with short- and medium-range interactions. Physica A: Statistical Mechanics and its Applications, 333(15), 257-268.

Gopal, K., Tripathy, S.S., Bersillon, J.L. and Dubey, S.P. (2007). Chlorination byproducts, their toxicodynamics and removal from drinking water. Journal of Hazardous Materials, 140(1-2), 1-6.

Gouzinis, A., Kosmidis, N., Vayenas, D.V. and Lyberatos, G. (1998). Removal of Mn and simultaneous removal of NH3, Fe and Mn from potable water using a trickling filter. Water Research, 32(8), 2442-2450.

Gray, S.R., Ritchie, C.B., Tran, T. and Bolto, B.A. (2007). Effect of NOM characteristics and membrane type on microfiltration performance. Water Research, 41(17), 3833-3841.

Griffin, A.E. (1960). Significance and removal of manganese in water supplies. Journal of the American Water Works Association, 52(10), 1326-1334.

Gregory, D. and Carlson, K. (2003). Effect of soluble Mn concentration on oxidation kinetics. Journal of the American Water Works Association, 95(1), 98-108.

Gregory, D. and Carlson, K.H. (2001). Ozonation of dissolved manganese in the presence of natural organic matter. Ozone: Science & Engineering, 23(2), 149-159.

Guan, J., Waite, T.D. and Amal R. (1998). Rapid structure characterization of bacterial aggregates. Environmental Science & Technology, 32(23), 3735-3742.

Guo, W., Ngo, H.-H. and Li, J. (2012). A mini-review on membrane fouling. Bioresource Technology, 122, 27-34.

Han, S.C., Choo, K.H., Choi, S.J. and Benjamin, M.M. (2007). Modeling manganese removal in chelating polymer-assisted membrane separation systems for water treatment. Journal of Membrane Science, 290(1-2), 55-61.

Han, S.C., Choo, K.H., Choi, S.J. and Benjamin, M.M. (2005). Removal of manganese from water using combined chelation-membrane separation systems. Water Science and Technology, 51(6-7), 349-355.

Hargette, A.C. and Knocke, W.R. (2001). Assessment of fate of manganese in oxide-coated filtration systems. Journal of Environmental Engineering-Asce, 127(12), 1132-1138.

He, X., Yang, H. and He, Y. (2010). Treatment of mine water high in Fe and Mn by modified manganese sand. Mining Science and Technology (China), 20(4), 571-575.

Health Canada. (2010). Guidelines for Canadian Drinking Water Quality-Summary Table. http://www.dieppe.ca/en/hoteldeville/resources/Canadiandrinkingwaterguidelines.pdf, (Dec. 23, 2015).

Health Canada. (2014). Guidelines for Canadian drinking water quality-Summary table. http://www.hc-sc.gc.ca/ewh-semt/alt_formats/pdf/pubs/water-eau/sum_guide-res_recom/sum_guide-res_recom_2014-10_eng.pdf (Jan. 07, 2017).

Health Canada. (2016). Manganese in drinking water. Federal-Provincial-Territorial Committee on Drinking Water, Ottawa, ON, Canada (pp. 116).

Healy, T.W., Herring, A.P. and Fuerstenau, D.W. (1966). The effect of crystal structure on the surface properties of a series of manganese dioxides. Journal of Colloid and Interface Science, 21(4), 435-444.

Hermia, J. (1982). Constant pressure blocking filtration laws - Application to power-law non-Newtonian fluids. Transactions of the Institute of Chemical Engineering, 60(3), 183-187.

Hofs, B., Ogier, J., Vries, D., Beerendonk, E.F. and Cornelissen, E.R. (2011). Comparison of ceramic and polymeric membrane permeability and fouling using surface water. Separation and Purification Technology, 79(3), 365-374.

Hu, P.-Y., Hsieh, Y.-H., Chen, J.-C. and Chang, C.-Y. (2004). Adsorption of divalent manganese ion on manganese-coated sand. Journal of Water Supply: Research and Technology-AQUA, 53(3), 151-158.

Huang, H., Lee, N., Young, T., Gary, A., Lozier, J.C. and Jacangelo, J.G. (2007). Natural organic matter fouling of low-pressure, hollow fiber membranes: effects of NOM source and hydrodynamic conditions. Water Research, 41 (17), 3823-3832.

Huang, H., Spinette, R. and O'Melia, C.R. (2008a). Direct-flow microfiltration of aquasols: I. Impacts of particle stabilities and size. Journal of Membrane Science, 314(1–2), 90-100.

Huang, H., Young, T.A. and Jacangelo, J.G. (2008b). Unified membrane fouling index for low pressure membrane filtration of natural waters: principles and methodology. Environmental Science & Technology, 42(3), 714-720.

Huisman, I.H., Dutre, B., Persson, K.M. and Tragardh, G. (1997). Water permeability in ultrafiltration and microfiltration-Viscous and electroviscous effects. Desalination, 113(1), 95-103.

Huisman, I.H., Vellenga, E., Tragardh, G. and Tragardh, C. (1999). The influence of the membrane zeta potential on the critical flux for crossflow microfiltration of particle suspensions. Journal of Membrane Science, 156(1), 153-158.

Hwang, K.J. and Hsueh, C.L. (2003). Dynamic analysis of cake properties in microfiltration of soft colloids. Journal of Membrane Science, 214(2), 259-273.

Islam, A.A., Goodwill, J.E., Bouchard, R., Tobiason , J.E. and Knocke, W.R. (2010). Characterization of filter media MnOx(s) Surfaces and Mn removal capabilit. Journal of the American Water Works Association, 102(9), 71-83.

Ito, Y., Inaba, M., Chung, D.J. and Imanishi, Y. (1992). Control of water permeation by pH and ionic strength through a porous membrane having poly(carboxylic acid) surface-grafted. Macromolecules, 25(26), 7313-7316.

Jefferson, B. and Jarvis, P.R. (2006). Practical application of fractal dimension. In: G. Newcombe and D. Dixon (Eds.), Interface Science in Drinking Water Treatment, Theory and Applications (pp. 45-61). Amsterdam, The Netherlands: Elsevier Ltd.

Jacobsen, F., Holcman, J. and Sehested, K. (1998). Oxidation of manganese(II) by ozone and reduction of manganese(III) by hydrogen peroxide in acidic solution. International Journal of Chemical Kinetics, 30(3), 207-214.

Kaiya, Y., Itoh, Y., Fujita, K. and Takizawa, S. (1996). Study on fouling materials in the membrane treatment process for potable water. Desalination, 106(1-3), 71-77.

Kallay, N. and Zalac, S. (2002). Stability of nanodispersions: a model for kinetics of aggregation of nanoparticles. Journal of Colloid Interface Science, 253(1), 70-76.

Karri, R. and Knowlton, T.M. (1999). Gas distributor and plenum design in fluidized beds. In: W.C. Yang (Ed.), Fluidization, Solids Handling and Processing: Industrial Applications (pp. 209-235). New Jersey, USA: Noyes.

Katsoufidou, K., Yiantsios, S.G. and Karabelas, A.J. (2005). A study of ultrafiltration membrane fouling by humic acids and flux recovery by backwashing: experiments and modeling. Journal of Membrane Science, 266(1-2), 40-50.

Kawakatsu, T., Nakao, S. and Kimura, S. (1993). Effects of size and compressibility of suspended particles and surface pore size of membrane on flux in crossflow filtration. Journal of Membrane Science, 81(1-2), 173-190.

Kaya, N., Karadurmus, E. and Alicilar, A. (2005). Catalytic air oxidation of manganese in synthetic waters. Central European Journal of Chemistry, 3(3), 511-519.

Knocke, W.R., Occiano, S. and Hungate, R. (1990a). Removal of soluble manganese from water by oxide-coated filter media. American Water Works Association Research Foundation (AWWARF), Denver, CO, USA.

Knocke, W.R., Van Benschoten, J.E., Kearney, M., Soborski, A. and Foundation, A.R. (1990b). Alternative oxidants for the removal of soluble iron and manganese. American Water Works Association Research Foundation (AWWARF), Denver, CO, USA.

Knocke, W.R., Van Benschoten, J.E., Kearney, M.J., Soborski, A.W. and Reckhow, D.A. (1991). Kinetics of manganese and iron oxidation by potassium-permanganate and chlorine dioxide. Journal of the American Water Works Association, 83(6), 80-87.

Knocke, W.R., Zuravnsky, L., Little, J.C. and Tobiason , J.E. (2010). Adsorptive contactors for removal of soluble manganese during drinking water treatment. Journal of the American Water Works Association, 102(8), 64-75.

Kontturi, K., Mafe, S., Manzanares, J.A., Svarfvar, B.L. and Viinikka, P. (1996). Modeling of the salt and ph effects on the permeability of grafted porous membranes. Macromolecules, 29(17), 5740-5746.

Kosmulski, M. (2009). Compilation of PZC and IEP of sparingly soluble metal oxides and hydroxides. Advanced in Colloid and Interface Science, 152(1-2), 14-25.

Krawczyk, H. and Jonsson, A.S. (2014). The influence of feed flow channel diameter on frictional pressure drop, membrane performance and process cost in full-scale tubular ceramic membranes. Chemical Engineering Research and Design, 92(1), 174-180.

Kunii, D. and Levenspiel, O. (1991). Fluidization Engineering. Boston, MA, USA: Butterworth-Heinemann.

Lee, E.K., Chen, V. and Fane, A.G. (2008). Natural organic matter (NOM) fouling in low pressure membrane filtration - effect of membranes and operation modes. Desalination, 218(1-3), 257-270.

Lee, S.A., Fane, A.G., Amal, R. and Waite, T.D. (2003). The effect of floc size and structure on specific cake resistance and compressibility in dead-end microfiltration. Separation Science and Technology, 38(4), 869-887.

Lee, S.-J. and Kim, J.-H. (2014). Differential natural organic matter fouling of ceramic versus polymeric ultrafiltration membranes. Water Research, 48(1), 43-51.

Lee, S.M., Tiwari, D., Choi, K.M., Yang, J.K., Chang, Y.Y. and Lee, H.D. (2009). Removal of Mn(ii) from aqueous solutions using manganese-coated sand samples. Journal of Chemical and Engineering Data, 54(6), 1823-1828.

Lee, C.I., Yang, W.F. and Hsieh, C.I. (2004). Removal of copper (II) by manganese-coated sand in a liquid fluidized-bed reactor. Journal of Hazardous Materials, 114(1-3), 45-51.

Li, L., Wray, H.E., Andrews, R.C. and Bérubé, P.R. (2014). Ultrafiltration fouling: Impact of backwash frequency and air sparging. Separation Science and Technology, 49(18), 2814-2823.

Lim, A.L. and Bai, R. (2003). Membrane fouling and cleaning in microfiltration of activated sludge wastewater. Journal of Membrane Science, 216(1–2), 279-290.

Logager, T., Holcman, J., Sehested, K. and Pedersenf, T. (1992). Oxidation of ferrous Ions by ozone in acidic solutions. Inorganic Chemistry, 31(17), 3523-3529.

Madaeni, S.S. (2001). The effect of large particles on microfiltration of small particles. Journal of Porous Materials, 8(2), 143-148.

Malvern Instruments Ltd. (1997). Sample dispersion and refractive index guide. <http://www.atomikateknik.com/pdf/Sample%20Dispersion%20&%20RI%20Guide.pdf> (Apr. 12, 2015).

Manttari, M., Pihlajamaki, A. and Nystrom, M. (2006). Effect of pH on hydrophilicity and charge and their effect on the filtration efficiency of NF membranes at different pH. Journal of Membrane Science, 280(1-2), 311-320.

Mastersizer 3000 user manual. (2011). Worcestershire, UK: Malvern Instruments Ltd.

Minnesota Department of Health (MDH). (2012). Health based guidance for groundwater. Manganese. Minnesota Department of Health.

Merkle, P.B., Knocke, W., Gallagher, D., Junta-Rosso, J. and Solberg, T. (1996). Characterizing filter media mineral coatings. Journal of the American Water Works Association, 88(12), 62-73.

Merkle, P.B., Knocke, W.R., Gallagher, D.L. and Little, J.C. (1997). Dynamic model for soluble Mn^{2+} removal by oxide-coated filter media. Journal of Environmental Engineering-Asce, 123(7), 650-658.

Ministère du développement durable de l'environnement et lutte contre les changements climatiques (MDDELCC). (2016). Règlement sur la qualité de l'eau potable. Loi sur la qualité de l'environnement.

Montgomery Watson Harza (MWH). (2005). Water treatment: principles and design (2ed Ed.). Hoboken, NJ, USA: John Wiley and Sons, Inc.

Morgan, J.J. and Stumm, W. (1964). Colloid-chemical properties of manganese dioxide. Journal of Colloid Science, 19(4), 347-359.

Morgan, J.J. and Stumm, W. (1965). The role of multivalent metal oxides in limnological transformations as exemplified by iron and manganese. In: O. Jaag (Ed.), Proceedings Second Water Pollusion Reasearch Conference (pp. 103-131). New York, NY, USA: Pergamon Press, Inc.

Muthukumaran, S. and Baskaran, K. (2014). Comparison of the performance of ceramic microfiltration and ultrafiltration membranes in the reclamation and reuse of secondary wastewater. Desalination and Water Treatment, 52(4-6), 670-677.

Nielsen, P.B., Christensen, T.C. and Vendrup, M. (1997). Continuous removal of heavy metals from FGD wastewater in a fluidised bed without sludge generation. Water Science and Technology, 36(2-3), 391-397.

Nilsson, M., Trägårdh, G. and Östergren, K. (2008). The influence of pH, salt and temperature on nanofiltration performance. Journal of Membrane Science, 312(1-2), 97-106.

Ning, R.Y. (2009). Colloidal Iron and Manganese in Water Affecting RO Operation. Desalination and Water Treatment, 12(1-3), 162-168.

Orts-Gil, G., Natte, K., Drescher, D., Bresch, H., Mantion, A., Kneipp, J. and Osterle, W. (2011). Characterisation of silica nanoparticles prior to in vitro studies: From primary particles to agglomerates. Journal of Nanoparticle Research, 13(4), 1593-1604.

Oulhote, Y., Mergler, D., Barbeau, B., Bellinger, D., Bouffard, T., Brodeur, M.E., Saint-Amour, D., Legrand, M., Sauvé, S. and Bouchard, M. (2014). Neurobehavioral function in school-age children exposed to manganese in drinking water. International Journal of Epidemiology, 122(12), 1343-1350.

Pantina, J.P. and Furst, E.M. (2006). Colloidal aggregate micromechanics in the presence of divalent ions. Langmuir, 22(12), 5282-5288.

Pell, M. (1990). Gas Fluidization. Amsterdam, The Netherlands: Elsevier Ltd.

Pendergast, M.M. and Hoek, E.M.V. (2011). A review of water treatment membrane nanotechnologies. Energy & Environmental Science, 4, 1946-1971.

Phatai, P., Wittayakun, J., Grisdanurak, N., Chen, W.H., Wan, M.W. and Kan, C.C. (2010). Removal of manganese ions from synthetic groundwater by oxidation using $KMnO_4$ and the characterization of produced MnO_2 particles. Water Science and Technology, 62(8), 1719-1726.

Piispanen, J.K. and Sallanko, J.T. (2010). Mn(II) removal from groundwater with manganese oxide-coated filter media. Journal of Environmental Science and Health, Part A: Toxic/Hazardous Substances and Environmental Engineering, 45(13), 1732-1740.

Post, J.E. (1999). Manganese oxide minerals: Crystal structures and economic and environmental significance. Proceedings of the National Academy of Sciences, 96(7), 3447-3454.

Potgieter, J.H., Mccrindle, R.I., Sihlali, Z., Schwarzer, R. and Basson, N. (2005). Removal of iron and manganese from water with a high organic carbon loading. Part I- The effect of various coagulants. Water Air and Soil Pollution, 162(1-4), 49-59.

Prasad, T.D. and Danso-Amoako, E. (2014). Influence of chemical and biological parameters on iron and manganese accumulation in water distribution networks. Procedia Engineering, 70, 1353-1361.

Ramachandra Rao, R., Roopa, H.N. and Kannan, T.S. (1999). Effect of pH on the dispersability of silicon carbide powders in aqueous media. Ceramic International, 25(3), 223-230.

Reckhow, D.A., Knocke, W.R., Kearney, M.J. and Parks, C.A. (1991). Oxidation of iron and manganese by ozone. Ozone: Science and Engineering, 13(6), 675-695

Reisz, E., Leitzke, A., Jarocki, A., Irmscher, R. and von Sonntag, C. (2008). Permanganate formation in the reactions of ozone with Mn(II): A mechanistic study. Journal of Water Supply: Research and Technology-AQUA, 57(6), 451-464.

Ren, Y.X., Yan, N., Wen, Q., Fan, Z., Wei, T., Zhang, M. and Ma, J. (2011). Graphene/δ-MnO2 composite as adsorbent for the removal of nickel ions from wastewater. Chemical Engineering Journal, 175, 1-7.

Richards, L.A., Richards, B.S. and Schäfer, A.I. (2011). Renewable energy powered membrane technology: Salt and inorganic contaminant removal by nanofiltration/reverse osmosis. Journal of Membrane Science, 369(1-2), 188-195.

Roccaro, P., Barone, C., Mancini, G. and Vagliasindi, F.G.A. (2007). Removal of manganese from water supplies intended for human consumption: a case study. Desalination, 210(1-3), 205-214.

Rudolfs, W. and Balmat, J.L. (1952). Colloids in sewage: I. separation of sewage colloids with the aid of the electron microscope. Water Environment Federation, 24(3), 247-256.

Safari, S., Sheikhi, A., and van de Ven, T.G.M. (2014). Electroacoustic characterization of conventional and electrosterically stabilized nanocrystalline celluloses. Journal of Colloid Interface Science, 432(15), 151-157.

Sallanko, J., Lakso, E. and Lehmikangas, M. (2005). The effect of ozonation on the size fractions of manganese. Ozone: Science and Engineering, 27(2), 147-152.

Santiwong, S.R., Guan, J. and Waite, T.D. (2008). Effect of ionic strength and pH on hydraulic properties and structure of accumulating solid assemblages during microfiltration of montmorillonite suspensions. Journal of Colloid and Interface Science, 317(1), 214-227.

Schneider, C., Johns, P. and Huehmer, R.P. (2001). Removal of manganese by microfiltration in a water treatment plant. Proceedings of the 2001 Membrane Technology Conference, San Antonio, Texas, USA: AWWA & IWA.

Shao, J., Hou, J. and Song, H. (2011). Comparison of humic acid rejection and flux decline during filtration with negatively charged and uncharged ultrafiltration membranes. Water Research, 45(2), 473-482.

Sharma, S.K., Greetham, M.R. and Schippers, J.C. (1999). Adsorption of iron(ii) onto filter media. Journal of Water Supply: Research and Technology-AQUA, 48(3), 84-91.

Sherman, D. M. and Waite, T. D. (1985). Electronic spectra of Fe^{3+} oxides and oxide hydroxides in the near IR to near UV. American Mineralogist, 70(11-12), 1262-1269.

Shirazi, S. Lin, C.J. and Chen D. (2010). Inorganic fouling of pressure-driven membrane processes-A critical review. Desalination, 250(1), 236-248.

Singh, G. and Song, L. (2006). Cake compressibility of silica colloids in membrane filtration processes. Industrial & Engineering Chemistry Research, 45(22), 7633-7638.

Sly, L.I., Hodgkinson, M.C. and Arunpairojana, V. (1990). Deposition of manganese in a drinking water distribution system. Applied and Environmental Microbiology, 56(3), 628-639.

Sommerfeld, E.O. (1999). Iron and manganese removal handbook. Denver, CO, USA: American Water Works Association.

Sorensen, C.M. (2001). Light scattering by fractal aggregates: A review. Aerosol Science and Technology, 35(2), 648-687.

Sorensen, B.L. and Sorensen, P.B. (1997). Applying cake filtration theory on membrane filtration data. Water Research, 31(3), 665-670.

Subramaniam, A. (2010). A pilot-scale evaluation of soluble manganese removal using pyrolucite media in a high-rate adsorptive contactor. Virginia Polytechnic Institute and State University, Blacksburg, VA.

Sung, B.W., Chu, K.H., Yun, S.L., Ahn, J.Y., Lee, J.H., Yoo, S.S., Lee, J.W. and Ko, K.B. (2015). Removal of iron and manganese ions from abandoned neutral or alkaline mine drainage via ozone oxidation and micro-sand filtration: a pilot-scale operation. Desalination and Water Treatment, 53(9), 2354-2362.

Takizawa, S., Fu, L., Pradhan, N., Ike, T., Ohtaki, M. and Ohgaki, S. (2001). Pretreatment processes for membrane filtration of raw water containing manganese. Water Science and Technology: Water Supply, 1(5-6), 341-348.

Tang, S., Preece, J.M., McFarlane, C.M. and Zhang, Z. (2000). Fractal morphology and breakage of DLCA and RLCA aggregates. Journal of Colloid and Interface Science, 221(1), 114-123.

Teng, Z., Huang, J.Y., Fujita, K. and Takizawa, S. (2001). Manganese removal by hollow fiber micro-filter. Membrane separation for drinking water. Desalination, 139(1-3), 411-418.

Theis, T.L. and Singer, P.C. (1974). Complexation of iron(II) by organic matter and its effect on iron(II) oxygenation. Environmental Science & Technology, 8(6), 569-573.

Tiller, F.M., Yeh, C.S. and Leu, W.F. (1987). Compressibility of paniculate structures in relation to thickening, filtration, and expression-A review. Separation Science and Technology, 22(2-3), 1037-1063.

Tiwari, D., Yu, M.R., Kim, M.N., Lee, S.M., Kwon, O.H., Choi, K.M., Lim, G.J. and Yang, J.K. (2007). Potential application of manganese coated sand in the removal of Mn(II) from aqueous solutions. Water Science and Technology, 56(7), 153-160.

Trudinger, P.A. (1979). Biogeochemical cycling of mineral forming elements. Amsterdam, The Netherlands: Elsevier Ltd.

Tobiason, J.E., Bazilio, A., Goodwill, J., Mai, X. and Nguyen, C. (2016). Manganese Removal from Drinking Water Sources. Current Pollution Reports, 2(3), 168-177.

Tobiason, J.E., Islam, A.A., Knocke, W.R., Goodwill, J., Hargette, P., Bouchard, R. and Zuravnsky, L. (2008). Characterization and performance of filter media for manganese control. Denver, CO, USA: American Water Works Association Research Foundation.

Tuschl, K., Mills, P.B. and Clayton, P.T. (2013). Manganese and the brain. International Review of Neurobiology, 110, 277-312.

United States Environmental Protection Agency (USEPA). (2000). Control of Gaseous Emissions (3[ed] Ed.). Air Pollution Training Institute (APTI) (pp. 341).

United States Environmental Protection Agency (USEPA). (2004). Drinking water health advisory for manganese. Office of Water (4304T). Health and Ecological Criteria Division, Washington, DC, USA (pp. 55).

United States Environmental Protection Agency (USEPA). (2005). Membrane filtration guidance manual. Office of Water (4601), Washington, DC, USA (pp. 332).

Van benschoten, J.E., Wei, L. and Knocke, W.R. (1992) Kinetic modeling of manganese(ii) oxidation by chlorine dioxide and potassium-permanganate. Environmental Science & Technology 26(7), 1327-1333.

Van Der Bruggen, B., Vandecasteele, C., Van Gestel, T., Doyen, W. and Leysen, R. (2003). A review of pressure-driven membrane processes in wastewater treatment and drinking water production. Environmental Progress, 22(1), 46-56.

van Wendel de Joode, B., Barbeau, B., Bouchard, M.F., Mora, A.M., Skytt, Å., Córdoba, L., Quesada, R., Lundh, T., Lindh, C.H. and Mergler, D. (2016). Manganese concentrations in drinking water from villages near banana plantations with aerial mancozeb spraying in Costa Rica: Results from the Infants' Environmental Health Study (ISA). Environmental Pollution, 215, 247-257.

Vane, L. M., and Zang, G. M. (1997). Effect of aqueous phase properties on clay particle zeta potential and electro-osmotic permeability: implications for electrokinetic soil remediation processes. Journal of Hazardous Materials, 55(1-3), 1-22.

Vela, M.C.V., Blanco, S.A., García, J.L. and Rodríguez, E.B. (2008). Analysis of membrane pore blocking models applied to the ultrafiltration of PEG. Separation and Purification Technology, 62(3), 491-500.

Vercellotti, J.M. (1988). Kinetics of iron removal using potassium permanganate and ozone. Ohio University, Athens, OH.

Wasserman, G.A., Liu, X.H., Parvez, F., Ahsan, H., Levy, D., Factor-Litvak, P., Kline, J., van Geen, A., Slavkovich, V., Lolacono, N.J., Cheng, Z.Q., Zheng, Y. and Graziano, J.H. (2006). Water manganese exposure and children's intellectual function in Araihazar, Bangladesh. Environmental Health Perspectives, 114(1), 124-129.

Weiner, B. (1992). Twenty seven years of QELS: a review of the advantages and disadvantages of particle sizing with QELS. In: N.G. Stanley-Wood and R.W. Lines (Eds.), Particle Size Analysis (pp. 173-185). Cambridge, UK: Royal Society of Chemistry.

Werther, J. (1978). Effect of gas distributor on the hydrodynamics of gas fluidized beds. German Chemical Engineering 1, 166-173.

Wong, J.M. (1984). Chlorination-filtration for iron and manganese removal. Journal of the American Water Resources Association, 76(1), 76-79.

World Health Organization (WHO). (2008). Guidelines for drinking water-quality. Third Edition incorporating the First and Second addenda Edition. Recommendations. Geneva, Switzerland (pp. 668).

World Health Organization (WHO). (2003). Iron in drinking water. Geneva, Switzerland (pp. 9).

Xu, R. (2000). Particle Characterization: Light Scattering Methods. Dordrecht, The Netherlands: Kluwer Academic Publishers.

Xu, W., Gao, B., Mao, R. and Yue, Q. (2011). Influence of floc size and structure on membrane fouling in coagulation–ultrafiltration hybrid process-The role of Al13 species. Journal of Hazardous Materials, 193, 249-256.

Yang, K., Xue, Y., He, J. and Yange, X. (2008). Case study: reducing manganese (Mn++) level in surface water with natural manganese-coated sand in sinopec Shanghai ltd. Journal of Water Supply: Research and Technology-AQUA, 57(3), 185-194.

Zhang, Y., Chen, Y.S., Westerhoff, P. and Crittenden, J. (2009). Impact of natural organic matter and divalent cations on the stability of aqueous nanoparticles. Water Research, 43(17), 4249-4257.

Zhang, Y.P., Fane, A.G. and Law, A.W.K. (2010). Critical flux and particle deposition of fractal flocs during crossflow microfiltration. Journal of Membrane Science, 353(1-2), 28-35.

Zhao, C., Nie, S., Tang, M. and Sun, S. (2011). Polymeric pH-sensitive membranes-A review. Progress in Polymer Science, 36(11), 1499-1520.

Zhao, Y., Xing, W., Xu, N. and Wong, F.S. (2005). Effects of inorganic salt on ceramic membrane microfiltration of titanium dioxide suspension. Journal of Membrane Science, 254(1-2), 81-88.

Zhao, Y., Zhang, Y., Xing, W. and Xu, N. (2005). Influences of pH and ionic strength on ceramic microfiltration of TiO_2 suspensions. Desalination, 177(1-3), 59-68.

Zogo, D., Bawa, L.M., Soclo, H.H. and Atchekpe, D. (2011). Influence of pre-oxidation with potassium permanganate on the efficiency of iron and manganese removal from surface water. Journal of Environmental Chemistry and Ecotoxicology, 3(1), 1-8.

Zularisam, A.W., Ismail, A.F. and Salim, R. (2006). Behaviours of natural organic matter in membrane filtration for surface water treatment-A review. Desalination, 194(1-3), 211-231.

Zuo, G. and Wang, R. (2013). Novel membrane surface modification to enhance anti-oil fouling property for membrane distillation application. Journal of Membrane Science 447, 26-35.

Zuravnsky, L. (2006). Development of soluble manganese sorptive contactors for enhancing potable water treatment practices. Virginia Polytechnic Institute and State University, Blacksburg, VA.

Zydney, A.L. and Pujar, N.S. (1998). Protein transport through porous membranes-effects of colloidal interactions. Colloids and Surfaces a-Physicochemical and Engineering Aspects, 138(2-3), 133-143.